AD-A193 577 INVESTIGATION OF THE HYPERSONIC FLOWFIELD SURROUNDING A 1/2
SHAPED CHARGE JET(U) ARMY BALLISTIC RESEARCH LAB
ABERDEEN PROVING GROUND MD H W MEYER DEC 87
UNCLASSIFIED BRL-TR-2883 F/G 19/1 NL

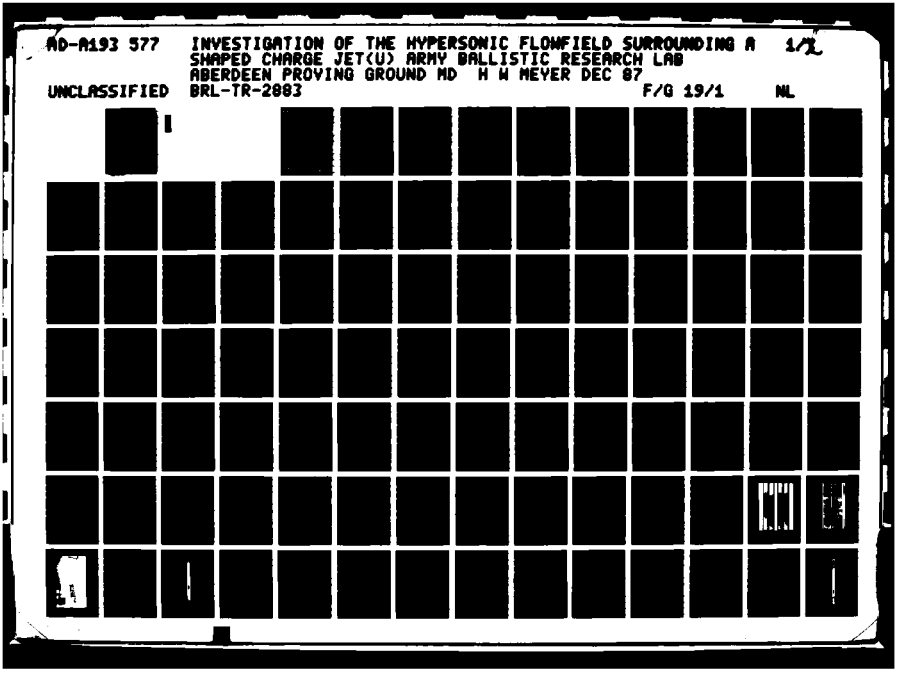

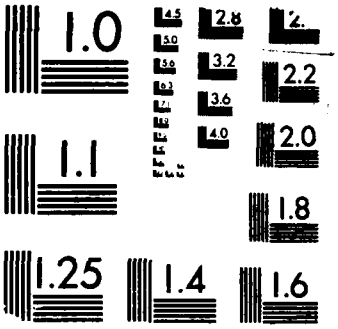

MICROCOPY RESOLUTION TEST CHART

BUREAU OF STANDARDS-1963-A

UNCLASSIFIED
SECURITY CLASSIFICATION OF THIS PAGE

ADA193577

REPORT DOCUMENTATION PAGE

Form Approved
OMB No. 0704-0188

1a. REPORT SECURITY CLASSIFICATION UNCLASSIFIED	1b. RESTRICTIVE MARKINGS
2a. SECURITY CLASSIFICATION AUTHORITY	3. DISTRIBUTION/AVAILABILITY OF REPORT Approved for Public Release; Distribution Unlimited
2b. DECLASSIFICATION/DOWNGRADING SCHEDULE	
4. PERFORMING ORGANIZATION REPORT NUMBER(S) BRL-TR-2883	5. MONITORING ORGANIZATION REPORT NUMBER(S)
6a. NAME OF PERFORMING ORGANIZATION Ballistic Research Laboratory 6b. OFFICE SYMBOL (If applicable) SLCBR-TB-A	7a. NAME OF MONITORING ORGANIZATION
6c. ADDRESS (City, State, and ZIP Code) Aberdeen Proving Ground, MD 21005-5066	7b. ADDRESS (City, State, and ZIP Code)
8a. NAME OF FUNDING/SPONSORING ORGANIZATION 8b. OFFICE SYMBOL (If applicable)	9. PROCUREMENT INSTRUMENT IDENTIFICATION NUMBER
8c. ADDRESS (City, State, and ZIP Code)	10. SOURCE OF FUNDING NUMBERS PROGRAM ELEMENT NO. / PROJECT NO. / TASK NO. / WORK UNIT ACCESSION NO.

11. TITLE (Include Security Classification)
Investigation of the Hypersonic Flowfield Surrounding a Shaped Charge Jet

12. PERSONAL AUTHOR(S)
Meyer, Hubert W. Jr.

13a. TYPE OF REPORT	13b. TIME COVERED FROM _____ TO _____	14. DATE OF REPORT (Year, Month, Day)	15. PAGE COUNT

16. SUPPLEMENTARY NOTATION

17. COSATI CODES			18. SUBJECT TERMS (Continue on reverse if necessary and identify by block number)
FIELD	GROUP	SUB-GROUP	Shaped Charge, Experimental, Godunov, Hypersonic, Numerical, Real Gas

19. ABSTRACT (Continue on reverse if necessary and identify by block number)

Explosively formed hypervelocity shaped charge jets for the defeat of armored targets have been the subject of a considerable amount of research, but little of this effort has been devoted to studying the aerodynamic forces acting on the jet particles, particularly the interference caused by nearby surfaces. The object here is to develop numerical methods and apply them to this problem. A Godunov inviscid technique is developed, modified to include high temperature thermodynamic properties, and used to obtain the flow field in front of a hemisphere. This solution is used as the initial condition for the computation of the flow field in the annular region between the jet and a surrounding cylindrical tube. Computations for Mach number 4.00 are compared to experimental data in order to validate the numerical technique. The actual shaped charge jet case at a Mach number of 20.45 is then solved. The predictions are compared to the results of an experiment under corresponding conditions.

Excellent correlation was obtained between the code prediction and experimental radio-

20. DISTRIBUTION/AVAILABILITY OF ABSTRACT	21. ABSTRACT SECURITY CLASSIFICATION
☒ UNCLASSIFIED/UNLIMITED ☐ SAME AS RPT. ☐ DTIC USERS	Unclassified

22a. NAME OF RESPONSIBLE INDIVIDUAL	22b. TELEPHONE (Include Area Code)	22c. OFFICE SYMBOL
Hubert W. Meyer, Jr.	301 278-6019	SLCBR-TB-A

DD Form 1473, JUN 86 — Previous editions are obsolete. — SECURITY CLASSIFICATION OF THIS PAGE UNCLASSIFIED

graphic data, with the predicted shock propagation characteristics being within 8% of the data. The computed pressure on the tube wall behind the reflected shock wave was 27% of the measured value, with poor repeatibility in the measurement.

Computations indicated the pressure on the side of the jet is 34 atm for a tube diameter of 2.50 jet diameters. This is insufficient to cause observed perturbations in the jet. A hypothesis was proposed to account for the perturbations; it considers the effect of the flow field on a cloud of particles, resulting from the explosive formation process, that surrounds the jet tip.

DTIC
COPY
INSPECTED
1

Accession For	
NTIS GRA&I	☑
DTIC TAB	☐
Unannounced	☐
Justification	
By	
Distribution/	
Availability Codes	
Dist	Avail and/or Special
A-1	

TABLE OF CONTENTS

LIST OF FIGURES

LIST OF TABLES

LIST OF SYMBOLS

General

$\vec{\omega}$	any vector function of time and position
σ	scalar element of surface area
$\hat{n}$	unit vector normal to σ; unit vector normal to boundary
Ψ	volume
S	surface of control volume
t	time
τ	length of time step

Flowfield

$\vec{V}$	fluid velocity
u	component of fluid velocity in positive x direction
v	component of fluid velocity in positive r direction
w	component of fluid velocity normal to cell boundary
y	component of fluid velocity tangent to cell boundary
ρ	fluid density
p	fluid pressure
e	fluid specific internal energy
ϵ	fluid specific total energy
∞	subscript to denote a property of the free stream fluid
γ	ratio of specific heats; = 1.4 (perfect air); eq 5-2 (real air)
Γ	isentropic γ; see eq 5-1

Grid

A	cell area
d	body diameter
D	tube diameter
x	axial position
r	radial position
θ	angle between negative x axis and radial boundary
ϕ	angle between negative x axis and circumferential boundary
$\hat{i}$	unit vector in positive x direction
$\hat{j}$	unit vector in positive r direction
n	circumferential or axial cell index
N	number of cells in circumferential or axial direction
m	radial cell index
M	number of cells in radial direction
S	length of cell boundary
ℓ	location of node as measured along the ray
q	cell boundary velocity
Ω	velocity of node along ray

Riemann Problem

U x component of fluid velocity at the boundary
V r component of fluid velocity at the boundary
W component of fluid velocity normal to the boundary
R fluid density at the boundary
P fluid pressure at the boundary
E specific internal energy of the fluid at the boundary
Ξ specific total energy of the fluid at the boundary
S length of the cell boundary
UR..suffix "R" denotes the property is for a radial boundary
UT..suffix "T" denotes the property is for a circumferential boundary
p_o pressure on the contact discontinuity
w_o velocity on the contact discontinuity
a mass velocity of both waves in the linear Riemann problem
a mass velocity of negative running wave in nonlinear Riemann prob
b mass velocity of positive running wave in nonlinear Riemann prob

ρ^+ density between positive running wave and contact discontinuity

ρ^- density between negative running wave and contact discontinuity

Δ^+ absolute velocity of positive running wave (radial boundary)

Δ^- absolute velocity of negative running wave (radial boundary)

D^+ absolute velocity of pos running wave (circumferential boundary)

D^- absolute velocity of neg running wave (circumferential boundary)

Chapter 1

INTRODUCTION

Background

The objective of this effort is to study the hypersonic flow field associated with a shaped charge jet. Of concern will be how and to what extent perturbations of the jet are caused by interactions of the flow field with objects the jet may encounter.

Shaped charges are explosive devices used in several widely differing applications. The mining industry uses them to penetrate and fracture subterranean rock for various purposes, among them creating drainage paths to the drilled hole of an oil well. They are also used in the metal fabrication industry to rough cut and drill heavy plates, for example a pilot hole for subsequent cutting with an oxy-acetylene torch. But by far the most common and the most demanding use is by the military for the defeat of armored targets. In this application, the shaped charge warhead most commonly is delivered to the target in a missle or a gun fired projectile. An on-board fuzing system senses the target and initiates the detonation of the warhead at the proper time, and the jet formation begins. This study considers the events that occur after the detonation and jet formation process is complete.

A shaped charge warhead consists of a cylindrical explosive charge with a conical cavity in one end. The cavity is typically lined with a hollow, thin walled conical copper liner. The shaped charge jet is formed when a detonation wave, traveling through the explosive, collapses the liner upon itself with such violence that a stream of copper is ejected along the axis of the cone. Obviously, symmetry of the charge plays a critical role in the lethality of the jet. A precision manufactured warhead with a 42° cone of 81 mm diameter at the base and a 1.9 mm wall thickness (figure 1) produces a pencil thin jet traveling at a speed of greater than Mach 20 in sea level air. This highly focused energy source is capable of penetrating over 450 mm (18 inches) of armor steel. The time scale of the cone collapse and jet formation is of the order of tens of microseconds.

Flash radiography is the most popular tool used in the study of shaped charge jets. The technique involves the use of a high energy (0.3 to 2.0 million volts) x-ray pulse of very short duration (30 to 50 nanoseconds) to project an image of the jet on conventional x-ray film. The high energy level is required for penetration of detonation products (gases and debris) and the short pulse time assures that the image of the hypervelocity jet is not noticeably blurred. The film

pack is sealed from visible light, so the burst of light from the detonation does not affect the film.

A flash radiograph of a typical jet is shown on the right in figure 2. As a consequence of the formation process, the jet tip travels at a greater speed than the trailing portion. This velocity gradient causes the jet to eventually break up into many small particles, as shown in the figure. As long as the particles are axially aligned, the jet is still quite lethal. The jet on the left in figure 2 has been perturbed by some target element, and its lethality has been seriously degraded. The armor designer searches for ways to achieve this degradation in a small and light armor package.

While considerable research has been conducted in the fields of jet formation and jet penetration, little effort has been devoted to studying the aerodynamic forces that influence the jet. At typical jet velocities of greater than Mach 20, an extremely strong flow field is developed which may cause severe perturbations in the jet. For example, an extremely strong bow shock wave is formed. As the jet from a missile-delivered warhead traverses the passage through the missile's guidance package, or through the hole in a skirting plate (the armored fender protecting the tracks and wheels of an armored vehicle) made by the leading portion of the jet, the bow shock is reflected back to impinge on a trailing portion of the jet, applying potentially disruptive forces. Another potentially disruptive force results from the strong wake behind a jet particle. The subsequent particles must fly through this highly turbulent region. The situation may be even more severe for particles farther back in the jet.

Numerous observations have been made in the past (ref 1) of obstacles that have perturbed the jet through some unknown mechanism. Under contract to the Ballistic Research Lab, Zernow et al. (ref 2) studied some armor configurations that caused perturbations in the jet, and concluded that aerodynamic forces must be responsible. In an attempt to verify this conclusion experimentally, they conducted a test in which the target and warhead were enclosed in a vacuum chamber, but the level of vacuum achieved was not low enough to absolutely preclude aerodynamic effects. The final report on their effort showed many examples of jets that were perturbed after passing through, but not touching, various armor configurations. Figure 3 is an example of one of these jets; at no time did this jet come in contact with any object.

Yen (ref 3), also under contract to the Ballistic Research Lab, conducted a preliminary study of the jet aerodynamics problem and identified some pressure levels and some general characteristics of the flow field associated with various rods passing through various apertures by varying the ratio of the rod radius to the aperture radius. Yen also studied the flow field around a leading jet particle and its influence on the motion of subsequent particles. The present effort is a detailed extension of the preliminary analytical work of Yen and the experimental study of Zernow, concentrating on the aerodynamic pressures exerted on the jet.

The hypersonic flow field is studied by numerical solution of the equations of motion utilizing a method developed by S. K. Godunov, a Russian mathematician. The method has been used at the BRL to solve a similar problem of a projectile passing through the muzzle brake of a gun (a blast deflector attached to the muzzle) (ref 4,5). This first order inviscid method is suitable to hypersonic flow regimes containing complicated shock patterns (ref 6). Holt (ref 7) discusses the method in some detail, devoting an entire chapter to it and to a second order sequel proposed by Godunov and his colleagues in 1970 (ref 8). In the first phase of this study (ref 9), the necessary equations were derived and a one-dimensional code written. Theoretical and experimental verifications were carried out (figures 4 and 5) which showed that the technique accurately predicts those flow phenomena critical to this study: shock and expansion wave formation, wave reflection, and wave/wave collisions. In the second phase of the study reported here, an axisymmetric code is written and validated by solving some problems with known solutions. Finally, jet passage through a cylindrical tube of circular cross section is studied, as shown in figure 6. These calculations are compared to experimental data. In the future, more complex geometries may be numerically studied.

The Godunov Technique

The one-dimensional scheme developed by Godunov is explained and expanded to two dimensions (and axisymmetric) in a 1961 paper in the Russian Journal of Mathematics and Mathematical Physics (Ref 10). The principal advantage of the method lies in the physically realistic approach used to obtain the numerical solution of the equations of fluid motion. That the solution technique can be so well expressed in physical terms is fascinating, and a fine comment on the beauty with which mathematics expresses the physical laws of nature. In fact, Godunov (Ref 11) derives all the necessary equations (not including the conservation equations) from purely mathematical considerations. As a final step, he indicates that his equations are the same as those that would result from consideration of a physical system. The physical system is the basis of the present derivations.

The physical system referred to above is the one-dimensional fluid discontinuity, sometimes called the Riemann problem after the German mathematician who was the first to attempt to calculate shock properties. Riemann's classical paper is given as reference 12. Courant and Friedrichs' text (ref 13) contains a few historical remarks as well as some theoretical discussion. For detailed derivations of the equations involved in the present application, the reader is referred to reference 9. The one-dimensional fluid discontinuity is used to estimate the fluxes of fluid properties at the cell boundaries, and imparts to the method an accuracy, stability and numerical efficiency that is better than many competing techniques. Several papers (ref 14, 15) report that the first order Godunov scheme is as accurate as some popular second order schemes. Also, while the Godunov method does smooth out discontinuities over several cells, it does not use

nonphysical methods like artificial viscosity as originally proposed by Von Neumann and Richtmyer (ref 16) and disdained by Moretti (ref 17).

To see how this Riemann problem helps in the solution of the equations of fluid motion, consider a one-dimensional fluid, divided into finite cells and at t_0 containing the pressure distribution as shown in figure 7a. Similar curves can be imagined for the other dependent variables, velocity (u), density (ρ) and internal energy (e). These quantities will be functions of time as well as functions of x for unsteady flow.

The gas is thus divided into one-dimensional regions of thickness Δx. Some appropriate average value of p, u, ρ, e is chosen for each layer (at $t = \tau$). These are denoted by $p_{m-1/2}$, $u_{m-1/2}$, etc. Consequently, the values in neighboring layers may not be the same, as seen in figure 7b. Because of the incremental nature of the assumed form of the pressure distribution, a pressure discontinuity exists at the boundary between cells. This is analogous to the classical shock tube problem (and to the problem studied by Riemann), which considers the solution of the problem depicted in figure 7c. Of course in the present case the diaphragm is imaginary. It is imagined to rupture by unfreezing the time variable, and permitting the discontinuities in pressure, density and velocity to seek equilibrium. The discontinuity at x_m is thus resolved into a shock wave, expansion wave and contact discontinuity (or some other combination), propagating from the cell boundary at x_m, or simply m, toward its neighbors at m-1 and m+1.

The conditions behind these waves are well known from shock tube theory, and can be computed from the known initial conditions on the two sides of the diaphragm. More importantly, the conditions behind the waves are constant. The essence of the Godunov technique is to utilize these constant conditions at the cell boundaries in the conservation equations to compute the flux of properties across that boundary during the time step. In this way new average properties are computed for each cell and the entire process is repeated in the next time step. The integral form of the conservation equations must be used if the solution is to be valid for flow fields containing discontinuities (shock waves).

The equations which constitute the general solution of the Riemann problem are nonlinear. For weak (sonic) waves, the equations can be linearized by use of the acoustic approximation, in which higher order terms in the flow variables and their derivatives are neglected. This approach is commonly used to reduce the momentum equation to a wave equation (ref 13,18), for which closed form solutions exist. Sound waves are an example of such weak waves. In the present application, a similar approximation is used to reduce the algebraic nonlinear Riemann equations to linear form. This approximation is valid in all cases except the case in which a discontinuity in the flow field (e.g. bow shock wave, reflected wave, etc.) passes near enough to

the two cells to cause large gradients between them. One can see from figure 7 that the magnitude of the discontinuities in each individual Riemann problem are governed in part by the size of the increment Δx. In the absence of strong gradients from a nearby shock wave, the Riemann waves can be guaranteed to be weak waves by selection of an appropriately fine grid.

The nonlinear equations resulting from the theoretical study of the Riemann problem, rather than approximations to those equations, were used for the solution of the nonlinear Riemann problem. This approach was chosen in order to retain a sound theoretical basis. Several approximate Riemann solvers have been developed which will reduce computation time while retaining an accuracy consistent with the finite difference method. The most popular of these is Roe's method (ref 19). Chakravarthy and Osher implemented this method and reported the results in reference 20. Osher has himself developed an approximate Riemann solver, and this work is presented in ref 21.

In order for the shock tube analogy cited above to be valid, the properties at the point x_m must remain constant during the time step; they must not be disturbed by the waves propagating from the neighboring points x_{m-1} and x_{m+1}. Thus the properties at x_m must only result from the resolution of the discontinuity at x_m. The fact that the region between points x_m and x_{m+1} (or x_m and x_{m-1}) is complicated by the presence of additional waves emanating from x_{m+1} (or x_{m-1}) is of no consequence to the properties at x_m. The properties computed for point x_m will remain valid until the waves from the neighboring points arrive at x_m. Thus the time interval Δt must be less than the time required for the wave to traverse the distance Δx. If W is the wave speed relative to the fixed coordinate frame,

$$\Delta t < \frac{\Delta x}{W}$$

is the physically required relationship between the step sizes. Godunov also derives this criterion by a purely mathematical stability analysis, again demonstrating the harmony between physical and mathematical descriptions of nature.

General Approach to Solving the Fluid Dynamics Problem

The Godunov technique requires the solution of two fluid dynamics problems. The primary problem involves use of the conservation laws to update the properties in each cell based on the flux of each property across the cell boundaries. The secondary fluid dynamics problem to be solved is the Riemann problem at the boundaries

of the cells. The fluid condition behind the waves constitutes the solution, and this condition governs the fluxes at the boundary.

Figure 8 shows a schematic of the conditions in the Riemann problem. The negative running wave and positive running wave may also fall in the same quadrant (either quadrant), but by definition the positive running wave has the more positive absolute (i.e. relative to the fixed cell boundary) velocity. The location of each wave (left or right quadrant) will depend on the initial fluid velocities in the two cells, and the resultant wave velocity relative to the fluid.

From classical shock tube theory, the pressure and velocity of the gas on either side of the contact discontinuity in figure 8 are known to be equal and constant; hence the terminology p_0 and u_0 in the regions behind the waves. Similarly, the density is known to be different on the two sides of the contact discontinuity, but to be constant in each of the regions 2 and 3. That is, the density is discontinuous across the contact discontinuity. p_1, u_1, ρ_1, and p_4, u_4, ρ_4 are the known and constant conditions of the gas prior to the passing of the wave.

Chapter 2

THE FINITE DIFFERENCE EQUATIONS

General Form of the Conservation Equations

The conservation laws are derived using the Lagrangian approach: a particular element of fluid is studied as it flows. The control volume in this case is that which encloses the element of fluid under study. It can change size and shape as it moves along in the flow field, but unlike the Eulerian control volume, the mass within it is constant. For this reason the Lagrangian approach seems more naturally suited to the derivation of conservation laws. Details of the derivation may be found in ref 9.

In the Lagrangian derivation, mass, momentum and energy is integrated over the volume of the element, but pressure must be integrated over the surface of the element. The Gauss Divergence Theorem (ref 22), used when the two types of integrals appear in the same equation, converts the surface integrals to volume integrals.

$$\int_{S(t)} \hat{n}\cdot\vec{\omega}\,d\sigma = \int_{\forall(t)} \vec{\nabla}\cdot\vec{\omega}\,d\forall \tag{2-1}$$

Equation 2-1 is the Gauss Divergence Theorem, where $\vec{\omega}$ is any vector function of time and position, $d\sigma$ is a scalar element of surface area, $\hat{n}$ is a unit vector normal to $d\sigma$ and directed outward, and $d\forall$ is a scalar element of volume.

The equations resulting from the Lagrangian derivation are then expressed in Eulerian terms by use of the Reynold's Transport Theorem.

$$\frac{d}{dt}\int_{\forall(t)} \alpha(t)\,d\forall = \int_{\forall} \left[\frac{\partial\alpha}{\partial t} + \vec{\nabla}\cdot\alpha\vec{V}\right] d\forall \tag{2-2}$$

Here α is any property of the fluid within $\forall$ and $\vec{V}$ is the velocity of the fluid within $\forall$. Reynold's Transport Theorem relates Lagrangian terms on the left hand side to Eulerian terms on the right hand side. In this form the volume on the right hand side is fixed, and the equality applies at the instant that the Lagrangian volume and the Eulerian volume coincide.

Conservation of Mass

To express the conservation of mass in a Lagrangian frame of reference is simple: The mass within the control volume is constant. An element of mass within $\forall$ is written $\rho d\forall$. The total mass of fluid within $\forall$ does not change with time.

$$\frac{d}{dt}\int_{\forall(t)} \rho d\forall = 0$$

With the help of Reynold's Transport Theorem, the three dimensional form of the continuity equation follows directly.

$$\frac{\partial \rho}{\partial t} + \vec{\nabla}\cdot\rho\vec{V} = 0 \qquad (2\text{-}3)$$

Conservation of Momentum

In Newton's Law, the resultant force acting on the fluid within the control volume is equal to the time rate of change of momentum. Neglecting shear forces (inviscid fluid) and body forces (gravity), pressure exerts the only force on the fluid.

$$-\int_S p\, d\vec{S} = \frac{d}{dt}\int_{\forall} \rho\vec{V}\, d\forall$$

The surface integral is converted to a volume integral by use of the Gauss Divergence Theorem. The general form of the axial momentum and radial momentum equations result from application of the Reynold's Transport Theorem to the above momentum balance. With the axial and radial components of the fluid velocity denoted by u and v respectively, the axial and radial momentum equations are written in the following general form.

$$\frac{\partial}{\partial t}(\rho u) + \vec{\nabla}\cdot\rho u\vec{V} + \frac{\partial p}{\partial x} = 0 \qquad (2\text{-}4)$$

$$\frac{\partial}{\partial t}(\rho v) + \vec{\nabla}\cdot\rho v\vec{V} + \frac{\partial p}{\partial r} = 0 \qquad (2\text{-}5)$$

Conservation of Energy

The principle of conservation of energy states that the rate of change of energy of the fluid within the control volume $\forall$ is equal to the rate at which heat is added plus the rate at which work is done on the fluid.

$$\begin{bmatrix}\text{rate at which heat}\\ \text{is added to fluid}\\ \text{within } \forall\end{bmatrix} + \begin{bmatrix}\text{rate at which work}\\ \text{is done on fluid}\\ \text{within } \forall\end{bmatrix} = \begin{bmatrix}\text{rate of change of}\\ \text{energy of fluid}\\ \text{within } \forall\end{bmatrix}$$

Heat conduction and radiation in the fluid will be neglected. This is permissible because of the extremely short time scale for the problem under study. Also, since no mass enters or leaves the Lagrangian control volume, no heat can be convected across S, the surface of $\forall$. Thus the first term in the energy balance is zero. The work in the second term is done by forces. Since body forces and shear stresses are being neglected, the only force is due to the pressure on S, $-p d\vec{S}$. Therefore the energy balance can be written in the following integral form.

$$-\int_S p\vec{V}\cdot d\vec{S} = \frac{d}{dt}\int_{\forall} \rho\epsilon \, d\forall \qquad (\epsilon = e+\tfrac{1}{2}V^2 = e+\tfrac{1}{2}\vec{V}\cdot\vec{V})$$

The term on the left hand side is converted to a volume integral by the Gauss divergence Theorem and the term on the right hand side is simplified by the Reynold's Transport Theorem. The result is the three dimensional form of the conservation of energy.

$$\frac{\partial}{\partial t}(\rho\epsilon) + \vec{\nabla}\cdot\rho\epsilon\vec{V} + \vec{\nabla}\cdot p\vec{V} = 0 \qquad (2\text{-}6)$$

Axisymmetric Equations of Motion

The general form of the velocity vector in cylindrical coordinates is

$$\vec{V} = u\hat{e}_x + v\hat{e}_r + w\hat{e}_\theta .$$

The axisymmetric assumption is that the fluid does not flow in the θ direction; ie. $w = 0$. This reduces the general form of the fluid velocity to the following.

$$\vec{V} = u\hat{e}_x + v\hat{e}_r \qquad (2\text{-}7)$$

With this substitution, and expanding the operator in eq. 2-3, the conservation of mass becomes

$$\frac{\partial\rho}{\partial t} + \frac{1}{r}\frac{\partial}{\partial r}(\rho v r) + \frac{\partial}{\partial x}(\rho u) = 0. \qquad (2\text{-}8)$$

Masson et al (ref 23) indicate, as do results presented below, that Godunov's formulation (equations 6.1 of ref 10) results in a loss of

accuracy at the stagnation point, r = 0. Godunov multiplies the above equation by r to arrive at his eq. 6.1, and this may contribute to the problem at the stagnation point. A more versatile formulation is the following.

$$\frac{\partial}{\partial t}(\rho) + \frac{\partial}{\partial x}(\rho u) + \frac{\partial}{\partial r}(\rho v) + \frac{\rho v}{r} = 0 \qquad (2\text{-}9)$$

The last term in eq. 2-9 will remain finite at the stagnation point, since $v \to 0$ as $r \to 0$.

Substitute eq. 2-7 into eq. 2-4 to obtain the conservation of momentum in the axial direction.

$$\frac{\partial}{\partial t}(\rho u) + \frac{\partial}{\partial x}(p+\rho u^2) + \frac{\partial}{\partial r}(\rho uv) + \frac{\rho uv}{r} = 0 \qquad (2\text{-}10)$$

Substitute eq. 2-7 into eq. 2-5 to obtain the conservation of momentum in the radial direction.

$$\frac{\partial}{\partial t}(\rho v) + \frac{\partial}{\partial x}(\rho uv) + \frac{\partial}{\partial r}(p+\rho v^2) + \frac{\rho v^2}{r} = 0 \qquad (2\text{-}11)$$

Substitute eq. 2-7 into eq. 2-6 to obtain the conservation of energy for the axisymmetric case. For simplicity, ϵ represents the specific total energy of the fluid (ie. internal + kinetic).

$$\frac{\partial}{\partial t}(\rho\epsilon) + \frac{\partial}{\partial x}\rho u(\epsilon+\frac{p}{\rho}) + \frac{\partial}{\partial r}\rho v(\epsilon+\frac{p}{\rho}) + \frac{\rho v}{r}(\epsilon+\frac{p}{\rho}) = 0 \qquad (2\text{-}12)$$

$$\epsilon = e + \tfrac{1}{2}(u^2+v^2)$$

Finite Difference Form of the Equations of Motion

A short discussion about conventions used is appropriate before proceding with the derivation of the finite difference form of the equations of motion.

The finite difference equations of motion are of the form

$$F_{new} = F_{old} - \tau[flux_1 + flux_2 + flux_3 + flux_4 + axisym]$$

where F represents the property being conserved, τ the length of the time step, $flux_i$ the flux of the property across the i boundary, and axisym an axisymmetric term as explained in the derivation below. Flux

out of the cell is considered positive. For the blunt body problem as pictured in figure 9, the circumferential boundaries are to be allowed to move radially so as to fit the shock layer exactly. For these boundaries, fluid velocity and boundary velocity in the direction away from the body are chosen as positive. Fluid velocity normal to the radial boundaries is considered positive if it is directed clockwise.

Conservation of Mass

For a flowfield containing discontinuities in the flow variables, the differential equations of motion are integrated over an arbitrary volume element. The axisymmetric assumption reduces this requirement to integration over an arbitrary area in the axisymmetric plane. A reasonable choice is the computational cell, as shown in figure 10. Equation 2-9 is integrated over the cell area.

$$\int_A \frac{\partial \rho}{\partial t}\, dA + \int_A \left[\frac{\partial}{\partial x}(\rho u) + \frac{\partial}{\partial r}(\rho v)\right] dA + \int_A \frac{\rho v}{r}\, dA = 0 \qquad (2\text{-}13)$$

Rewrite the first term using polar coordinates (z,θ) in the axisymmetric plane.

$$\int_A \frac{\partial \rho}{\partial t}\, dA = \int_\theta \int_{z_4}^{z_2} \frac{\partial \rho}{\partial t}\, z\, dz\, d\theta$$

The inner integral is simplified by substituting $x = z^2/2$.

$$\int_A \frac{\partial \rho}{\partial t}\, dA = \int_\theta \int_{x_4}^{x_2} \frac{\partial \rho}{\partial t}\, dx\, d\theta$$

Leibnitz' rule (ref 19) may now be used on the inner integral. When the original variable z is replaced, the inner integral is written as follows.

$$\int_A \frac{\partial \rho}{\partial t}\, dA = \int_\theta \left\{ \frac{d}{dt} \int_{z_4}^{z_2} (\rho z)\, dz - \left[\rho z\right]_{z_2,t} \frac{dz_2}{dt} + \left[\rho z\right]_{z_4,t} \frac{dz_4}{dt} \right\} d\theta$$

Note that the radial boundaries do not move. That is, $\theta \neq \theta(t)$, and the integration over θ can be moved inside the differentiation. This is done, and the following boundary velocities are substituted.

$$q_{n-1/2,m} = \frac{dz_4}{dt}$$

$$q_{n-1/2,m-1} = \frac{dz_2}{dt}$$

The result is

$$\int_A \frac{\partial \rho}{\partial t} dA = \frac{d}{dt} \int_\theta \int_z \rho z dz d\theta - \int_\theta \rho z_2 q_{n-1/2,m-1} \, d\theta + \int_\theta \rho z_4 q_{n-1/2,m} \, d\theta \, .$$

The integrals over $z_2\theta$ and $z_4\theta$ are simply integrals along the two circumferential boundaries of the cell. These are rewritten as line integrals, and the double integral is written in notation which is independent of whether the cell's area is described in polar or cylindrical coordinates.

$$\int_A \frac{\partial \rho}{\partial t} dA = \frac{d}{dt} \int_A \rho \, dA - \int_{s_2} \rho q_{n-1/2,m-1} \, ds + \int_{s_4} \rho q_{n-1/2,m} \, ds \qquad (2\text{-}14)$$

The boundary velocity is considered constant along the length of the boundary by assigning an average velocity to the entire boundary. The assumption is now made that the fluid properties (axial velocity, radial velocity, outward normal velocity, density, pressure, energy) are all constant along each of the four boundaries. This of course is consistent with the Riemann model being used to compute the conditions at each boundary. These constant conditions are denoted by capital letters (U,V,W,R,P,E). The integrals along the boundaries s_2 and s_4 are replaced as follows:

$$\int_A \frac{\partial \rho}{\partial t} dA \approx \frac{d}{dt} \int_A \rho \, dA - \left[RqS\right]_{n-1/2,m-1} + \left[RqS\right]_{n-1/2,m} \qquad (2\text{-}15)$$

where S represents the length of the boundary.

Consider next the second integral in eq. 2-13. Notice that the integrand is the two dimensional divergence of $\rho\bar{V}$.

$$\bar{\nabla} \cdot \rho\bar{V} = \frac{\partial}{\partial x}(\rho u) + \frac{\partial}{\partial r}(\rho v)$$

The corresponding two dimensional divergence theorem states that

$$\int_A \bar{\nabla} \cdot \rho\bar{V} \, dA = \int_s \rho\bar{V} \cdot \hat{n} \, ds,$$

where S is the closed boundary around the cell area A, ds is an incremental length of S, and $\hat{n}$ is a unit vector perpendicular to S and directed outward. Therefore $\bar{V}\cdot\hat{n}$ is the normal component of the outward fluid velocity across the cell boundary (w), so the second integral in eq. 2-13 may be written as follows.

$$\int_A \left[\frac{\partial}{\partial x}(\rho u) + \frac{\partial}{\partial r}(\rho v)\right] dA = \int_S \rho w \, ds$$

The integral on the right hand side is replaced by four integrals, one along each of the four cell boundaries. Since the fluid properties are constant along each of these boundaries, each integral reduces to simply RWS, where S is the length of the boundary.

$$\int_A \left[\frac{\partial}{\partial x}(\rho u) + \frac{\partial}{\partial r}(\rho v)\right] dA$$

$$\approx \left[[RWS]_{n,m-1/2} + [RWS]_{n-1/2,m-1} - [RWS]_{n-1,m-1/2} - [RWS]_{n-1/2,m}\right] \quad (2\text{-}16)$$

Flux out of the cell has been chosen as positive, so the flux across the negative-most boundaries (where a positive W is directed into the cell) will be positive if the negative of the velocity W is used.

Finally, consider the third integral in eq. 2-13. An average value (r) is chosen for the distance from the centroid of the cell to the x axis, measured perpendicular to the x axis. All fluid properties within the cell (distinct from those at the boundary), including r, are assumed constant for the duration of the time step. Of course, u,v,ρ,p,e and r may vary from time step to time step, so they are all functions of time, but the integration is over a single time step only. The third integral in eq. 2-13 therefore reduces to

$$\int_A \frac{\rho v}{r} dA \approx \left[\frac{\rho v}{r} A\right]_{n-1/2,m-1/2} \quad (2\text{-}17)$$

in the notation of figure 9. Except when appearing in an integral, the above lower case letters (u,v,ρ,p,e), plus w,y,r, and A, will refer to average cell properties, considered constant over the entire cell for the duration of the time step. Next, eqs. 2-15, 2-16, and 2-17 are substituted into eq. 2-13.

$$\frac{d}{dt}\int_A \rho \, dA - \left[RqS\right]_{n-1/2,m-1} + \left[RqS\right]_{n-1/2,m} +$$

$$\left[[RWS]_{n,m-1/2} + [RWS]_{n-1/2,m-1} - [RWS]_{n-1,m-1/2} - [RWS]_{n-1/2,m}\right] + \left[\frac{\rho v}{r} A\right]_{n-1/2,m-1/2} \approx 0$$

The terms for the circumferential boundaries may be combined, with the following result.

$$\frac{d}{dt}\int_A \rho\ dA + \Big\{ [RWS]_{n,m-1/2} + [R(W-q)S]_{n-1/2,m-1} + \\ + [-RWS]_{n-1,m-1/2} + [R(q-W)S]_{n-1/2,m} + \left[\frac{\rho v}{r}A\right]_{n-1/2,m-1/2} \Big\} \approx 0 \qquad (2\text{-}18)$$

Notice that the flux terms use fluid velocity relative to the boundary (the velocities of the radial boundaries are zero). This result also may be obtained by use of the form of Reynold's Transport theorem for moving and deforming control volumes (this form is discussed, for example, in reference 24).

Equation 2-18 must be integrated over the time step in order to remove the differentiation. The general cell is denoted by the notation (n-1/2,m-1/2). If τ is the length of the time step, and values at t are denoted by subscripts and values at t+τ by superscripts, the first term in eq. 2-18 becomes

$$\int_t^{t+\Delta t} \frac{d}{dt}\int_A \rho\ dA\ dt \approx \left[\rho A\right]^{n-1/2,\ m-1/2} - \left[\rho A\right]_{n-1/2,\ m-1/2}$$

Since all the other terms in eq. 2-18 contain properties that are constant over the time step, those integrals simplify to algebraic expressions, and the conservation of mass results.

$$\left[\rho A\right]^{n-1/2,m-1/2} \approx \left[\rho A\right]_{n-1/2,m-1/2} - \tau\Big\{ [RWS]_{n,m-1/2} + [R(W-q)S]_{n-1/2,m-1} + \\ + [-RWS]_{n-1,m-1/2} + [R(q-W)S]_{n-1/2,m} + \left[\frac{\rho v}{r}A\right]_{n-1/2,m-1/2} \Big\} \qquad (2\text{-}19)$$

Conservation of Axial Momentum

The steps used in deriving the finite difference form of the conservation of axial momentum are the same as those used above. Begin by rearranging eq. 2-10 and integrating over the cell area.

$$\int_A \frac{\partial}{\partial t}(\rho u)\ dA + \int_A \left[\frac{\partial}{\partial x}(\rho u^2) + \frac{\partial}{\partial r}(\rho uv)\right] dA + \int_A \frac{\partial p}{\partial x}\ dA + \int_A \frac{\rho uv}{r}\ dA = 0 \qquad (2\text{-}20)$$

The first, second, and fourth integrals are approximated in the same manner as was done for the conservation of mass, as follows.

$$\int_A \frac{\partial}{\partial t}(\rho u)\,dA \approx \frac{d}{dt}\int_A \rho u\ dA - \Big[RUqS\Big]_{n-1/2,m-1} + \Big[RUqS\Big]_{n-1/2,m} \tag{2-21}$$

$$\int_A \left[\frac{\partial}{\partial x}(\rho u^2) + \frac{\partial}{\partial r}(\rho uv)\right] dA$$

$$\approx \Big[[RUWS]_{n,m-1/2} + [RUWS]_{n-1/2,m-1} - [RUWS]_{n-1,m-1/2} - [RUWS]_{n\ \ 2,m}\Big] \tag{2-22}$$

$$\int_A \frac{\rho uv}{r}\,dA \approx \left[\frac{\rho uv}{r}A\right]_{n-1/2,m-1/2} \tag{2-23}$$

The third integral in eq. 2-20 can be simplified, also with the two dimensional divergence theorem, as shown below.

$$\int_A \frac{\partial p}{\partial x}\ dA = \int_A \bar{\nabla}\cdot p\hat{i}\ dA$$

$$\int_A \frac{\partial p}{\partial x}\ dA = \int_S p\hat{i}\cdot\hat{n}\ ds \tag{2-24}$$

The scalar product $(\hat{i}\cdot\hat{n})$ is a direction cosine, and is evaluated along each of the four boundaries in turn. Closed path S is again taken to be the sequence of the four boundaries, and θ and ϕ represent respectively the angles between radial and circumferential boundaries and the negative x axis. The scalar product is evaluated as follows.

$$\hat{i}\cdot\hat{n}_{n,m-1/2} = |\hat{i}||\hat{n}|\cos\left(\frac{\pi}{2}-\theta_n\right) = \sin\theta_n$$

The other scalar products are evaluated in a similar manner.

$$\hat{i}\cdot\hat{n}_{n-1/2,m-1} = -\sin\phi_{n-1/2,m-1}$$

$$\hat{i}\cdot\hat{n}_{n-1,m-1/2} = -\sin\theta_{n-1}$$

$$\hat{i}\cdot\hat{n}_{n-1/2,m} = \sin\phi_{n-1/2,m}$$

The integral on the right hand side of eq. 2-24 is divided into four

integrals and the direction cosines above are substituted. The resulting integrals are approximated as was done previously (eq. 2-16). Equation 2-24 is then written:

$$\int_A \frac{\partial p}{\partial x}\, dA \approx \Big\{ [PS\sin\theta]_{n,m-1/2} - [PS\sin\phi]_{n-1/2,m-1} - [PS\sin\theta]_{n-1,m-1/2} + [PS\sin\phi]_{n-1/2,m} \Big\} . \qquad (2\text{-}25)$$

Equations 2-21, 2-22, 2-23, and 2-25 are substituted into eq. 2-20, and the circumferential boundary terms combined. The entire equation is integrated over the time step to obtain the finite difference form of the conservation of axial momentum.

$$\left[\rho uA\right]^{n-1/2,m-1/2} = \left[\rho uA\right]_{n-1/2,m-1/2} - \tau\Big\{ [(RUW+P\sin\theta)S]_{n,m-1/2} + [(RU(W-q)-P\sin\phi)S]_{n-1/2,m-1} + [(-RUW-P\sin\theta)S]_{n-1,m-1/2} + [(RU(q-W)+P\sin\phi)S]_{n-1/2,m} + \left[\frac{\rho uv}{r}A\right]_{n-1/2,m-1/2} \Big\} \qquad (2\text{-}26)$$

Conservation of Radial Momentum

The finite difference form of the conservation of radial momentum is completely analogous to that of the axial momentum. The only difference is in the direction cosines.

$$\hat{j}\cdot\hat{n}_{n,m-1/2} = \cos\theta_n$$

$$\hat{j}\cdot\hat{n}_{n-1/2,m-1} = -\cos\phi_{n-1/2,m-1}$$

$$\hat{j}\cdot\hat{n}_{n-1,m-1/2} = -\cos\theta_{n-1}$$

$$\hat{j}\cdot\hat{n}_{n-1/2,m} = \cos\phi_{n-1/2,m}$$

The resulting finite difference form of the conservation of radial momentum is very similar to that of axial momentum.

$$\left[\rho vA\right]^{n-1/2,m-1/2} = \left[\rho vA\right]_{n-1/2,m-1/2} - \tau\Big\{\left[(RVW+P\cos\theta)S\right]_{n,m-1/2} +$$

$$+\left[(RV(W-q)-P\cos\phi)S\right]_{n-1/2,m-1} + \left[(-RVW-P\cos\theta)S\right]_{n-1,m-1/2} +$$

$$+\left[(RV(q-W)+P\cos\phi)S\right]_{n-1/2,m} + \left[\frac{\rho v^2}{r}A\right]_{n-1/2,m-1/2}\Big\} \qquad (2\text{-}27)$$

Conservation of Energy

The procedure for the energy equation parallels that of the mass and momentum equations. The general differential form of the conservation of energy is

$$\frac{\partial}{\partial t}(\rho\epsilon) + \bar{\nabla}\cdot\rho\epsilon\vec{V} + \bar{\nabla}\cdot p\vec{V} = 0 \qquad (2\text{-}5)$$

where ϵ is the specific total energy of the fluid, as defined above for eq. 2-12. Also required will be Ξ, the specific total energy of the fluid at the boundary (from the Riemann problem):

$$\Xi = E + \tfrac{1}{2}(U^2+V^2) \qquad (E = \text{specific internal energy at boundary}).$$

Again, begin by integrating the differential equation of motion over the cell area.

$$\int_A \frac{\partial}{\partial t}(\rho\epsilon)dA + \int_A \bar{\nabla}\cdot\rho\epsilon\vec{V}\,dA + \int_A \bar{\nabla}\cdot p\vec{V}\,dA = 0 \qquad (2\text{-}28)$$

Leibnitz's rule is applied to the first integral in eq. 2-28.

$$\int_A \frac{\partial}{\partial t}(\rho\epsilon)dA = \int_\theta \left\{ \frac{d}{dt}\int_{z_4}^{z_2}(\rho\epsilon z)dz - \left[\rho\epsilon z\right]_{z_2,t}\frac{dz_2}{dt} + \left[\rho\epsilon z\right]_{z_4,t}\frac{dz_4}{dt}\right\} d\theta$$

The numerical approximation is constructed analogously to eq. 2-15.

$$\int_A \frac{\partial}{\partial t}(\rho\epsilon)dA \approx \frac{d}{dt}\int_A \rho\epsilon dA - \left[R\Xi qS\right]_{n-1/2,m-1} + \left[R\Xi qS\right]_{n-1/2,m} \qquad (2\text{-}29)$$

Approximation of the second integral in eq. 2-28 is analogous to that of eq. 2-16.

$$\int_A \bar{\nabla}\cdot\rho\epsilon\vec{V}\ dA \approx \Big\{ [R\Xi WS]_{n,m-1/2} + [R\Xi WS]_{n-1/2,m-1} + $$

$$-[R\Xi WS]_{n-1,m-1/2} - [R\Xi WS]_{n-1/2,m} + \left[\frac{\rho\epsilon V}{r}A\right]_{n-1/2,m-1/2} \Big\} \qquad (2\text{-}30)$$

The third integral in eq. 2-28 is analogous to the second, except that the scalar function p replaces the scalar function $\rho\epsilon$.

$$\int_A \bar{\nabla}\cdot p\vec{V}\ dA \approx \Big\{ [PWS]_{n,m-1/2} + [PWS]_{n-1/2,m-1} + $$

$$- [PWS]_{n-1,m-1/2} - [PWS]_{n-1/2,m} + \left[\frac{pV}{r}A\right]_{n-1/2,m-1/2} \Big\} \qquad (2\text{-}31)$$

Equation 2-31 represents the change in energy of the fluid in the cell from work done on the fluid by forces exerted by the pressure of the surrounding fluid. Notice that although the fluid must move in order that these forces do work on the fluid, the moving boundaries do not contribute to any work done on the fluid.

Equations 2-29, 2-30, and 2-31 are substituted into eq. 2-28 and the result integrated over the time step to obtain the finite difference form of the conservation of energy.

$$\left[\rho\epsilon A\right]^{n-1/2,m-1/2} = \left[\rho\epsilon A\right]_{n-1/2,m-1/2} - \tau\Big\{ [(P+R\Xi)WS]_{n,m-1/2} +$$

$$+[(PW+R\Xi(W-q))S]_{n-1/2,m-1} + [-(P+R\Xi)WS]_{n-1,m-1/2} +$$

$$+[(-PW+R\Xi(q-W))S]_{n-1/2,m} + \left[(p+\rho\epsilon)\frac{V}{r}A\right]_{n-1/2,m-1/2} \Big\} \qquad (2\text{-}32)$$

Chapter 3

THE SPHERE IN UNIFORM FLOW

The problem of the jet in a tunnel, as pictured in figure 6, is naturally divided into two axisymmetric problems: a hemisphere described by a spherical grid, and an annulus described by a rectangular grid. Two similar but distinct codes are written to solve the two problems; the boundary conditions for the sphere being those of uniform flow, and the boundary conditions for the annulus coming from the solution of the sphere problem. This chapter deals with the solution of the sphere problem, and some comparisons to experimental data. Many of the developments of this chapter are also applicable to the code used to solve the rectangular grid. The analysis in this chapter considers a perfect gas. Modifications required to include real gas effects are considered in a later chapter. A listing of the code used to solve the hemisphere problem, including real gas effects, is given in Appendix A.

The Grid

The general notation for the grid for the sphere problem is shown in figure 9. The grid pattern used in this work straddles the axis of symmetry, with one-half of the first cell below the axis and one half above. This approach simplifies statement of the boundary condition, forces the shock to be perpendicular to the axis at the axis, and facilitates computations on the axis. Considerable effort was expended on the approach in which each of the first cells has the axis as as one of its boundaries. This approach could not be made accurate at the stagnation point of the sphere. The subject of boundary conditions will be dealt with in more detail later.

The grid is defined by specifying three independent variables:

$\ell_{n,m}$ location, measured along the ray from the x axis, of the intersection of each circumferential boundary with each ray.

x_n coordinate of the point of intersection of the nth ray with the x axis (for this problem, $x_0 = x_1 = \ldots = x_{nt} = 0$).

θ_n angle between the nth ray and the negative x axis.

All remaining grid attributes are derived from these three.

1. Length of radial boundary, SR:

$$SR_{n,m-1/2} = \ell_{n,m-1} - \ell_{n,m} \tag{3-1}$$

2. r component of length of circumferential boundary of cell:

$$\eta_{n-1/2,m} = \ell_{n,m} \sin \theta_n - \ell_{n-1,m} \sin \theta_{n-1} \tag{3-2}$$

3. x component of length of circumferential boundary of cell:

$$\xi_{n-1/2,m} = \ell_{n-1,m} \cos \theta_{n-1} - \ell_{n,m} \cos \theta_n \tag{3-3}$$

4. Length of circumferential boundary, ST:

$$ST_{n-1/2,m} = \sqrt{\xi^2_{n-1/2,m} + \eta^2_{n-1/2,m}} \tag{3-4}$$

5. Distance from x axis to centroid of cell, r:

$$r_{n-1/2,m-1/2} = \tfrac{1}{4}\left[[\ell_{n-1,m-1}+\ell_{n-1,m}]\sin \theta_{n-1} + [\ell_{n,m-1}+\ell_{n,m}]\sin \theta_n\right] \tag{3-5}$$

6. Area of cell, A:

$$A_{n-1/2,m-1/2} = \tfrac{1}{2}\left[\ell_{n-1,m-1}\ \ell_{n,m-1} - \ell_{n-1,m}\ \ell_{n,m}\right]\sin[\theta_n - \theta_{n-1}] \tag{3-6}$$

7. Angle between negative x axis and circumferential boundary, ϕ:

Four cases are possible for ϕ.

1. $0 \le \phi \le \frac{1}{2}\pi$ $\quad \eta \ge 0$ $\quad \xi \le 0$ $\quad \phi_{n-1/2,m} = \arcsin \dfrac{\eta}{ST_{n-1/2,m}}$ (3-7)

2. $\frac{1}{2}\pi \le \phi \le \pi$ $\quad \eta \ge 0$ $\quad \xi \ge 0$ $\quad \phi_{n-1/2,m} = \pi - \arcsin \dfrac{\eta}{ST_{n-1/2,m}}$ (3-8)

3. $\pi \le \phi \le \frac{3}{2}\pi$ $\quad \eta \le 0$ $\quad \xi \ge 0$ $\quad \phi_{n-1/2,m} = \pi - \arcsin \dfrac{\eta}{ST_{n-1/2,m}}$ (3-9)

4. $\frac{3}{2}\pi \le \phi \le 2\pi$ $\quad \eta \le 0$ $\quad \xi \le 0$ This is not possible in the first quadrant.

Fluid Properties on Radial Cell Boundaries

The Riemann model may be used on any cell boundary if the component of fluid velocity normal to the boundary is the only one

considered. In figure 9, the conditions at boundary (n,m-1/2) are found by considering it to be a diaphragm in a shock tube surrounded by fluid of pressure and density as they exist in the two adjacent cells, but fluid of velocity equal to the normal velocity in the two cells, $w_{n-1/2,m-1/2}$ and $w_{n+1/2,m-1/2}$. The fluid velocity component parallel to the boundary (denoted by y) is assumed to remain constant during the resolution of the discontinuity on the boundary. The components of fluid velocity are as follows.

$$w_{n-1/2,m-1/2} = u_{n-1/2,m-1/2} \sin \theta_n + v_{n-1/2,m-1/2} \cos \theta_n \tag{3-10}$$

$$w_{n+1/2,m-1/2} = u_{n+1/2,m-1/2} \sin \theta_n + v_{n+1/2,m-1/2} \cos \theta_n \tag{3-11}$$

$$y_{n-1/2,m-1/2} = -u_{n-1/2,m-1/2} \cos \theta_n + v_{n-1/2,m-1/2} \sin \theta_n \tag{3-12}$$

$$y_{n+1/2,m-1/2} = -u_{n+1/2,m-1/2} \cos \theta_n + v_{n+1/2,m-1/2} \sin \theta_n \tag{3-13}$$

For the radial boundaries of the grid around the sphere, the linear approximation to the solution of the Riemann problem may be used, since these boundaries are not influenced by the severe gradients associated with the bow shock wave. These equations were derived in detail in reference 9. The variable names are defined in figure 8 (except for a, the mass velocity of both positive running and negative running linear waves).

$$a = \left\{ \frac{\gamma}{4} \left[p_{n-1/2,m-1/2} + p_{n+1/2,m-1/2} \right] \left[\rho_{n-1/2,m-1/2} + \rho_{n+1/2,m-1/2} \right] \right\}^{\frac{1}{2}} \tag{3-14}$$

$$p_0 = \frac{1}{2} \left[p_{n-1/2,m-1/2} + p_{n+1/2,m-1/2} \right] + \frac{1}{2} a \left[w_{n-1/2,m-1/2} - w_{n+1/2,m-1/2} \right] \tag{3-15}$$

$$w_0 = \frac{1}{2} \left[w_{n-1/2,m-1/2} + w_{n+1/2,m-1/2} \right] + \frac{1}{2a} \left[p_{n-1/2,m-1/2} - p_{n+1/2,m-1/2} \right] \tag{3-16}$$

$$\rho^+ = \left[\frac{(\gamma+1)p_0 + (\gamma-1)p_{n+1/2,m-1/2}}{(\gamma-1)p_0 + (\gamma+1)p_{n+1/2,m-1/2}} \right] \rho_{n+1/2,m-1/2} \tag{3-17}$$

$$\rho^- = \left[\frac{(\gamma+1)p_0 + (\gamma-1)p_{n-1/2,m-1/2}}{(\gamma-1)p_0 + (\gamma+1)p_{n-1/2,m-1/2}} \right] \rho_{n-1/2,m-1/2} \tag{3-18}$$

$$\Delta^+_{n,m-1/2} = w_{n+1/2,m-1/2} + \frac{a}{\rho_{n+1/2,m-1/2}} \tag{3-19}$$

$$\Delta^-_{n,m-1/2} = w_{n-1/2,m-1/2} - \frac{a}{\rho_{n-1/2,m-1/2}} \tag{3-20}$$

Any one of four possible states may result from the resolution of the discontinuity at the radial boundary. Recall that the constant conditions behind the waves in the Riemann problem are denoted by capital letters, while lower case letters indicate average properties in the cell. One further distinction is required: the constant conditions on radial boundaries will be specified by adding a capital R to the name, for example PR for pressure on the radial boundary. By contrast, circumferential boundaries will be denoted by a capital T, as in PT. The four possible states are given in Table 1.

Table 1. The four possible states for a radial boundary.

$\Delta^+ > 0 \ , \ \Delta^- > 0$	$PR_{n,m-1/2} = p_{n-1/2,m-1/2}$ $RR_{n,m-1/2} = \rho_{n-1/2,m-1/2}$ $WR_{n,m-1/2} = w_{n-1/2,m-1/2}$ $UR_{n,m-1/2} = u_{n-1/2,m-1/2}$ $VR_{n,m-1/2} = v_{n-1/2,m-1/2}$
$\Delta^+ > 0 \ , \ \Delta^- < 0 \ , \ w_0 > 0$	$PR_{n,m-1/2} = p_{0_-}$ $RR_{n,m-1/2} = \rho$ $WR_{n,m-1/2} = w_0$ $UR_{n,m-1/2} = w_0 \sin \theta_n - y_{n-1/2,m-1/2} \cos \theta_n$ $VR_{n,m-1/2} = w_0 \cos \theta_n + y_{n-1/2,m-1/2} \sin \theta_n$
$\Delta^+ > 0 \ , \ \Delta^- < 0 \ , \ w_0 \leq 0$	$PR_{n,m-1/2} = p_{0_+}$ $RR_{n,m-1/2} = \rho$ $WR_{n,m-1/2} = w_0$ $UR_{n,m-1/2} = w_0 \sin \theta_n - y_{n+1/2,m-1/2} \cos \theta_n$ $VR_{n,m-1/2} = w_0 \cos \theta_n + y_{n+1/2,m-1/2} \sin \theta_n$
$\Delta^+ < 0 \ , \ \Delta^- < 0$	$PR_{n,m-1/2} = p_{n+1/2,m-1/2}$ $RR_{n,m-1/2} = \rho_{n+1/2,m-1/2}$ $WR_{n,m-1/2} = w_{n+1/2,m-1/2}$ $UR_{n,m-1/2} = u_{n+1/2,m-1/2}$ $VR_{n,m-1/2} = v_{n+1/2,m-1/2}$

The total energy of the fluid at the boundary is used in the flux terms of the conservation of energy equation. For a perfect gas, the following equation of state is used to compute that energy.

$$ER_{n,m-1/2} = \frac{1}{\gamma-1} \frac{PR_{n,m-1/2}}{RR_{n,m-1/2}} + \tfrac{1}{2}[UR^2_{n,m-1/2} + VR^2_{n,m-1/2}] \qquad (3\text{-}21)$$

Fluid Properties on Circumferential Cell Boundaries

Despite the fact that the circumferential boundaries are moving, the solution of the Riemann problem there is analogous to that

of the stationary radial boundary, with one exception, to be discussed later. The components of fluid velocity normal to the boundary (w) and parallel to the boundary (y) are given by the following equations.

$$w_{n-1/2,m-1/2} = -u_{n-1/2,m-1/2} \sin \phi_{n-1/2,m} - v_{n-1/2,m-1/2} \cos \phi_{n-1/2,m} \tag{3-22}$$

$$w_{n-1/2,m+1/2} = -u_{n-1/2,m+1/2} \sin \phi_{n-1/2,m} - v_{n-1/2,m+1/2} \cos \phi_{n-1/2,m} \tag{3-23}$$

$$y_{n-1/2,m-1/2} = -u_{n-1/2,m-1/2} \cos \phi_{n-1/2,m} + v_{n-1/2,m-1/2} \sin \phi_{n-1/2,m} \tag{3-24}$$

$$y_{n-1/2,m+1/2} = -u_{n-1/2,m+1/2} \cos \phi_{n-1/2,m} + v_{n-1/2,m+1/2} \sin \phi_{n-1/2,m} \tag{3-25}$$

The linear approximation to the solution of the Riemann problem may be used for the interior circumferential boundaries. The circumferential boundaries that coincide with the shock and those that coincide with the body surface will require the nonlinear equations, so these are treated separately. The conditions on the interior circumferential boundaries are presented here.

$$a = \left\{ \frac{\gamma}{4} \left[p_{n-1/2,m+1/2} + p_{n-1/2,m-1/2} \right] \left[\rho_{n-1/2,m+1/2} + \rho_{n-1/2,m-1/2} \right] \right\}^{\frac{1}{2}} \tag{3-26}$$

$$p_o = \frac{1}{2} \left[p_{n-1/2,m+1/2} + p_{n-1/2,m-1/2} \right] + \frac{1}{2} a \left[w_{n-1/2,m+1/2} - w_{n-1/2,m-1/2} \right] \tag{3-27}$$

$$w_o = \frac{1}{2} \left[w_{n-1/2,m+1/2} + w_{n-1/2,m-1/2} \right] + \frac{1}{2a} \left[p_{n-1/2,m+1/2} - p_{n-1/2,m-1/2} \right] \tag{3-28}$$

$$\rho^+ = \left[\frac{(\gamma+1)p_o + (\gamma-1)p_{n-1/2,m-1/2}}{(\gamma-1)p_o + (\gamma+1)p_{n-1/2,m-1/2}} \right] \rho_{n-1/2,m-1/2} \tag{3-29}$$

$$\rho^- = \left[\frac{(\gamma+1)p_o + (\gamma-1)p_{n-1/2,m+1/2}}{(\gamma-1)p_o + (\gamma+1)p_{n-1/2,m+1/2}} \right] \rho_{n-1/2,m+1/2} \tag{3-30}$$

$$D^+_{n-1/2,m} = w_{n-1/2,m-1/2} + \frac{a}{\rho_{n-1/2,m-1/2}} \tag{3-31}$$

$$D^-_{n-1/2,m} = w_{n-1/2,m+1/2} - \frac{a}{\rho_{n-1/2,m+1/2}} \tag{3-32}$$

The effect of a moving boundary on the Riemann problem can be seen in figure 8. The figure shows that a moving boundary is represented as a sloped line. Thus the fluid conditions at the boundary will depend on the boundary's velocity (or slope) q with respect to the velocities (or slopes) of the waves shown in the figure.

The effect of the moving boundary, then, is manifested in the conditions for the four possible states, as presented in Table 2.

Table 2. The four possible states for a circumferential boundary.

$D^+ < q$

$$
\begin{aligned}
PT_{n-1/2,m} &= p_{n-1/2,m-1/2} \\
RT_{n-1/2,m} &= \rho_{n-1/2,m-1/2} \\
WT_{n-1/2,m} &= w_{n-1/2,m-1/2} \\
UT_{n-1/2,m} &= u_{n-1/2,m-1/2} \\
VT_{n-1/2,m} &= v_{n-1/2,m-1/2}
\end{aligned}
$$

$w_0 < q \leq D^+$

$$
\begin{aligned}
PT_{n-1/2,m} &= p_{0_+} \\
RT_{n-1/2,m} &= \rho \\
WT_{n-1/2,m} &= w_0 \\
UT_{n-1/2,m} &= -w_0 \sin \phi_{n-1/2,m} - y_{n-1/2,m-1/2} \cos \phi_{n-1/2,m} \\
VT_{n-1/2,m} &= -w_0 \cos \phi_{n-1/2,m} + y_{n-1/2,m-1/2} \sin \phi_{n-1/2,m}
\end{aligned}
$$

$D^- \leq q \leq w_0$

$$
\begin{aligned}
PT_{n-1/2,m} &= p_{0_-} \\
RT_{n-1/2,m} &= \rho \\
WT_{n-1/2,m} &= w_0 \\
UT_{n-1/2,m} &= -w_0 \sin \phi_{n-1/2,m} - y_{n-1/2,m+1/2} \cos \phi_{n-1/2,m} \\
VT_{n-1/2,m} &= -w_0 \cos \phi_{n-1/2,m} + y_{n-1/2,m+1/2} \sin \phi_{n-1/2,m}
\end{aligned}
$$

$q < D^-$

$$
\begin{aligned}
PT_{n-1/2,m} &= p_{n-1/2,m+1/2} \\
RT_{n-1/2,m} &= \rho_{n-1/2,m+1/2} \\
WT_{n-1/2,m} &= w_{n-1/2,m+1/2} \\
UT_{n-1/2,m} &= u_{n-1/2,m+1/2} \\
VT_{n-1/2,m} &= v_{n-1/2,m+1/2}
\end{aligned}
$$

For a perfect gas, the following equation of state is used to compute the total energy of the fluid at the boundary.

$$ET_{n,m-1/2} = \frac{1}{\gamma-1} \frac{PT_{n-1/2,m}}{RT_{n-1/2,m}} + \tfrac{1}{2}[UT^2_{n-1/2,m} + VT^2_{n-1/2,m}] \qquad (3\text{-}33)$$

Boundary Conditions on the Shock Wave

The circumferential boundaries of the computational field are adjusted during computations so that the outer boundary (m = 0) coincides with the bow shock wave (figure 9). Solution of the Riemann problem there provides the boundary conditions for subsequent computations in the shock layer. The subscript ∞ will be used to denote properties of the incoming uniform flow. Fluid velocity normal to the shock (w) and parallel to the shock (y) are given below.

$$w_{n-1/2,1/2} = -u_{n-1/2,1/2} \sin \phi_{n-1/2,0} - v_{n-1/2,1/2} \cos \phi_{n-1/2,0} \quad (3\text{-}34)$$

$$w_{n-1/2,-1/2} = -u_{\infty} \sin \phi_{n-1/2,0} \quad (3\text{-}35)$$

$$y_{n-1/2,1/2} = -u_{n-1/2,1/2} \cos \phi_{n-1/2,0} + v_{n-1/2,1/2} \sin \phi_{n-1/2,0} \quad (3\text{-}36)$$

$$y_{n-1/2,-1/2} = -u_{\infty} \cos \phi_{n-1/2,0} \quad (3\text{-}37)$$

Because this boundary coincides with the bow shock wave, a large difference in properties exists between the two adjacent cells, so this Riemann problem will require the nonlinear equations, as follows. The derivation is detailed in reference 9.

$p_0 \geq p_{n-1/2,1/2}$ (Negative running compression wave):

$$a = \left\{ \left[\gamma p_{n-1/2,1/2} \rho_{n-1/2,1/2} \right] \left[1 - \frac{\gamma+1}{2\gamma} (1 - p_0/p_{n-1/2,1/2}) \right] \right\}^{\frac{1}{2}} \quad (3\text{-}38)$$

$p_0 < p_{n-1/2,1/2}$ (Negative running expansion wave):

$$a = \frac{\gamma-1}{2\gamma} \left[\gamma p_{n-1/2,1/2} \rho_{n-1/2,1/2} \right]^{\frac{1}{2}} \frac{1 - \left[p_0/p_{n-1/2,1/2} \right]}{1 - \left[p_0/p_{n-1/2,1/2} \right]^{(\gamma-1)/2\gamma}} \quad (3\text{-}39)$$

$p_0 \geq p_{\infty}$ (Positive running compression wave):

$$b = \left\{ \left[\gamma p_{\infty} \rho_{\infty} \right] \left[1 - \frac{\gamma+1}{2\gamma} (1 - p_0/p_{\infty}) \right] \right\}^{\frac{1}{2}} \quad (3\text{-}40)$$

$p_0 < p_{\infty}$ (Positive running expansion wave):

$$b = \frac{\gamma-1}{2\gamma} \left[\gamma p_{\infty} \rho_{\infty} \right]^{\frac{1}{2}} \frac{1 - \left[p_0/p_{\infty} \right]}{1 - \left[p_0/p_{\infty} \right]^{(\gamma-1)/2\gamma}} \quad (3\text{-}41)$$

$$p_0 = \frac{b p_{n-1/2,1/2} + a p_{\infty} + ab(w_{n-1/2,1/2} - w_{n-1/2,-1/2})}{a + b} \quad (3\text{-}42)$$

$$w_0 = \frac{a w_{n-1/2,1/2} + b w_{n-1/2,-1/2} + p_{n-1/2,1/2} - p_{\infty}}{a + b} \quad (3\text{-}43)$$

$$\rho^+ = \left[\frac{(\gamma+1)p_0 + (\gamma-1)p_\infty}{(\gamma-1)p_0 + (\gamma+1)p_\infty} \right] \rho_\infty \tag{3-44}$$

$$D^+_{n-1/2,0} = w_{n-1/2,-1/2} + \frac{b}{\rho_\infty} \tag{3-45}$$

Equations 3-38 through 3-42 comprise a nonlinear system of equations for the computation of the pressure on the boundary. These equations must be solved by iteration. A detailed study of the method that follows is given in reference 9. This method is similar to Godunov's (ref 11), and is an extension of the method used by Chorin (ref 25) and Sod (ref 14). Several textbooks were useful in deriving the technique, and these are given as references 26 - 28. The recommended iterating function is:

$$p_0^{i+1} = \frac{f(p_0^i)\Delta p_0^i - p_0^i \Delta f^i}{\Delta p_0^i - \Delta f^i} \tag{3-46}$$

where $f(p_0)$ is the right hand side of eq. 3-42. The following notation was used in eq. 3-46 to improve readability.

$$\Delta p_0^i = p_0^i - p_0^{i-1} \tag{3-47}$$

$$\Delta f^i = f(p_0^i) - f(p_0^{i-1}) \tag{3-48}$$

To begin the computations, p_0^0 and p_0^1 are required. These may be computed with the following equations.

$$p_0^0 = \frac{1}{2}\,(p_\infty + p_{n-1/2,1/2}) \tag{3-49}$$

$$p_0^1 = f(p_0^0) \tag{3-50}$$

Equation 3-49 is suggested by several authors as a good initial estimate. Equation 3-50 is simply the first revised estimate based on the standard (unmodified) iterating technique (eq. 3-42). Thus the first two iterates are the same as would be obtained in either a standard method (ie. one in which eq's. 3-38 through 3-42 are themselves used iteratively) or Chorin's method (ref 25). Reference 9, however, shows that the method presented here will guarantee convergence in all cases, and will converge faster than either the standard method or Chorin's method.

Van Leer (ref 29) notes that during the course of the iteration large negative values of $(u_\infty - u_{n-1/2,1/2})$ may lead to a negative value for p_0. Hence he suggests defining a minimum allowable value for p_0, say ϵ, which is the minimum meaningful pressure for the flowfield under study. If the next iteration also results in a negative pressure, he suggests stopping the iteration and setting $p_0 = \epsilon$.

$D^+_{n-1/2,0}$ in eq. 3-45 is the velocity of the Riemann wave that propagates into the free stream. The outer boundary of the computational field is made to move with this wave, so $q = D^+$ and the second state listed in Table 2 is applicable. The properties on the shock boundary, including the total energy of a perfect fluid, follow.

$$w_0 < q \le D^+$$

$$\begin{aligned} PT_{n-1/2,0} &= p_{0_+} \\ RT_{n-1/2,0} &= \rho \\ WT_{n-1/2,0} &= w_0 \\ UT_{n-1/2,0} &= -w_0 \sin \phi_{n-1/2,0} - y_{n-1/2,-1/2} \cos \phi_{n-1/2,0} \\ VT_{n-1/2,0} &= -w_0 \cos \phi_{n-1/2,0} + y_{n-1/2,-1/2} \sin \phi_{n-1/2,0} \end{aligned}$$

$$ET_{n-1/2,0} = \frac{1}{\gamma-1} \frac{PT_{n-1/2,0}}{RT_{n-1/2,0}} + \tfrac{1}{2}[UT^2_{n-1/2,0} + VT^2_{n-1/2,0}] \qquad (3\text{-}51)$$

To determine grid movement during the time step, nodal point velocity ($\Omega_{n,m}$) is found approximately from the boundary velocities ($D^+_{n-1/2,0}$) just determined. The nodal point velocities are used to compute the grid movement during the timestep. The new nodal point positions are then used to compute a consistent set of circumferential boundary velocities. The velocity of the boundary on the shock will differ slightly from the originally intended D^+, but will nonetheless vanish as the steady state shock position is approached. Furthermore, it will be consistent with the velocities of the inner circumferential boundaries during the unsteady calculations.

The nodal point velocity $\Omega_{n,0}$ is approximately proportional to the components in the direction of ray n of the velocities of the adjacent cell boundaries ($D^+_{n+1/2,0}$ and $D^+_{n-1/2,0}$), and approximately inversely proportional to the lengths of these boundaries ($ST_{n+1/2,0}$ and $ST_{n-1/2,0}$). The components in the direction of ray n of the velocities of the adjacent cell boundaries are in the square brackets in the following equation. The approximate proportions will yield the following nodal point velocity.

$$\Omega_{n,0} = \frac{\left[\dfrac{D^+_{n+1/2,0}}{\sin(\phi_{n+1/2,0} - \theta_n)}\right] ST_{n-1/2,0} + \left[\dfrac{D^+_{n-1/2,0}}{\sin(\phi_{n-1/2,0} - \theta_n)}\right] ST_{n+1/2,0}}{ST_{n+1/2,0} + ST_{n-1/2,0}} \qquad (3\text{-}52)$$

Special attention is required for the rays at the extreme ends of the computational grid: below the axis of symmetry (n = 0) and beyond the downstream boundary (n = N).

$$\Omega_{0,0} = \Omega_{1,0} \tag{3-53}$$

$$\Omega_{N,0} = \left[\frac{D^{+}_{N-1/2,0}}{\sin\ (\phi_{N-1/2,0}-\theta_{N})}\right] \tag{3-54}$$

Having determined all the $\Omega_{n,0}$, the new positions of the nodal points on the shock may now be computed. Recall from Chapter 2 that superscripted variables indicate conditions for the new timestep.

$$\ell^{n,0} = \ell_{n,0} + \Omega_{n,0}\tau \tag{3-55}$$

If M represents the number of cells in the radial direction (ie. M is the index for the boundary on the body), and the sphere radius is 1 (ie. all dimensions are normalized by the sphere radius), then the new positions of the interior nodes are given by the following equation.

$$\ell^{n,m} = \ell^{n,0} - \frac{m}{M}(\ell^{n,0}-1) \tag{3-56}$$

Having thus defined what the grid will be for the start of the next timestep, the boundary velocities for the present timestep may be calculated. The velocity of the circumferential boundary in a direction perpendicular to itself is computed as follows.

$$q_{n-1/2,m} = \frac{1}{2\tau}\left[(\ell^{n-1,m}-\ell_{n-1,m})\sin(\phi_{n-1/2,m}-\theta_{n-1})+(\ell^{n,m}-\ell_{n,m})\sin(\phi_{n-1/2,m}-\theta_{n})\right] \tag{3-57}$$

This formula is to be applied to the cell boundaries on the shock also, where it will yield a velocity only approximately equal to the velocity of the positive running Riemann wave, as previously noted.

Boundary Conditions on the Sphere

The sphere in figure 9 forms the inner boundary (m = M) of the computational field. Solution of the Riemann problem there provides the boundary condition for subsequent computations in the shock layer. Since the fluid velocity normal to the surface (w) must be zero at the surface, and the body does not transfer any heat to the fluid, the mass

and energy flux is zero. However, the body does exert a force on the fluid (the equal and opposite reaction to the fluid pressure on the body), so momentum is imparted to the fluid through this boundary. As a result, u,v,ρ and e need not be computed here, and p is the only fluid property required. This can be seen mathematically by first noting that this circumferential boundary is fixed, and by substituting q = w = 0 into the finite difference conservation equations previously derived.

Fluid velocity parallel to the body is not required for computation of the pressure in the Riemann problem at the boundary. Fluid velocity normal to the body (but in the center of the first cell) is given below.

$$w_{n-1/2,M-1/2} = -u_{n-1/2,M-1/2} \sin \phi_{n-1/2,M} - v_{n-1/2,M-1/2} \cos \phi_{n-1/2,M} \qquad (3\text{-}58)$$

Because of the large gradients in fluid properties that exist near the surface of a submerged body, the Riemann problem there will require the nonlinear equations. The momentum equation for the fluid crossing a positive running wave (expansion or compression) provides the starting point of the analysis (see ref 9 for the derivation).

$$b[w] - [p] = 0$$

Here the square brackets indicate that the jump conditions across the wave are to be used. The mass velocity of the wave (b) is computed by using the appropriate one of the two following equations.

$p_0 \geq p_{n-1/2,M-1/2}$ (Positive running compression wave):

$$b = \left\{ \left[\gamma p_{n-1/2,M-1/2} \, \rho_{n-1/2,M-1/2} \right] \left[1 - \frac{\gamma+1}{2\gamma} \left(1 - p_0 / p_{n-1/2,M-1/2} \right) \right] \right\}^{\frac{1}{2}} \qquad (3\text{-}59)$$

$p_0 < p_{n-1/2,M-1/2}$ (Positive running expansion wave):

$$b = \frac{\gamma-1}{2\gamma} \left[\gamma p_{n-1/2,M-1/2} \, \rho_{n-1/2,M-1/2} \right]^{\frac{1}{2}} \frac{1 - \left[p_0 / p_{n-1/2,M-1/2} \right]}{1 - \left[p_0 / p_{n-1/2,M-1/2} \right]^{(\gamma-1)/2\gamma}} \qquad (3\text{-}60)$$

For this problem the momentum equation is expanded in the following form.

$$b\left[w_{n-1/2,M-1/2} - w_0 \right] - \left[p_{n-1/2,M-1/2} - p_0 \right] = 0$$

As previously discussed, subscript 0 denotes conditions behind the wave, which also will be the conditions at the cell boundary on the body (n-1/2,M). Since the normal velocity there must be zero, $w_0 = 0$ and the momentum equation simplifies to the following.

$$p_0 = p_{n-1/2,M-1/2} - w_{n-1/2,M-1/2}\,b \qquad (3\text{-}61)$$

This system of equations (3-59 through 3-61) must be solved by iteration. The method used is the same as was used for the Riemann problem on the shock wave, with one addition. These equations are more sensitive to the starting guess, so a refinement of the iteration process was required. Normally the initial estimate p_0^0 is set equal to the pressure in the cell from the previous time step (ref 30). The second estimate, p_0^1, is obtained by substituting p_0^0 into the system of equations. The iteration process then continues with the same recursion formula as described previously (eq. 3-46), except of course eq. 3-61 is used for $f(p_0)$. In the unsteady startup of computations, a strong shock is immediately reflected from the body surface. This results in a pressure in the first cell that is much lower than the pressure at the surface. Thus the pressure in the first cell (from the previous time step) is a poor estimate with which to begin the iteration; it causes the first value computed by the recursion formula (p_0^2) to be negative. Succeeding calculations are not possible, since b becomes imaginary. In general, therefore, whenever p_0^{i+1} is negative, the iteration scheme is restarted with p_0^0 set equal to p_0^i, the most recent positive value for p_0.

Since only the pressure on the body surface is required in the conservation equations, the solution of the Riemann problem there involves only the following relationship.

$$PT_{n-1/2,M} = p_0$$

Boundary Conditions on the Axis

Originally, the axis of symmetry formed one boundary of each of the first row of cells in the computational grid. This approach has a basic flaw, and even after considerable effort did not produce results at the stagnation point of the body that were within about ten per cent of experimental data for Mach 4 flow. The flaw is that this geometry is inconsistent with the basic premise of the Godunov method: that conditions at the cell boundaries may be obtained by use of a one dimensional Riemann model. In an axisymmetric problem, this model considers the boundary to be a plane diaphragm, whose edge is seen in a drawing of the grid such as figure 9. But the boundary on the axis is not even a sharply curved plane; it is actually just a line. Further, although the mass and energy fluxes are zero on that line by symmetry, the pressure and v/r terms are not.

A grid configuration in which the first radial row of cells is centered on the axis of symmetry is better suited to the Godunov method. Although the radial boundaries for the first row of cells may be significantly curved, the assumption of plane waves is a much better approximation for this geometry than for the geometry discussed above. In addition, the statement of the boundary condition is greatly simplified. Also, shock orientation on the axis is automatically normal to the axis as a natural consequence of the grid and the boundary conditions imposed. In practice, the superiority of this grid was upheld and results at the stagnation point were greatly improved.

The mathematical statement of the boundary condition for a cell on the axis is quite simple, and results from the symmetry of the flow at points in the flowfield equally displaced from the axis.

$$
\begin{aligned}
PR_{0,m-1/2} &= PR_{1,m-1/2} \\
RR_{0,m-1/2} &= RR_{1,m-1/2} \\
WR_{0,m-1/2} &= WR_{1,m-1/2} \\
UR_{0,m-1/2} &= UR_{1,m-1/2} \\
VR_{0,m-1/2} &= -VR_{1,m-1/2}
\end{aligned}
$$

In addition to the boundary condition, an adjustment to the computational scheme was required in this region. Each of the conservation equations makes use of the ratio v/r. Approaching the stagnation region (the axis of symmetry) both v and r go to zero, but the ratio remains finite (ref 23). Computationally, the ratio cannot be evaluated in the row of cells on the axis if it is simply based on the value of v and r in the cell. Taylor and Lin discuss a similar problem on the axis and their treatment of it in reference 31. The method used here is based on a discussion of the problem found in reference 32.

The object of this section is to obtain an estimate of the ratio v/r for the cells on the axis. Since v approaches zero as r approaches zero, l'Hôpital's rule applies.

$$
\left[\frac{v}{r} \right]_{r \to 0} = \left[\frac{\partial v / \partial r}{\partial r / \partial r} \right]_{r \to 0} = \left[\frac{\partial v}{\partial r} \right]_{r \to 0}
$$

The velocity gradient near the axis of symmetry is assumed to be linear along any locus of points equidistant from the sphere's center. This is consistent with computations presented in reference 33. The technique consists of using the method of least squares to find the best linear fit to the computed data for v and r in the second and third cells (n=3/2,5/2). The velocity is constrained to be zero at the axis by requiring that the y intercept of the linear regression be zero. The slope of this line (m) is the approximation for the ratio v/r at the axis. The distance between the line and a plotted point

(v_i, r_i) is δ_i, as follows.

$$\delta_i = (v_i - m r_i)$$

In the least squares method the error ϵ is the governing parameter.

$$\epsilon = \Sigma \delta_i^2$$

The error ϵ is to be minimized with respect to the slope, m.

$$\frac{\partial \epsilon}{\partial m} = \frac{\partial}{\partial m} \sum (v_i - m r_i)^2 = 0$$

The derivative is moved inside the summation, the differentiation carried out, and the result rearranged to obtain the slope, m.

$$m = \frac{\Sigma r_i v_i}{\Sigma r_i^2}$$

This is the approximation for the velocity gradient to be used for the row of cells on the axis. In the notation of figure 9, it is written

$$\nabla_{1/2,m-1/2} = \frac{(rv)_{3/2,m-1/2} + (rv)_{5/2,m-1/2}}{r^2_{3/2,m-1/2} + r^2_{5/2,m-1/2}} , \qquad (3\text{-}62)$$

where ∇ stands for the velocity gradient, v/r.

One additional comment on this subject is appropriate. The grid originally used to solve the sphere problem (ie. where the first row of cells has the axis of symmetry forming one of the cell boundaries) would seem to be immune from the problem of evaluating v/r as $r \to 0$, since r is never zero in a finite grid of this type. In practice, however, a velocity gradient scheme similar to eq. 3-62 was required for the first row of cells. Without it, pressures in the first row of cells were in error by 4% (based on experimental data at Mach 4). Also, numerical oscillations about the erroneous value of pressure of about ±2% remained after 400 time steps. When v/r was computed by the above method for the first row of cells, the error was reduced to 2%, the oscillations vanished and the steady solution was reached in 200 time steps. Surprisingly, the greatest error in the original computations occurred in the second radial rows of cells, where the pressure and density were low by 20% or more. These errors were eliminated by the improved grid.

Downstream Boundary Conditions

Boundary conditions at the downstream boundary of the computational grid shown in figure 9 are the easiest to describe, since this boundary has been placed in a region of supersonic flow. This means that disturbances at this boundary cannot propagate upstream and disrupt the computational domain (ref 17). (A similar argument justifies use of the free stream conditions outside the shock.) This is a qualitative way of saying that the assumedly sonic waves arising from the Riemann problem at these cell boundaries will be swept downstream by the higher (ie. greater than sonic) velocity fluid. Thus the applicable state in Table 2 is the first one, in which both the positive and negative running waves have a positive velocity relative to the fixed coordinate system. The conditions at this boundary are given by the following equations.

$$\Delta^+ > 0 \ , \ \Delta^- > 0$$

$$\begin{aligned} PR_{N,m-1/2} &= p_{N-1/2,m-1/2} \\ RR_{N,m-1/2} &= \rho_{N-1/2,m-1/2} \\ WR_{N,m-1/2} &= w_{N-1/2,m-1/2} \\ UR_{N,m-1/2} &= u_{N-1/2,m-1/2} \\ VR_{N,m-1/2} &= v_{N-1/2,m-1/2} \end{aligned}$$

One can readily see that conditions downstream of this boundary play no part in the conditions at the boundary.

Computation of the Time Step

The basic requirement for stability of the one dimensional Godunov method is given in Godunov's two papers (ref 10,11) as

$$\tau < \frac{\Delta x}{W}$$

where τ is the length of the time step, Δx is the width of the cell, and W is the velocity of the Riemann wave normal to the boundary. Although he arrives at this conclusion by way of a mathematical analysis, the result is intuitively satisfying, in that it states that no Riemann wave shall be allowed to reach the far side of the cell, where it will interfere with the Riemann problem (and associated constant properties) used to determine the fluxes there.

The length of the time step cannot be computed explicitly, since the wave velocities and final cell dimensions are not known until the computations for the time step have been completed. To overcome this difficulty, one assumes that only a small change will occur in τ from one time step to the next. One then applies a safety factor to the τ computed in the present time step and uses this reduced time for the length of the next time step (for example, $\tau_{t+1} = 0.9\tau_t$).

Godunov discusses the stability of finite difference schemes in reference 34 and at great length in his text, The Theory of Difference Schemes (ref 35). He presents a stability analysis in reference 10 for the two dimensional case, the result of which is the following equation for the maximum time step.

$$\tau_{n-1/2,m-1/2} = \left[\frac{\tau_r \tau_\theta}{\tau_r + \tau_\theta}\right]_{n-1/2,m-1/2} \tag{3-63}$$

Here τ_r is the one dimensional time step for waves traveling in the radial direction, and τ_θ is the one dimensional time step for waves traveling in the circumferential direction. In this way τ is computed for each cell in the grid, and the minimum value is chosen as the time step. Equation 3-63 was used in the present work. In most cases numerical instability was avoided by a time step that was 90% of that computed by eq. 3-63. However a smaller time step was required in the unsteady start of computations to main- tain the stability of the computations. This was because a strong shock wave is reflected from the body when fluid motion begins. This wave can alter significantly the (average) properties in a cell as it passes through. This may cause the Riemann problem at each boundary, which is based on the assumed constant average properties from the previous time step, to be seriously in error. The solution to this dilemma is to reduce the length of the time step, so the reflected wave cannot significantly alter the properties in the cell before updated values are computed. Eventually the reflected wave coalesces with the shock wave, and normal size time steps may be resumed. To compute the Mach 24 case, a time step of 20% of eq. 3-63 was arbitrarily chosen for the entire computation. No attempt was made to determine if this factor could be increased.

To compute τ_θ, the two waves that travel into the cell from each of the two radial boundaries must be considered. The wave velocities are resolved into components along the circumferential boundaries, and the time required for each wave to reach each opposite node is computed. The least of these four times will be τ_θ.

The four waves that travel into cell (n-1/2,m-1/2) are shown in figure 11. Two considerations must be addressed before proceding. First, since the circumferential boundaries are moving and in general are not perpendicular to the radial boundaries, the nodes will have a slight velocity component in the direction of the circumferential boundary. This small velocity has been neglected. The second concerns the direction of travel of the Riemann waves. If $\Delta_{n-1,m-1/2}$ is less than zero, the wave travels in the negative direction; ie. the wave does not enter the (n-1/2,m-1/2) cell, and cannot affect computation of the minimum τ_θ there. It will instead enter the adjacent cell (n-3/2,m-1/2), but its presence there will not alter the computation of the minimum τ_θ there. This is because it is the positive running wave emanating from the boundary (n-1,m-1/2), which is by

definition that wave with the most positive velocity, although in this case it travels in the negative direction. Since the negative running wave is automatically considered for cell (n-3/2,m-1/2), it will result in a lower time than the positive running wave emanating from the boundary (n-1,m-1/2). In fact, this argument is true for any of the four waves in cell (n-1/2,m-1/2), resulting in the following general rule: Only those Riemann waves that actually enter the cell under study need to be considered in determining the time step.

The time required for the positive running radial wave (Δ^+ in figure 11) to reach the node at (n,m) is

$$\tau^+_{n-1/2,m} = \frac{ST_{n-1/2,m}\ \sin(\phi_{n-1/2,m} - \theta_{n-1})}{\Delta^+_{n-1,m-1/2}} \quad . \tag{3-64}$$

The time required for the positive running radial wave to reach the node at (n,m-1) is

$$\tau^+_{n-1/2,m-1} = \frac{ST_{n-1/2,m-1}\ \sin(\phi_{n-1/2,m-1} - \theta_{n-1})}{\Delta^+_{n-1,m-1/2}} \quad . \tag{3-65}$$

Angle limits for grids restricted to the fourth quadrant follow.

$$0 \le (\phi_{n-1/2,m} - \theta_{n-1}) \le \pi$$

$$0 \le (\phi_{n-1/2,m-1} - \theta_{n-1}) \le \pi$$

Also, $ST_{n-1/2,m}$ and $ST_{n-1/2,m-1}$ are positive, so both $\tau^+_{n-1/2,m}$ and $\tau^+_{n-1/2,m-1}$ will be negative if the wave velocity $\Delta^+_{n-1,m-1/2}$ is negative (ie. the wave doesn't enter the cell). Hence any negative τ may be disregarded.

The time required for the negative running radial wave (Δ^- in figure 11) to reach the node at (n-1,m) is

$$\tau^-_{n-1/2,m} = \frac{ST_{n-1/2,m}\ \sin(\phi_{n-1/2,m} - \theta_{n})}{-\Delta^-_{n,m-1/2}} \quad . \tag{3-66}$$

The time required for the negative running radial wave to reach the node at (n-1,m-1) is

$$\tau^-_{n-1/2,m-1} = \frac{ST_{n-1/2,m-1}\ \sin(\phi_{n-1/2,m-1} - \theta_{n})}{-\Delta^-_{n,m-1/2}} \quad . \tag{3-67}$$

The negative velocity in the last two equations is required to make τ positive for the case in which $\Delta^{-}_{n,m-1/2}$ is negative (ie. the wave enters the cell). As before, if either τ is negative, it may be disregarded.

The time based on the waves traveling in the θ direction, τ_θ, is the smallest non-negative value of the four times computed above. For simplicity, let

$$\tau_{\theta 1} = \text{MAX}\ (\epsilon, \tau^{+}_{n-1/2,m})$$

$$\tau_{\theta 2} = \text{MAX}\ (\epsilon, \tau^{+}_{n-1/2,m-1})$$

$$\tau_{\theta 3} = \text{MAX}\ (\epsilon, \tau^{-}_{n-1/2,m})$$

$$\tau_{\theta 4} = \text{MAX}\ (\epsilon, \tau^{-}_{n-1/2,m-1})$$

where ϵ is some suitably small positive time, say 0.1 μs. The minimum of these times is required for eq. 3-63.

$$\tau_\theta = \text{MIN}\ (\tau_{\theta 1}, \tau_{\theta 2}, \tau_{\theta 3}, \tau_{\theta 4}) \qquad (3\text{-}68)$$

The situation is more complicated for the waves emanating from the circumferential boundaries, since the nodes at the opposite side of the cell move along the ray due to the motion of the boundary there. The component of the Riemann wave velocity along the ray is computed as in the radial case, then the node velocity along the ray is subtracted. The balance of the procedure is identical to the radial case.

The time required for the positive running circumferential wave (D^+ in figure 11) to reach the node at (n,m-1) is

$$\tau^{+}_{n,m-1/2} = \frac{SR_{n,m-1/2}}{\dfrac{D^{+}_{n-1/2,m}}{\sin(\phi_{n-1/2,m} - \theta_n)} - \Omega_{n,m-1}} \qquad (3\text{-}69)$$

The time required for the positive running circumferential wave to reach the node at (n-1,m-1) is

$$\tau^{+}_{n-1,m-1/2} = \frac{SR_{n-1,m-1/2}}{\frac{D^{+}_{n-1/2,m}}{\sin(\phi_{n-1/2,m}-\theta_{n-1})} - \Omega_{n-1,m-1}} \quad . \tag{3-70}$$

The time required for the negative running circumferential wave (D^{-} in figure 11) to reach the node at (n,m) is

$$\tau^{-}_{n,m-1/2} = \frac{SR_{n,m-1/2}}{\frac{-D^{-}_{n-1/2,m-1}}{\sin(\phi_{n-1/2,m-1}-\theta_{n})} + \Omega_{n,m}} \quad . \tag{3-71}$$

The time required for the negative running circumferential wave to reach the node at (n-1,m) is

$$\tau^{-}_{n-1,m-1/2} = \frac{SR_{n-1,m-1/2}}{\frac{-D^{-}_{n-1/2,m-1}}{\sin(\phi_{n-1/2,m-1}-\theta_{n-1})} + \Omega_{n-1,m}} \quad . \tag{3-72}$$

Again, the negative velocity in the last two equations assures that the time will be positive for the case in which the wave enters the cell. Therefore, if any of the four times is found to be negative, it may be disregarded.

The time based on the waves traveling in the r direction, τ_r, is the smallest non-negative value of the four times computed above. Again, with ϵ some suitably small time, compute the following four times.

$$\tau_{r1} = \text{MAX}\ (\epsilon, \tau^{+}_{n,m-1/2})$$

$$\tau_{r2} = \text{MAX}\ (\epsilon, \tau^{+}_{n-1,m-1/2})$$

$$\tau_{r3} = \text{MAX}\ (\epsilon, \tau^{-}_{n,m-1/2})$$

$$\tau_{r4} = \text{MAX}\ (\epsilon, \tau^{-}_{n-1,m-1/2})$$

The minimum time is selected for use in eq. 3-63.

$$\tau_r = \text{MIN}\ (\tau_{r1}, \tau_{r2}, \tau_{r3}, \tau_{r4}) \qquad (3\text{-}73)$$

Upon substitution of eq's. 3-68 and 3-73 into eq. 3-63, computation of the time step based on conditions in cell $(n\text{-}1/2, m\text{-}1/2)$ is complete. This procedure is repeated for each cell in the grid, and the minimum value noted. Call this minimum time $\bar{\tau}$.

$$\bar{\tau} = \text{MIN}\ (\tau_{n\text{-}1/2, m\text{-}1/2}) \qquad (3\text{-}74)$$

Since this time step is to be used in the next series of finite difference computations, a simple safety factor (k) is applied.

$$\tau = k\bar{\tau} \qquad 0 < k < 1 \qquad (3\text{-}75)$$

The τ in eq. 3-75 is the timestep that appears in the earlier derivations (eg. finite difference equations) and that will be used in subsequent computations.

Experimental Data for the Hemisphere at Mach 4

A computer code was written using the equations presented above. The code was run on the CRAY X-MP/48 computer at the Ballistic Research Laboratory for the case of Mach 4 flow, with a grid of eight radial cells and twenty-five circumferential cells. The code predictions were compared to experimental data gathered by Belotserkovskii (ref 33). Data on spheres in uniform flow are plentiful, and numerous additional references for sphere data are given in reference 36, along with calculations at Mach 1.2.

The code predictions for the Mach 4 case are presented graphically in figures 12 through 16. The figures indicate elapsed time in seconds, which may be non-dimensionalized as follows.

$$\bar{t} = \frac{t}{d/u_\infty} \qquad (3\text{-}76)$$

Substituting t = .0107 s, d = 2.0 m, u_∞ = 1506 m/s yields a dimensionless time of $\bar{t}$ = 8.1, which means the flow has had time to travel over eight sphere diameters. Taylor and Masson (ref 37) indicate that the flow field around smooth bodies will achieve steady state after flowing two body lengths.

Figure 12 shows the shock position. Code predictions and experimental data generally agree. A slight variation between the two,

however, can be seen at the axis. At this point, the code predicts a standoff distance of 0.189 sphere radii while the data indicates 0.174, a difference of 8.6%. Experimental curves in Liepmann and Roshko (ref 38) indicate a standoff of 0.164, and Godunov (ref 10) indicates 0.180. The axis of symmetry is characteristically a difficult place to compute. The important area in this study, however, is the downstream boundary, since the conditions there will be input to the cylindrical portion of the problem. The code accurately predicts the Mach 4 shock position at this boundary, predicting within 1% of the experimental data.

Figure 13 shows the pressure distribution on the sphere. The code computes a pressure for each cell, which is assigned to the center of each cell. Therefore an extrapolation must be performed to obtain the value at the edge of the cell that borders the sphere. These extrapolations are compared to Belotserkovskii's data, and agreement between the two is apparent. A slight variation (2.3%) can be seen at the stagnation point. This, however, is an improvement over code predictions using the original grid (see discussion of grid above), which varied from experimental data by more than 5%. The code accurately predicts the Mach 4 pressure at the downstream boundary, predicting within 5% of the experimental data. Note that the low magnitude of the pressure at this point causes the relative error to seem high.

Extrapolation of the density predictions yields the density distribution along the surface of the sphere, as plotted in figure 14. The code predictions are compared to computations of Godunov (ref 10) and Belotserkovskii (ref 39). Belotserkovskii used the method of integral relations for his computations. The method was originated by Dorodnitsyn and adapted by Belotserkovskii for his particular problem. Hayes and Probstein (ref 40) discuss the method at some length. The code predictions for the present work are very close to those of Belotserkovskii. Godunov used the grid that begins at the axis of symmetry. When the same grid was used in the present work, results agreed more closely with Godunov's. But the improved grid not only removed the cusp (local minimum) in the density at the stagnation point, it provided marked improvements in the pressure at the stagnation point and in the shock position on the axis. Because of these improvements, the density predictions are considered to be more accurate than Godunov's original computations. The density at the downstream boundary is predicted within 5% of Belotserkovskii's computation.

Figures 15 and 16 plot the code's prediction of pressure and density extrapolated to the shock wave. The predictions are compared to theoretical calculation of the conditions behind a plane oblique wave. These calculations were based on the following equations from Anderson (ref 41). M represents Mach number, and subscript N indicates that the Mach number is for the component of flow normal to the oblique shock wave.

$$\frac{\rho_{n-1/2,0}}{\rho_\infty} = \frac{(\gamma+1)M_N^2}{(\gamma-1)M_N^2 + 2} \tag{3-77}$$

$$\frac{p_{n-1/2,0}}{p_\infty} = 1 + \frac{2\gamma}{\gamma+1}(M_N^2 - 1) \tag{3-78}$$

$$M_N = M_\infty \sin \phi_{n-1/2,0} \tag{3-79}$$

The theoretical calculation was based on the assumption that the boundary of the first cell behind the shock, (ie. the boundary that coincides with the shock), is approximately a plane at some angle to the free stream. This assumption is less accurate near the axis of symmetry than it is at the downstream boundary. This inaccuracy is manifested by a wider discrepancy between the two predictions near the axis. The two predictions also seem to parallel each other. This is due to the fact that the theoretical calculations used the shock angle that was predicted by the code. Figures 15 and 16 indicate that the code is giving reasonable results behind the shock wave, with results at the downstream boundary being within 3% of the theoretical (perfect gas) prediction.

Chapter 4

FLOW IN THE ANNULUS

Attention is now turned to the second part of the problem pictured in figure 6, flow in the annulus between the jet and the tube wall. The polar coordinate code described in Chapter 3 for solving the sphere problem is modified to suit this cylindrical problem. The discussion is again limited to the case of a perfect gas. Real gas modifications will be discussed in the next chapter. A listing of the code used to solve the cylinder problem, including real gas effects, is given in Appendix B.

The Grid

The grid for the cylindrical problem is shown in figure 17. It is a greatly simplified version of the spherical grid primarily owing to its being fixed. This means that all angles for the vertical grid lines (θ_n) are equal and constant, and all angles for the horizontal grid lines ($\phi_{n-1/2,m}$) are equal and constant. Furthermore, the cell area, radial position and boundary lengths are constant. The cells were chosen to be square, and the computational field was chosen to be divided into forty cells in the radial direction. Given these two choices, the computational field is completely defined by the following three independent variables.

d = body diameter (= 2 -normalized by the body radius)

D = tube diameter (also normalized by the body radius)

δ = downstream length of grid in multiples of (ie. normalized by) channel width

The length of the grid, δ, is also arbitrary, but the grid must be long enough to include all of the flow features of interest. Since the points of interest are the point at which the shock hits the wall and the point at which the reflected shock hits the body, $\delta = 5$ was found to be required for the Mach 4.00 problem. Thus the grid consists of 40 cells in the radial direction and 200 cells in the axial direction. For the Mach 20.45 case discussed in Chapter 6, $\delta = 10$ (400 axial cells) was required. All remaining grid attributes are easily derived from the above information. Positive directions for all computations were chosen in the positive axis directions: upward for the radial direction and to the right for the axial direction.

Fluid Properties on Radial Cell Boundaries

The equations for the solution of the Riemann problem on the radial cell boundaries are the same as those given in the sphere problem. The fluid velocities normal and parallel to the radial boundary under study are given by eq. 3-10 through 3-13. Use of the nonlinear equations must be completely general, since shock waves can appear anywhere in the flowfield. As a result of this generality, the first step is to determine the magnitude of the discontinuity at the boundary, then decide whether the nonlinear equations are required. The following test is performed for each radial boundary to make this determination.

$$\left| \frac{p_{n-1/2,m-1/2} - p_{n+1/2,m-1/2}}{p_{n-1/2,m-1/2}} \right| > \eta$$

$$\left| \frac{w_{n-1/2,m-1/2} - w_{n+1/2,m-1/2}}{w_{n-1/2,m-1/2}} \right| > \eta$$

The parameter η was set to 0.1 for the present work. If either inequality is satisfied, the nonlinear equations are used to compute a, b, p_0, and w_0. The iteration scheme is the same as that discussed above for the shock wave boundary of the sphere problem. The nonlinear equations are identical in form to equations 3-38 through 3-43, with the following subscript changes:

subscript $n-1/2,1/2$	is changed to subscript $n-1/2,m-1/2$
subscript ∞	is changed to subscript $n+1/2,m-1/2$

In the linear case, equations 3-14 through 3-16 are appropriate. Next, ρ^+ and ρ^- are computed from equations 3-17 and 3-18. For either case (linear or nonlinear), the velocities of the waves are computed from the following equations. Recall that for the linear case, a = b.

$$\Delta^+_{n,m-1/2} = w_{n+1/2,m-1/2} + \frac{b}{\rho_{n+1/2,m-1/2}}$$

$$\Delta^-_{n,m-1/2} = w_{n-1/2,m-1/2} - \frac{a}{\rho_{n-1/2,m-1/2}}$$

The four possible states for the boundary are those given by Table 1. The total energy of the fluid on the radial boundary is computed with eq. 3 21.

Fluid Properties on Circumferential Cell Boundaries

The equations for the solution of the Riemann problem on the circumferential cell boundaries are the same as those given for the sphere. The fluid velocities normal and parallel to the circumferential boundary under study are given by eq. 3-22 through 3-25. Again, use of the nonlinear equations must be completely general. The following inequalities are evaluated to determine if the nonlinear equations are required.

$$\left| \frac{p_{n-1/2,m-1/2} - p_{n-1/2,m+1/2}}{p_{n-1/2,m-1/2}} \right| > \eta$$

$$\left| \frac{w_{n-1/2,m-1/2} - w_{n-1/2,m+1/2}}{w_{n-1/2,m-1/2}} \right| > \eta$$

The parameter η was set to 0.1 for the present work. If either inequality is satisfied, the nonlinear equations are used to compute a, b, p_0, and w_0. The iteration scheme is the same as that discussed above for the shock wave boundary of the sphere problem. The nonlinear equations are identical in form to equations 3-38 through 3-43, with the following subscript changes:

subscript n-1/2,1/2	is changed to subscript n-1/2,m+1/2
subscript ∞	is changed to subscript n-1/2,m-1/2

In the linear case, equations 3-26 through 3-28 are appropriate. Next, ρ^+ and ρ^- are computed from equations 3-29 and 3-30. For either case (linear or nonlinear), the velocities of the waves are computed from the following equations. Recall that for the linear case, a = b.

$$D^+_{n-1/2,m} = w_{n-1/2,m-1/2} + \frac{b}{\rho_{n-1/2,m-1/2}}$$

$$D^-_{n-1/2,m} = w_{n-1/2,m+1/2} - \frac{a}{\rho_{n-1/2,m+1/2}}$$

The four possible states for the boundary are those given by Table 2. The total energy of the fluid on the circumferential boundary is computed with eq. 3-33.

The Conservation Equations

The conservation equations are the same as those presented in chapter 2: equations 2-19, 2-26, 2-27, and 2-32. In this cylindrical case the grid is fixed, so q = 0 in the conservation equations. Also,

since the computational field does not include the axis of symmetry, the difficulty of estimating the ratio v/r as r goes to zero was not encountered.

Boundary Conditions

The upstream boundary condition for the cylindrical grid of figure 17 is obtained from the results of the sphere computation for the cells $N-1/2,m$. A column of virtual cells is placed to the left of the first column of cells in the grid. The data from the sphere problem is adjusted to the new amount of cells and assigned to these virtual cells. The downstream boundary condition is the same as that used for the sphere grid; the flow is assumed to be supersonic there, and therefore will not affect computations upstream of the boundary. Results of the calculations show this assumption to be valid for incoming flow at Mach 20.45. Disturbances did not propagate into the computational domain for incoming speeds as low as Mach 4.00.

The boundary condition on the body was identical in all respects to the boundary condition on the sphere discussed above. Since this technique involves iteration, the less critical boundary at the wall of the tube was stated as a reflection surface, where the tangential component of fluid velocity, the density, the pressure, and the energy of the fluid are symmetrical across the boundary, and the normal component of fluid velocity is anti-symmetric.

The Time Step

Computation of the time step is quite similar to the procedure discussed for the sphere problem. The equations will be slightly simplified because the grid is fixed, but the basic technique and equations are the same.

Computational Results at Mach 4.00

Figure 18 summarizes the computational results for three geometries. The fluid velocity ahead of the sphere was Mach 4.00 in each case. The middle plot represents the case in which the bow shock hits the tube wall directly above the tangent point ($\theta = \pi/2$ in figure 9). The reflection point in the top plot is slightly ahead of the tangent point, since the tube diameter is slightly reduced. The tube diameter was increased in the bottom graph, and the reflection point is noticeably displaced from the tangent point. The pressure behind the reflected wave varies as a function of wall diameter, being 19 atm for $D/d = 1.689$, 17 atm for $D/d = 1.766$, and only 11 atm for $D/d = 1.958$. Notice also that in each case a Mach stem appears. This condition is forced by mass flow requirements; the oblique reflected wave cannot satisfy the mass flow requirement near the body.

Density contour plots for the same three cases are given in figure 19. The bottom plot (D/d = 1.958) can be compared to similar work by Woodward and Colella (ref 42). Although their problem differed somewhat (Mach 3, blunt nose, D/d = 5), the flow structure is very similar. For example, both plots show a similar reflection, the Mach stem, the expansion region near the tangent point, and qualitatively similar density patterns aft of the reflected wave.

Chapter 5

REAL GAS CONSIDERATIONS

In order to compute the flow conditions for a jet traveling at Mach 20, real gas effects must be accounted for in the code. The thermodynamic properties of high temperature equilibrium air are computed from approximate partition functions for the major components of air using a technique developed by Hansen (ref 43). The model assumes air to be a mixture of 20% oxygen and 80% nitrogen; other components are neglected. The model is designed to compute the properties of air for temperatures and pressures up to those of escape velocity (37,000 fps, or Mach 30 for sea level air), so dissociation and ionization of the molecules are included. The model computes ten properties of air: compressibility, energy, enthalpy, entropy, the specific heats, sonic velocity, viscosity, thermal conductivity, and Prandtl number.

Hansen begins with the standard definition of the partition function for the various components of air,

$$Q = \Sigma\, g_i \exp[-\epsilon_i/kT],$$

where g_i is the degeneracy of the i^{th} state of the gas, and ϵ_i its energy level. The partition functions for the various energy modes for diatomic molecules (translational, rotational, vibrational and electronic) are derived from this by the methods of statistical mechanics. The partition functions for monatomic particles (atoms, ions and electrons) are special cases of these. Hansen gives the constants required to compute the partition functions for seven types of particles found in high temperature air: N_2, O_2, N, O, N^+, O^+, and electrons. He uses these partition functions to obtain closed form approximate expressions for the properties of the air. In the process, he indicates that only four chemical reactions of the air need to be considered: the dissociation of molecular oxygen and molecular nitrogen, and the ionization of atomic oxygen and atomic nitrogen. The formation of nitric oxide (NO), while resulting in significant quantities, has little effect on the resulting properties of the air. All other reactions form very little product, and do not influence the properties of the air. Hansen then goes on to consider the transport properties of high temperature air (viscosity, thermal conductivity, Prandtl number). These are not of interest to the present work. The result of Hansen's work is a model that can be used to predict the properties of equilibrium air at temperatures from 500 K to 15,000 K and at pressures up to 100 atm.

Deschambault extended Hansen's method by including two additional levels of ionization, for a total of eleven different species involved in eight different reactions. This raises the limits of applicability of the model to 50,000 K for densities up to one-hundred times the density of sea level air. Deschambault wrote a FORTRAN program implementing this revised model (ref 44), and this code is included in the present work as a subroutine called REALGAS. Real gas considerations are required in two distinct places in the code: in conjunction with the conservation equations, and in conjunction with the solution of the Riemann problem. These two applications are handled in two distinctly different ways.

Conservation Equations

Knowledge of two thermodynamic properties is sufficient to completely define the thermodynamic state of a gas. Hansen's method uses pressure and temperature as the principal variables. This approach is inconvenient when coupled with the Godunov method, since density and energy are computed by the finite difference form of the conservation equations. As a result, an iterative procedure is required to find the pressure and temperature of the gas given the density and energy. This process is represented graphically in figure 20, which shows the range of pressures and temperatures expected for this problem. To obtain the initial iterate, Deschambault includes a subroutine with his code that computes the pressure and temperature based on the perfect gas equation of state. This approach was found to be ineffective for the present application, so the procedure was changed to one in which the cell's pressure and temperature from the previous time step is the first iterate. Iteration is begun with these values, and continues until the proper values for density and energy are reached.

The REALGAS subroutine is called from the main program after the finite difference form of the conservation equations have been evaluated, and the density, velocity, and total energy of the gas determined. The subroutine is entered with the density and internal energy (total energy less the kinetic energy) from the present time step, and the pressure and temperature from the previous time step. The subroutine conducts its iterative search for the proper pressure and temperature, finally returning the pressure, temperature, and the sonic velocity of the gas in the cell.

Riemann Problem

The iteration in the REALGAS subroutine presents a considerable complication for the Godunov method when computing the Riemann problem for a strong discontinuity. As described previously, iteration is required to compute this nonlinear case. If this iteration is coupled with the REALGAS iteration, computation time would be enormous. Colella and Glaz (ref 45) devised a procedure that eliminates the

double iteration in the Riemann problem by computing the pressure and velocity at the boundary (ie. behind the waves), p_0 and w_0, without precise knowledge of real gas conditions there. Rather they are computed with approximate information based on real gas conditions in the adjacent cells (ie. ahead of the waves). The Riemann iteration remains, but is now accompanied by noniterative algebraic equations, as described below.

Colella and Glaz begin by defining an "isentropic Γ",

$$\Gamma = \frac{c^2 \rho}{p} \tag{5-1}$$

where c is the speed of sound. They note another dimensionless quantity γ,

$$\gamma = \frac{p}{\rho \epsilon} + 1 \tag{5-2}$$

where ϵ is the internal energy of the gas. For a perfect gas, γ is the ratio of specific heats, and $\gamma = \Gamma$. For a real gas, the two variables are intimately involved in determining the thermodynamic properties. All fluid properties in eqs. 5-1 and 5-2 are known for each cell from the computations of the previous time step: ρ and ϵ from the conservation equations; p and c from subroutine REALGAS. Consequently, $\gamma_{n-1/2,m-1/2}$ and $\Gamma_{n-1/2,m-1/2}$ are computed from eqs. 5-1 and 5-2 using these cell properties.

In the following analysis, the equations for the radial boundaries will be given. Equations for the circumferential boundaries may be obtained by the following subscript changes.

change	$n-1/2,m-1/2$	to	$n-1/2,m+1/2$
change	$n+1/2,m-1/2$	to	$n-1/2,m-1/2$
change	$n,m-1/2$	to	$n-1/2,m$

An important step in the technique advanced by Colella and Glaz is approximating the values of γ and Γ for the boundary under study by averaging the values in the adjacent cells (computed during the previous time step). For example, for a radial boundary the averages are as follows.

$$\bar{\Gamma}_{n,m-1/2} = \frac{1}{2}\left[\Gamma_{n-1/2,m-1/2} + \Gamma_{n+1/2,m-1/2}\right] \tag{5-3}$$

$$\bar{\gamma}_{n,m-1/2} = \frac{1}{2}\left[\gamma_{n-1/2,m-1/2} + \gamma_{n+1/2,m-1/2}\right] \tag{5-4}$$

In the nonlinear Riemann problem, the iteration for p_0 is begun by

choosing an initial iterate for p_0. More will be said about this choice later. p_0, $\bar{\gamma}$, and $\bar{\Gamma}$ are then used in the following equations to compute new constants for the fluid behind the negative and positive running waves, respectively.

$$\hat{\gamma}_- = \gamma_{n-1/2,m-1/2} + \left[1 - \frac{\bar{\gamma}_{n,m-1/2}}{\bar{\Gamma}_{n,m-1/2}}\right](\bar{\gamma}_{n,m-1/2}-1)\left[\frac{p_0 - p_{n-1/2,m-1/2}}{\frac{1}{2}(p_0+p_{n-1/2,m-1/2})}\right] \tag{5-5}$$

$$\hat{\gamma}_+ = \gamma_{n+1/2,m-1/2} + \left[1 - \frac{\bar{\gamma}_{n,m-1/2}}{\bar{\Gamma}_{n,m-1/2}}\right](\bar{\gamma}_{n,m-1/2}-1)\left[\frac{p_0 - p_{n+1/2,m-1/2}}{\frac{1}{2}(p_0+p_{n+1/2,m-1/2})}\right] \tag{5-6}$$

Physically meaningful limits (minimum and maximum values) for $\hat{\gamma}$ are chosen for the problem under study and the computed $\hat{\gamma}$'s are checked and adjusted if necessary to assure conformity with the limits.

The next step in the procedure is to compute the mass velocities from the following equations.

$$a^2 = \frac{[p_0 - p_{n-1/2,m-1/2}][p_0 + \frac{1}{2}(\hat{\gamma}_- - 1)(p_0 + p_{n-1/2,m-1/2})]}{\frac{p_0}{\rho_{n-1/2,m-1/2}} - \left[\frac{\hat{\gamma}_- - 1}{\gamma_{n-1/2,m-1/2} - 1}\right]\frac{p_{n-1/2,m-1/2}}{\rho_{n-1/2,m-1/2}}} \tag{5-7}$$

$$b^2 = \frac{[p_0 - p_{n+1/2,m-1/2}][p_0 + \frac{1}{2}(\hat{\gamma}_+ - 1)(p_0 + p_{n+1/2,m-1/2})]}{\frac{p_0}{\rho_{n+1/2,m-1/2}} - \left[\frac{\hat{\gamma}_+ - 1}{\gamma_{n+1/2,m-1/2} - 1}\right]\frac{p_{n+1/2,m-1/2}}{\rho_{n+1/2,m-1/2}}} \tag{5-8}$$

In taking the square root of these expressions, the absolute value of the right hand side is to be used. The mass velocities are then used in eq. 3-46 to compute the next iteration of p_0. The procedure is repeated until convergence in p_0 is reached. Notice that no iteration due to the REALGAS subroutine is required for the Riemann problem.

At the beginning of each Riemann iteration, the following test is performed.

$$\left| \frac{p_0 - p_{n-1/2,m-1/2}}{p_{n-1/2,m-1/2}} \right| \leq \lambda \tag{5-9}$$

where λ is a constant suitable for distinguishing between the linear and the nonlinear case, say 0.1. If the test is true, the linear approximation is valid and the following equations are used to compute the mass velocity of the negative running and positive running waves respectively.

$$a = \sqrt{\Gamma_{n-1/2,m-1/2}\ p_{n-1/2,m-1/2}\ \rho_{n-1/2,m-1/2}} \tag{5-10}$$

$$b = \sqrt{\Gamma_{n+1/2,m-1/2}\ p_{n+1/2,m-1/2}\ \rho_{n+1/2,m-1/2}} \tag{5-11}$$

The approximation was carried one step further in the present work by replacing eqs. 5-10 and 5-11 with the following.

$$a = b = \left[\bar{\Gamma}\ \bar{p}\ \bar{\rho}\right]^{1/2} \tag{5-12}$$

Here $\bar{\Gamma}$ is given by eq. 5-3, and $\bar{p}$ and $\bar{\rho}$ are the following.

$$\bar{p}_{n,m-1/2} = \frac{1}{2}\left[p_{n-1/2,m-1/2} + p_{n+1/2,m-1/2}\right] \tag{5-13}$$

$$\bar{\rho}_{n,m-1/2} = \frac{1}{2}\left[\rho_{n-1/2,m-1/2} + \rho_{n+1/2,m-1/2}\right] \tag{5-14}$$

In the linear case, then, eq. 5-12 replaces eqs. 5-7 and 5-8, and the resulting Riemann computation is not iterative.

The following estimate is used to begin the Riemann iteration.

$$p_0 = \tfrac{1}{2}(p_{n-1/2,m-1/2} + p_{n+1/2,m-1/2}) \tag{5-15}$$

The mass velocity as computed by eq. 5-7 will be zero if

$$p_0 = p_{n-1/2,m-1/2}$$

which results quite frequently from eq. 5-15, for example in the beginning of computations when all cells in the flow field are set to the same initial condition. A similar situation exists for eq. 5-8. These possibilities are avoided by application of the linear check (eq. 5-9) in the manner described above, since eq. 5-12 will then be used.

Density and Energy in the Riemann Problem

Computing the density and internal energy for a real gas in the Riemann problem requires special consideration. The following equations are general; they may be used for expansion or compression waves, and for positive or negative running waves. To emphasize this

generality, they will be written with the following general notation:

subscript a denotes conditions ahead of the wave
subscript b denotes conditions behind the wave.

Colella and Glaz give the following equation for the density behind a shock wave in the Riemann problem.

$$\rho_b = \frac{1}{\frac{1}{\rho_a} - \frac{p_0 - p_a}{\omega^2}} \tag{5-16}$$

where ω is the mass velocity of the shock wave. The same equation is approximately true in the case of a rarefaction wave. The following derivation will show this approximation to be consistent with the first order level of approximation of the overall Godunov scheme. The isentropic law can be written as follows.

$$\frac{d}{dp}\left(\frac{1}{\rho}\right) = -\frac{1}{\omega^2} \tag{5-17}$$

Equation 5-17 is integrated across the rarefaction in order to relate conditions behind the wave to those ahead.

$$\frac{1}{\rho_b} - \frac{1}{\rho_a} = -\frac{1}{\omega^2}(p_b - p_a) \tag{5-18}$$

The mass velocity ω was assumed to be constant over the entire expansion wave. This is approximately true for a short time after the wave's formation. This assumption is implied in Godunov's technique, and has been shown to be valid in the previous ideal gas studies. Equation 5-18 is rearranged to obtain the density behind the rarefaction wave.

$$\rho_b = \frac{1}{\frac{1}{\rho_a} - \frac{p_0 - p_a}{\omega^2}} \tag{5-19}$$

This is the same as eq. 5-16 for the density behind the shock wave.

To find the total energy of the gas behind the wave, another basic assumption is made: The flow of gas through the wave (shock or rarefaction) is an adiabatic process. Therefore total enthalpy is preserved.

$$H_b = H_a$$

$$E_b + \frac{P_0}{\rho_b} = E_a + \frac{P_a}{\rho_a}$$

This equation is solved for E_b and equation 5-16 is substituted with the following result.

$$E_b = E_a + \left[\frac{1}{\rho_a} - \frac{P_0}{\omega^2} \right] (p_a - p_0) \qquad (5\text{-}20)$$

Thus, after the Riemann problem has been solved (either iteratively or non-iteratively) for p_0 and w_0, eq's. 5-16 and 5-20 are used to find the density and energy behind the Riemann waves. Thus the fluid properties (velocity, density, pressure and total energy) are all known at the cell boundary under study. The advantage of this method is worth reiterating: these properties have been found entirely from cell conditions known from the previous time step; that is REALGAS iterations are not required in this procedure. The properties thus computed are then used in the conservation equations. Note that the conservation of energy equation requires the total energy of the fluid, as given by eq. 5-20.

Implementation in the Riemann Problem

In the case of the bow shock wave for the sphere, the cell boundary under study moves with the positive running wave (of mass velocity b), so $\omega = b$ in eqs. 5-16 and 5-20. The conditions ahead of the wave are those of the free stream.

For cell boundaries on the surface of the sphere, the density and energy behind the wave are not required, since there is no mass or energy flux at this surface.

For radial boundaries in either the sphere or the annulus problem, the density and energy behind the positive running wave are obtained by making the following substitutions in eqs. 5-16 and 5-20.

$\omega = b$
subscript a = subscript $n+1/2,m-1/2$

For the negative running wave, the substitutions are the following.

$\omega = a$
subscript a = subscript $n-1/2,m-1/2$

For circumferential boundaries, the density and energy behind

the positive running wave are obtained from eqs. 5-16 and 5-20 by making the following substitutions.

ω = b
subscript a = subscript n-1/2,m-1/2

For the negative running wave, the substitutions are the following.

ω = a
subscript a = subscript n-1/2,m+1/2

Chapter 6

EXPERIMENTAL AND COMPUTATIONAL RESULTS

A series of exploratory experiments has been conducted in which an explosively formed shaped charge jet was directed along the axis of a tube which contained a fast response pressure transducer mounted in the wall. The pressure on the wall was monitored as the jet's bow shock swept past the transducer. This was an extremely difficult experiment to conduct, requiring an orderly and delicate acquisition of data from a disorderly and violent event.

Test Hardware and Instrumentation

Figure 21 is a schematic of the test setup. The shaped charge warhead is positioned on an adjustable cradle behind a six inch thick armor plate. The spike of the warhead extends into a three inch diameter hole in the plate. An alignment device is assembled to the spike. The tube through which the jet is to pass is laid on an adjustable cradle and positioned on the axis of the warhead with the help of the alignment device. The pressure transducer has been previously assembled to the thick wall tube in the manner shown in the detail in figure 21. The exposed face of the transducer is insulated from thermal shock by a layer of electrical tape and a coating of silicone grease. These do not affect the pressure measurement appreciably. Behind the tube is a film cassette, which will capture an x-ray image of the dynamic process.

The hardware setup is shown in figure 22. This photograph shows the tube on its cradle, the film cassette behind it, and the six inch thick armor plate that isolates the warhead. The x-ray heads (sources) are located out of view to the right of this photograph.

Figure 23 is a close up view of the tube, showing the alignment device, cradle and transducer. The tube is 152 mm (6 in) long, with the transducer mounted at the midpoint. The inside diameter of the tube is 19 mm (0.75 in). The tube begins at 3 cone diameters from the base of the liner (cone). Since the jet tip is 7.6 mm (0.30 inch) in diameter, the tube is 20 jet diameters long with a diameter of 2.5 jet diameters. This length insures that the tip of the jet will be within the tube when the shock passes the transducer for shock angles as low as 5°, although ideally there is no need to satisfy such a requirement. The tube length had to be kept as short as possible from a practical viewpoint, due to the difficulty of aligning it with the axis of the warhead so the jet would not hit the wall.

The actual hardware is shown in figure 24. The warhead is at the left, with the spike next to it. The tube is third from the left, with a threaded adapter, pressure transducer, and another threaded adapter in front of it. The alignment device is at the right.

Figure 25 shows an overall view of the test area from behind the warhead enclosure. The warhead itself can be seen on the test stand inside the enclosure. The white building at the left houses the x-ray heads and pulsers.

The x-ray heads are the devices that emit the bursts of x-ray radiation; they are shown in figure 26. Three heads are mounted at different elevations, but all are focused at the same point on the "shot line", the imaginary line along which the jet will travel. Each head will emit a 10 nanosecond burst of x-ray radiation which reduces blurring of the jet image on the film to a negligible amount. The timing of the burst from each head can be set to within a microsecond. Note that the jet used in these tests travels 7.69 mm/μs.

The large cables attached to the x-ray heads in figure 26 are coming from the pulsers shown in figure 27 (only two are shown). These pulsers are essentially large capacitors that are charged to 27 kvolts prior to the test. This electrical energy is dumped to the head at the proper instant, causing it to emit a burst of x-rays.

The test instrumentation is shown schematically in figure 28. The left side of the figure shows the pressure transducer, its power supply, and the oscilloscopes used to record the transducer's signal. The oscilloscopes are triggered by a delay generator. The timing of the trigger signal is monitored by an electronic counter.

The pressure transducers were model 113A23, manufactured by PCB Piezotronics Inc. of Depew, NY. These transducers are designed to respond accurately to extremely fast pressure pulses, ie. rise times as little as 1 μs/volt, and are quite linear over their 5 volt (680 atm or 10,000 psi) range of operation. The transducer contains a compression mode quartz element with a matching accelerometer to reduce the effects of vibration and resonance. The transducer is connected to a PCB model 483A02 power supply. This powers the transducer and couples it to the oscilloscope(s). In this configuration, the transducer signal is almost independent of cable length and motion. In these tests, the cable length was about 250 feet.

The right side of figure 28 shows the x-ray instrumentation and warhead firing circuitry. A power supply generates the energy required to initiate the detonator/warhead. Delivery of this signal to the detonator initiates all the instrumentation timing sequences (four counters and four delay generators). The warhead requires about 30 μs to form the jet, and the jet takes about 47 μs to travel to the pressure transducer, so the first x-ray flash was set for 77 μs. This was done on channel 2 (the middle head in figure 26) since this is the only head with a view of the transducer area. Consequently, the first

image on the film is the center image. In order to begin recording the pressure transducer output prior to passage of the jet tip, the delay generator on channel 4 is set for 50 μs. Channel 3 is set for a delay of 161 μs to show the jet just prior to the tip passing the end of the film cassette. Channel 2 is set for a convenient time (131 μs) between the first and third flashes, to provide a means for observing the time dependent behavior of the jet. The counters for channels 1, 2, and 3 receive their stop signals from the pulsers, thus confirming the timing of the x-ray burst. The counter for channel 4 receives its stop signal from the output of the delay generator.

Figure 29 is a photograph of the instrumentation. The cart at the left holds the transducer power supply (top), the analog oscilloscope, and the digital recording oscilloscope (bottom). The digital recording oscilloscope (Nicolet) was used in addition to the analog oscilloscope on tests 14 and 15. The Nicolet is capable of recording and storing a total of 2000 data points, at a sampling rate of up to 20 points per microsecond. The Nicolet holds the trace on the screen following the test, and then can record the information on a $5\frac{1}{4}$ inch diskette for later analysis. The Nicolet also contains controls that allow the user to measure precisely the time and voltage level of each digital point, and to expand or compress any section of the trace for visual emphasis.

To the right of the cart are three x-ray consoles. The console farthest away was not used for this test. The middle console houses the four electronic counters (bottom two rows), and the detonator firing circuit power supply (directly above the counters). The near console contains the power supply used to charge the pulsers (top), and the four delay generators below. At the bottom of this console are valves used to purge the air from inside the pulsers and fill them with dry nitrogen, to enhance the system's ability to withstand high voltages without arcing.

X-ray Data

The principle motivation for this study is to try to understand the effect observed by several independent researchers, in which a shaped charge jet is perturbed while traveling through a cylindrical passage, for example the hole in a guidance package, even though the jet never touches the walls of the passage. This effect was observed during this study as well, and figure 30 is the best example of the effect. Notice the upward pitch of the lead particle, three areas of severe perturbation, and the poor quality of the jet between these areas. The rear portion of the jet is undisturbed. These images were taken at the times discussed above. The jet did not touch the tube wall, but is about 2mm off center. The entire length of the tube and the image of the jet within the tube are visible in the center image of the original x-ray negative, but not visible in prints of the original negatives.

Useable x-ray data was obtained on four tests. These tests were labelled 11, 13, 14, and 15, and are shown in figures 30, 31, 32, and 33, respectively. A pressure trace was obtained in the last three tests only. The lead particle on all four tests is pitched upward and the jets are all perturbed, although not to the degree of the jet from test 11 (figure 30). A serious perturbation is evident in the late portion of the jet in figure 33, but this is due to a grazing impact by this portion of the jet with the end of the tube. The delay generators were set in the wrong sequence in test 13 (figure 31), so the short time is in the bottom image. The measurements taken from the four x-ray images are summarized in Table 3.

Table 3. Summary of Measurements taken from the X-Ray Images.

test	figure	tip vel	tip diameter
		km/s	d,mm
11	30	7.57	8.1
13	31	7.73	9.7
14	32	7.66	8.1
15	33	7.71	7.6

Three studies of the x-ray data follow: shock length, shock angle, and perturbed length of jet.

Shock Length

The geometry of the shock wave is quantified by the shock length. This is defined as the distance between the tip of the jet and the transducer location when the peak of the initial pressure pulse is sensed by the transducer, measured along the axis of the jet. Image (x-ray) data from test number 13 is not useful in computing the shock length. The delay generators were set in the wrong sequence on this test, resulting in the view of the jet in the tube being obscured by part of the test apparatus (the transducer region is visible only in the center image on the film).

The time of the first x-ray flash on each test was inadvertently set for the same time that the pressure pulse was seen by the transducer (77 μs), so the distance between the tip and the shock reflection point on the tube wall can be measured directly on the film. Of course it could have been computed knowing the jet velocity if the flash did not coincide in time with the passing of the shock wave by the transducer. This distance was 24.7 mm for test 14 and 25.2 mm for test 15.

The ratio of tube diameter to jet diameter (D/d) is required for input to the cylindrical code in order to compute the flow field. Ideally, the ratio is 2.3; the tube diameter (19mm) divided by the

average jet diameter (8.4mm). In the experiment, however, the jet was slightly off center in the tube, and the effective diameter ratio varied from this figure. The x-ray images were analysed as follows to determine the experimental ratio. First the diameter of the tip of the jet was measured directly. Then the distance from the jet centerline to the inside of the tube wall (where the transducer was mounted) was measured. The inside tube radius was considered to be equivalent to this second measurement, thus accounting for the possibility that the jet may be off center in the tube and actually traveling closer to or farther from the wall than a simple ratio of the part's diameters would indicate. Division of these two measurements yields the effective diameter ratio. The derived dimensions for the four tests are detailed in Table 4. Test 11 data is not included in the following evaluation since its geometry (D/d) is distinctly different from that of tests 14 and 15. The average effective ratio for tests 14 and 15 is D/d = 2.90.

Table 4. Parameters Computed from the X-Ray Measurements.

test	actual tip diameter d,(mm)	effective tube diameter D,(mm)	effective D/d	derived shock length l,(mm)
11	8.1	11.6	1.43	9.0
13	9.7	16.3	1.68	?
14	8.1	23.9	2.93	24.7
15	7.6	21.8	2.87	25.2

The shock length predicted by the code was obtained as follows. The average jet tip velocity of 7.69 km/s was input to the real gas sphere code, with the result as given in figures 34 and 35. Details of the computation are given at the end of this chapter. The properties at the sphere's downstream boundary, along with the diameter ratio (D/d = 2.90), were then input to the real gas axisymmetric code. This result is shown in figure 36.

The computational results used to plot figure 36 were examined to determine that the peak pressure on the wall occurs at axial cell number 125 (n = 125). The length of the computational field is 9.5 jet diameters (400 cells), so reflection occurs at 2.95 diameters aft of the tangent point, or 3.45 diameters from the tip of the jet. For a jet diameter of 7.8 mm, this corresponds to a distance of 26.9 mm, which is within 8% of the experimental value.

Shock Angle

The shock angle at the wall can not be explicitly determined from the x-ray images since the shock is not visible in the films. However, this angle can be inferred by a combination of experimental and computational facts, as follows.

1. A scaled layout is made showing the jet with a hemispherical tip within the tube according to the dimensions determined from the x-rays.

2. The point of shock reflection from the wall (relative to the tip) is located and the shock sketched in using the following criteria.

3a. The shock stand off at the stagnation point is about .035d (figure 34), and the shape near the axis is the same as the blunt body, spherical.

3b. The angle of the shock and its distance from the body above the tangent point on the body (θ = 90° in the sphere grid) are 28° and approximately .375 d respectively (figure 34).

3c. Curvature of the shock is significant even aft of the tangent point (figure 36).

Notice that although 1 and 2 are based on experimental data, 3a, 3b, and 3c are based on code predictions. When a smooth curve was drawn in accordance with these steps, the shock angle at the wall was found to be 12.2°. The computed angle was found to be 12.8° (figure 36). This is a very coarse comparison, but it is useful for providing insight into the problem. Using the shock length as discussed above is a more precise comparison of experiment and code.

Length of Perturbed Jet

One more analysis of the x-ray data was made: determining the length of jet perturbed by the tube. This was done by measuring the perturbed length in the second and third images, and extrapolating this length back to the point in time when the jet tip is at the exit of the tube. This can be done because the jet possesses a constant (in time) velocity gradient along its length which causes the jet to stretch. In fact, this stretching of the jet causes the eventual break up of the continuous jet into the particles seen in later images. If x is the distance between the tip particle and the last perturbed particle, and the subscripts 77, 131, 161 refer to the time (in microseconds) of the image in which the measurement is made, then the proportionality is written as follows.

$$\frac{x_{161} - x_{131}}{t_{161} - t_{131}} = \frac{x_{131} - x_{77}}{t_{131} - t_{77}}$$

Substitute t_{77} = 77 μs, t_{131} = 131 μs, and t_{161} = 161 μs, and rearrange.

$$x_{77} = x_{131} - \frac{54}{30}\,(x_{161} - x_{131})$$

Measurements of the perturbed areas in the two later views were possible for all four shots (figures 30 through 33). When these measurements were substituted into the above equation, the results were 157 mm (6.2 inches), 142 mm (5.6 inches), 143 mm (5.6 inches), and 156 mm (6.2 inches) respectively, for an average of 150 mm (5.9 inches). This is interesting because it is quite close to the length of the tube (152 mm, or 6 inches). Apparently the perturbing of the jet ceases at about the time that the jet tip emerges from the confines of the tube. This may be coincidence, as similar perturbations (precise length unknown) have been reported by other researchers when using much shorter tubes. However, this information does lend some support to the hypothesis that shock wave reflection is a factor in the cause of the perturbations. The length of perturbed jet should be the subject of further study.

Measurement of the Pressure on the Wall

Pressure traces were obtained for test numbers 13, 14, and 15. Calibration curves for these traces are given in figures 37 through 39 respectively. The analog traces are shown in figure 40. The sweep rate for these traces was 10 μs/div, and the voltage sensitivity was 500 mv/div. The trigger for tests 14 and 15 occurred 50 μs after warhead initiation, while number 13 was delayed by 1 μs. The trace for test 13 also shows an upper beam trace set at 1000 mv/div.

The digital oscilloscope traces for tests 14 and 15 are shown in figure 41. The sampling rate for these tests was 20 points per microsecond. The Nicolet was triggered 50 μs after the warhead was detonated. The expanded views show the rise time and peak voltage of each initial pressure pulse.

All three tests show no output from the transducer until 77 μs after warhead initiation, then a rapid rise (4 μs) to a peak pressure, then a rapid fall in pressure for about 4 μs, followed by a noisy signal. The peak pressures recorded for these tests were 252 atm (3700 psi), 354 atm (5200 psi), and 190 atm (2800 psi) for tests 13, 14, and 15 respectively. The average pressure was 265 atm (3900 psi) ±40%. The average ratio of the tube diameter to body diameter (D/d) was 2.50, and the average jet velocity was 7.70 km/s.

Based on the numerical predictions of the shock length, the observed 77 μs is precisely the time that the shock wave should pass the transducer. Coincidentally, the flash time for the first x-ray image was set for 77 μs. The coincidence was accidental, since the shock length was not available when the experiment was conducted. The remarkable consistency for the three tests (all are 77 μs) seems to indicate that the observed transducer pulse is caused by the high voltage x-ray pulse. But the instrumentation and the warhead are capable of this consistency, and in a static test (no warhead) to check crosstalk, triggering of the x-rays caused no response from the transducer. Despite this, a test in which the first flash is set for

say 100 μs would be informative.

The temperature of the air behind the shock is thousands of Kelvins. According to a representative of the transducer manufacturer, this may cause a very fast (less than 1μs rise time) positive spike very early in the event. At the representative's suggestion, a single layer of electrical tape and a coating of silicone grease were put over the end of the transducer. The intent of these precautions was to reduce the level of this signal to a small amount relative to the 4 μs pulse actually observed. The long term effects of a high temperature are to cause a negative output from the transducer. This might explain the negative voltages seen on tests 13 and 14, except that the manifestation of this effect probably takes milliseconds.

Computation of the Pressure on the Wall

To predict the pressure on the wall and other flow properties for the average experimental case, a diameter ratio (D/d) of 2.50 (the average for the three tests, 13 through 15) was input to the code, along with the output from the sphere problem for u_∞ = 7.69 km/s. The result is shown in Figure 42. The bow shock wave can be seen, as well as its reflection from the wall and its subsequent reflection from the surface of the jet. The peak pressure on the wall of the tube is 71 atm (1040 psi) at the reflection point, 18.8 mm (0.74 inches) from the tip of the jet. This corresponds to a shock angle at the wall of 16°. This shock length and angle varies significantly from the values for the case of D/d = 2.90 (25.0 mm and 12°). Obviously moving the wall in or out will change the shock length; the shock angle also changes because the shock still has noticeable curvature at the wall.

The predicted pressure on the wall of the tube is shown in figure 43a for D/d = 2.50 and in figure 43b for D/d = 2.90. The two curves are plotted to the same scale for ease in comparison, but this causes the plot for D/d = 2.50 to end at 7.5 jet diameters on the abscissa, since the axial length of the computational domain was a fixed multiple of the annular width. The abscissas in the two figures represent the same physical distance of 72.2 mm (2.85 inches), since the jet diameter in both cases was 7.6 mm (0.30 inches).

Evaluation of Both the Measured and the Computed Pressure

If figure 43a (D/d = 2.50) is compared directly to the pressure trace for test 15 (figure 41), two differences stand out: the time scale of the events recorded, and the magnitude of the initial pressure pulse. These are discussed separately in the next two sections.

Time Scale of Pressure Trace

Although figure 43a shows pressure plotted versus position along the wall, and not time as in figure 41, the curve of figure 43a

can be imagined to move past the pressure transducer at the jet velocity, which would have the effect of converting the independent variable to time. In fact, the jet moves at very nearly one jet diameter per microsecond, so the abscissa units in figure 43a may be considered microseconds as well as jet diameters.

The time scale of the initial pressure pulse in figure 41 seems too slow, since the wave sweeps past the 2 mm diameter pressure port at 7.69 mm/μs. The actual rise time is 3.35 μs, about ten times slower than expected. The extreme angle of the shock (12°) may contribute to the slow rise time, although no calculations were done (eg. shock thickness) to study this contention. The slow rise time is not simply a view of the transducer's limitation, since the transducer is capable of responding more quickly than the observed rise time. According to the manufacturer, the transducer will rise to an output of one volt in 1 μs. The peak voltage in test 15 was 1.44 volts. Clearly, the expected rise time and the transducer response are quite close in magnitude. Ideally, the transducer should have a response time an order of magnitude faster than the event being recorded.

If the noise is filtered out of the rest of the pressure trace, it becomes a decaying pressure starting at a pressure of about 95 atm. The computation (figure 43a) shows a similarly decaying pressure starting at a pressure of 71 atm. Although the general shape of the curve is qualitatively the same as the transducer trace for test 15, the transducer trace again seems to be about ten times slower than expected.

Magnitude of Pressure Trace

The initial pressure pulse on the traces matches the expected passing of the shock wave qualitatively, in that the transducer reads a constant atmospheric pressure for a while, then suddenly jumps to a large value. Furthermore, this jump begins at precisely the expected time, according to the known jet position and the code predicted shock length. Quantitatively, however, the pressure traces do not match expectations; the magnitude of the initial pressure pulses are all higher than expected, based on both the real gas code and on a simple perfect gas analysis.

The perfect gas analysis used equations from Anderson (ref 41) which describe an oblique shock wave in a calorically perfect gas. The conditions ahead of the incident shock wave are known (these are the free stream conditions), and the angle of the incident wave at the wall is taken from the code computation. With this information, the pressure, temperature, and fluid velocity behind the incident wave may be computed. These conditions are then used to compute the jump conditions across the reflected wave, although in this case the angle of the wave is not known. Instead the flow is known to be parallel to the wall after crossing this wave. With this information, the equations can be solved iteratively for the properties behind this wave. When these operations are carried out, the result is a pressure

behind the reflected wave of 135 atm, and a temperature of 2700 K. Real gas effects are generally considered negligible up to about 2500 K at 1 atm, so even this analysis indicates that conditions are well into the real gas regime. Nevertheless, the predicted pressure is one-half of the measured pressure of 265 atm.

The code prediction of 71 atm is only 27% of the experimentally observed pressure. The reasons for this can be divided into two broad catagories: the code is in error, or the measurement is in error. The following paragraphs discuss these two issues.

The first issue, the code is in error, seems unlikely to account for the entire discrepancy in the pressure determination, in view of the excellent agreement with the geometric measurements as previously discussed. However, some uncertainty does exist in the computation, partly from the inviscid assumption, but primarily from resolution due to the finite cell size and round off errors. The physical size of the cells in the cylinder problem was 0.146 mm on a side. The shock in figure 43a is smeared over about 27 cells. Thus the shock is not as sharp as the physical phenomenon, and its position is uncertain. The uncertainty in the shock strength could be as significant as that of position.

Also, the modeling of the jet tip is definitely causing an error in the computations, and this error could be quite large. The shape of the jet tip is poorly modeled by a hemisphere. Inspection of the x-ray images of the jet tip particle for the three tests shows that it is more blunt than a hemisphere. In fact it is nearly flat across most of its diameter. Considering a more realistic shape in the code will increase the pressure behind the shock at the wall in two ways. First, the shock angle at the wall will be larger. This will increase the component of the free stream velocity that is normal to the shock, and therefore increase the pressure jump across the shock. Second, although the stagnation pressure will not change much, the pressure distribution on the face of the blunt tip will be more constant than for the hemisphere, and higher pressures will exist at points much closer to the wall. In effect, the hemispherical tip has been moved closer to the wall. As seen above, the pressure at the wall is very sensitive to this separation distance.

The second possibility, that the measurement is in error, is entirely possible given the difficulty of making the measurement and the fact that a negative transducer output signal was recorded on each test. In addition, the qualitative appearance of the initial pulse indicates the measurement is in error: the rise time is too slow, and there is a wide variation in the peak magnitude for the three measurements. The transducer response time is barely fast enough. Computational results indicate that the 161 μs of the recorded event is not enough time for the flowfield to achieve steady state. High air temperature effects have already been discussed, and assumed to have negligible influence on the transducer response. Notice, however, that the experimental apparatus provides no indication of how well the jet

is centered in the tube in the horizontal plane, that is the plane that is perpendicular to the plane of the film. But the pressure measurement is sensitive to the distance from the jet to the wall. Notice from figure 43 that the peak pressure increases from 51 atm to 71 atm (40%) when the diameter ratio is reduced from 2.90 to 2.50 (14%). The 14% represents the experimental variation in the diameter ratio observed in the vertical plane. The variation in the horizontal plane may be of the same magnitude, and could be responsible for much of the observed variation in pressure measurements of ±40%.

The air inside the copper cone is compressed and shot through the tube before the copper jet, and this has an unknown effect on the pressure measurement. For example, the air in front of the jet may have a density and pressure much greater than atmospheric conditions. The velocity of the copper jet may be greater than the air jet, causing it to pass through the bow shock of the air jet at some point, with unknown effects on the jet's bow shock.

Pressure on the Jet

The pressure on the jet is the object of this entire study. This pressure cannot be measured, so computations yield the only knowledge of it. The predicted pressure on the surface of the jet is plotted in figure 44 for both D/d = 2.50 and D/d = 2.90. The two cases can be considered to indicate the effect of eccentricity of the jet in the tube. For a small eccentricity of 0.20 jet diameters = 1.6 mm (0.06 inches), there is quite a difference in the pressure field experienced by the jet. The magnitude of the pressure behind the reflected shock jumps from 25 atm on the side of the jet farthest from the tube wall (approximated by the D/d = 2.90 case) to 34 atm on the side closest to the wall (D/d = 2.50). More importantly, the location of the shock reflection varies by two jet diameters (15.2 mm or 0.60 inches). Thus for a distance of two jet diameters, there is a pressure imbalance of up to 30 atm. The following simple analysis indicates that this is not sufficient to cause significant lateral displacement of a particle of the jet in the timeframe indicated by the x-rays.

Newton's Second Law was written for a cylindrical particle under the influence of a pressure exerted over one-half of its lateral surface. It was integrated twice to yield the following equation for the radial position of the particle as a function of time.

$$r = \frac{2p}{\pi d \rho} t^2 \qquad (6\text{-}1)$$

where d is the particle diameter (taken as 6 mm - less than the tip diameter as indicated figures 30 - 33), ρ its density (nominally the density of copper, 8.9 g/cc, but it could be less due to porosity in the jet), and p the constant pressure acting on the particle. The particle is assumed to begin its radial motion from rest at r = 0, the

axis of the tube. The pressure is taken to be the maximum experimental pressure at the wall of the tube, 354 atm. The time is the tube length divided by the jet velocity, or the time that the particle is in the tube, 20 μs. The resulting lateral displacement of the particle is 0.17 mm (0.007 inch), which is about 3% of the observed displacement of about 6 mm. This simple analysis does not consider the possibility that the pressure imbalance could cause the particle to pitch, and the pitch could grow due to other aerodynamic forces.

Entrained Particles

The existence of a cloud of copper particles surrounding the tip of the jet is a well known phenomenon for certain apex designs, observable using a different test apparatus than that used here (see, for example, ref 46). The explosive process that forms the jet is far from ideal, and not all elements of the copper liner end up on the axis. These minute copper particles are given the same velocity as the jet tip during the formation process and have been observed to be entrained by the bow shock wave. Another source of particles, this one continuous, is ablation from the jet tip. These particles would also be entrained by the bow shock wave. As the jet travels through the air, the air flowing across the bow shock is turned away from the jet, and causes these particles to move obliquely away from the jet. These particles must cross the reflected shock in their journey outward, but unlike air molecules, they retain some of their radial momentum after crossing the shock. Many of them impact the tube wall, as evidenced by the roughened surface on the inside of all recovered tubes.

Recovered transducers all show definite signs of erosive particle impact. In related studies of dusty flow, dust in the air was found to increase the dynamic pressure measurement by as much as four times (eg. ref 47). Figure 45 shows an example of pressure measurement of dusty air at Mach 3 (ref 48). The top plot is a record of the measurement of a transducer (similar to the type used here) protected from impact of the dust particles, and the bottom plot is from an identical transducer exposed to the dust. Both transducers were mounted next to each other (about 1/2 inch apart), inclined at 45° to the flow, and exposed to the air motion near the ground caused by a large nearby explosion. The total time scale is 200 ms, 2000 times as long as the time scale in figure 41. The spikes caused by the impact of the dust particles are apparent in the bottom graph of figure 45.

Based on this data, plus the eroded face of the transducer in the tests conducted here, one must conclude that particle impacts are contributing to the pressure measurements. There are two differences between the data in figure 45 and the data obtained here. The transducer used here was inclined at 90° to the flow (ie. static pressure), while that of figure 45 was inclined at 45°. However this angle is probably quite similar if the direction of motion of the copper particles is considered. In any case, the difference is offset by the greater density of the particles in this test. The particles

here are copper, while those of figure 45 were dust picked up off the ground by the blast wave.

The particle impacts on the transducer should lag behind the passing of the shock wave by a small time, of order of magnitude of the pulse width (the time required for the shock to pass the transducer). This is the case; the initial pressure pulses in test 14 and 15 are free from noise of the type generated by particle impacts. Consequently the phenomenon cannot explain the high magnitude of the initial pressure pulse reading, but the noise in the signal that follows the initial pulse is likely to be caused by the particle impacts.

The motion of the tube, transducer, and signal lead due to the detonation blast probably does not contribute to the noise following the initial pressure spike. Following all tests, the tube and transducer assembly was found about ten meters from its original position. The tube was not rigidly mounted in order to reduce noise in the transducer output due to any shock waves from the explosion propagating through the metal parts. The manufacturer feels that transducer and cable motion will not affect the transducer's output. In any case, the tube does not start to move until the interesting part of the event is over, as evidenced by the x-ray images.

General notes on the computation

The problem was broken down into two simpler flowfields: a hemisphere in uniform flow and the flow between concentric cylinders. The grid used for the hemisphere problem had eight radial cells and twenty-five circumferential cells. The problem was run until the flow traveled 2.3 sphere diameters, (1770 time steps) which took about thirty minutes on the BRL's CRAY X-MP/48 computer. A fixed grid of square cells was used to solve the cylindrical problem, with forty cells in the radial direction and 400 cells in the axial direction. This problem was run until the mass flow out of the grid was 98% of the mass flow in, which took 60 hours on a single cpu of the CRAY X-MP/48. About 1.25 million variables were computed each time step (not including iteration, logical tests, etc), each requiring numerous additions, multiplications, exponentiations, etc. Each of these time steps required two minutes of cpu time. The problem required a memory of one million words.

CONCLUSIONS

1. The problem of shock reflection for a hypersonic shaped charge jet traveling through a tube was solved numerically using a Godunov code with real gas modifications.

2. An experiment was conducted to test some of the code predictions. Measurements were made of the pressure on the tube wall, and flash radiographs were taken of the jet in the tube.

3. Excellent correlation was found between the code prediction and the radiographic data, with the shock length prediction being within 8% of the data. The computed pressure on the tube wall behind the reflected shock was only 27% of the measured value, however.

4. The pressure of the flow field alone is insufficient to cause the severe perturbations seen in figure 30.

5. Evidence of particle impacts was observed on the transducer and tube wall on each test conducted. This data leads to the following hypothesis to explain the perturbations of the jet:

> Copper particles from the jet formation process and ablation are entrained by the bow shock of the jet, and caused to move radially outward by the flow field behind the shock. These copper particles are reflected by the tube wall and travel radially inward, eventually impacting the jet and causing radial displacement (perturbation) of jet particles. The distribution of particles is asymmetric, and the asymmetry of the flowfield (due to eccentricity of the jet in the tube) compounds the asymmetry.

Experimental results obtained here are consistent with this hypothesis, but do not prove it.

6. The first six inches of the jet is perturbed by the six inch long tube. This is also consistent with conclusion 5, since the cloud of particles exists only at the tip of the jet, and these particles get used up or exit the tube before the late portions of the jet enter the tube. This observation and its influence on conclusion 5 are in need of further experimentation (recommendations 7 and 8).

RECOMMENDATIONS

1. Change the configuration of the tip of the jet in the code to more closely match the blunt shape seen in the radiographs.

2. Do a computational run at say D/d = 2.0 to evaluate the dependence of the reflected pressure on this parameter.

3. Conduct additional tests to obtain more pressure measurements to build confidence in the data. Try tourmaline transducers (PCB Piezotronics model 134a), with a rise time of about one-tenth that of the transducers used here, but with the same full scale range (available with either a 10,000 or a 20,000 psi range). Alas, they are more difficult and more expensive to use.

4. Change the time of the first x-ray flash to ≈100 μs for several of the additional tests.

5. Modify the test apparatus to try to avoid damage to the transducer. For example, use a breakaway transducer lead and/or rigidly attach the lead to the tube. Mount the tube like a pendulum so it won't fly away and damage the transducer.

6. Isolate the transducer from particle impacts for a comparison test.

7. Investigate the effect of tube length on the perturbed length of the jet.

8. Test several "sharp apex" 3.2 inch precision shaped charges. These charges do not form a debris cloud around the tip. Direct the jet through the tube, and take flash radiographs (pressure measurements are optional). Observe whether the jet is perturbed. This will test conclusion 5.

9. Jet breakup time (the time, after warhead initiation, that the stretching jet begins to separate into individual particles) may be influenced by the shock reflection that impinges on the body. Combine information learned on this program with the current BRL model for jet breakup to test this.

FIGURES

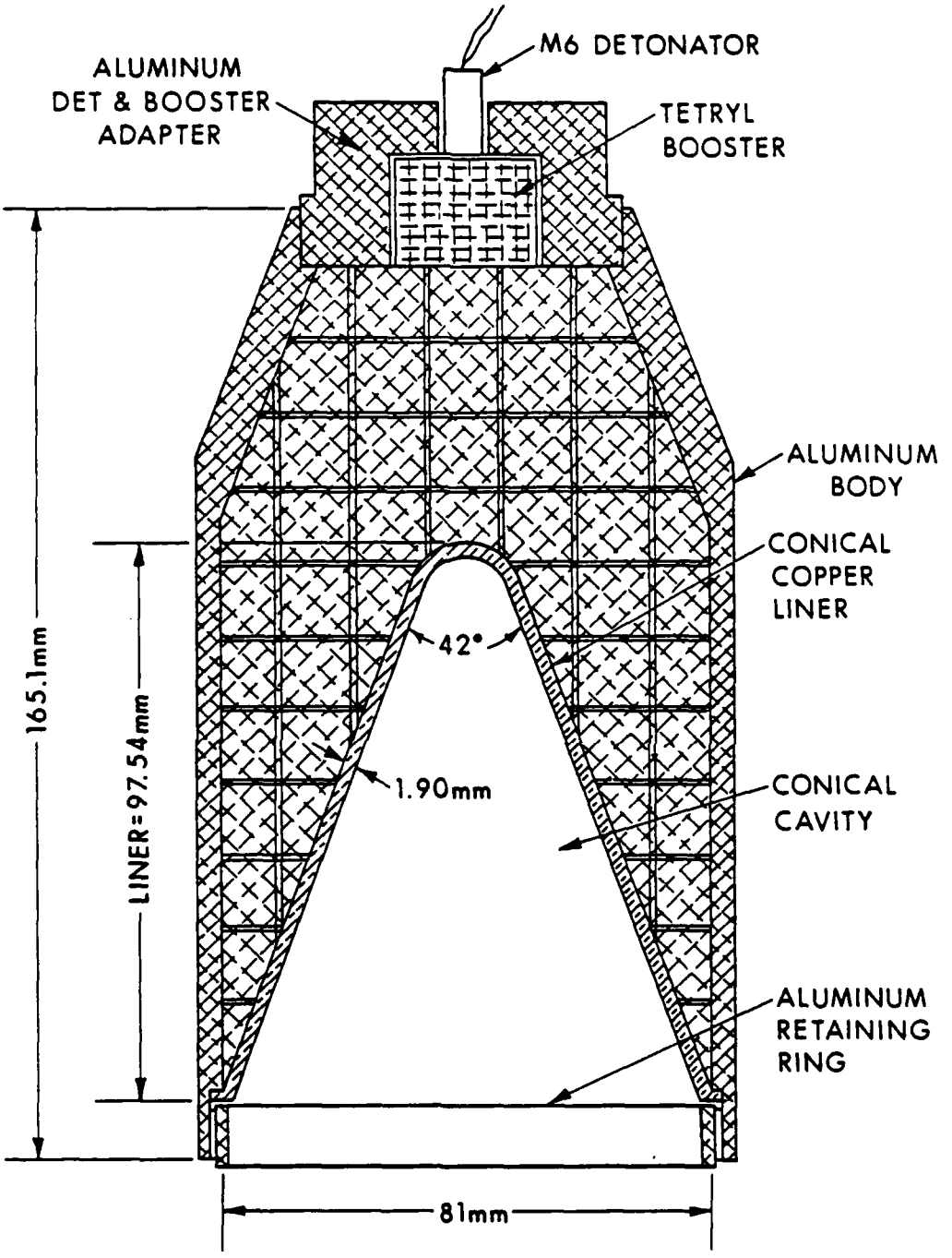

Figure 1. The BRL 81mm precision shaped charge.

Figure 2. The jet from the BRL 127mm precision shaped charge.

Figure 3. Flash radiograph of a perturbed jet (ref 2).

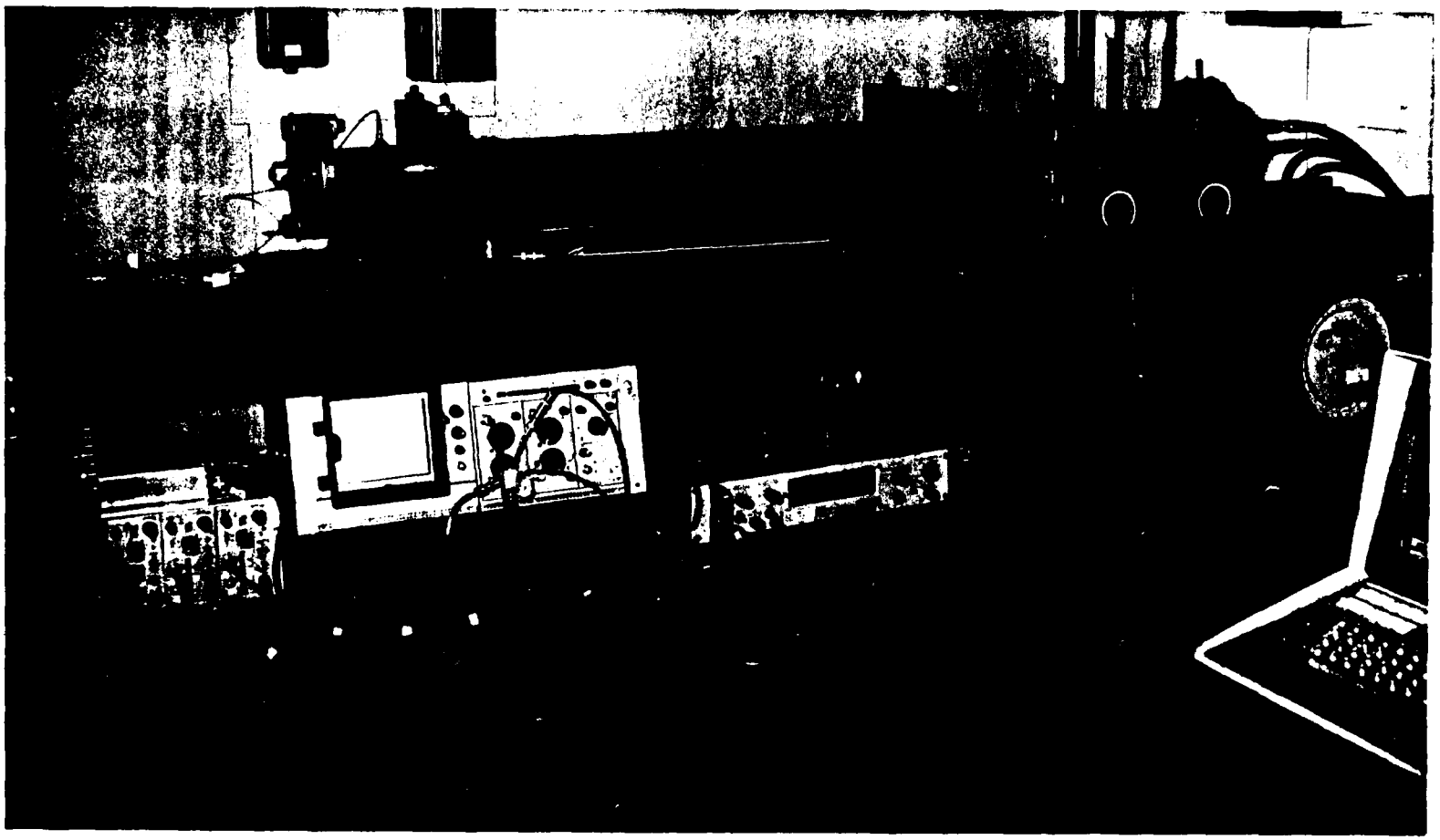

Figure 4. The two inch shock tube and related instrumentation.

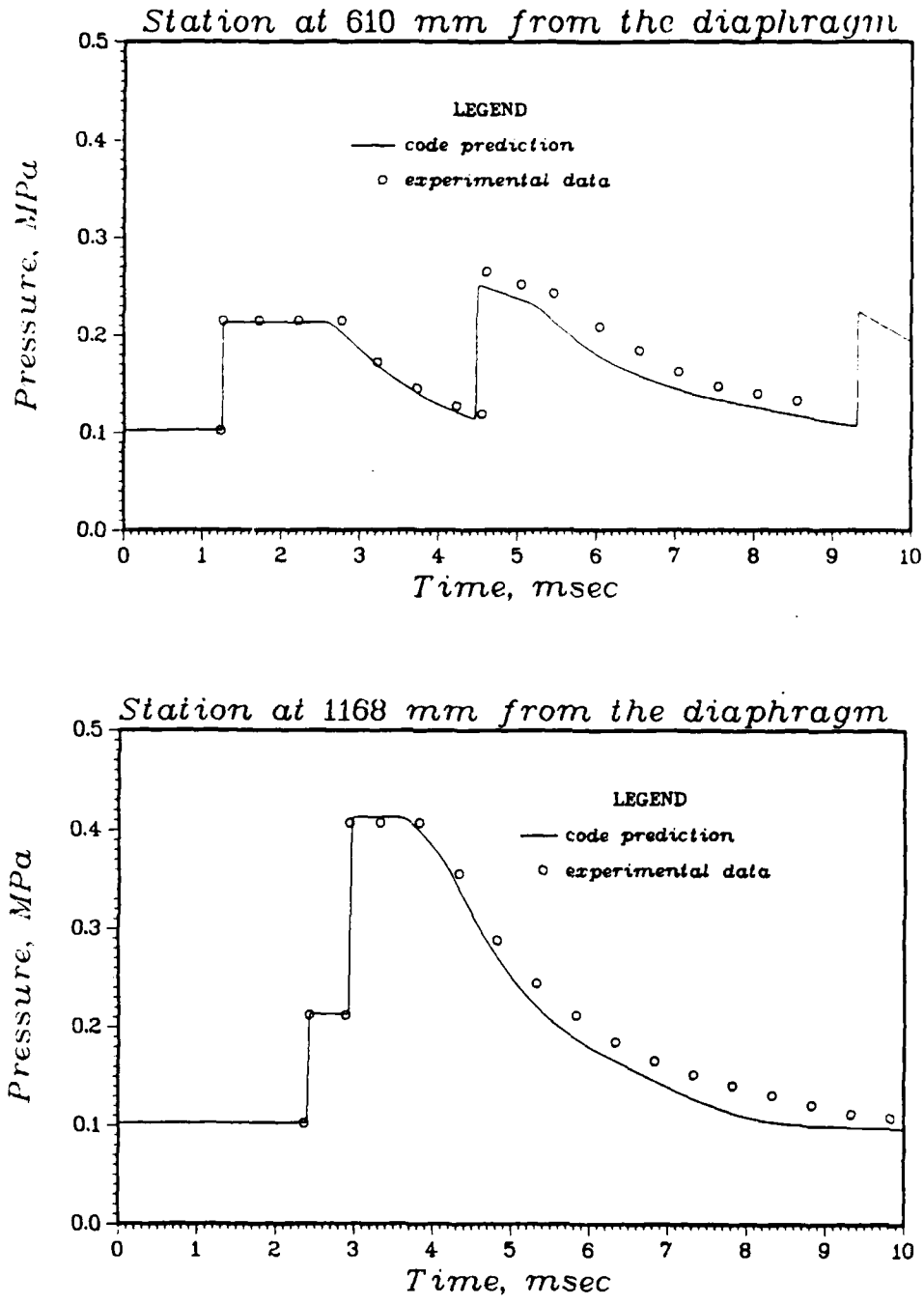

Figure 5. Comparison of 1-d code predictions and shock tube data.

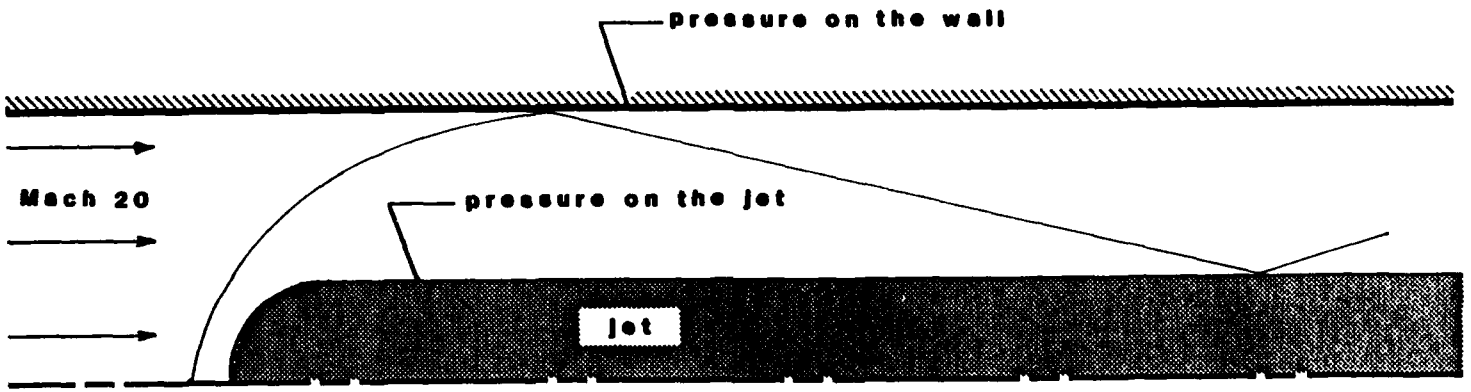

Figure 6. The problem under study.

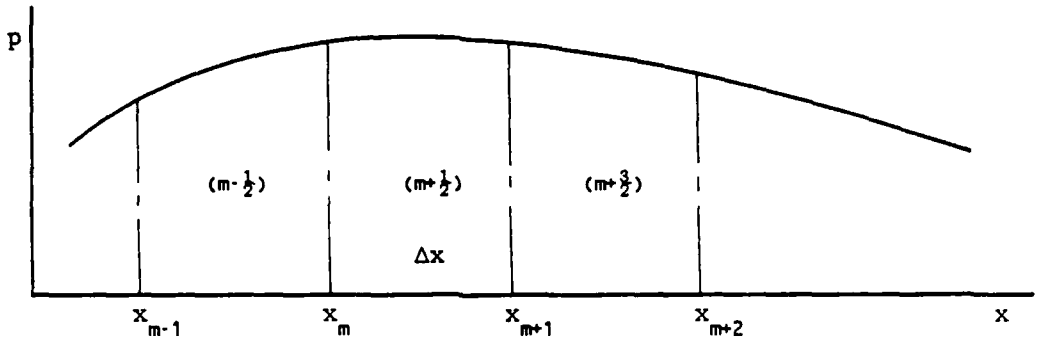

a. Pressure in a one-dimensional fluid.

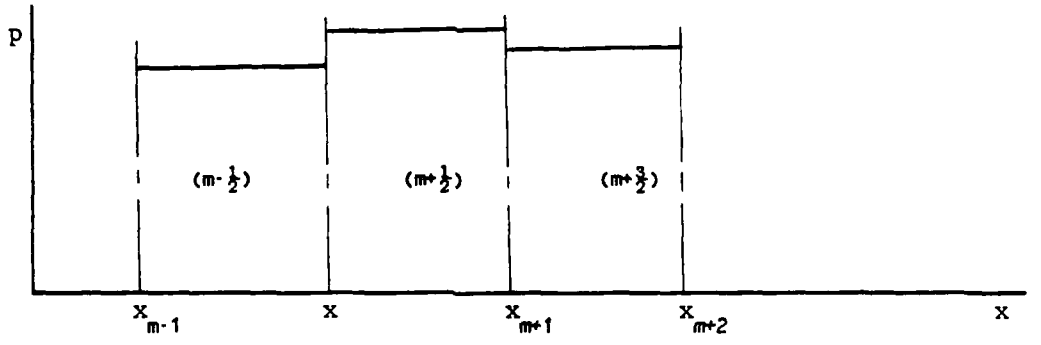

b. Discretized pressure in a one-dimensional fluid.

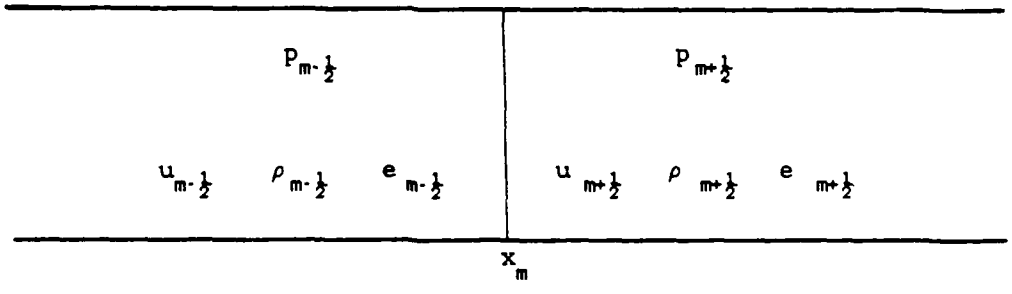

c. The classical shock tube problem.

Figure 7. The descretized flowfield.

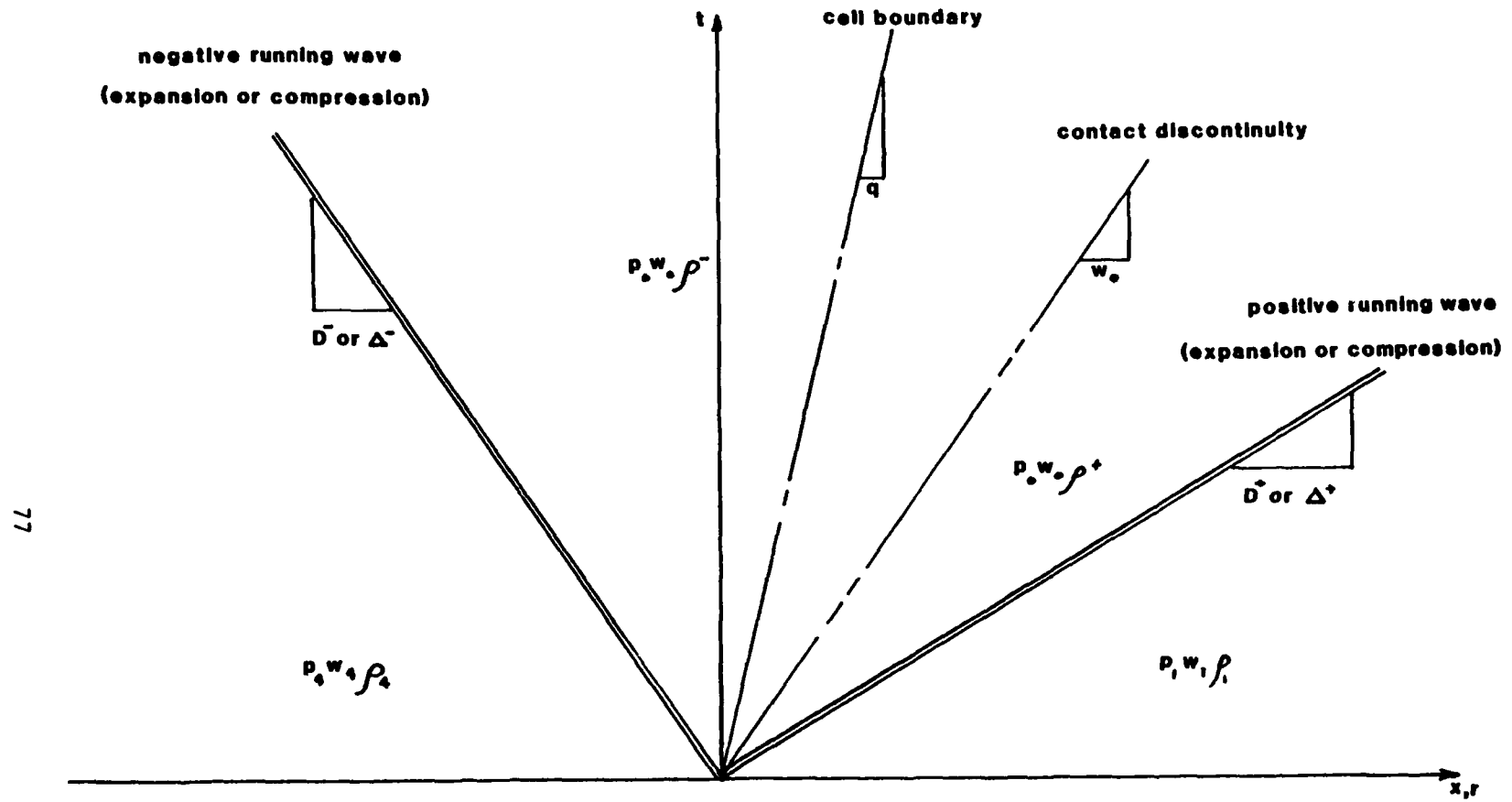

Figure 8. The x-t diagram for the Riemann problem.

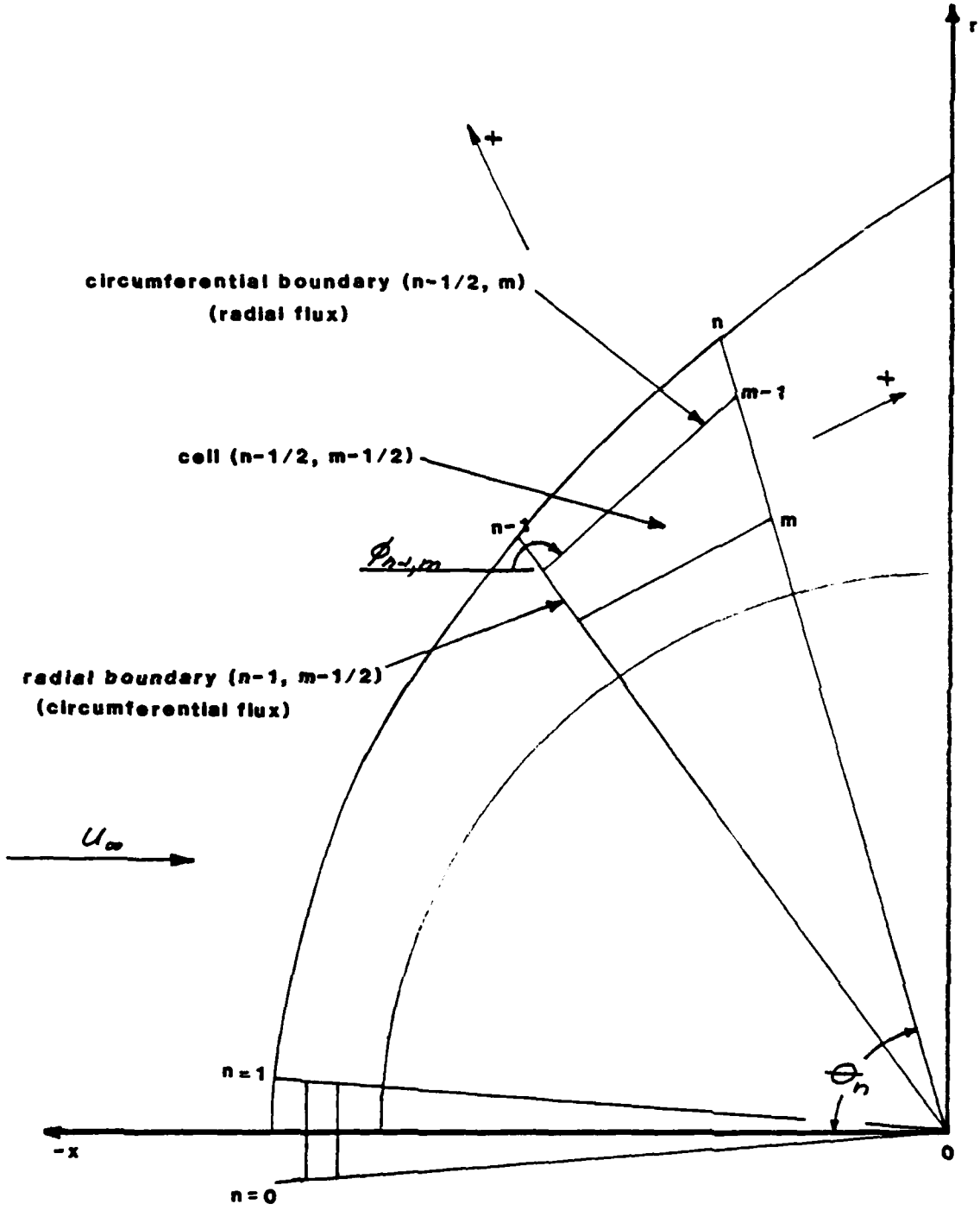

Figure 9. The hemisphere shock layer with a typical cell.

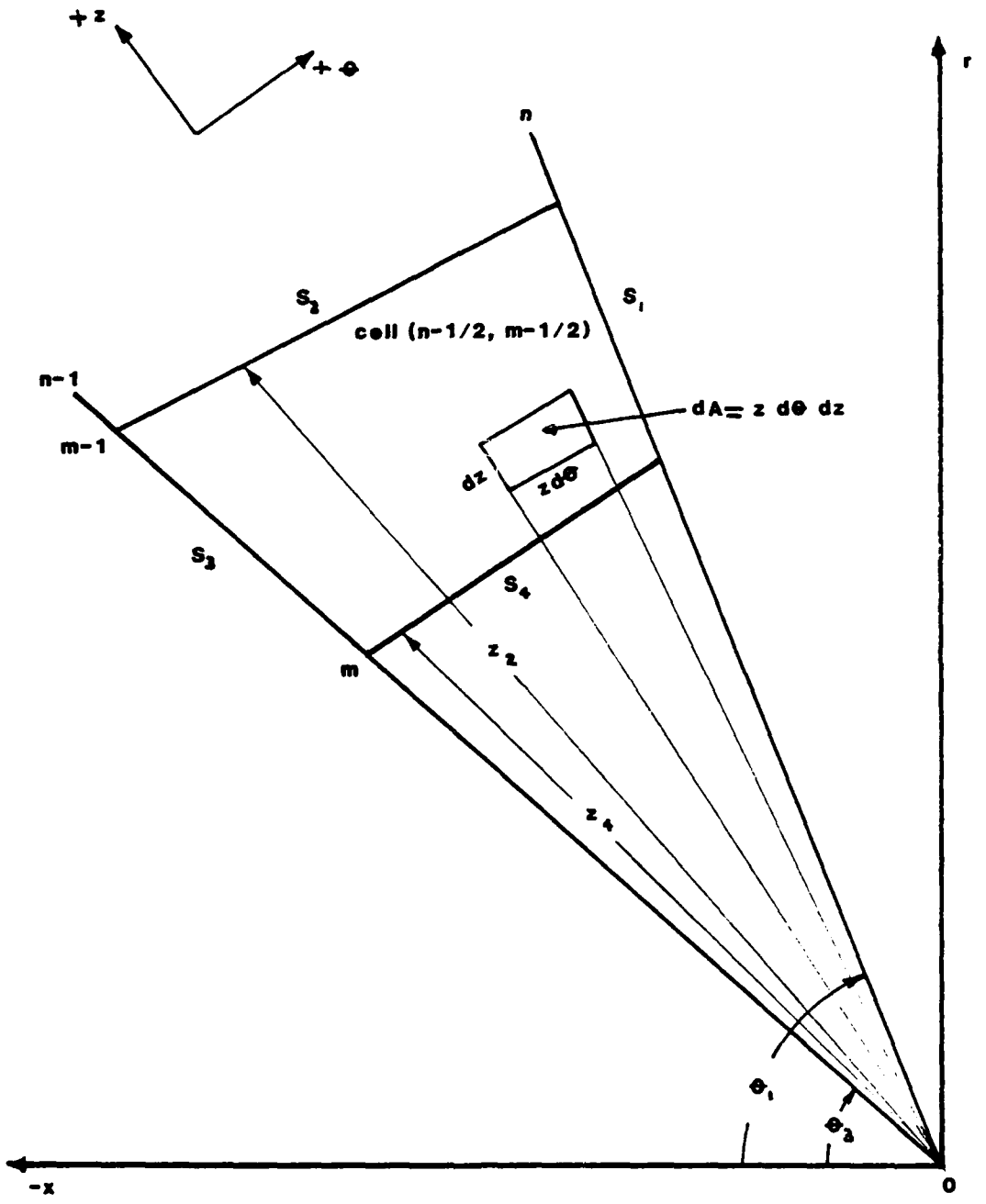

Figure 10. Integration over the cell area.

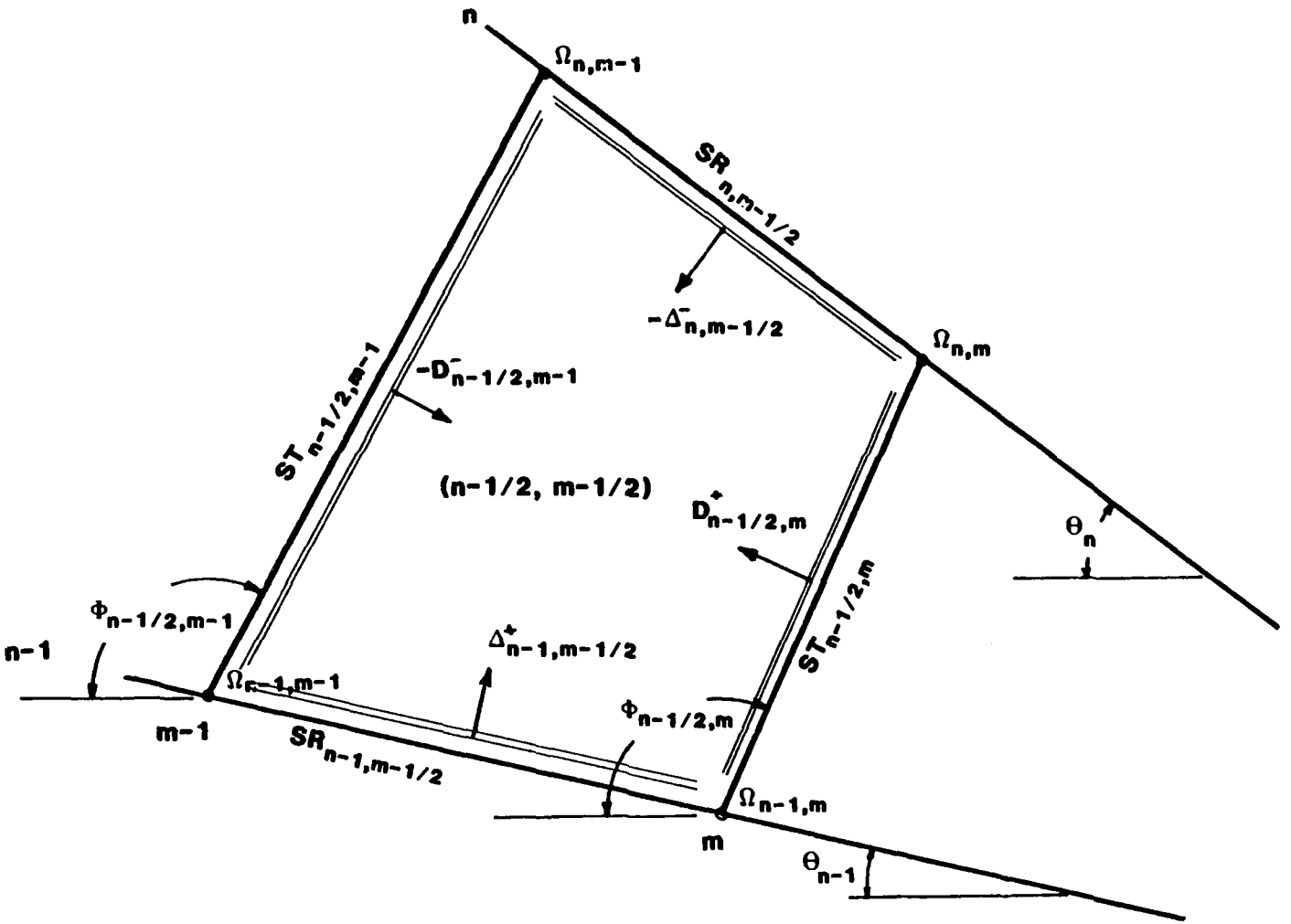

Figure 11. Riemann waves entering the computational cell.

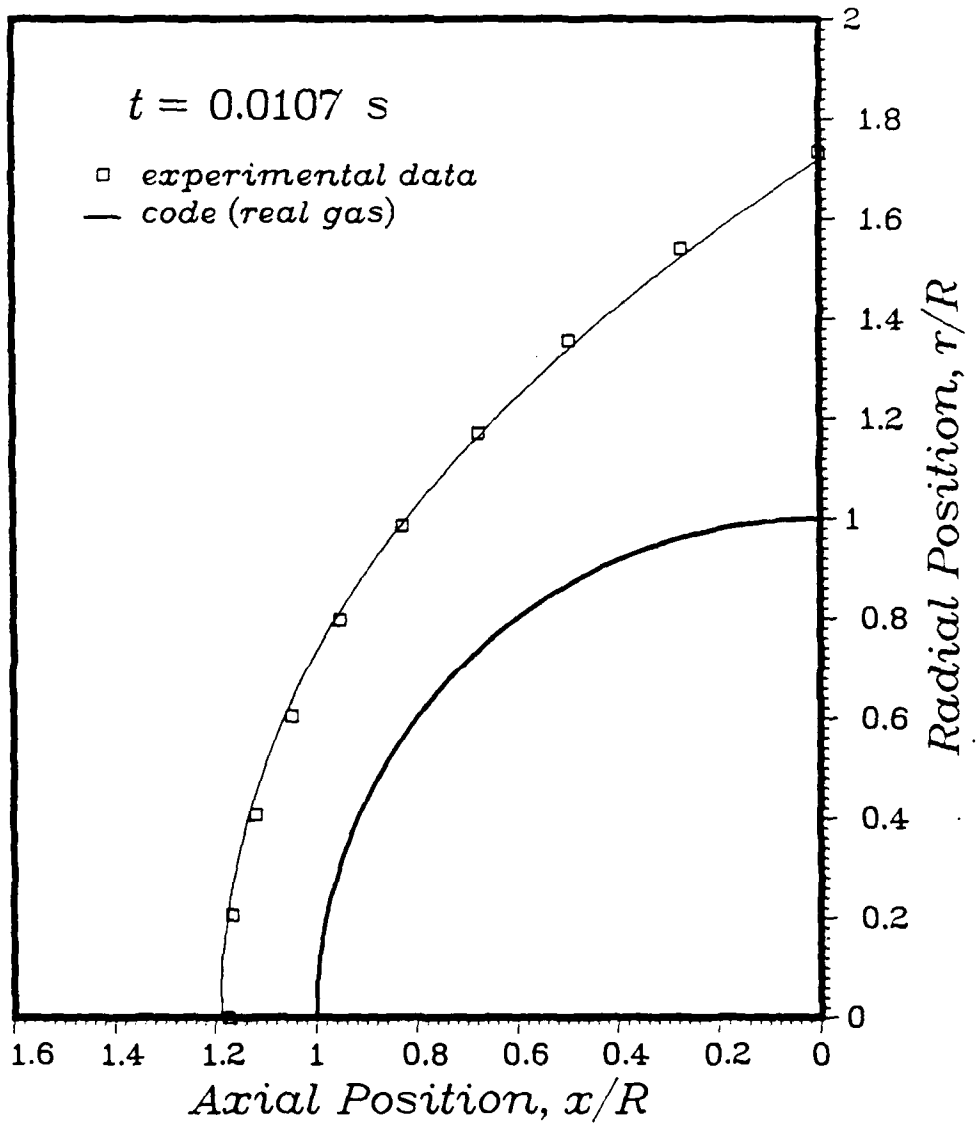

Figure 12. Shock position on the hemisphere, Mach 4.00.

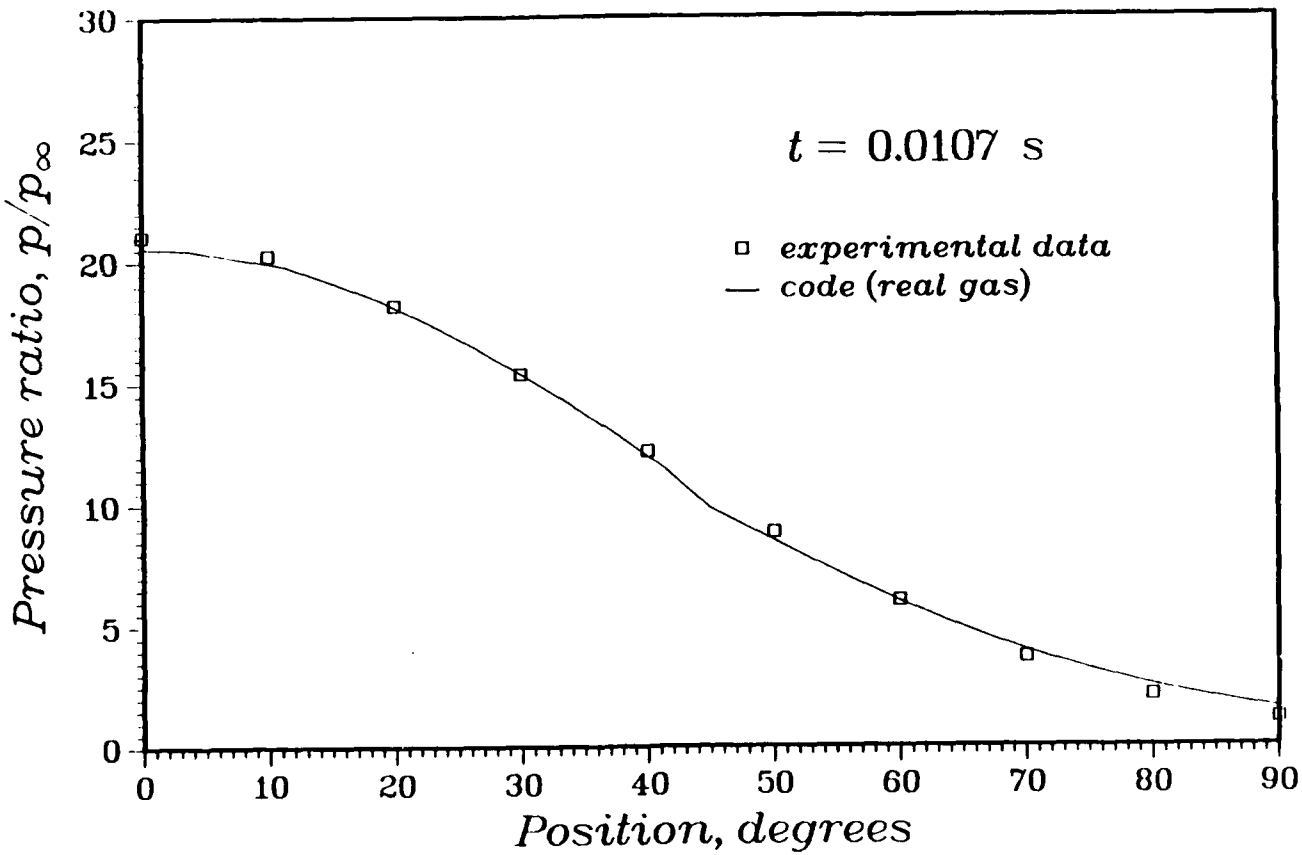

Figure 13. Pressure distribution on the hemisphere, Mach 4.00.

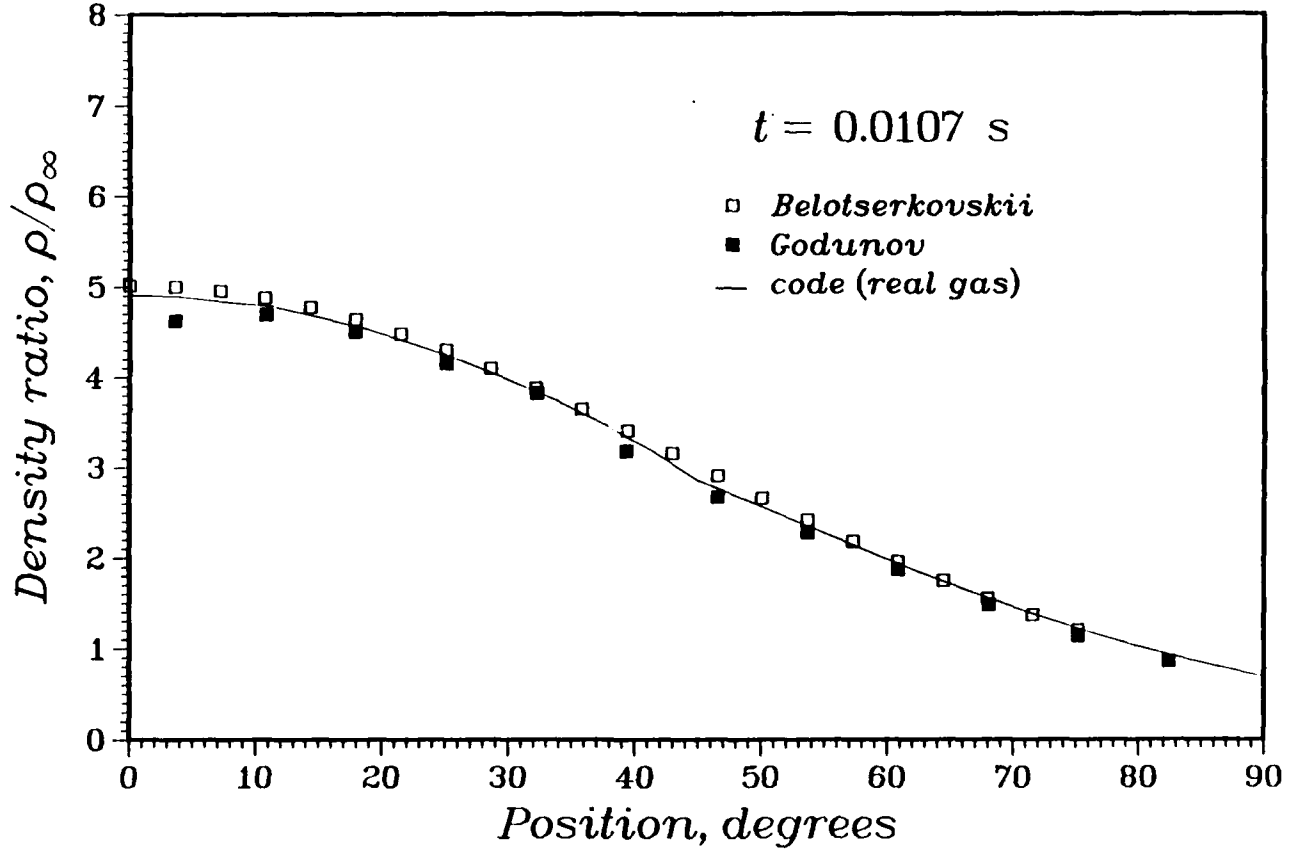

Figure 14. Density distribution on the hemisphere, Mach 4.00.

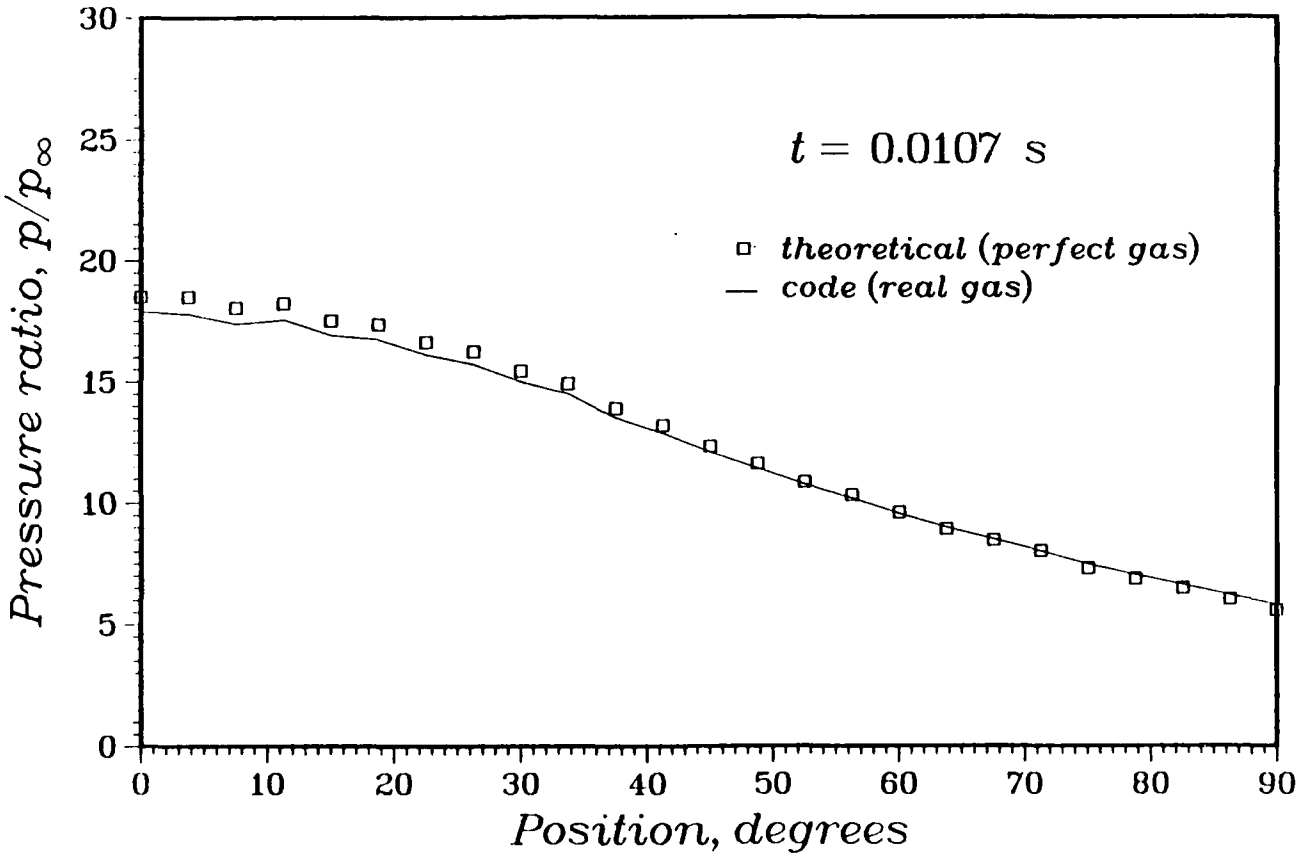

Figure 15. Pressure behind the bow shock wave, Mach 4.00.

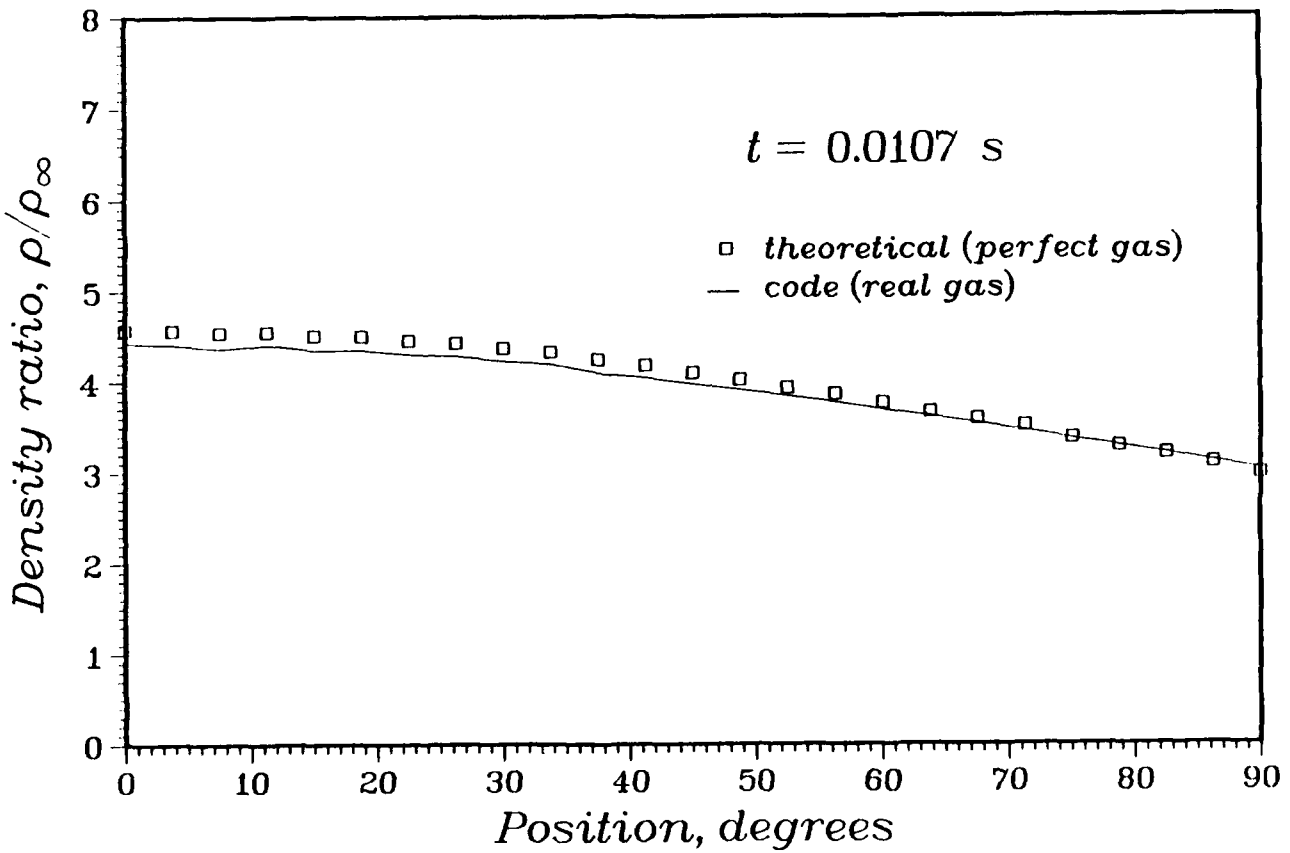

Figure 16. Density behind the bow shock wave, Mach 4.00.

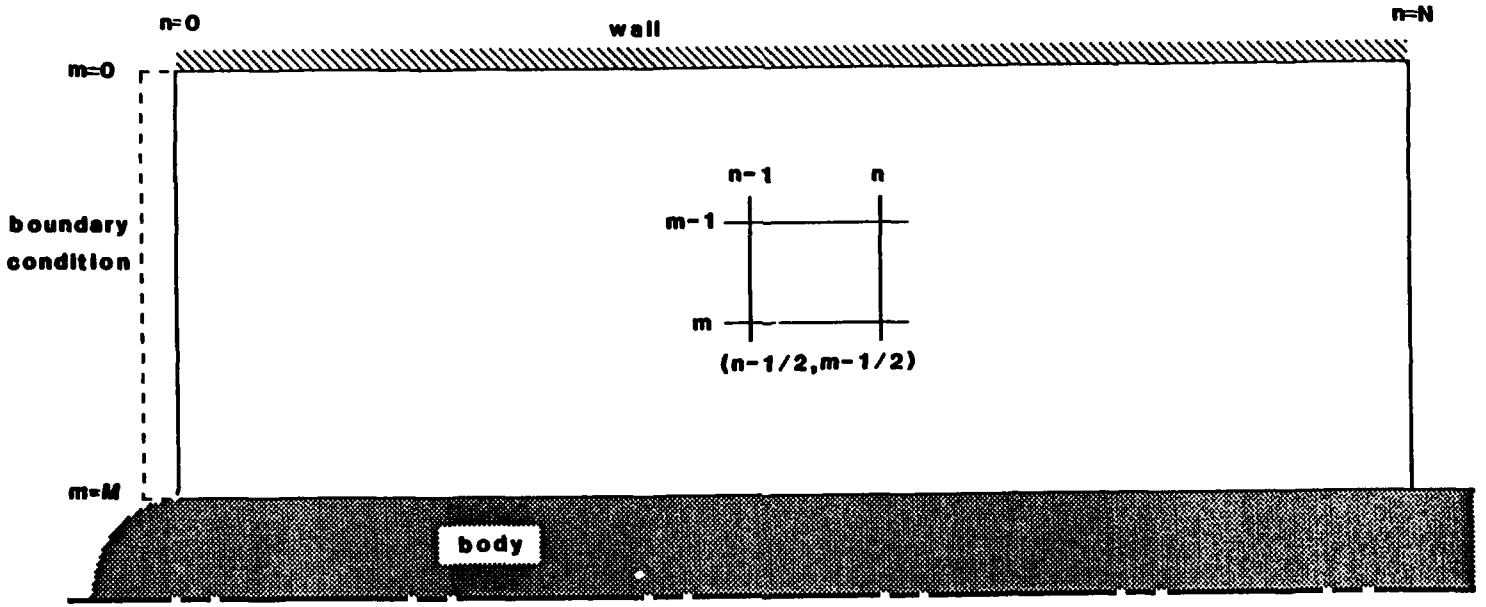

Figure 17. Grid for the cylindrical problem.

AD-A193 577 INVESTIGATION OF THE HYPERSONIC FLOWFIELD SURROUNDING A SHAPED CHARGE JET(U) ARMY BALLISTIC RESEARCH LAB ABERDEEN PROVING GROUND MD H W MEYER DEC 87 2/2

UNCLASSIFIED BRL-TR-2883 F/G 19/1 NL

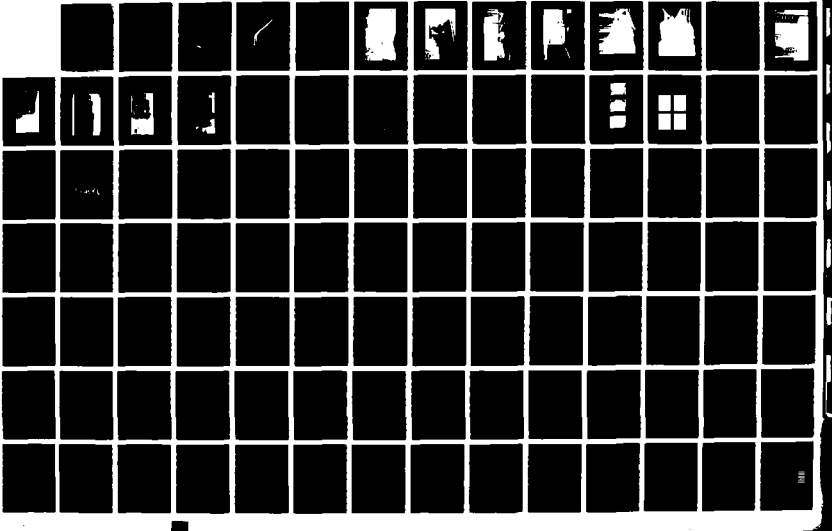

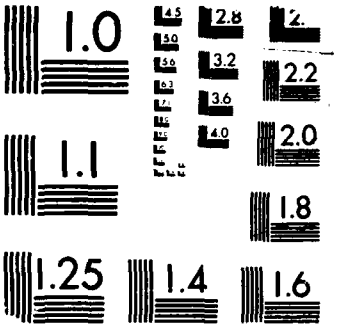

MICROCOPY RESOLUTION TEST CHART

BUREAU OF STANDARDS-1963-A

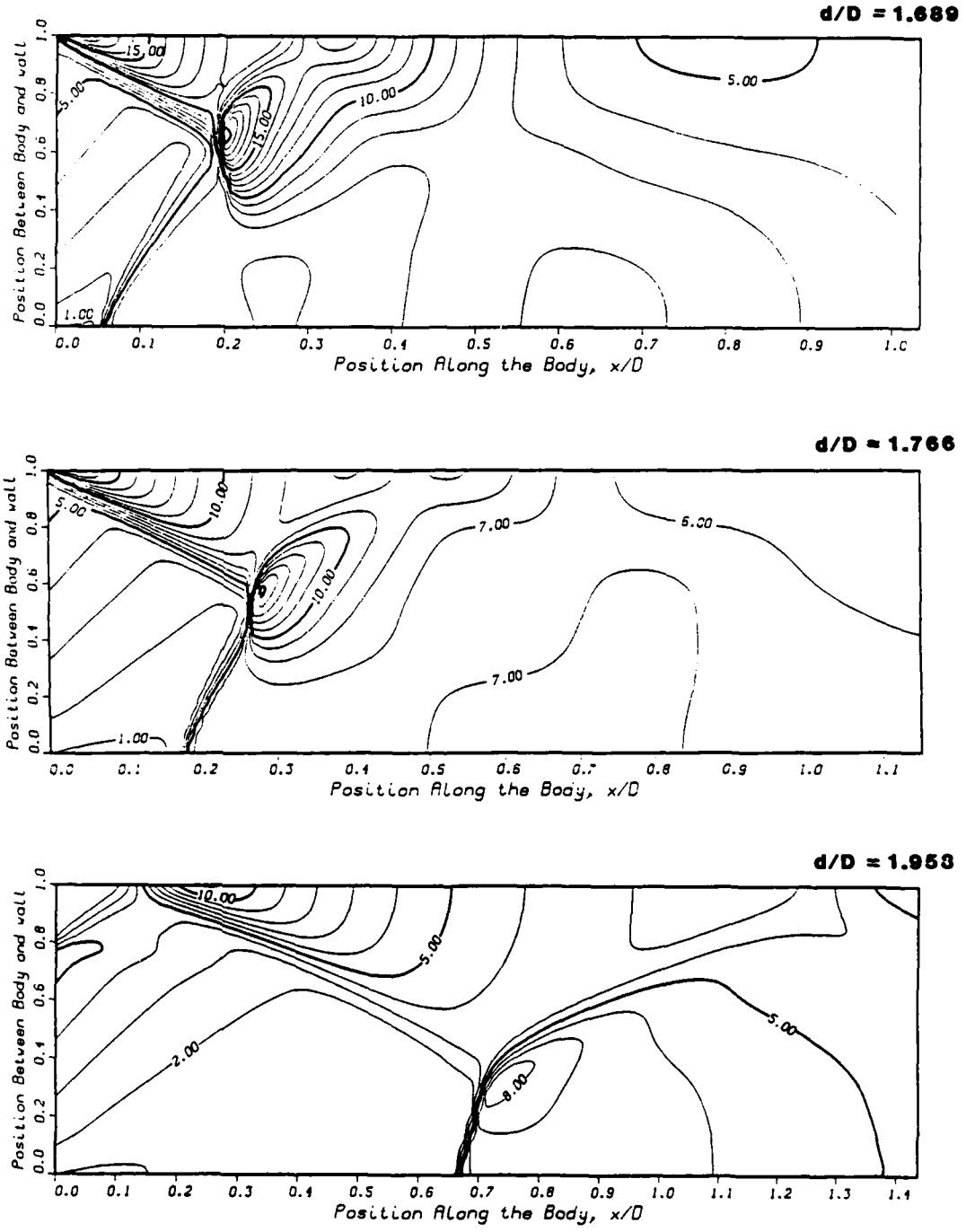

Figure 18. Pressure contours for three wall diameters, Mach 4.00.

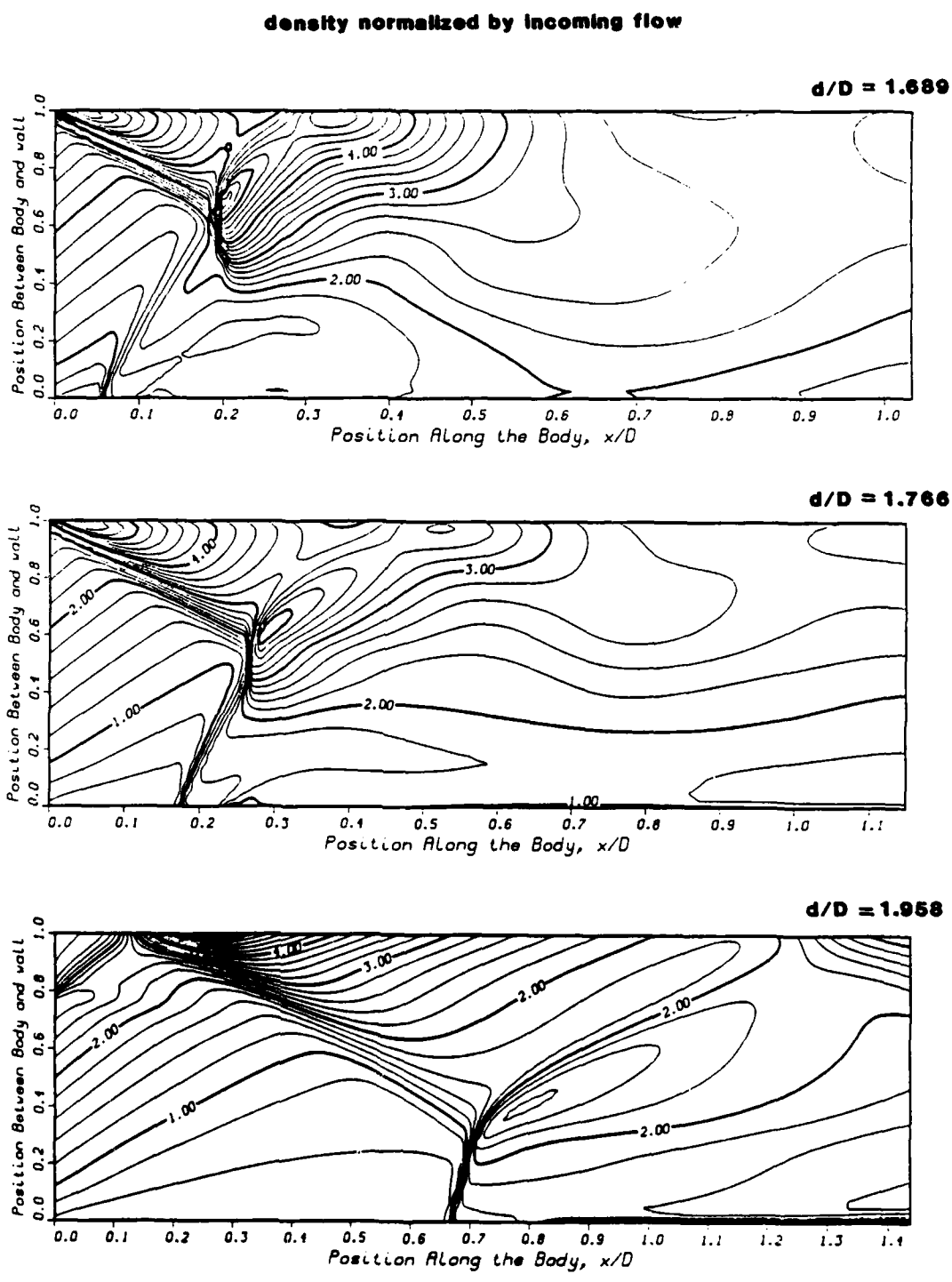

Figure 19. Density contours for three wall diameters, Mach 4.00.

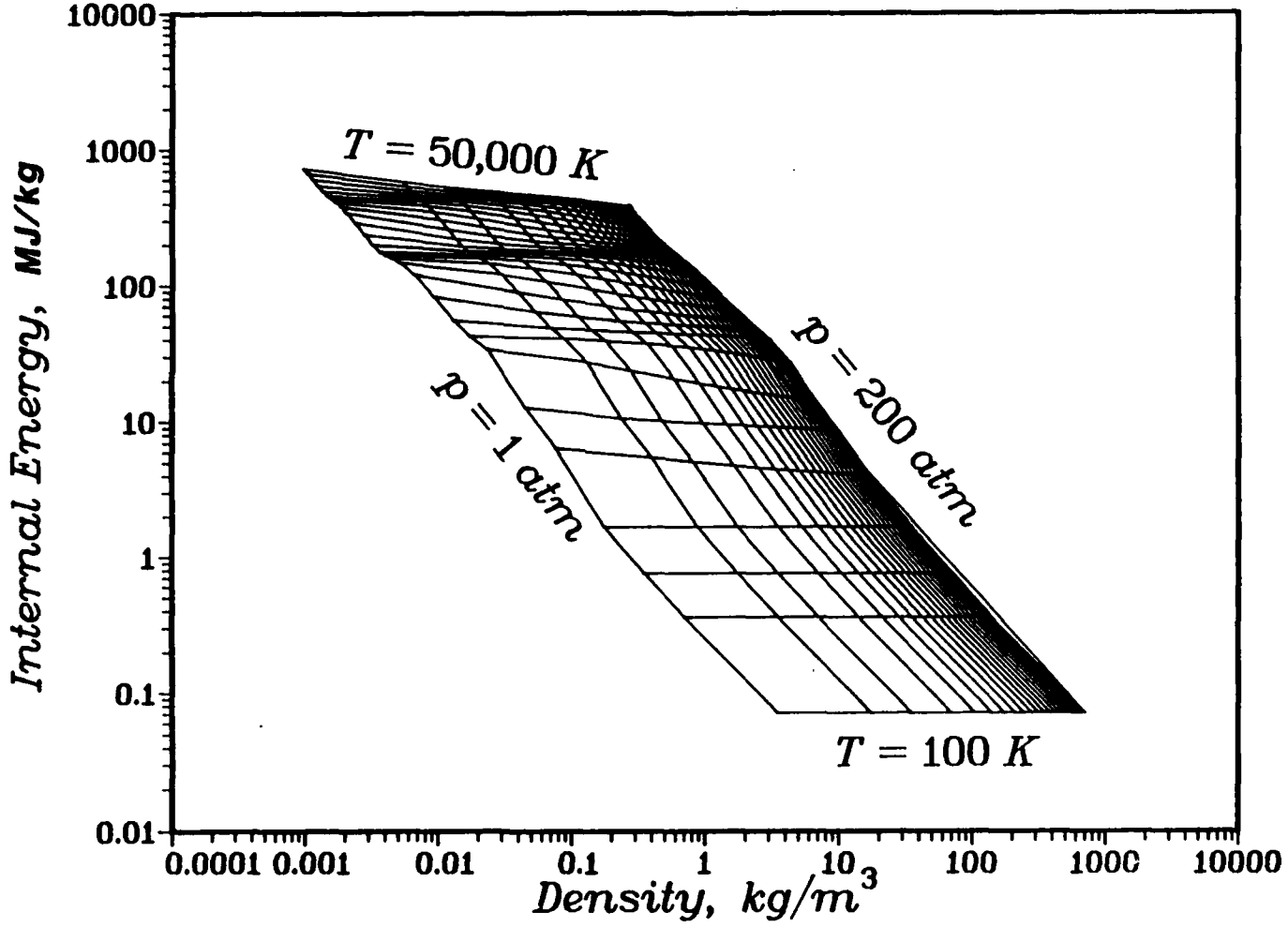

Figure 20. Thermodynamic properties of air.

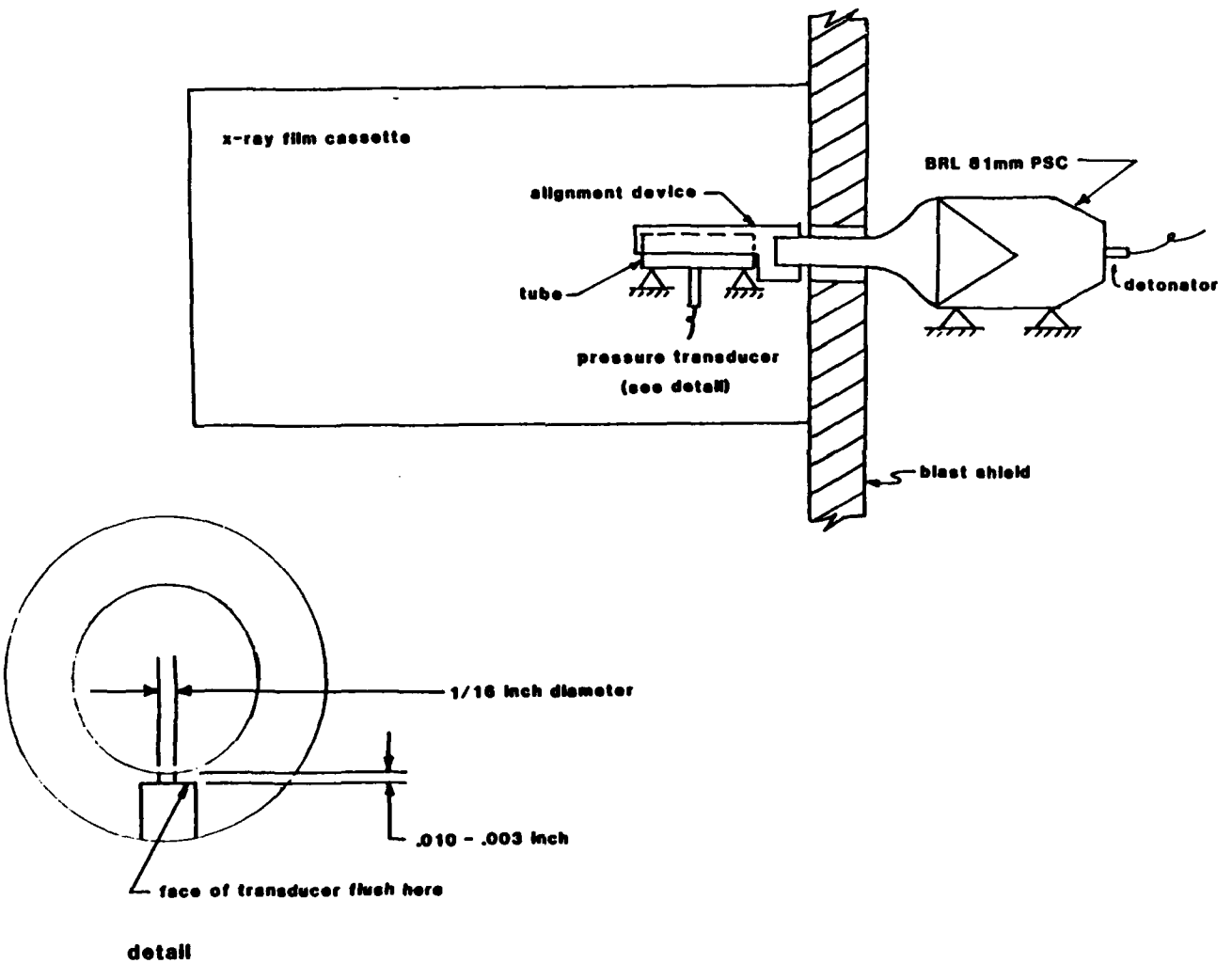

Figure 21. Schematic of the experimental apparatus.

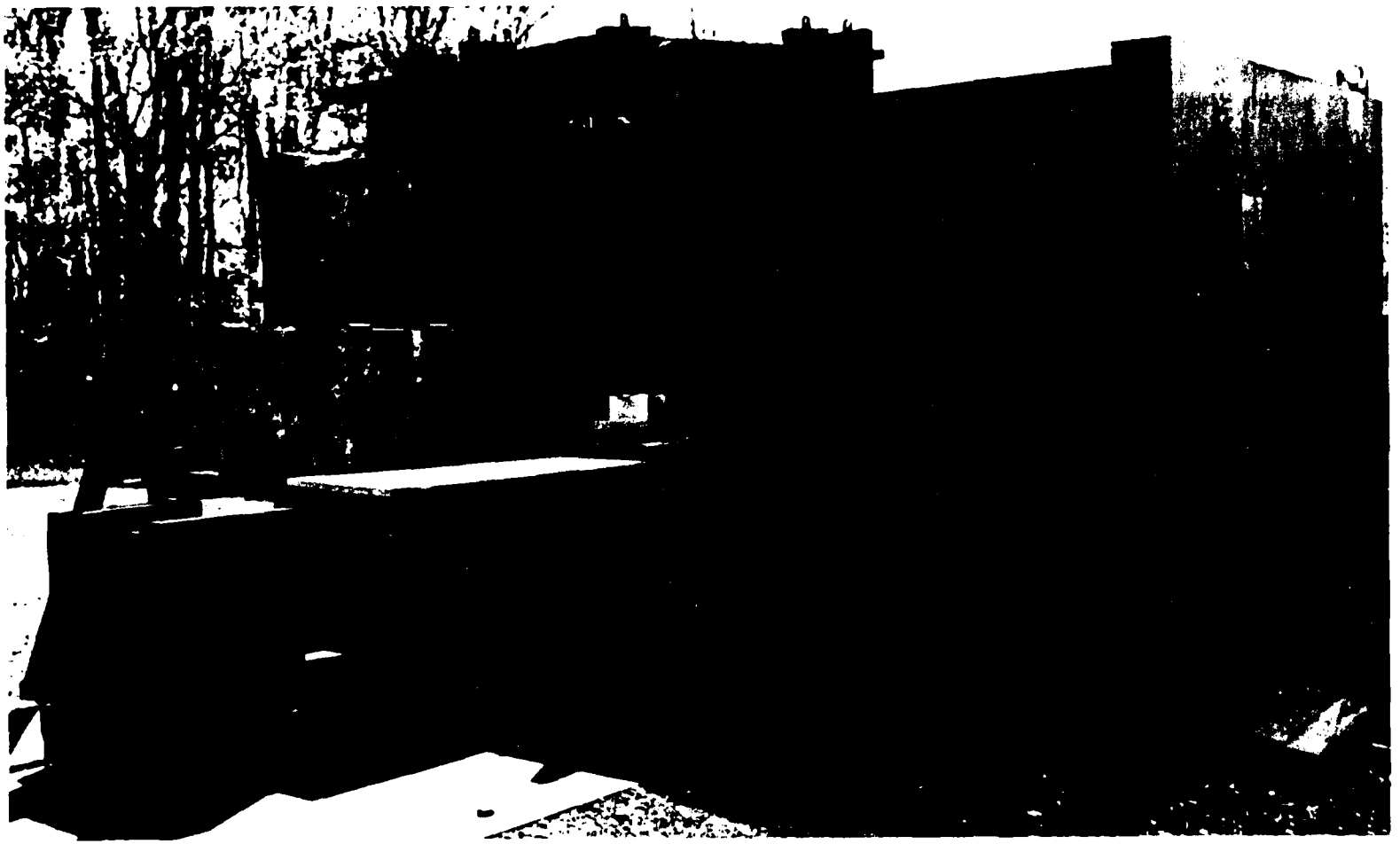

Figure 22. View of the test area in front of the explosive barricade.

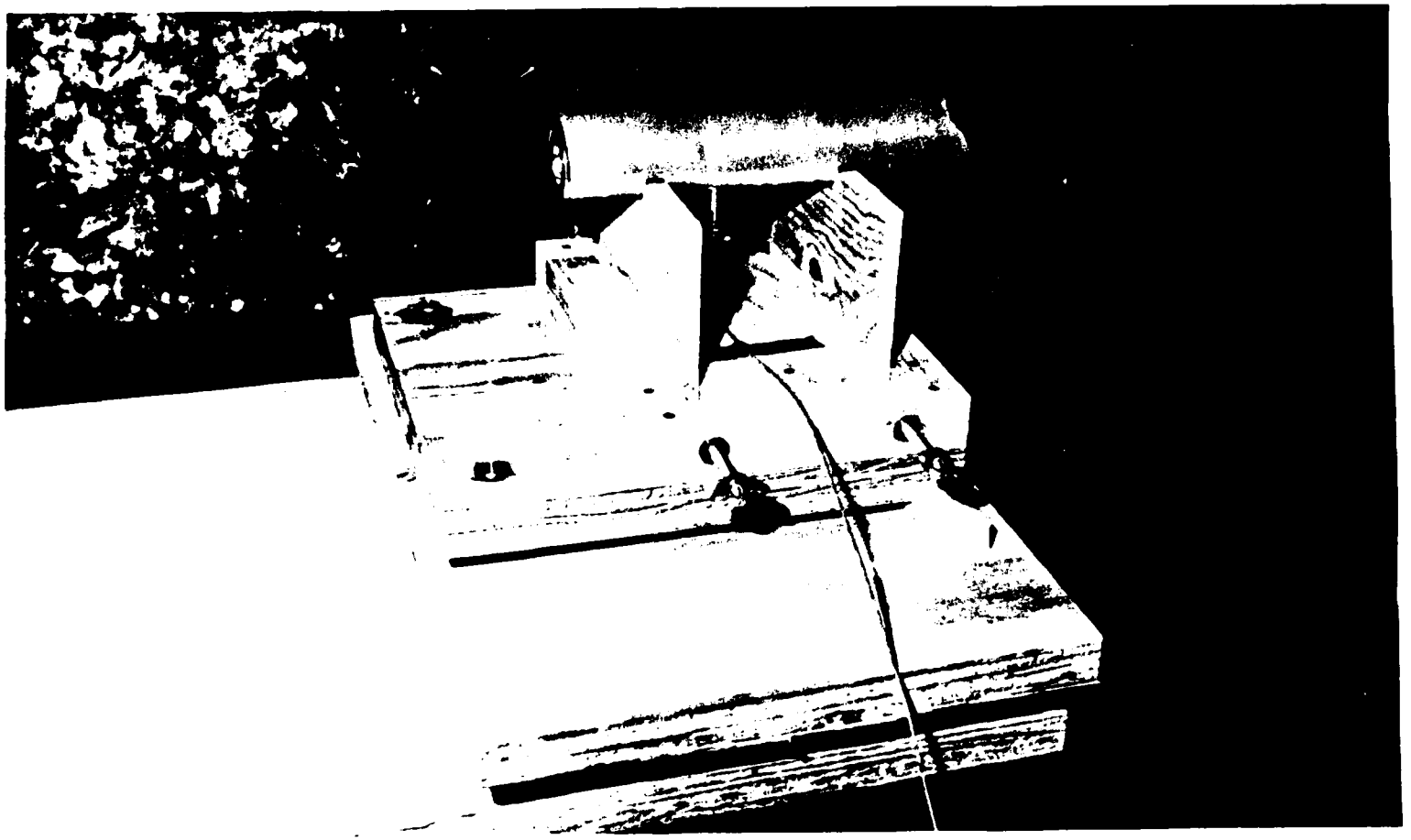

Figure 23. View of the pressure transducer and tube in position.

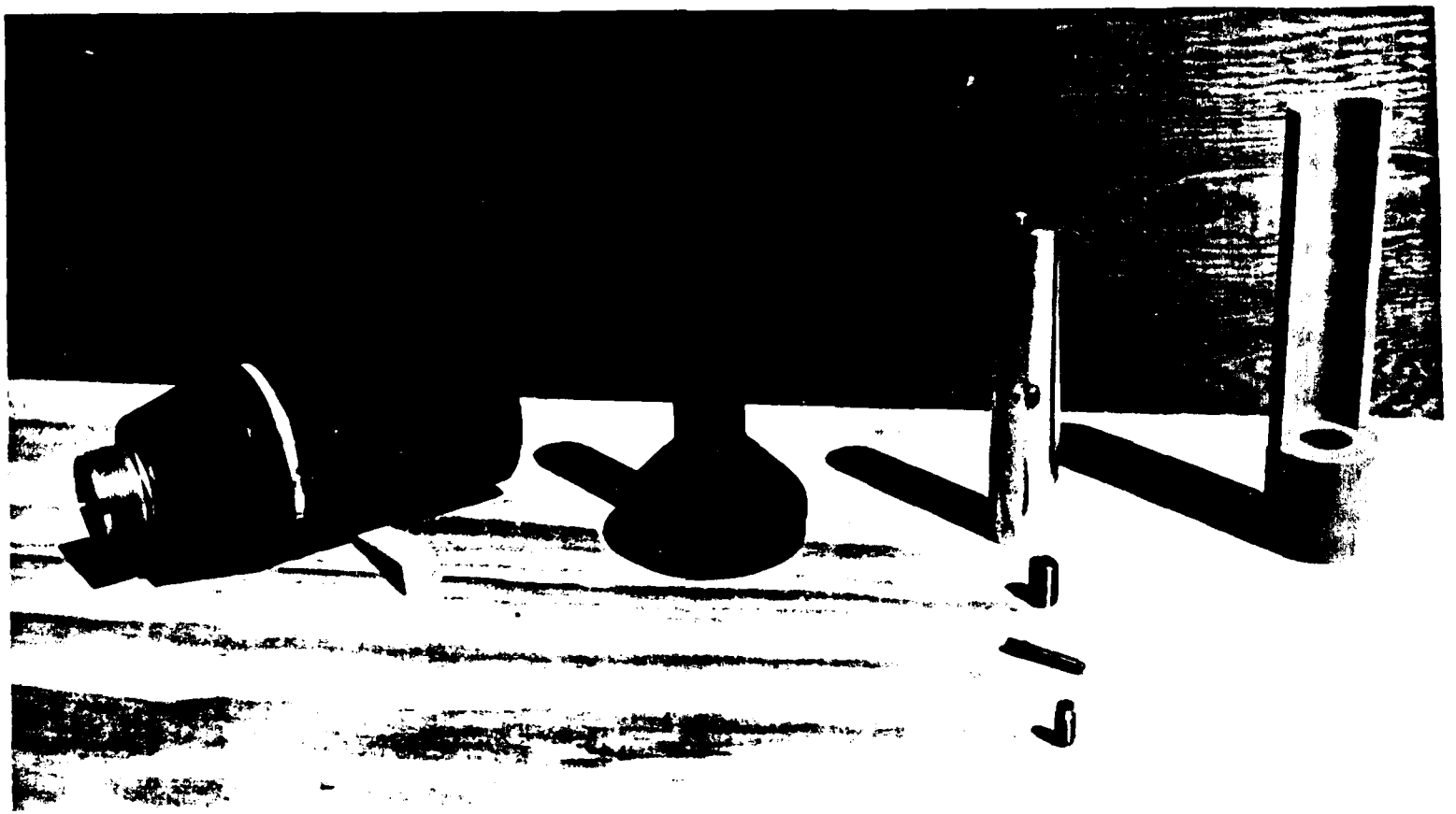

Figure 24. Disassembled view of the warhead, transducer and tube.

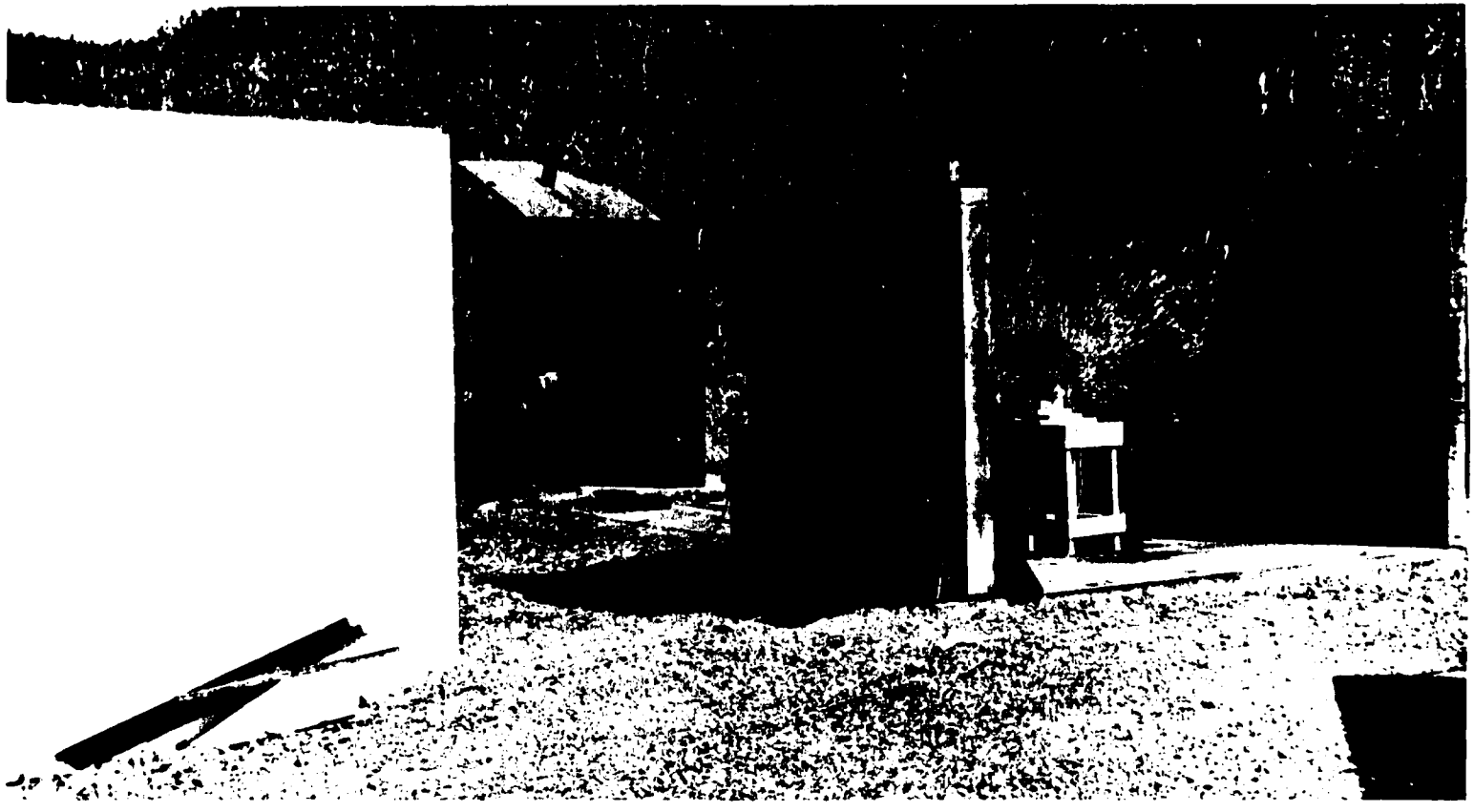

Figure 25. View of the test area behind the explosive barricade.

Figure 26. Photograph of the x-ray heads.

Figure 27. Photograph of the x-ray pulsers.

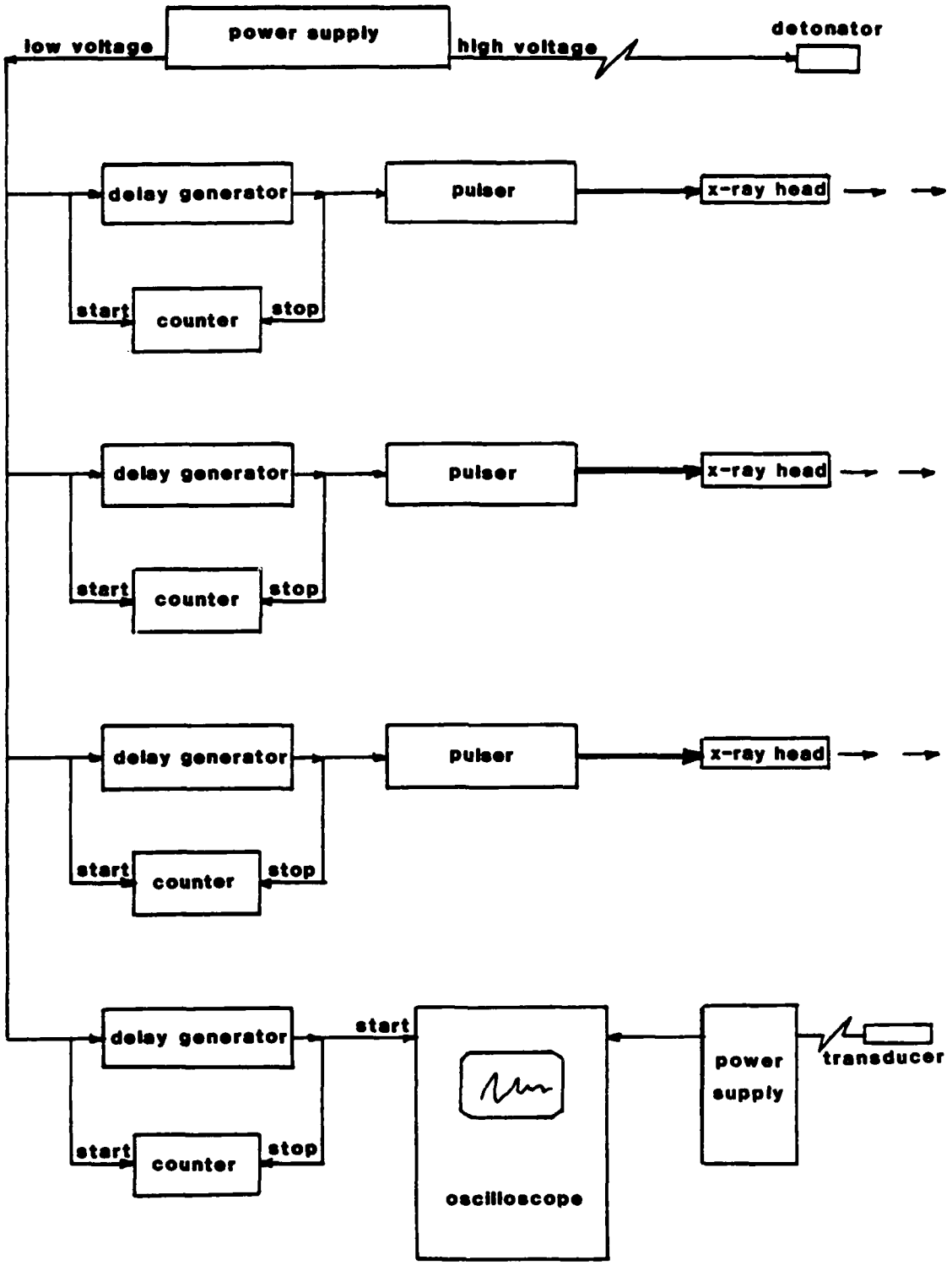

Figure 28. Schematic of the test instrumentation.

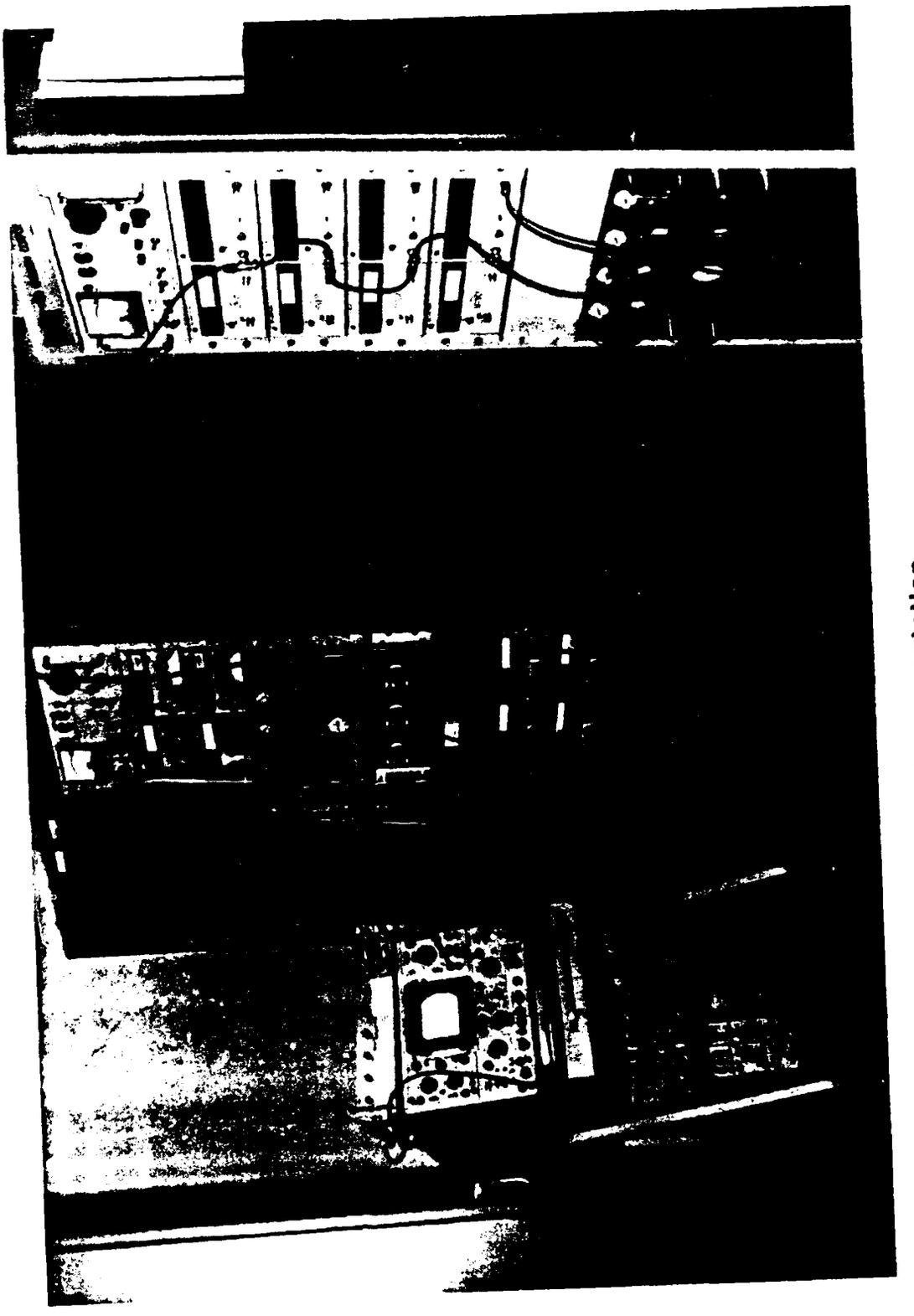

Figure 29. Photograph of the test instrumentation.

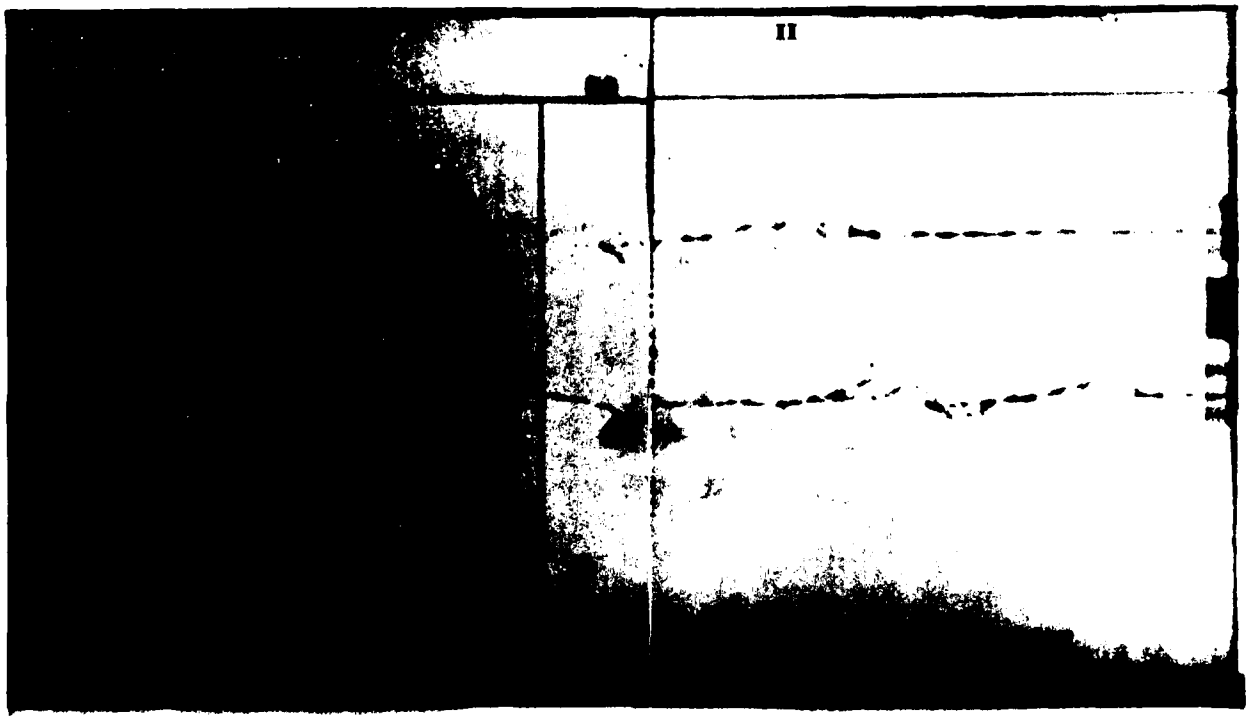

Figure 30. Flash radiograph of the jet from test 11.

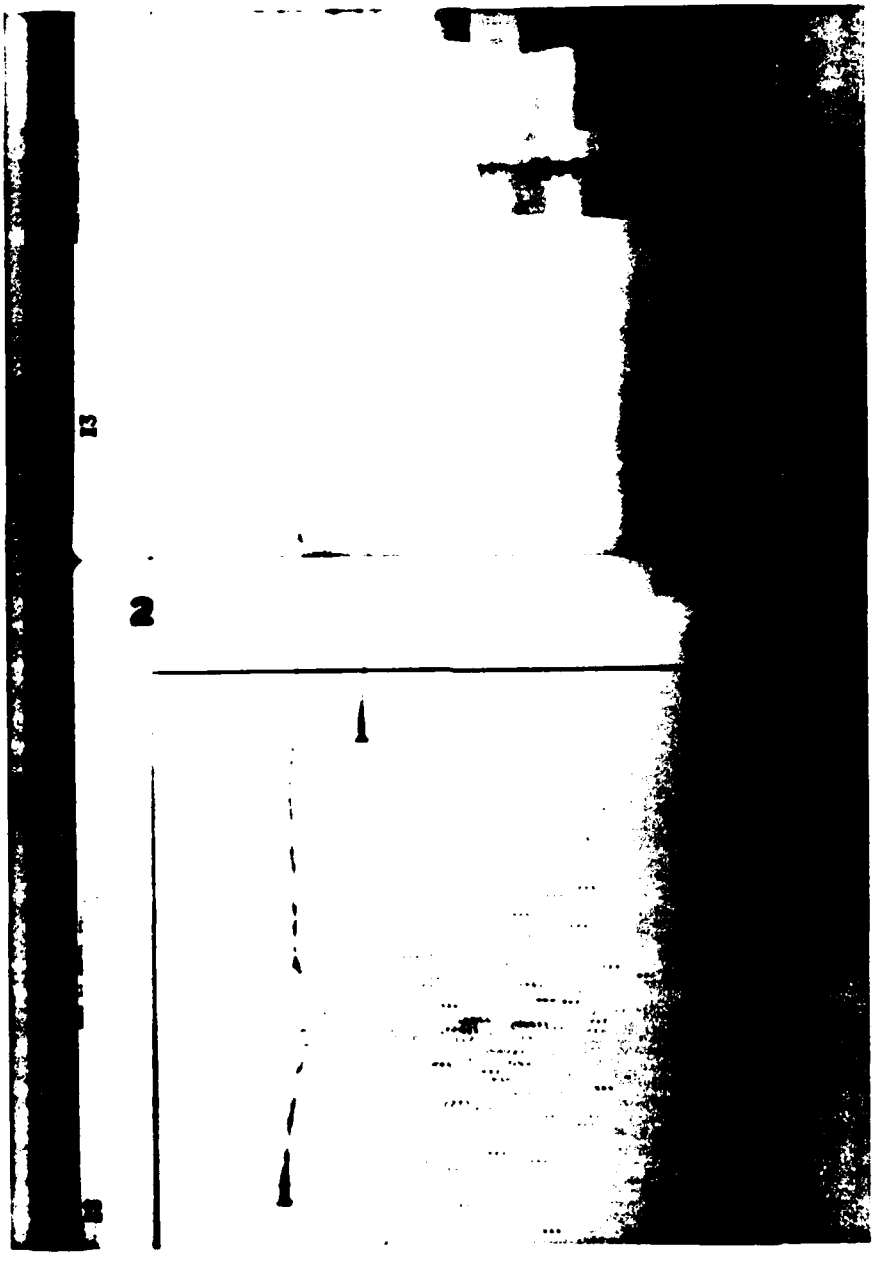

Figure 31. Flash radiograph of the jet from test 13.

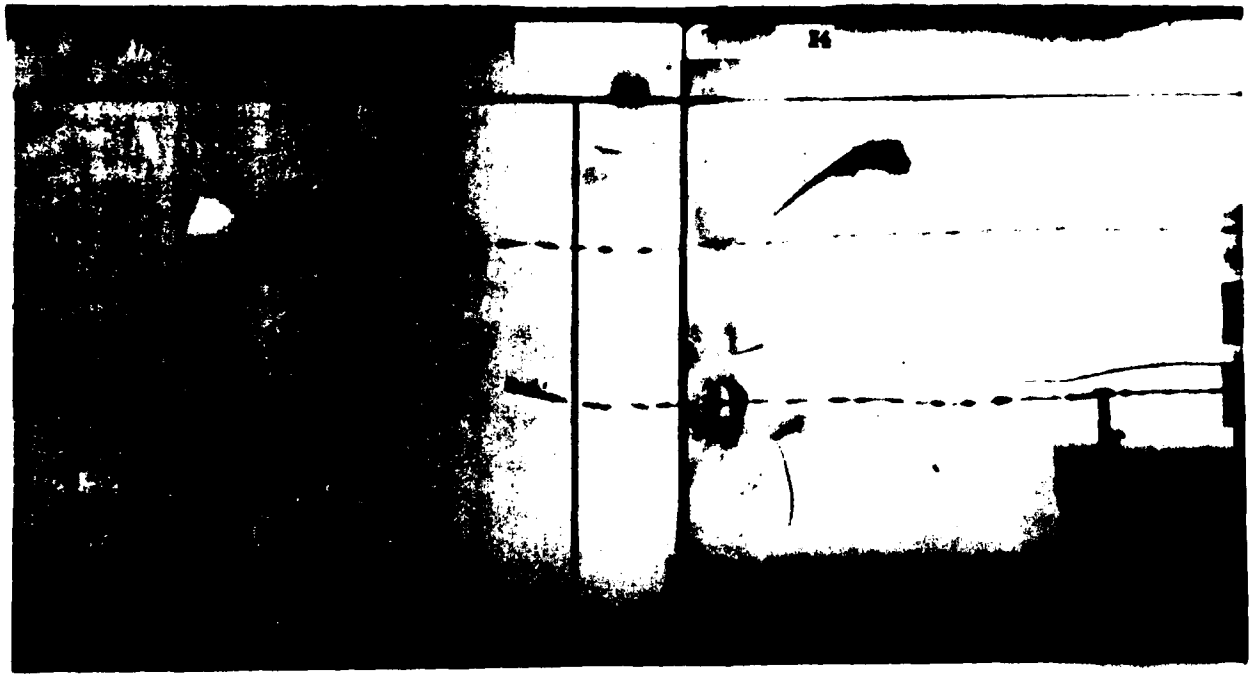

Figure 32. Flash radiograph of the jet from test 14.

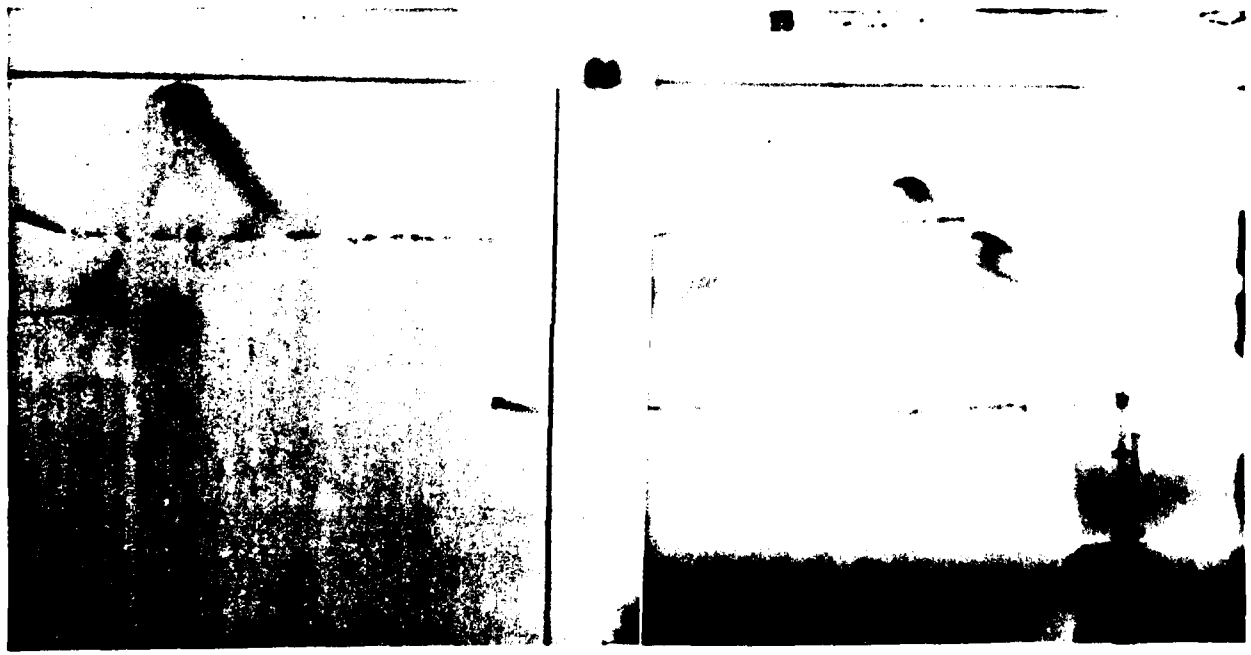

Figure 33. Flash radiograph of the jet from test 15.

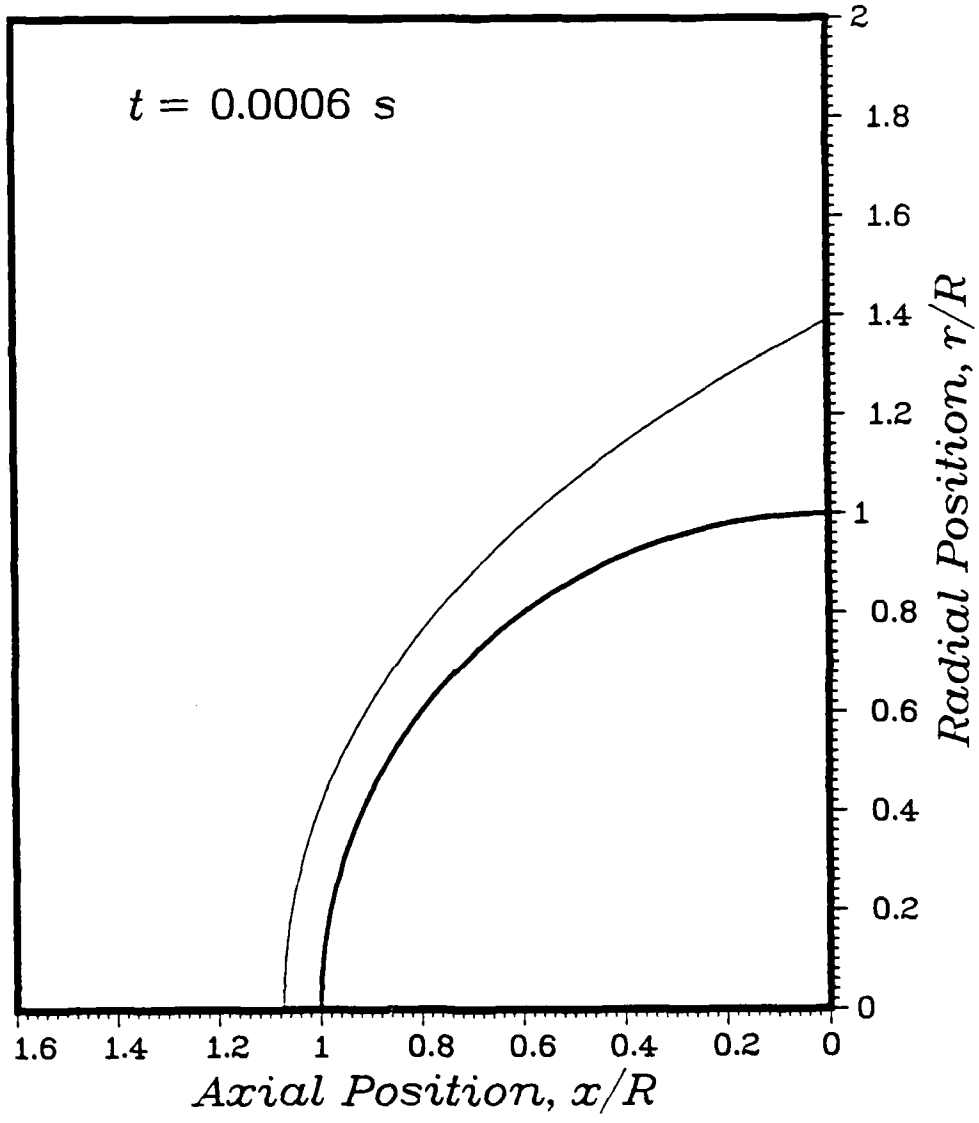

Figure 34. Shock position on the hemisphere, Mach 20.45.

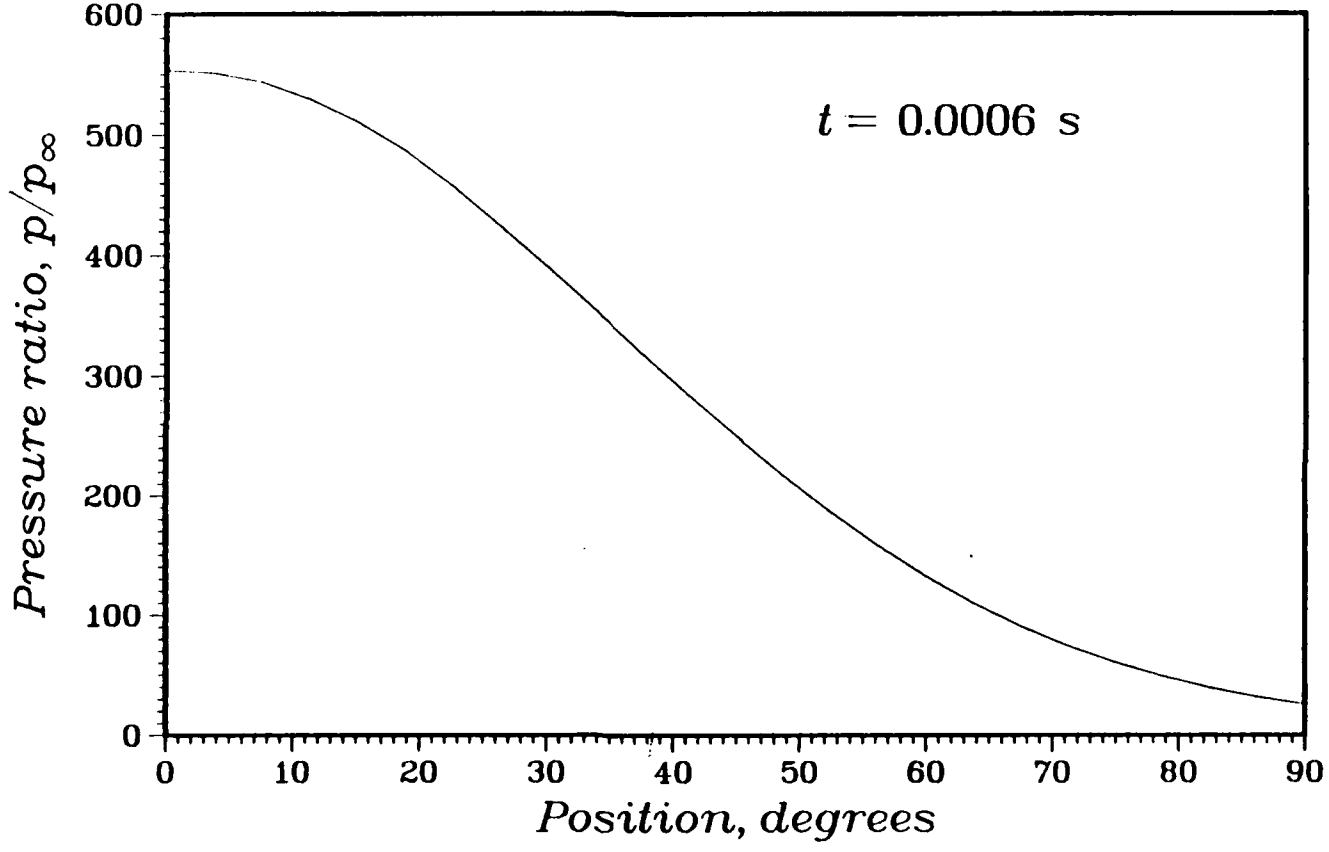

Figure 35. Pressure distribution on the hemisphere, Mach 20.45.

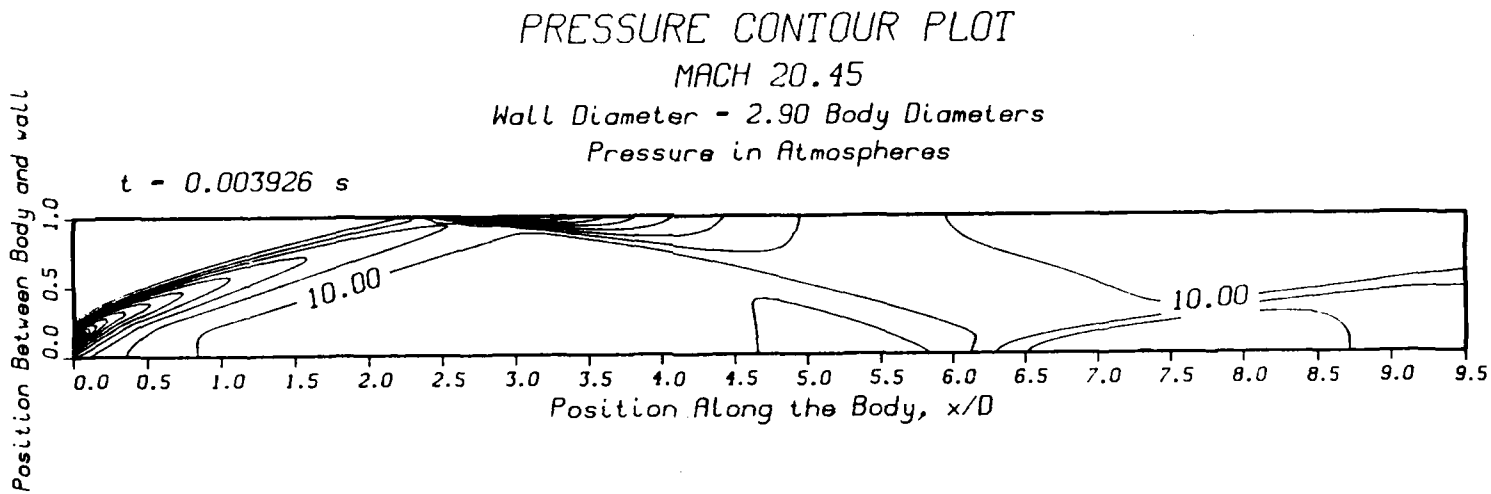

Figure 36. Pressure contours in the annulus, Mach 20.45, D/d = 2.90.

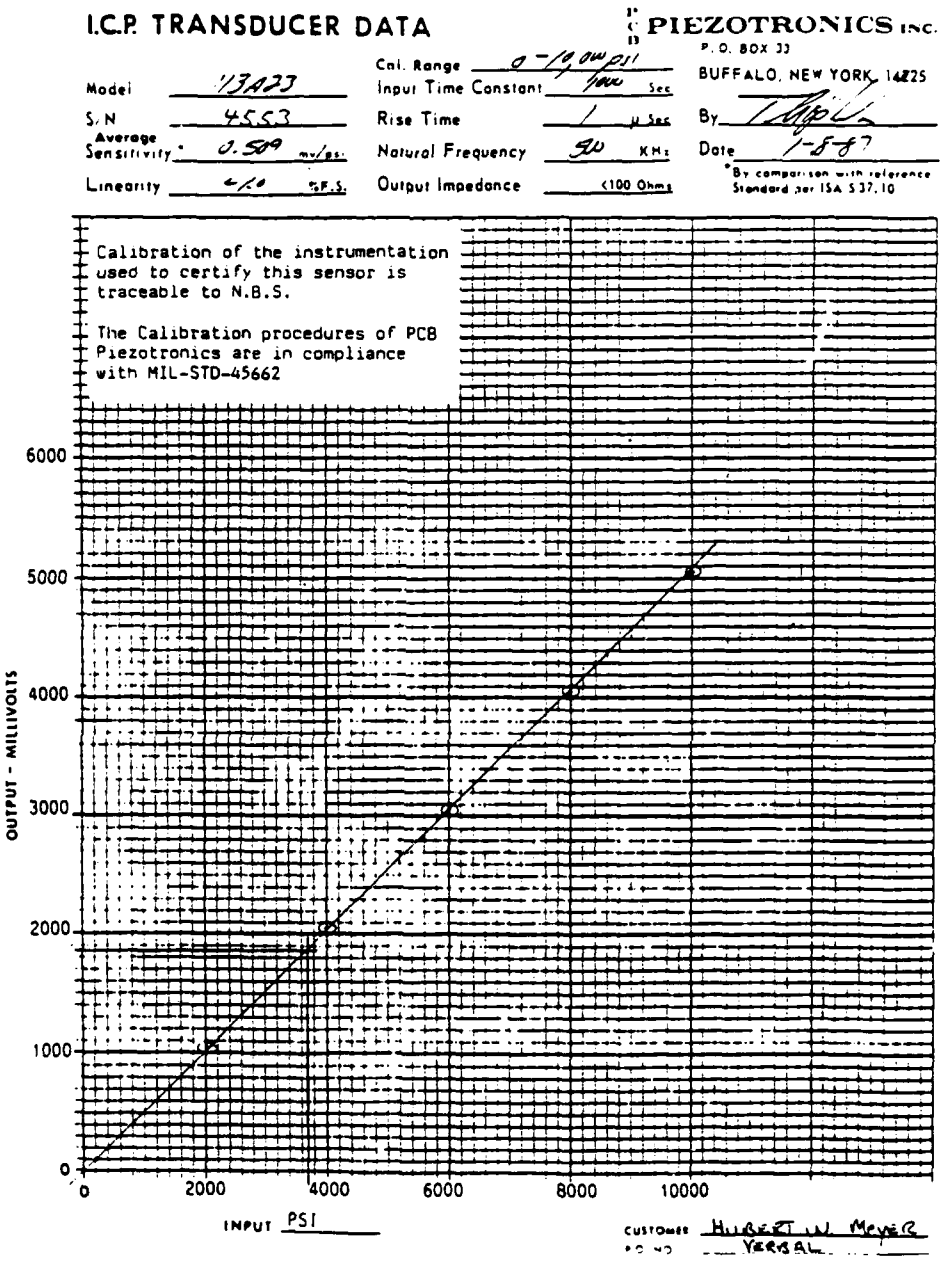

Figure 37. Calibration curve for test 13.

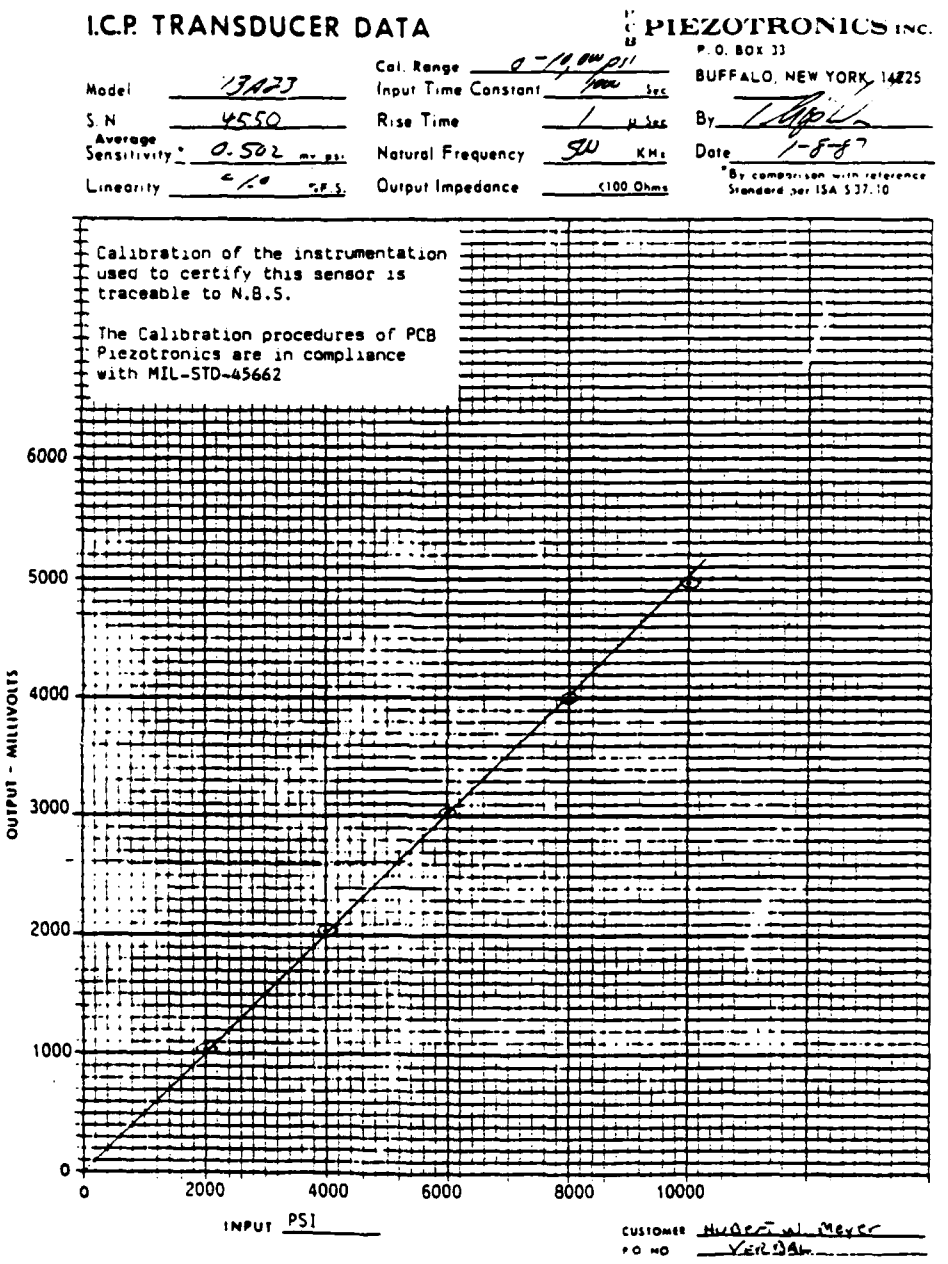

Figure 38. Calibration curve for test 14.

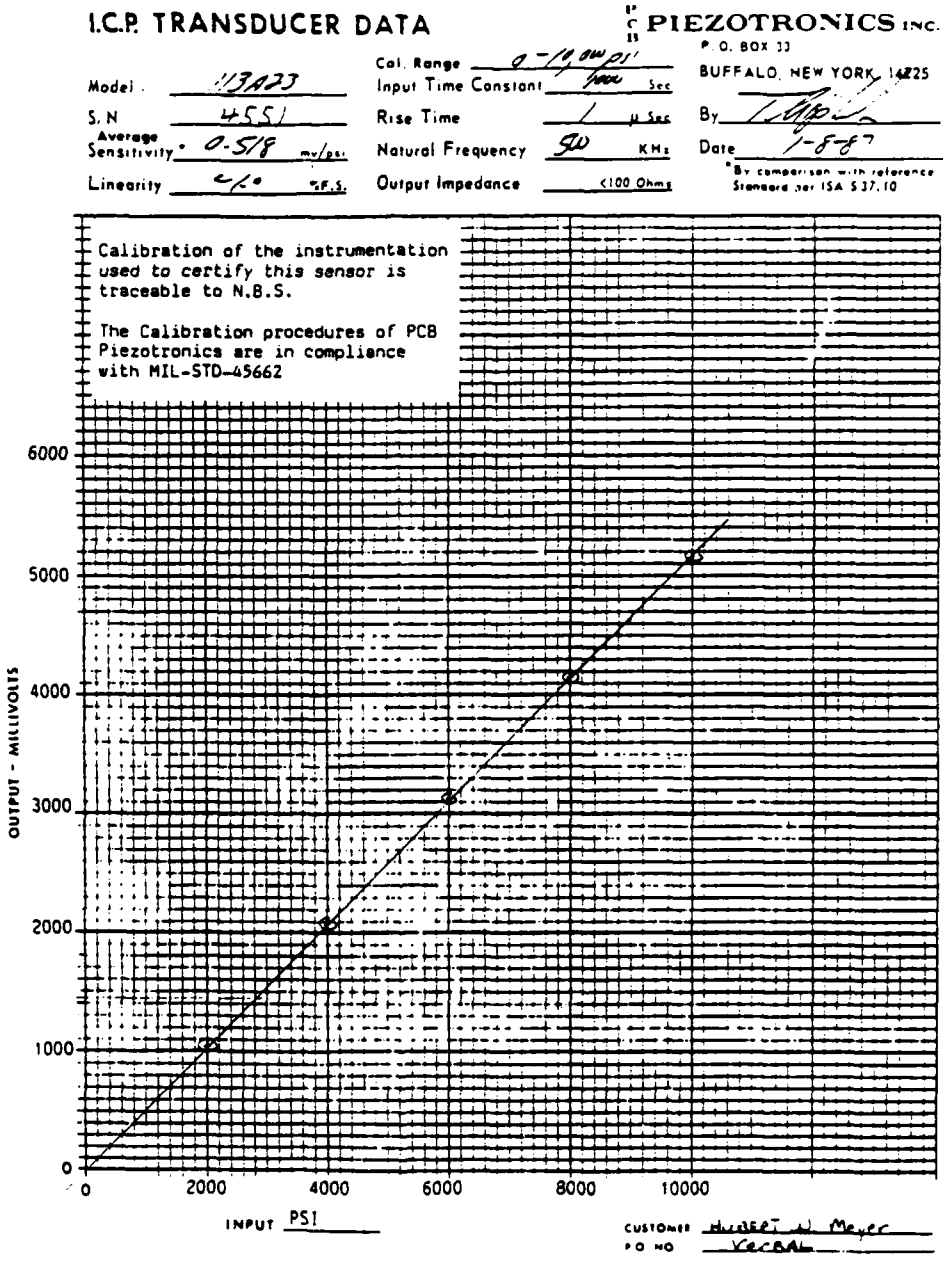

Figure 39. Calibration curve for test 15.

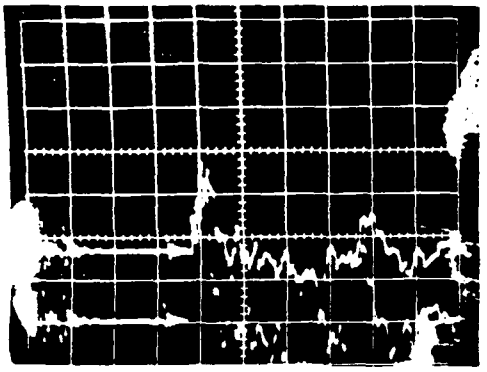

a. Test 13.

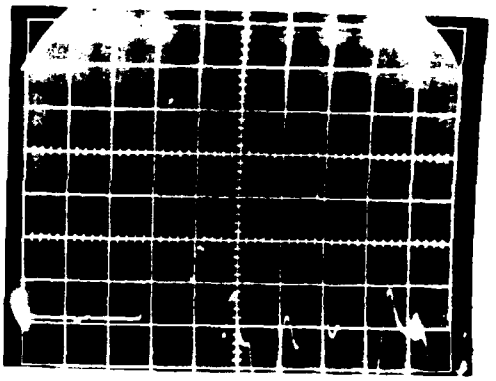

b. Test 14.

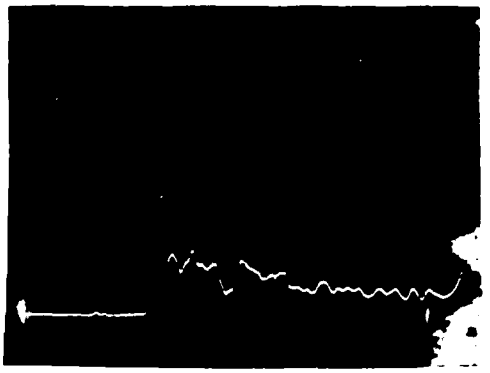

c. Test 15.

Figure 40. Pressure transducer output on an analog oscilloscope.

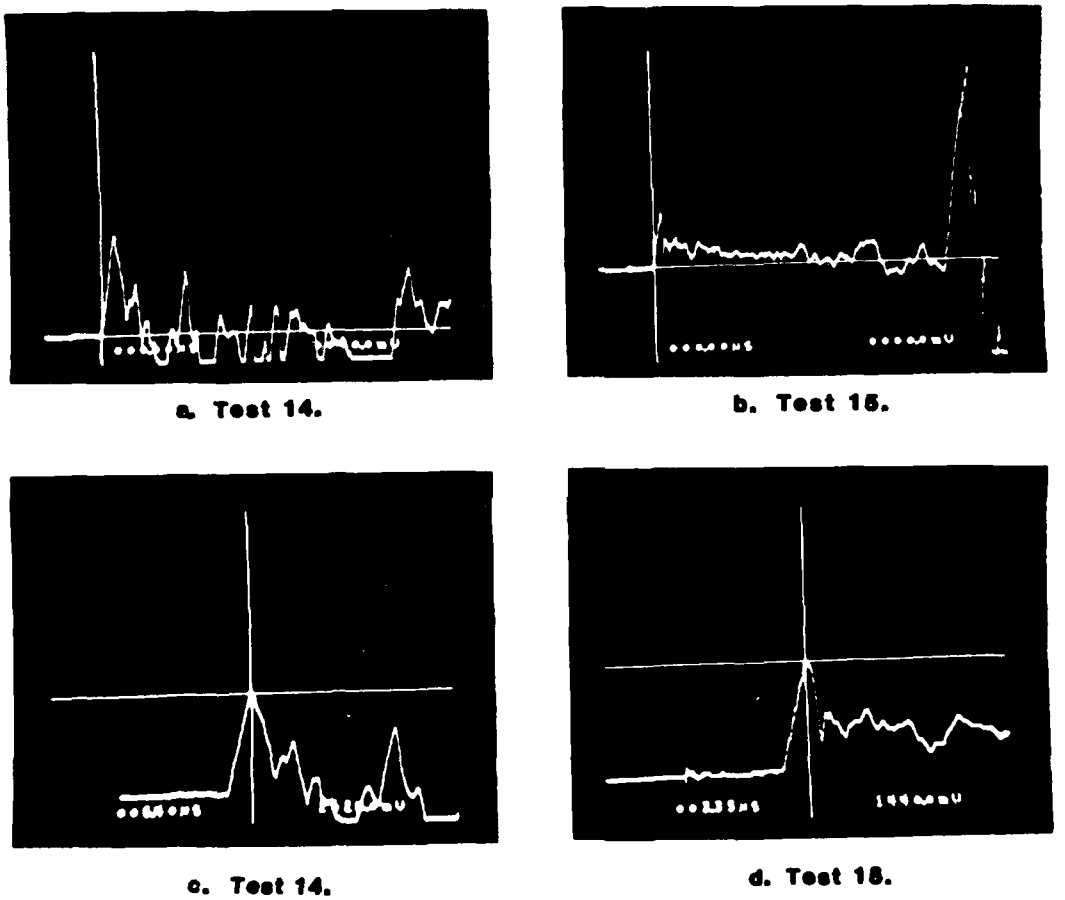

a. Test 14.

b. Test 15.

c. Test 14.

d. Test 18.

Figure 41. Pressure transducer output on a digital oscilloscope.

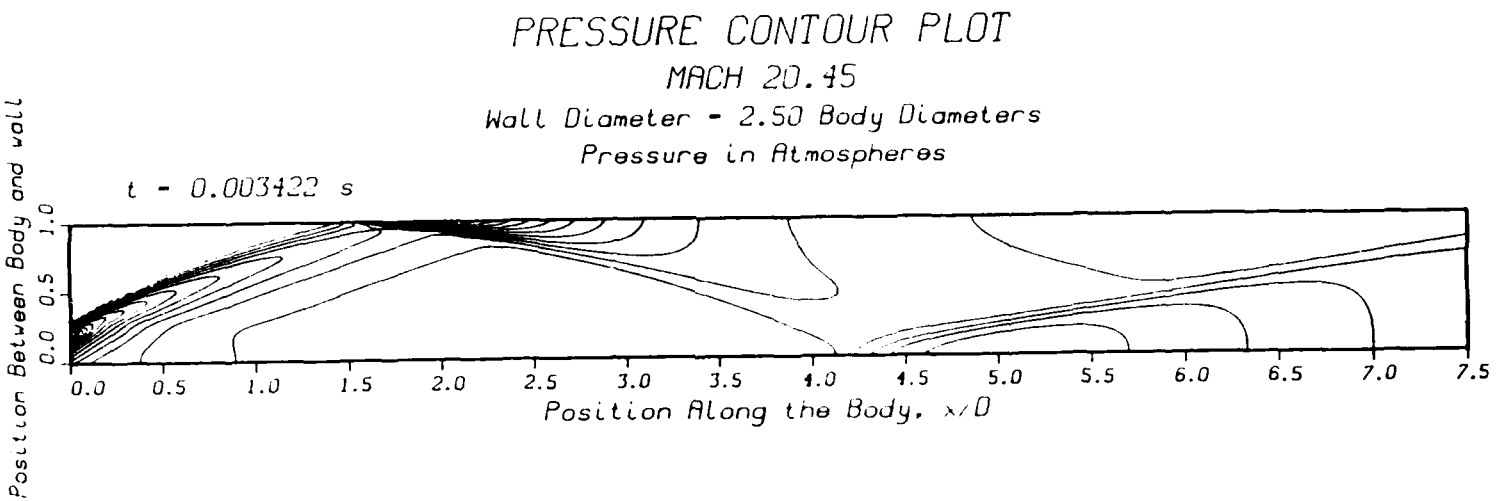

Figure 42. Pressure contours in the annulus, Mach 20.45, D/d = 2.50.

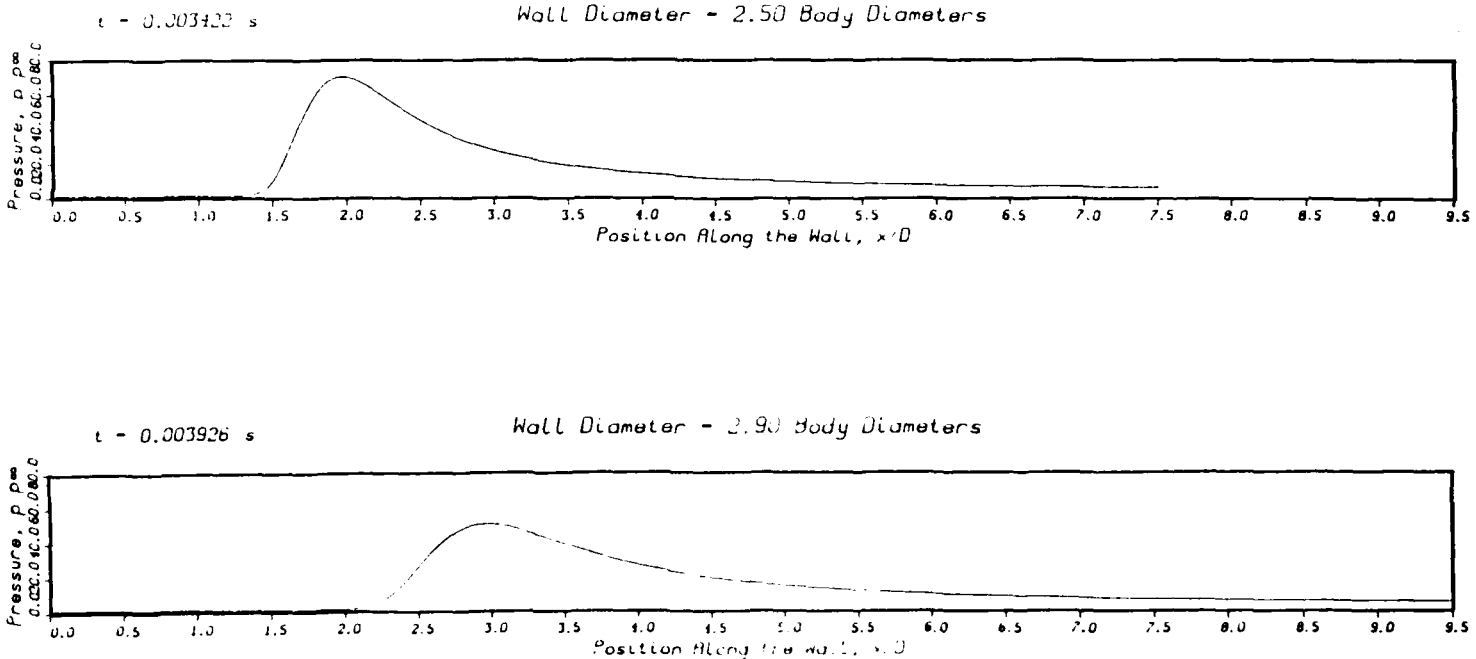

Figure 43. Pressure on the tube wall, Mach 20.45.

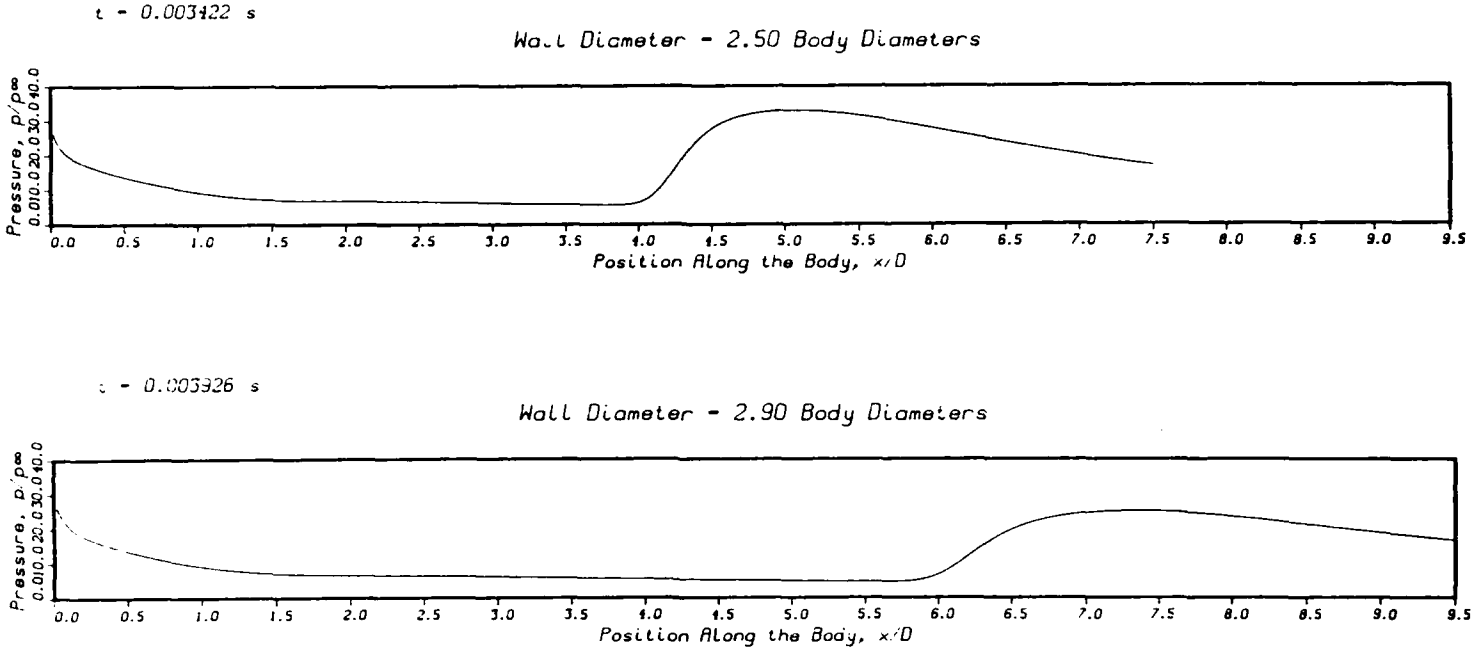

Figure 44. Pressure on the jet, Mach 20.45.

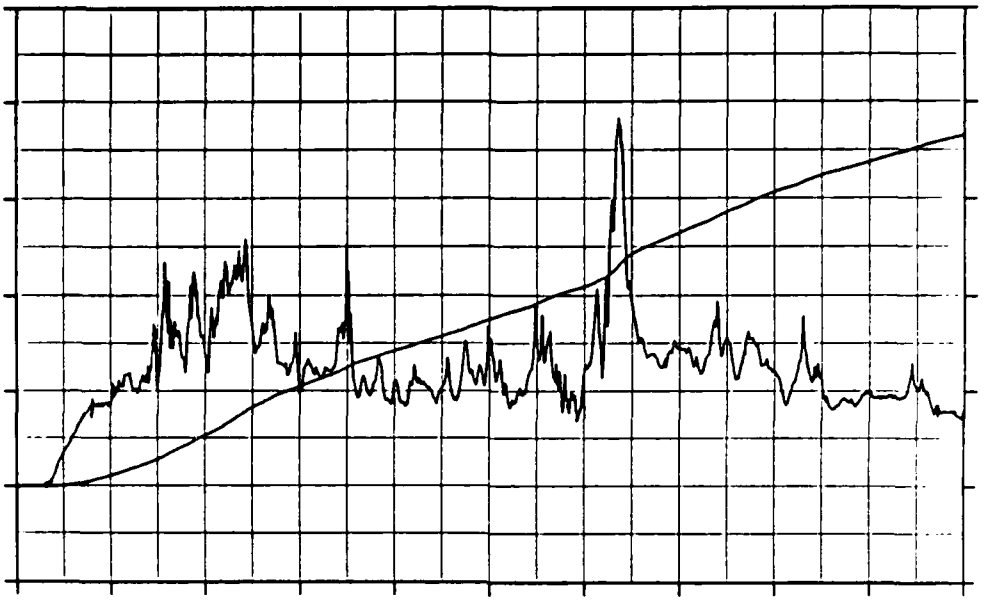

a. Transducer not exposed to dust.

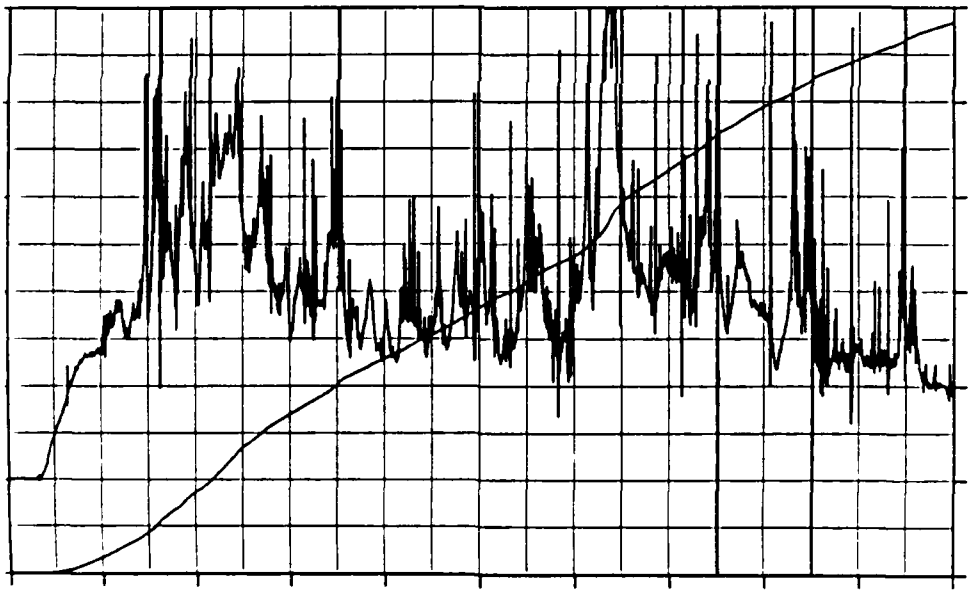

b. Transducer exposed to dust.

Figure 45. Pressure measurement in dusty air, Mach 3.00.

REFERENCES

1. Engineering Design Handbook, AMCP706-170, Headquarters, U.S. Army Materiel Command, Alexandria, VA, 1973.

2. Zernow, L., Garfinkle, D., Buhman, D., and Burchfield, J., "Final Report on the Evaluation of New Armor Concepts (U)", Report No. 220, Shock Hydrodynamics Inc., Sherman Oaks, CA, April 1975.

3. Yen, S.M., "Interactions Between Multiple Objects in a Hypervelocity Flow Regime", Contract DAAK 11-81-C-0011, Aeronautical and Astronautical Engineering Department, Engineering Experiment Station, College of Engineering, University of Illinois, Urbana, IL. June 1983.

4. Widhopf, G. and Schmidt, E., "Time-Dependent Near Muzzle Brake Flow Simulations", AIAA/ASME Third Joint Thermophysics, Fluids, Plasma and Heat Transfer Conference, paper AIAA-82-0973, St. Louis, MO. June 1982.

5. Fansler, K.S., "Gasdynamic Quantities about a Ramjet Projectile while in the Transitional Ballistics Region", AIAA Twelfth Atmospheric Flight Mechanics Conference, paper AIAA-85-1840-CP, Snowmass, CO. August 1985.

6. Peyret, R. and Taylor, T.D., Computational Methods for Fluid Flow, Springer-Verlag, Berlin, 1983.

7. Holt, M., Numerical Methods in Fluid Dynamics, Springer-Verlag, Heidelberg, 1977.

8. Alalykin, G.B., Godunov, S.K., Kireeva, I.L., Pliner, L.H.: Solutions of One Dimensional Problems in Gas Dynamics in Moving Networks, Moscow: NAUKA, 1970.

9. Meyer, H.W. Jr., "A One Dimensional Fluid Dynamics Code Using the Godunov Method", U.S. Army Ballistic Research Laboratory, Aberdeen Proving Ground, MD., in printing.

10. Godunov, S.K., et al., "A Difference Scheme for Two Dimensional Unsteady Problems of Gas Dynamics and Computation of Flow with a Detached Shock Wave". Moscow: Zh. Vychyslitelnoi Mat. i Mat. Fiziki, Vol. I, No. 6, pp. 1020, 1961. Also Cornell Aeronautical Lab translation By I. Bohachevsky.

11. Godunov, S.K., "Finite Difference Method for Numerical Computation of Discontinuous Solutions of the Equations of Fluid Dynamics". Mathematicheskii Sbornik, Vol. 47, No. 3, pp. 271, Moscow, 1959. Cornell Aeronautical Lab translation by I. Bohachevsky.

12. Riemann, B., "Uberdie Fortpflanzung ebener Luftwellen von endlicher Schwingungsweite", Abhandlungen der Gesellschaft der Wissenschaften zu Gottingen, Mathematisch-physikalische Klasse 8, 43 (1860), or Gesammelte Werke, 1876, pp. 144.

13. Courant, R. and Friedrichs, K.O., Supersonic Flow and Shock Waves, Interscience Publishers, Inc., New York, 1948.

14. Sod, G.A., "A Survey of Several finite Difference Methods for Systems of Nonlinear Hyperbolic Conservation Laws". Journal of Computational Physics 27, pp. 1-31, (1978).

15. Taylor, T.D., Ndefo, E. and Masson, B.S., "A Study of Numerical Methods for Solving Viscous and Inviscid Flow Problems". Journal of Computational Physics 9, pp. 99-119, (1972).

16. Von Neumann, J. and Richtmyer, R.D., "A Method for the Numerical Calculation of Hydrodynamic Shocks". Journal of Applied Physics, Vol. 21, pp. 232, (1950).

17. Moretti, G., "Importance of Boundary Conditions in the Numerical Treatment of Hyperblic Equations". The Physics of Fluids Supplement II, pp. 13, (1969).

18. Meyer, R.E., Introduction to Mathematical Fluid Dynamics, John Wiley & Sons, Inc., New York, 1971.

19. Roe, P. L., "Approximate Riemann Solvers, Parameter Vectors, and Difference Schemes". Journal of Computational Physics 43, pp. 357-372, (1981).

20. Chakravarthy, S.R. and Osher, S., "A New Class of High Accuracy TVD Schemes for Hyperbolic Conservation Laws". AIAA 23rd Aerospace Sciences Meeting, paper AIAA-85-0363, Reno, NV. January 1985.

21. Osher, S., "Numerical Solution of Singular Perturbation Problems and Hyperbolic Systems of Conservation Laws," North Holland Mathematical Studies No. 47, Ed. S. Axelsson, L.S. Frank, and A. van der Sluis, pp. 179-205.

22. Greenberg, M. D., Foundations of Applied Mathematics, Prentice-Hall, Inc., Englewood Cliffs, NJ. 1978.

23. Masson, B.S., Taylor, T.D.,and Foster, R.M., "Application of Godunov's Method to Blunt-Body Calculations". AIAA Journal, Vol. 7, No. 4, pp. 694-698, April 1969.

24. White, Frank M., Viscous Fluid Flow, 2nd ed., McGraw-Hill Inc., New York, 1974.

25. Chorin, A. J., "Random Choice Solution of Hyperbolic Systems". Journal of Computational Physics 22, pp. 517-533, 1976.

26. Scarborough, J.B., Numerical Mathematical Analysis, John Hopkins Press, 4th ed., Baltimore, 1958.

27. Pizer, S.M., Numerical Computing and Mathematical Analysis, Science Research Associates, Inc., Chicago, 1975.

28. Ostrowski, A.M., Solution of Equations and Systems of Equations, Academic Press, 2nd ed., New York, 1966.

29. Van Leer, B., "Towards the Ultimate Conservative Difference Scheme. V. A Second-Order Sequel to Godunov's Method". Journal of Computational Physics 32, pp. 101-136, 1979.

30. Richtmyer, R.D. and Morton, K.W., Difference Methods for Initial-Value Problems, John Wiley & Sons, 2nd ed., New York, 1967.

31. Taylor, T.D. and Lin, T.C., "Numerical Model for Muzzle Blast Flowfields". AIAA Journal, Vol. 19, No. 3, pp. 346-349, March 1981.

32. Bohachevsky, I. O., "A Direct Method for Computation of Nonequilibrium Flows with Detached Shock Waves". AIAA Journal, Vol. 4, No. 4, pp. 600-607, April 1966.

33. Belotserkovskiy, O.M., ed., Supersonic Gas Flow Past Blunt Bodies; Theoretical and Experimental Studies, USSR Academy of Sciences, Transactions of the Computation Center, Sochi, May 1967. Also U.S. Army Foreign Science and Technology Center translation, FSTC-HT-23-447-68.

34. Bagrynovskii, K.A. and Godunov, S.K., "Difference Schemes for Many Dimesional Problems". Doklady A. N., U.S.S.R., Vol. 115, No. 3, pp. 431-433, 1957. Also Cornell Aeronautical Lab translation by I. O. Bohachevsky.

35. Godunov, S.K. and Ryabenki, V.S., Theory of Difference Schemes, North-Holland Publishing Company, Amsterdam, 1964.

36. Salas, M.D., "Flow Properties for a Spherical Body at Low Supersonic Speeds". Symposium on Computer in Aerodynamics, Twenty-Fifth Anniversary of Aerodynamics Laboratories, Polytechnic Institute of New York, Long Island Center, Farmingdale, New York, June 1979.

37. Taylor, T.D. and Masson, B.S., "Application of the Unsteady Numerical Method of Godunov to Computation of Supersonic Flows Past Bell-Shaped Bodies". Journal of Computational Physics 5, pp. 443-454, (1970).

38. Liepman H.W., and Roshko, A., Elements of Gas Dynamics, John Wiley and Sons, Inc., New York, 1957.

39. Belotserkovskii, O.M., "On the Calculation of Flow Past Axi-symmetric Bodies with Detached Shock Waves Using an Electronic Computing Machine". Prikl. Math. i Mech. Vol. 24, No. 3, pp. 511-517, 1960. (translation)

40. Hayes, W.E. and Probstein, R.F., Hypersonic Flow Theory, Academic Press, New York, 1959.

41. Anderson, J.D. Jr., Modern Compressible Flow, McGraw-Hill Book Company, New York, 1982.

42. Woodward, P. and Colella, P., "High Resolution Difference Schemes for Compressible Gas Dynamics". 7th Int'l Conf. on Numerical Methods in Fluid Dynamics, pp. 434-441, (1981).

43. Hansen, C F., "Approximations for the Thermodynamic and Transport Properties of High-Temperature Air", NASA TR-R-50, 1959.

44. Deschambault, Robert, "An Equation of State for Real Air", Version 1.2, Institute for Aerospace Studies, University of Toronto, June 1980.

45. Colella, P. and Glaz, H.M., "Efficient Solution Algorithms for the Riemann Problem for Real Gases". Journal of Computational Physics 59, pp. 264-289, (1985).

46. Backofen, J.E. Jr., "Shaped Charge Jet Aerodynamics, Particulation and Blast Field Modeling", Proceedings from the Tenth International Symposium on Ballistics, San Diego, CA., October 1987.

47. Rosenblatt, M. and Schlamp, R., "Misty Picture Real Surface Airblast Predictions", CRT-TM-3780-2, California Research and Technology, Inc., Chatsworth, California, September 1986.

48. Ethridge, N., Aberdeen Research Corporation, private communication, 30 July 1987.

APPENDIX A

PROGRAM LISTING FOR THE SPHERE PROBLEM

```
*COMDECK COMMON
      LOGICAL RESTART
      INTEGER T,T1,TSTEPS,TLAST
      CHARACTER PROBLEM*13
      PARAMETER (NT=25,MT=8,TSTEPS=500)
      COMMON / HWM / U(0:NT+1, 0:MT,0:1), V(0:NT+1, 0:MT,0:1),
     +               W(0:NT+1, 0:MT,0:1), R(0:NT+1, 0:MT,0:1),
     +               W1(0:NT+1, 0:MT,0:1), W2(0:NT+1, 0:MT,0:1),
     +               W3(0:NT+1, 0:MT,0:1), W4(0:NT+1, 0:MT,0:1),
     +               E(0:NT+1, 0:MT,0:1), UR(0:NT+1, 0:MT),
     +               P(0:NT+1, 0:MT,0:1), ER(0:NT+1, 0:MT),
     +               VR(0:NT+1, 0:MT),    WR(0:NT+1, 0:MT),
     +               RR(0:NT+1, 0:MT),    PR(0:NT+1, 0:MT),
     +               UT(0:NT+1, 0:MT),    VT(0:NT+1, 0:MT),
     +               WT(0:NT+1, 0:MT),    RT(0:NT+1, 0:MT),
     +               PT(0:NT+1, 0:MT),    ET(0:NT+1, 0:MT)
      COMMON / HWM1 /
     +               Y(0:NT+1, 0:MT),     RL(0:NT+1, 0:MT,0:1),
     +               SR(0:NT+1, 0:MT),    ST(0:NT+1, 0:MT),
     +               Q(0:NT+1, 0:MT),     PHI(0:NT+1, 0:MT),
     +               DPOS(0:NT+1, 0:MT),  PCD(0:50), FPCD(0:50),
     +               TT(8),THETA(0:NT+1),RESTART,T1,VELGRAD(3,MT),
     +               OMEGA(0:NT+1, 0:MT), AREA(0:NT+1, 0:MT,0:1),
     +               DPOST(0:NT+1, 0:MT), RADIUS(0:NT+1, 0:MT),
     +               DNEGT(0:NT+1, 0:MT), DPOSR(0:NT+1, 0:MT),
     +               DNEGR(0:NT+1, 0:MT), GAMMA,PMIN,UINF,VINF,RINF,
     +               PINF, EINF, TINF, DELTA, TAU, T, TIME, XMACH,
     +               TEMP(0:NT+1,0:MT+1), SONIC(0:NT+1,0:MT+1),
     +               G5(0:NT+1,0:MT+1),   G6(0:NT+1,0:MT+1), GMAX, GMIN
*DECK AXIS
      PROGRAM AXIS
*CALL COMMON
C THIS PROGRAM COMPUTES PROPERTIES IN THE SHOCK LAYER OF A HEMISPHERE
C LIST OF VARIABLES
C
C U,V,R,P,E: AXIAL VELOCITY, RADIAL VEL, DENSITY, PRESSURE, TOT ENERGY
C UINF,VINF,RINF,PINF,EINF,TINF: U,V,R,P,E,TEMP OF FREE STREAM AIR
C UR,VR,RR,PR,ER: PROPERTIES (AS ABOVE) ON RADIAL BOUNDARIES (RIEMANN)
C UT,VT,RT,PT,ET: PROPERTIES ON CIRCUMFERENTIAL BOUNDARIES (RIEMANN)
C W,W1,W2,W3,W4: FLUID VEL COMPONENT NORMAL TO THE BOUNDARY
C Y: FLUID VELOCITY COMPONENT PARALLEL TO THE BOUNDARY
C RL: POSITION OF NODES MEASURED FROM SPHERE CENTER ALONG RAYS
C SR,ST: LENGTH OF RADIAL AND CIRCUMFERENTIAL BOUNDARIES
C PHI: ANGLE BETWEEN NEGATIVE X AXIS AND CIRCUMFERENTIAL BOUNDARY
C THETA: ANGLE BETWEEN NEGATIVE X AXIS AND RADIAL BOUNDARY
C DPOSR: ABSOLUTE VEL OF POSITIVE RUNNING WAVE FOR RADIAL BOUNDARIES
C DNEGR: ABSOLUTE VEL OF NEGATIVE RUNNING WAVE FOR RADIAL BOUNDARIES
C DPOST: ABSOLUTE VEL OF POSITIVE RUNNING WAVE FOR CIRCUM BOUNDARIES
C DNEGT: ABSOLUTE VEL OF NEGATIVE RUNNING WAVE FOR CIRCUM BOUNDARIES
C OMEGA: VELOCITY OF NODES ALONG THE RAY
C Q: VELOCITY OF CIRCUMFERENTIAL BOUNDARIES
C AREA, RADIUS: CELL AREA AND DISTANCE OF CENTROID TO X AXIS
C VELGRAD: RATIO OF V/R (RADIAL VEL/RADIUS) AT THE AXIS OF SYMMETRY
```

```
C T: TIME STEP INDEX
C TAU: LENGTH OF TIME STEP IN SECONDS
C TIME: ELAPSED TIME IN SECONDS
C TSTEPS: NUMBER OF TIME STEPS TO BE COMPUTED
C TEMP: AIR TEMPERATURE IN KELVINS
C SONIC: SPEED OF SOUND IN THE AIR
C G5,G6: REAL GAS CONSTANTS, REPLACE GAMMA=1.4, SEE SUBR FLUX FOR DEFT
C GMAX,GMIN: MAXIMUM AND MINIMUM VALUES FOR G5 AND G6
C PMIN: MINIMUM ALLOWABLE PRESSURE IN RIEMANN ITERATIONS
C A,B: MASS VEL OF NEG AND POS RUNNING WAVE IN RIEMANN PROBLEM
C NT: NUMBER OF CELLS IN THE THETA DIRECTION
C MT: NUMBER OF CELLS IN THE RADIAL (R) DIRECTION
C
C CONSTANTS
      GAMMA=1.4
      GMAX=1.667
      GMIN=1.000
      PMIN=1.
C
C IF RESTARTING A PREVIOUS RUN, SET RESTART EQUAL TO TRUE.
      RESTART=.TRUE.
C     RESTART=.FALSE.
C FREE STREAM CONDITIONS
      MACH=24
      UINF=376.59*REAL(MACH)
      VINF=0.
      RINF=1.0
      PINF=101300.
      TINF=293.
C THE FREE STREAM AIR IS AT STANDARD ATMOSPHERIC CONDITIONS, SO IT
C CAN BE CONSIDERED IDEAL.  THEREFORE, EINF AND XMACH ARE:
      EINF=PINF/((GAMMA-1.)*RINF)+(UINF**2.+VINF**2.)/2.
      XMACH=UINF/SQRT(GAMMA*PINF/RINF)
C
C OUTPUT DESCRIPTION
C TAPE3: THEORETICAL PRESSURE AND DENSITY BEHIND THE SHOCK WAVE
C TAPE5: COMPUTATIONAL DATA (U,V,R,P,E,UR,...UT,...RL,ETC)
C TAPE6: DATA USED FOR INPUT TO CYLINDRICAL PORTION OF PROBLEM
C TAPE 24: MAIN OUTPUT - ALSO RESTART FILE
C
C
C
*****************************************************************************
C
C MAIN COMPUTATION
C
C
*****************************************************************************
C
C
      IF (RESTART) THEN
C     READ (24,113) T1,TAU,TIME
      READ (24,113) T1,TAU,TIME,UINF,VINF,RINF,PINF,TINF
```

```
      ELSE
      T1=0
      TAU=1.E-7
      TIME=0.
      END IF
      PRINT*, 'PROGRAM IS RUNNING...'
      CALL IC
      DO 1 T=1,TSTEPS
      IF (MOD(T,100).EQ.0) PRINT*, 'T=',T
      TIME=TIME+TAU
C
      CALL GRID
      CALL SHOCK
      CALL RAY
      CALL ARC
      CALL BODY
      CALL FLUX
      CALL TIMESTP
      CALL UPDATE
    1 CONTINUE
C
C COMPUTE THEORETICAL CONDITIONS BEHIND THE SHOCK WAVE
      CALL GRID
      WRITE (3,10) TIME
      DO 2 N=1,NT
      XMACHN=XMACH*SIN(PHI(N-1,0))
      DENSITY=((GAMMA+1.)*(XMACHN**2.))/((GAMMA-1.)*(XMACHN**2.)+2.)
      DN=1./(GAMMA*((2./(GAMMA-1.))+XMACH**2.))
      PRESSUR=DN*(1.+(2.*GAMMA*((XMACHN**2.)-1.))/(GAMMA+1.))
      WRITE (3,11) N,DENSITY,PRESSUR
    2 CONTINUE
C
   10 FORMAT (1X,E14.7)
   11 FORMAT (1X,I5,2F10.4)
  113 FORMAT (1X,I5,7E16.9)
      END
C
C
C
*******************************************************************************
C
      SUBROUTINE IC
C
C
*******************************************************************************
C
*CALL COMMON
      DATA (RL(N,0,0),N=0,NT) / 1.10, NT*1.10 /
      IF (RESTART) THEN
      READ (24,301) ((I,J,U(N,M,0),V(N,M,0),R(N,M,0),P(N,M,0),E(N,M,0),
     +RL(N,M,0),G5(N,M),G6(N,M),TEMP(N,M),M=0,MT),N=0,NT)
      ELSE
C INITIAL CONDITIONS IN ALL CELLS ARE THOSE OF THE FREE STREAM
```

```
      DO 31 N=1,NT
      DO 32 M=0,MT
      G5(N,M)=1.4
      G6(N,M)=1.4
      U(N,M,0)=UINF
      V(N,M,0)=VINF
      R(N,M,0)=RINF
      P(N,M,0)=PINF
      E(N,M,0)=EINF
      TEMP(N,M)=TINF
   32 CONTINUE
   31 CONTINUE
      END IF
  301 FORMAT (1X,2I2,9E14.7)
      RETURN
      END
C
C
C
*******************************************************************************
C
      SUBROUTINE GRID
C
C *******************************************************************************
C
*CALL COMMON
C
      TN=REAL(NT)
      DELTA=3.14159265359/(2.*(TN-1.))
      DO 17 N=0,NT
      RN=REAL(N)
      THETA(N)=((2.*RN)-1.)*DELTA/2.
   17 CONTINUE
C
      DO 11, N=0,NT
      DO 12, M=0,MT
      IF (T.EQ.1) THEN
      RL(N,M,0)=RL(N,0,0)-(REAL(M)/REAL(MT))*(RL(N,0,0)-1.)
      END IF
      IF (M.EQ.0) GO TO 12
      SR(N,M)=RL(N,M-1,0)-RL(N,M,0)
   12 CONTINUE
   11 CONTINUE
C
      DO 14 N=1,NT
      DO 13 M=0,MT
      H1=RL(N,M,0)*SIN(THETA(N))-RL(N-1,M,0)*SIN(THETA(N-1))
      H2=RL(N-1,M,0)*COS(THETA(N-1))-RL(N,M,0)*COS(THETA(N))
      ST(N,M)=SQRT(H1**2.+H2**2.)
      IF (H2.GT.0.) THEN
      PHI(N-1,M)=3.1415926535898-ARCSIN(H1/ST(N,M))
      ELSE
      PHI(N-1,M)=ARCSIN(H1/ST(N,M))
```

```
      END IF
   13 CONTINUE
   14 CONTINUE
C
      DO 15 N=1,NT
      DO 16 M=1,MT
      AREA(N,M,0)=.5*((RL(N-1,M-1,0)*RL(N,M-1,0))-(RL(N-1,M,0)*RL(N,M,0
     +)))*SIN(DELTA)
      RADIUS(N,M)=.25*(RL(N,M-1,0)+RL(N,M,0))*SIN(THETA(N))+
     +.25*(RL(N-1,M-1,0)+RL(N-1,M,0))*SIN(THETA(N-1))
      IF (N.EQ.1) RADIUS(N,M)=0.
   16 CONTINUE
   15 CONTINUE
      END IF
C
      RETURN
      END
C
C
C ***********************************************************************
C
      SUBROUTINE RAY
C
C ***********************************************************************
C
*CALL COMMON
C THIS SUBROUTINE COMPUTES THE RIEMANN PROBLEM ON RADIAL (RAY)
C BOUNDARIES
C
      DO 42 N=1,NT-1
      DO 43 M=1,MT
C VEL COMPONENTS NORMAL (W) AND TANGENTIAL (Y) TO RADIAL BOUNDARY (N,M)
      W1(N,M,0)=U(N,M,0)*SIN(THETA(N))+V(N,M,0)*COS(THETA(N))
      W1(N+1,M,0)=U(N+1,M,0)*SIN(THETA(N))+V(N+1,M,0)*COS(THETA(N))
      Y(N,M)=-U(N,M,0)*COS(THETA(N))+V(N,M,0)*SIN(THETA(N))
      Y(N+1,M)=-U(N+1,M,0)*COS(THETA(N))+V(N+1,M,0)*SIN(THETA(N))
      G6BAR=(G6(N,M)+G6(N+1,M))/2.
      A2=.25*G6BAR*(P(N,M,0)+P(N+1,M,0))*(R(N,M,0)+R(N+1,M,0))
      A=SQRT(A2)
      P0=(P(N,M,0)+P(N+1,M,0)+A*(W1(N,M,0)-W1(N+1,M,0)))/2.
      W0=(W1(N,M,0)+W1(N+1,M,0)+(1./A)*(P(N,M,0)-P(N+1,M,0)))/2.
      DNEGR(N,M)=W1(N,M,0)-A/R(N,M,0)
      DPOSR(N,M)=W1(N+1,M,0)+A/R(N+1,M,0)
C
      IF (DNEGR(N,M).GT.0.) THEN
      PR(N,M)=P(N,M,0)
      RR(N,M)=R(N,M,0)
      WR(N,M)=W1(N,M,0)
      UR(N,M)=U(N,M,0)
      VR(N,M)=V(N,M,0)
      ER(N,M)=E(N,M,0)
      ELSE IF (DPOSR(N,M).LT.0.) THEN
      PR(N,M)=P(N+1,M,0)
```

```
      RR(N,M)=R(N+1,M,0)
      WR(N,M)=W1(N+1,M,0)
      UR(N,M)=U(N+1,M,0)
      VR(N,M)=V(N+1,M,0)
      ER(N,M)=E(N+1,M,0)
      ELSE IF (W0.GT.0.) THEN
      RNEG=1./((1./R(N,M,0))-((P0-P(N,M,0))/A**2.))
      PR(N,M)=P0
      RR(N,M)=RNEG
      WR(N,M)=W0
      UR(N,M)=W0*SIN(THETA(N))-Y(N,M)*COS(THETA(N))
      VR(N,M)=W0*COS(THETA(N))+Y(N,M)*SIN(THETA(N))
      ER(N,M)=E(N,M,0)+((1./R(N,M,0))-(P0/A**2.))*(P(N,M,0)-P0)
      ELSE IF (W0.LE.0.) THEN
      RPOS=1./((1./R(N+1,M,0))-((P0-P(N+1,M,0))/A**2.))
      PR(N,M)=P0
      RR(N,M)=RPOS
      WR(N,M)=W0
      UR(N,M)=W0*SIN(THETA(N))-Y(N+1,M)*COS(THETA(N))
      VR(N,M)=W0*COS(THETA(N))+Y(N+1,M)*SIN(THETA(N))
      ER(N,M)=E(N+1,M,0)+((1./R(N+1,M,0))-(P0/A**2.))*(P(N+1,M,0)-P0)
      END IF
C
C AXIS BOUNDARY CONDITIONS
      IF (N.EQ.1) THEN
      UR(0,M)=UR(1,M)
      VR(0,M)=-VR(1,M)
      WR(0,M)=-WR(1,M)
      RR(0,M)=RR(1,M)
      PR(0,M)=PR(1,M)
      ER(0,M)=ER(1,M)
      END IF
C DOWNSTREAM B C (ASSUMES SUPERSONIC FLOW ACROSS BOUNDARY)
      IF (N.EQ.NT-1) THEN
      UR(NT,M)=U(NT,M,0)
      VR(NT,M)=V(NT,M,0)
      WR(NT,M)=U(NT,M,0)*SIN(THETA(NT))+V(NT,M,0)*COS(THETA(NT))
      RR(NT,M)=R(NT,M,0)
      PR(NT,M)=P(NT,M,0)
      ER(NT,M)=E(NT,M,0)
      END IF
C
   43 CONTINUE
   42 CONTINUE
      RETURN
      END
C
C
C ***************************************************************************
C
      SUBROUTINE SHOCK
C
C ***************************************************************************
```

```
C
*CALL COMMON
C THIS SUBROUTINE COMPUTES CONDITIONS BEHIND THE SHOCK WAVE
C BY ITERATION OF THE NON-LINEAR EQUATIONS
C
C FREE STREAM (IE AHEAD OF SHOCK) BOUNDARY CONDITIONS
      DO 54 N=1,NT
      U(N,0,0)=UINF
      V(N,0,0)=VINF
      R(N,0,0)=RINF
      P(N,0,0)=PINF
      E(N,0,0)=EINF
      TEMP(N,0)=TINF
   54 CONTINUE
      DO 51 N=1,NT
      W2(N,1,0)=-U(N,1,0)*SIN(PHI(N-1,0))-V(N,1,0)*COS(PHI(N-1,0))
      W2(N,0,0)=-U(N,0,0)*SIN(PHI(N-1,0))
      Y(N,1)=-U(N,1,0)*COS(PHI(N-1,0))+V(N,1,0)*SIN(PHI(N-1,0))
      Y(N,0)=-U(N,0,0)*COS(PHI(N-1,0))
      PCD(0)=(P(N,1,0)+P(N,0,0))/2.
      G5BAR=(G5(N,0)+G5(N,1))/2.
      G6BAR=(G6(N,0)+G6(N,1))/2.
      J=0
   58 IF (J.GT.50) THEN
      P0=PCD(J)
      GO TO 59
      END IF
C
C COMPUTATION OF MASS VELOCITIES
C COMPUTATION FOR NEGATIVE-MOST CELL
        IF (PCD(J).EQ.P(N,1,0)) THEN
        A=SQRT(G5(N,1)*P(N,1,0)*R(N,1,0))
        GO TO 56
        END IF
      GHATNEG=G5(N,1)+(1.-(G5BAR/G6BAR))*(G5BAR-1.)*
     +        ((PCD(J)-P(N,1,0))/(0.5*(PCD(J)+P(N,1,0))))
      GNEG=MAX(GMIN,MIN(GHATNEG,GMAX))
      A11=(PCD(J)-P(N,1,0))*(PCD(J)+0.5*(GNEG-1.)*(PCD(J)+P(N,1,0)))
      A12=(PCD(J)/R(N,1,0))-((GNEG-1.)*P(N,1,0)/((G5(N,1)-1.)*R(N,1,0))
     +)
      A=SQRT(ABS(A11/A12))
C COMPUTATION FOR POSITIVE-MOST CELL
   56   IF (PCD(J).EQ.P(N,0,0)) THEN
        B=SQRT(G5(N,0)*P(N,0,0)*R(N,0,0))
        GO TO 57
        END IF
      GHATPOS=G5(N,0)+(1.-(G5BAR/G6BAR))*(G5BAR-1.)*
     +        ((PCD(J)-P(N,0,0))/(0.5*(PCD(J)+P(N,0,0))))
      GPOS=MAX(GMIN,MIN(GHATPOS,GMAX))
      B11=(PCD(J)-P(N,0,0))*(PCD(J)+0.5*(GPOS-1.)*(PCD(J)+P(N,0,0)))
      B12=(PCD(J)/R(N,0,0))-((GPOS-1.)*P(N,0,0)/((G5(N,0)-1.)*R(N,0,0)
     +)
      B=SQRT(ABS(B11/B12))
```

```
C
   57 F=(B*P(N,1,0)+A*P(N,0,0)+A*B*(W2(N,1,0)-W2(N,0,0)))/(A+B)
      FPCD(J)=MAX(PMIN,F)
      IF (J.EQ.0) THEN
      PCD(J+1)=FPCD(J)
      J=J+1
      GO TO 58
      END IF
      IF ((FPCD(J-1).EQ.PMIN).AND.(FPCD(J).EQ.PMIN)) THEN
      P0=PMIN
      GO TO 59
      END IF
      DPCD=PCD(J)-PCD(J-1)
      DFPCD=FPCD(J)-FPCD(J-1)
      IF (ABS(DPCD).LT.ABS(PCD(J)/10000.)) THEN
      P0=PCD(J)
      ELSE
      PCD(J+1)=(FPCD(J)*DPCD-PCD(J)*DFPCD)/(DPCD-DFPCD)
      J=J+1
      GO TO 58
      END IF
   59 W0=(A*W2(N,1,0)+B*W2(N,0,0)+P(N,1,0)-P(N,0,0))/(A+B)
      RPOS=1./((1./RINF)-((P0-PINF)/B**2.))
      PT(N,0)=P0
      RT(N,0)=RPOS
      WT(N,0)=W0
      UT(N,0)=-W0*SIN(PHI(N-1,0))-Y(N,0)*COS(PHI(N-1,0))
      VT(N,0)=-W0*COS(PHI(N-1,0))+Y(N,0)*SIN(PHI(N-1,0))
      ET(N,0)=EINF+((1./RINF)-(P0/B**2.))*(PINF-P0)
      DNEGT(N,0)=W2(N,1,0)-A/R(N,1,0)
      DPOST(N,0)=W2(N,0,0)+B/R(N,0,0)
   51 CONTINUE
C
C VEL OF BOUNDARY AT SHOCK (M=0) IS SET EQUAL TO POSITIVE RUNNING WAVE;
C THE VEL OF ALL NODES IS NOW APPROXIMATED, BASED ON M=0 BOUNDARY VEL'S
      DO 53 N=1,NT-1
      D1=DPOST(N,0)/SIN(PHI(N-1,0)-THETA(N))
      D2=DPOST(N+1,0)/SIN(PHI(N,0)-THETA(N))
      OMEGA(N,0)=(D2*ST(N,0)+D1*ST(N+1,0))/(ST(N,0)+ST(N+1,0))
   53 CONTINUE
      OMEGA(0,0)=OMEGA(1,0)
      OMEGA(NT,0)=-DPOST(NT,0)/COS(PHI(NT-1,0)-DELTA/2.)
C
      DO 52 N=0,NT
      RL(N,0,1)=RL(N,0,0)+OMEGA(N,0)*TAU
C
      DO 55,M=0,MT
      RL(N,M,1)=RL(N,0,1)-(REAL(M)/REAL(MT))*(RL(N,0,1)-1.)
      OMEGA(N,M)=(RL(N,M,1)-RL(N,M,0))/TAU
      IF (N.EQ.0) GO TO 55
C THE VELOCITIES OF ALL TANGENTIAL BOUNDARIES ARE NOW COMPUTED.
C THESE VELOCITIES ARE BASED ON THE NODAL VELOCITIES APPROXIMATED ABOVE
      Q1=(RL(N-1,M,1)-RL(N-1,M,0))*SIN(PHI(N-1,M)-THETA(N-1))
```

```
      Q2=(RL(N,M,1)-RL(N,M,0))*SIN(PHI(N-1,M)-THETA(N))
      Q(N,M)=(Q1+Q2)/(2.*TAU)
   55 CONTINUE
   52 CONTINUE
      RETURN
      END
C
C
C ***************************************************************************
C
      SUBROUTINE ARC
C
C ***************************************************************************
C
*CALL COMMON
C THIS SUBROUTINE COMPUTES THE RIEMANN PROBLEM ON TANGENTIAL BOUNDARIES
C
      DO 62 N=1,NT
      Q(N,MT)=0.
      DO 63 M=1,MT-1
      W3(N,M,0)=-U(N,M,0)*SIN(PHI(N-1,M))-V(N,M,0)*COS(PHI(N-1,M))
      W3(N,M+1,0)=-U(N,M+1,0)*SIN(PHI(N-1,M))-V(N,M+1,0)*COS(PHI(N-1,M)
     +)
      Y(N,M)=-U(N,M,0)*COS(PHI(N-1,M))+V(N,M,0)*SIN(PHI(N-1,M))
      Y(N,M+1)=-U(N,M+1,0)*COS(PHI(N-1,M))+V(N,M+1,0)*SIN(PHI(N-1,M))
      G6BAR=(G6(N,M)+G6(N,M+1))/2.
      A2=.25*G6BAR*(P(N,M,0)+P(N,M+1,0))*(R(N,M,0)+R(N,M+1,0))
      A=SQRT(A2)
      P0=(P(N,M,0)+P(N,M+1,0)+A*(W3(N,M+1,0)-W3(N,M,0)))/2.
      W0=(W3(N,M,0)+W3(N,M+1,0)+(1./A)*(P(N,M+1,0)-P(N,M,0)))/2.
      DNEGT(N,M)=W3(N,M+1,0)-A/R(N,M+1,0)
      DPOST(N,M)=W3(N,M,0)+A/R(N,M,0)
C
      IF (Q(N,M).GT.DPOST(N,M)) THEN
      PT(N,M)=P(N,M,0)
      RT(N,M)=R(N,M,0)
      WT(N,M)=W3(N,M,0)
      UT(N,M)=U(N,M,0)
      VT(N,M)=V(N,M,0)
      ET(N,M)=E(N,M,0)
      ELSE IF (Q(N,M).LT.DNEGT(N,M)) THEN
      PT(N,M)=P(N,M+1,0)
      RT(N,M)=R(N,M+1,0)
      WT(N,M)=W3(N,M+1,0)
      UT(N,M)=U(N,M+1,0)
      VT(N,M)=V(N,M+1,0)
      ET(N,M)=E(N,M+1,0)
      ELSE IF (Q(N,M).GT.W0) THEN
      RPOS=1./((1./R(N,M,0))-((P0-P(N,M,0))/A**2.))
      PT(N,M)=P0
      RT(N,M)=RPOS
      WT(N,M)=W0
      UT(N,M)=-W0*SIN(PHI(N-1,M))-Y(N,M)*COS(PHI(N-1,M))
```

```
      VT(N,M)=-W0*COS(PHI(N-1,M))+Y(N,M)*SIN(PHI(N-1,M))
      ET(N,M)=E(N,M,0)+((1./R(N,M,0))-(P0/A**2.))*(P(N,M,0)-P0)
      ELSE IF (Q(N,M).LE.W0) THEN
      RNEG=1./((1./R(N,M+1,0))-((P0-P(N,M+1,0))/A**2.))
      PT(N,M)=P0
      RT(N,M)=RNEG
      WT(N,M)=W0
      UT(N,M)=-W0*SIN(PHI(N-1,M))-Y(N,M+1)*COS(PHI(N-1,M))
      VT(N,M)=-W0*COS(PHI(N-1,M))+Y(N,M+1)*SIN(PHI(N-1,M))
      ET(N,M)=E(N,M+1,0)+((1./R(N,M+1,0))-(P0/A**2.))*(P(N,M+1,0)-P0)
      END IF
   63 CONTINUE
   62 CONTINUE
      RETURN
      END
C
C
C ***************************************************************************
C
      SUBROUTINE BODY
C
C ***************************************************************************
C
*CALL COMMON
C THIS SUBROUTINE COMPUTES THE PROJECTILE BOUNDARY CONDITION.
C COMPUTE REFLECTED PRESSURE BY ITERATION OF NON-LINEAR EQUATIONS.
C THE BOUNDARY ON THE BODY IS A ONE-D REFLECTION PROBLEM, WHERE
C W = VEL OF INCIDENT FLUID, WT = VEL BEHIND REFLECTED SHOCK = 0.
C
      DO 72 N=1,NT
      WT(N,MT)=0.
C VALUES FOR UT,VT,RT AND ET ON THE BODY SURFACE BOUNDARY ARE NOT
C REQUIRED, SINCE AT THIS BOUNDARY WT = Q = 0 , SO THESE TERMS DROP OUT
C OF THE CONSERVATION EQUATIONS.  HOWEVER, FOR DATA INITIALIZATION,
C THEY WILL BE SET TO ZERO.
      UT(N,MT)=0.
      VT(N,MT)=0.
      RT(N,MT)=0.
      ET(N,MT)=0.
      W4(N,MT,0)=-U(N,MT,0)*SIN(PHI(N-1,MT))-V(N,MT,0)*COS(PHI(N-1,MT))
      G5BAR=G5(N,MT)
      G6BAR=G6(N,MT)
      L=0
      PCD(L)=P(N,MT,0)
   73 IF (L.GE.50) THEN
      PT(N,MT)=PCD(L)
      DPOST(N,MT)=W4(N,MT,0)+B/R(N,MT,0)
      GO TO 77
      END IF
C COMPUTATION OF MASS VELOCITY OF THE RIEMANN WAVE
        IF (PCD(L).EQ.P(N,MT,0)) THEN
        B=SQRT(G5(N,MT)*P(N,MT,0)*R(N,MT,0))
        GO TO 71
```

```
        END IF
       GHATPOS=G5(N,MT)+(1.-(G5BAR/G6BAR))*(G5BAR-1.)*
      +        ((PCD(L)-P(N,MT,0))/(0.5*(PCD(L)+P(N,MT,0))))
       GPOS=MAX(GMIN,MIN(GHATPOS,GMAX))
       B1=(PCD(L)-P(N,MT,0))*(PCD(L)+0.5*(GPOS-1.)*(PCD(L)+P(N,MT,0)))
       B2=(PCD(L)/R(N,MT,0))-((GPOS-1.)*P(N,MT,0)/((G5(N,MT)-1.)*R(N,MT,
      +0)))
       B=SQRT(ABS(B1/B2))
C
C COMPUTATION OF THE PRESSURE BEHIND THE RIEMANN WAVE
   71 F=P(N,MT,0)-W4(N,MT,0)*B
      FPCD(L)=MAX(PMIN,F)
      IF (L.EQ.0) THEN
      PCD(L+1)=FPCD(L)
      L=L+1
      GO TO 73
      END IF
      IF ((FPCD(L-1).EQ.PMIN).AND.(FPCD(L).EQ.PMIN)) THEN
      PT(N,MT)=PMIN
      DPOST(N,MT)=W4(N,MT,0)+B/R(N,MT,0)
      GO TO 77
      END IF
      DPCD=PCD(L)-PCD(L-1)
      DFPCD=FPCD(L)-FPCD(L-1)
      IF (ABS(DPCD).LT.ABS(PCD(L)/10000.)) THEN
      PT(N,MT)=PCD(L)
      DPOST(N,MT)=W4(N,MT,0)+B/R(N,MT,0)
      ELSE
      PCD(L+1)=(FPCD(L)*DPCD-PCD(L)*DFPCD)/(DPCD-DFPCD)
        IF (PCD(L+1).LE.0.) THEN
        PCD(0)=PCD(L)
        L=0
        GO TO 73
        END IF
      L=L+1
      GO TO 73
      END IF
   77 CONTINUE
   72 CONTINUE
      END
C
C
C ***************************************************************************
C
      SUBROUTINE FLUX
C
C ***************************************************************************
C
*CALL COMMON
C
C V/R RATIO FOR CELLS ON THE AXIS IS TAKEN AS THAT VALUE WHICH YIELDS
C V=0 ON THE AXIS.  THE SIMPLEST WAY TO DO THIS IS TO ESTIMATE V/R
C ON THE AXIS BASED ON NEARBY CELLS, AND TO ARTIFICIALLY RESTRAIN
```

```
C V TO BE ZERO ON THE AXIS.
      DO 88 M=1,MT
      VELGRAD(1,M)=(RADIUS(3,M)*V(3,M,0)+RADIUS(2,M)*V(2,M,0))/
     +(RADIUS(3,M)**2.+RADIUS(2,M)**2.)
   88 CONTINUE
C
      DO 81 N=1,NT
      DO 82 M=1,MT
C
C CONSERVATION OF MASS
      AREA(N,M,1)=.5*((RL(N-1,M-1,1)*RL(N,M-1,1))-(RL(N-1,M,1)*RL(N,M,1
     +)))*SIN(DELTA)
      C1=RR(N,M)*WR(N,M)*SR(N,M)
      C2=RT(N,M-1)*(WT(N,M-1)-Q(N,M-1))*ST(N,M-1)
      C3=RR(N-1,M)*(-WR(N-1,M))*SR(N-1,M)
      C4=RT(N,M)*(Q(N,M)-WT(N,M))*ST(N,M)
      IF (N.EQ.1) C5=R(N,M,0)*AREA(N,M,0)*VELGRAD(1,M)
      IF (N.NE.1) C5=R(N,M,0)*V(N,M,0)*AREA(N,M,0)/RADIUS(N,M)
      C6=R(N,M,0)*AREA(N,M,0)
      R(N,M,1)=(C6-TAU*(C1+C2+C3+C4+C5))/AREA(N,M,1)
C
C CONSERVATION OF AXIAL MOMENTUM
      AM1=SR(N,M)*(RR(N,M)*UR(N,M)*WR(N,M)+PR(N,M)*SIN(THETA(N)
     +))
      AM2=ST(N,M-1)*(RT(N,M-1)*UT(N,M-1)*(WT(N,M-1)-Q(N,M-1))-
     +PT(N,M-1)*SIN(PHI(N-1,M-1)))
      AM3=SR(N-1,M)*(RR(N-1,M)*UR(N-1,M)*(-WR(N-1,M))-PR(N-1,M)*
     +SIN(THETA(N-1)))
      AM4=ST(N,M)*(RT(N,M)*UT(N,M)*(Q(N,M)-WT(N,M))+
     +PT(N,M)*SIN(PHI(N-1,M)))
      IF (N.EQ.1) AM5=R(N,M,0)*U(N,M,0)*AREA(N,M,0)*VELGRAD(1,M)
      IF(N.NE.1) AM5=R(N,M,0)*U(N,M,0)*V(N,M,0)*AREA(N,M,0)/RADIUS(N,M)
      AM6=R(N,M,0)*U(N,M,0)*AREA(N,M,0)
      U(N,M,1)=(AM6-TAU*(AM1+AM2+AM3+AM4+AM5))/(R(N,M,1)*AREA(N,M,1))
C
C CONSERVATION OF RADIAL MOMENTUM
      RM1=SR(N,M)*(RR(N,M)*VR(N,M)*WR(N,M)+PR(N,M)*COS(THETA(N)
     +))
      RM2=ST(N,M-1)*(RT(N,M-1)*VT(N,M-1)*(WT(N,M-1)-Q(N,M-1))-
     +PT(N,M-1)*COS(PHI(N-1,M-1)))
      RM3=SR(N-1,M)*(RR(N-1,M)*VR(N-1,M)*(-WR(N-1,M))-PR(N-1,M)*
     +COS(THETA(N-1)))
      RM4=ST(N,M)*(RT(N,M)*VT(N,M)*(Q(N,M)-WT(N,M))+PT(N,M)*
     +COS(PHI(N-1,M)))
      IF (N.EQ.1) RM5=R(N,M,0)*V(N,M,0)*AREA(N,M,0)*VELGRAD(1,M)
      IF(N.NE.1) RM5=R(N,M,0)*V(N,M,0)*V(N,M,0)*AREA(N,M,0)/RADIUS(N,M)
      RM6=R(N,M,0)*V(N,M,0)*AREA(N,M,0)
      V(N,M,1)=(RM6-TAU*(RM1+RM2+RM3+RM4+RM5))/(R(N,M,1)*AREA(N,M,1))
      IF (N.EQ.1) V(N,M,1)=0.
C
C CONSERVATION OF ENERGY
      E1=(PR(N,M)+RR(N,M)*ER(N,M))*WR(N,M)*SR(N,M)
      E2=(PT(N,M-1)*WT(N,M-1)+RT(N,M-1)*ET(N,M-1)*(WT(N,M-1)-
```

```
     +Q(N,M-1)))*ST(N,M-1)
      E3=(PR(N-1,M)+RR(N-1,M)*ER(N-1,M))*(-WR(N-1,M))*SR(N-1,M)
      E4=(PT(N,M)*(-WT(N,M))+RT(N,M)*ET(N,M)*(Q(N,M)-WT(N,M)
     +))*ST(N,M)
      IF(N.EQ.1)E5=(P(N,M,0)+R(N,M,0)*E(N,M,0))*AREA(N,M,0)*VELGRAD(1,M
     +)
      IF (N.NE.1) E5=(P(N,M,0)+R(N,M,0)*E(N,M,0))*V(N,M,0)*AREA(N,M,0)/
     +RADIUS(N,M)
      E6=R(N,M,0)*E(N,M,0)*AREA(N,M,0)
      E(N,M,1)=(E6-TAU*(E1+E2+E3+E4+E5))/(R(N,M,1)*AREA(N,M,1))
C
      PROBLEM='R AND E GIVEN'
      DENSITY=R(N,M,1)
      ENERGY=E(N,M,1)-(U(N,M,1)**2.+V(N,M,1)**2.)/2.
      ESAVE=ENERGY
      OLDP=P(N,M,0)
      OLDT=TEMP(N,M)
      CALL REALGAS (DENSITY,ENERGY,SOUND,PRESSUR,TEMPERA,PROBLEM,
     +OLDP,OLDT)
      P(N,M,1)=PRESSUR
      TEMP(N,M)=TEMPERA
      SONIC(N,M)=SOUND
      G5(N,M)=1.+P(N,M,1)/(R(N,M,1)*ESAVE)
      G6(N,M)=(SONIC(N,M)**2.)*R(N,M,1)/P(N,M,1)
      IF (P(N,M,1).LT.0) P(N,M,1)=PMIN
   82 CONTINUE
   81 CONTINUE
C
C     IF (T.EQ.TSTEPS) THEN
      TLAST=T1+T
      REWIND 24
      WRITE (24,805) TLAST,TAU,TIME,UINF,VINF,RINF,PINF,TINF
C     WRITE (24,807)
      DO 85 N=0,NT
      DO 86 M=0,MT
      IF (M.EQ.0) THEN
      WRITE (24,806) N,M,U(N,M,0),V(N,M,0),R(N,M,0),P(N,M,0),E(N,M,0),
     +RL(N,M,1),G5(N,M),G6(N,M),TEMP(N,M)
      ELSE
      WRITE (24,806) N,M,U(N,M,1),V(N,M,1),R(N,M,1),P(N,M,1),E(N,M,1),
     +RL(N,M,1),G5(N,M),G6(N,M),TEMP(N,M)
      END IF
   86 CONTINUE
   85 CONTINUE
C     END IF
  805 FORMAT (1X,I5,7E16.9)
  806 FORMAT (1X,2I2,9E14.7)
  807 FORMAT (3X,'N   M   U',15X,'V',15X,'R',15X,'P',15X,'E',15X,
     +'RL',15X,'G5',15X,'G6'/)
C
C
      IF ((T.EQ.1).OR.(T.EQ.TSTEPS)) THEN
      WRITE (5,808) T,TIME
```

```
      WRITE (5,811)
      DO 83 N=0,NT
      DO 84 M=0,MT
      IF ((N.EQ.0).OR.(M.EQ.0)) THEN
      WRITE (5,810) N,M,RL(N,M,0),SR(N,M),ST(N,M),RADIUS(N,M),
     +AREA(N,M,0),PHI(N,M),Q(N,M),U(N,M,0),V(N,M,0),R(N,M,0),P(N,M,0),
     +E(N,M,0)
      ELSE
      WRITE (5,810) N,M,RL(N,M,0),SR(N,M),ST(N,M),RADIUS(N,M),
     +AREA(N,M,0),PHI(N,M),Q(N,M),U(N,M,1),V(N,M,1),R(N,M,1),P(N,M,1),
     +E(N,M,1)
      END IF
   84 CONTINUE
   83 CONTINUE
      WRITE (5,812)
      WRITE (5,802) ((N,M,UR(N,M),VR(N,M),WR(N,M),RR(N,M),PR(N,M),
     +ER(N,M),UT(N,M),VT(N,M),WT(N,M),RT(N,M),PT(N,M),ET(N,M),M=0,MT),
     +N=0,NT)
      END IF
C
      IF (T.EQ.TSTEPS) WRITE (6,803) (U(NT,M,0),V(NT,M,0),R(NT,M,0),
     +P(NT,M,0),M=1,MT)
C
  800 FORMAT (1X,E14.7)
  801 FORMAT (1X,I5,2F10.4,10X,2F10.4)
  802 FORMAT (1X,2I3,3F10.3,F7.4,2E12.5,3F10.3,F7.4,2E12.5)
  803 FORMAT (1X,4E16.9)
  804 FORMAT (1X,2I3,5E14.7)
  808 FORMAT (///1H1,1X,'TIME(',I4,')=',E14.7/)
  810 FORMAT (1X,2I3,6F10.7,F12.5,2F11.5,F7.4,2E12.5)
  811 FORMAT (3X,'N',2X,'M',5X,'RL',8X,'SR',8X,'ST',6X,'RADIUS',5X,
     +'AREA',6X,'PHI',9X,'Q',10X,'U',10X,'V',8X,'R',9X,'P',11X,'E'/)
  812 FORMAT (//3X,'N',2X,'M',5X,'UR',8X,'VR',8X,'WR',6X,'RR',8X,
     +'PR',10X,'ER',8X,'UT',8X,'VT',8X,'WT',7X,'RT',8X,'PT',10X,
     +'ET'/)
  824 FORMAT (1X,I5,F14.7)
  825 FORMAT (1X,I5,9E14.7)
      RETURN
      END
C
C
C ***************************************************************************
C
      SUBROUTINE UPDATE
C
C ***************************************************************************
C
*CALL COMMON
C
      DO 93 N=0,NT
      DO 94 M=0,MT
      U(N,M,0)=U(N,M,1)
      V(N,M,0)=V(N,M,1)
```

```
      R(N,M,0)=R(N,M,1)
      P(N,M,0)=P(N,M,1)
      E(N,M,0)=E(N,M,1)
      RL(N,M,0)=RL(N,M,1)
   94 CONTINUE
   93 CONTINUE
C
  900 FORMAT (1X,2I5,6E19.12)
  901 FORMAT (1X,I10,E20.13)
      RETURN
      END
C
C
C ***********************************************************************
C
      SUBROUTINE TIMESTP
C
C ***********************************************************************
C
*CALL COMMON
      SF=0.2
C SMALL TIMESTEPS ARE REQUIRED BEFORE THE REFLECTED WAVE COLLIDES
C WITH THE SHOCK IN THE UNSTEADY STARTUP.  THIS TAKES ABOUT 100 STEPS
C AT MACH 4 AND 200 STEPS AT MACH 8.
      TLAST=T1+T
C     IF (TLAST.LE.2000) SF=0.1
      DO 101 N=1,NT
      DO 102 M=1,MT
C
      IF (N.EQ.1) THEN
      TT(1)=1.E100
      TT(2)=1.E100
      ELSE
      TT(1)=ST(N,M)*SIN(PHI(N-1,M)-THETA(N-1))/DPOSR(N-1,M)
      TT(2)=ST(N,M-1)*SIN(PHI(N-1,M-1)-THETA(N-1))/DPOSR(N-1,M)
      END IF
C
      IF (N.EQ.NT) THEN
      TT(3)=1.E100
      TT(4)=1.E100
      ELSE
      TT(3)=ST(N,M)*SIN(PHI(N-1,M)-THETA(N))/(-DNEGR(N,M))
      TT(4)=ST(N,M-1)*SIN(PHI(N-1,M-1)-THETA(N))/(-DNEGR(N,M))
      END IF
C
      IF (M.EQ.MT) THEN
      TT(5)=1.E100
      TT(6)=1.E100
      ELSE
      TT(5)=(RL(N,M-1,0)-RL(N,M,0))/
     +((DPOST(N,M)/SIN(PHI(N-1,M)-THETA(N)))-OMEGA(N,M-1))
      TT(6)=(RL(N-1,M-1,0)-RL(N-1,M,0))/
     +((DPOST(N,M)/SIN(PHI(N-1,M)-THETA(N-1)))-OMEGA(N-1,M-1))
```

```
      END IF
C
      TT(7)=(RL(N,M-1,0)-RL(N,M,0))/
     +(OMEGA(N,M)-(DNEGT(N,M-1)/SIN(PHI(N-1,M-1)-THETA(N))))
      TT(8)=(RL(N-1,M-1,0)-RL(N-1,M,0))/
     +(OMEGA(N-1,M)-(DNEGT(N,M-1)/SIN(PHI(N-1,M-1)-THETA(N-1))))
C
      TAUT=1.E100
      TAUR=1.E100
      DO 1006 J=1,8
      IF (J.LE.4) THEN
      IF ((TT(J).GT.0.).AND.(TT(J).LT.TAUT)) TAUT=TT(J)
      ELSE
      IF ((TT(J).GT.0.).AND.(TT(J).LT.TAUR)) TAUR=TT(J)
      END IF
 1006 CONTINUE
      TAU9=TAUT*TAUR/(TAUT+TAUR)
      IF ((N.EQ.1).AND.(M.EQ.1)) THEN
      TAUBAR=TAU9
      ELSE
      TAUBAR=MIN(TAUBAR,TAU9)
      END IF
  102 CONTINUE
  101 CONTINUE
      TAU=SF*TAUBAR
C
      RETURN
      END
C
C
C
C*********************************************************************
C ////////////////////////////////////////////////////////////////////
C*********************************************************************
C
C
C*********************************************************************
C
      SUBROUTINE REALGAS(DENSITY,ENERGY,SOUND,PRESSUR,TEMPERA,PROBLEM,
     +OLDP,OLDT)
C
C*********************************************************************
C
C THIS SUBROUTINE WILL RETURN THE THERMODYNAMIC PROPERTIES OF REAL AIR.
C GIVEN THE DENSITY AND INTERNAL ENERGY OF THE AIR (PROBLEM='R AND E
C GIVEN'), OR GIVEN THE PRESSURE AND TEMPERATURE OF THE AIR (PROBLEM=
C 'P AND T GIVEN').
      CHARACTER PROBLEM*13
      COMMON/XYZ/GAMMAE
      COMMON/ENTRO/ZSR
      COMMON/BERT/ENRG,ENTH,RHO,COMPRES
C
C VARIABLES AND UNITS ARE:
```

```
C     ROGIVE:     GIVEN DENSITY, KG/M**3
C     EGIVE:      GIVEN ENERGY, J/KG
C     P:          PRESSURE, N/M**2
C     T:          KELVIN
C     GAMMA:      RATIO OF SPECIFIC HEATS, DIMENSIONLESS
C     Z:          COMPRESSIBILITY, DIMENSIONLESS
C     ALPHA:      DEGREE OF DISOCCIATION, DIMENSIONLESS
C     A:          SONIC VELOCITY, M/S
C     ZSR:        DIMENSIONLESS ENTROPY, -S/R, S-ENTROPY, R-GAS CONSTANT
C
C CONVERT SI UNITS (USED IN MAIN PROGRAM) TO CGS (USED IN SUBROUTINE)
      DENSITY=DENSITY*(1.E-3)
      ENERGY=ENERGY*(1.E4)
C     PRESSUR=PRESSUR*(1.E1)
C     TEMPERA=TEMPERA
C     SOUND=SOUND*(1.E2)
C
C COMPUTE PROPERTIES OF THE REAL GAS
      IF (PROBLEM.EQ.'R AND E GIVEN') THEN
        CALL USERGP (DENSITY,ENERGY,SOUND,PRESSUR,TEMPERA,OLDP,OLDT)
      ELSE IF (PROBLEM.EQ.'P AND T GIVEN') THEN
        CALL RGP (PRESSUR,TEMPERA,ALPHA,DENSITY,ENERGY,SOUND)
      ELSE
        PRINT*, 'TROUBLE IN SUBROUTINE REALGAS'
      END IF
C
C CONVERT CGS UNITS TO SI
      DENSITY=DENSITY*(1.E3)
      ENERGY=ENERGY*(1.E-4)
      PRESSUR=PRESSUR*(1.E-1)
      TEMPERA=TEMPERA
      SOUND=SOUND*(1.E-2)
C
      RETURN
      END
C
*****************************************************************************
*
      SUBROUTINE USERGP(ROGIVE,EGIVE,A,P,T,OLDP,OLDT)
*
*****************************************************************************
C
      COMMON /RGPCOM/ GAMA,GAMAE,IRGPOPT,PLEFT,TLEFT,GAMLFT,ROLEFT

        DIMENSION AJAC(2,2),F(2),DELTA(2)

      DATA GAMA,GAMAE/1.4,1.4/
      DATA EMAX/1.E+13/
      EGIVE=AMIN1(EGIVE,EMAX)
C SUBROUTINE GUESS IS NOT USED HERE - STARTING POINT FOR ITERATION IS
C TAKEN AS THE P AND T IN THE CELL FROM THE PREVIOUS TIME STEP
C     CALL GUESS(P,T,ROGIVE,EGIVE)
      P=OLDP
```

```
      T=OLDT
      DEL=.01
      TOLER = 2.0E-5
      IRGPOPT = 1
C        NEWTON ITERATION TO FIND P,T WITH GIVEN RO,E
      DO 500 ITER=1,10
        ITNUM=ITER
      CALL RGP(P,T,ALPHA,RONEW,ENEW,ANEW)
      DELP=DEL*P
       P1=P+DELP
      CALL RGP(P1,T,ALPHA,RO1,E1,A)
      DELT=DEL*T
       T2=T+DELT
      CALL RGP(P,T2,ALPHA,RO2,E2,A)
      AJAC(1,1)=(RO1-RONEW)/DELP
      DRODP=AJAC(1,1)
        AJAC(2,1)=(E1-ENEW)/DELP
      DEDP=AJAC(2,1)
        AJAC(1,2)=(RO2-RONEW)/DELT
      DRODT=AJAC(1,2)
        AJAC(2,2)=(E2-ENEW)/DELT
      DEDT=AJAC(2,2)
        F(1)=-RONEW+ROGIVE
      F(2)=-ENEW+EGIVE
      CALL SOL2BY2(AJAC,DELTA,F)
      IF(ABS(DELTA(1)) .GT. TOLER*P)GO TO 300
      IF(ABS(DELTA(2)) .GT. TOLER*T)GO TO 300
      GO TO 600
  300 CONTINUE
      P=P+DELTA(1)
      T=T+DELTA(2)
  500 CONTINUE
C        NO CONVERGENCE
C     WRITE(6,1234)
 1234 FORMAT(' NO CONVERGENCE IN USERGP ITERATION')
  600 CONTINUE
      PBACK=P
      GBACK = PBACK/(ROGIVE*EGIVE) + 1.
      GCBACK = ANEW*ANEW*ROGIVE/PBACK
        PLEFT=P
        TLEFT=T
        ROLEFT=ROGIVE
      RETURN
       END
C
*****************************************************************************
*
      SUBROUTINE SOL2BY2(A,X,B)
*
*****************************************************************************
C

      REAL A(2,2),X(2),B(2)
```

```
      DET = A(1,1) * A(2,2)  -  A(1,2) * A(2,1)
      X(1) = (A(2,2) * B(1)  -  A(1,2) * B(2)) / DET
      X(2) = (-A(2,1) * B(1)  +  A(1,1) * B(2)) / DET

      RETURN
      END
C
C
*******************************************************************************
*
      SUBROUTINE GUESS(P,T,RO,E)
*
*******************************************************************************
C
      DATA R,GM1 /2.9677E6,.4/
      P=GM1*RO*E
      T=GM1*E/R
      RETURN
       END
C
C
*******************************************************************************
*
      SUBROUTINE RGP(P,T,ALPHA,RO,H,A)
*
*******************************************************************************
C
C     ****************************************
C     *                                      *
C     *   AN EQUATION OF STATE FOR REAL AIR  *
C     *                                      *
C     *   UNIVERSITY OF TORONTO              *
C     *   INSTITUTE FOR AEROSPACE STUDIES    *
C     *                                      *
C     *   WRITTEN BY ROBERT DESCHAMBAULT     *
C     *   VERSION 1.2  JUNE, 1980            *
C     *                                      *
C     ****************************************
C
C     THE SUBROUTINE RGP IS AN ENGINEERING APPROXIMATION OF THE
C     EOS (EQUATION OF STATE) FOR PERFECT AND REAL AIR.
C     RGP CALCULATES VARIOUS THERMODYNAMIC QUANTITIES GIVEN THE EQUILIB
C     PRESSURE AND TEMPERATURE.  IT IS ADAPTED FROM THE NASA TECHNICAL
C     REPORT TR R-50 BY DR. C. F. HANSEN(1959).  EXTENSIONS HAVE BEEN
C     MADE TO THE ORIGINAL WORK TO INCLUDE TWO MORE LEVELS OF
C     IONIZATION.  HENCE, THE CALCULATION IS RELIABLE TO 50000 DEGREES
C     KELVIN IF DENSITIES ARE KEPT UNDER 100 TIMES STANDARD ATMOSPHERIC
C     CONDITIONS.
C     THE MODEL ASSUMES A MIXTURE OF 20 PERCENT OXYGEN AND 80 PERCENT
C     NITROGEN AT STP CONDITIONS.  AS THE TEMPERATURE IS INCREASED,
C     FOR A GIVEN INITIAL PRESSURE, A TOTAL OF 11 DIFFERENT SPECIES
C     INVOLVED IN 8 REACTIONS MAY BE PRODUCED.
```

```
C
C     VARIABLE LIST
C
C     P - PRESSURE (ATMOSPHERE)
C     T - TEMPERATURE (DEGREE KELVIN)
C     ITYPE - TYPE OF EOS USED, 1 = PERFECT GAS, 2 = REAL GAS
C     ALPHA - DEGREE OF DISSOCIATION AND IONIZATION
C     RO - EQUILIBRIUM DENSITY (GRAMS PER CUBIC CENTIMETER)
C     H - EQUILIBRIUM ENTHALPY (ERGS)
C     A - EQUILIBRIUM SPEED OF SOUND (CENTIMETER PER SECOND)
C     GAMMAE - EQUILIBRIUM RATIO OF SPECIFIC HEATS
C     R - UNIVERSAL GAS CONSTANT (ERG PER GRAMMOLE PER DEGREE KELVIN)
C     ZSR - NONDIMENSIONAL ENTROPY
C
C     REQUIRED SUBROUTINES FOR RGP (SIX ROUTINES)
C     ENTHSP
C     RVPART
C     TEPART
C     DERLNK
C     DERZ
C     MOLFRA
C
      COMMON/ABC/ITYPE
      COMMON/RGASP/ID
      COMMON/XYZ/GAMMAE
      COMMON/ENTRO/ZSR
      COMMON/BERT/ENRG,ENTH,RHO,COMPRES
      DIMENSION LA(11),EA(11,21),TETE(11),TETV(2),TETR(2),X(11),TDRLKC(
     +5),TDRLKP(5),DERXR(11),DERXP(11),HMEO(11),EMEO(11),CP(11),CV(11),
     +TETH(11),SR(11)
      DIMENSION EA1(11),EA2(11),EA3(11),EA4(11),EA5(11),EA6(11),EA7(11)
     +,EA8(11),EA9(11),EA10(11),EA11(11),EA12(11),EA13(11),EA14(11),EA
     +15(11),EA16(11),EA17(11),EA18(11),EA19(11),EA20(11),EA21(11)
      REAL MGAS,MGS(11),LNQ(11),LNQP(11),LNQT(11),LNQRV(11),LNQE(11),LN
     +KP(8),KP(8),KPA(3)
      INTEGER GA(11,21),SIGMA(2)
      INTEGER GA1(11),GA2(11),GA3(11),GA4(11),GA5(11),GA6(11),GA7(11),
     +GA8(11),GA9(11),GA10(11),GA11(11),GA12(11),GA13(11),GA14(11),GA15
     +(11),GA16(11),GA17(11),GA18(11),GA19(11),GA20(11),GA21(11)
      EQUIVALENCE (GA(1,1),GA1(1)),(GA(1,2),GA2(1)),(GA(1,3),GA3(1)),(G
     +A(1,4),GA4(1)),(GA(1,5),GA5(1)),(GA(1,6),GA6(1)),(GA(1,7),GA7(1))
     +,(GA(1,8),GA8(1)),(GA(1,9),GA9(1)),(GA(1,10),GA10(1)),(GA(1,11),G
     +A11(1)),(GA(1,12),GA12(1)),(GA(1,13),GA13(1)),(GA(1,14),GA14(1)),
     +(GA(1,15),GA15(1)),(GA(1,16),GA16(1)),(GA(1,17),GA17(1)),(GA(1,18
     +),GA18(1)),(GA(1,19),GA19(1)),(GA(1,20),GA20(1)),(GA(1,21),GA21(1
     +))
      EQUIVALENCE (EA(1,1),EA1(1)),(EA(1,2),EA2(1)),(EA(1,3),EA3(1)),(E
     +A(1,4),EA4(1)),(EA(1,5),EA5(1)),(EA(1,6),EA6(1)),(EA(1,7),EA7(1))
     +,(EA(1,8),EA8(1)),(EA(1,9),EA9(1)),(EA(1,10),EA10(1)),(EA(1,11),E
     +A11(1)),(EA(1,12),EA12(1)),(EA(1,13),EA13(1)),(EA(1,14),EA14(1)),
     +(EA(1,15),EA15(1)),(EA(1,16),EA16(1)),(EA(1,17),EA17(1)),(EA(1,18
     +),EA18(1)),(EA(1,19),EA19(1)),(EA(1,20),EA20(1)),(EA(1,21),EA21(1
     +))
```

```
C
C     INITIALIZE CONSTANTS REQUIRED FOR PARTITION FUNCTION CALCULATIONS
C
      DATA TETH/0.0,0.0,56608.,29669.5,225469.,187726.,569172.,595759.,
     +1119774.,1233519.,0.0/
      DATA MGS/28.0134,31.9988,14.0067,15.9994,14.00615,15.99885,14.005
     +6,15.9983,14.00505,15.99775,0.54905E-03/
      DATA LA/2,14,15,21,10,5,7,7,4,6,1/
      DATA TETE/113216.,59339.8,168861.,158056.,343703.,408033.6,550602
     +.4,637760.5,898381.8,896989.,0.0/
      DATA TETV/3371.0,2256.0/
      DATA TETR/2.88,2.069/
      DATA SIGMA/2,2/
      DATA GA1/1,3,4,5,1,4,2,1,1,2,2/,GA2/3,2,10,3,3,10,4,3,4,4,2/,GA3/
     +0,1,6,1,5,6,2,5,5,2,0/,GA4/0,3,12,5,5,6,4,5,3,4,0/,GA5/0,0,6,1,1,
     +6,6,1,0,6,0/,GA6/2*0,12,5,5,0,10,5,0,10,0/,GA7/2*0,2,3,15,0,2,15,
     +3*0/,GA8/2*0,20,15,9,6*0/,GA9/2*0,12,9,5,6*0/,GA10/2*0,14,5,12,6*
     +0/,GA11/2*0,6,3,7*0/,GA12/2*0,10,45,7*0/,GA13/2*0,12,15,7*0/,GA14
     +/2*0,6,9,7*0/,GA15/2*0,34,15,7*0/,GA16/3*0,5,7*0/,GA17/3*0,3,7*0/
     +,GA18/3*0,5,7*0/,GA19/3*0,25,7*0/,GA20/3*0,15,7*0/,GA21/3*0,9,7*0
     +/
      DATA EA1/11*0.0/,EA2/72224.73,11390.85,27653.59,228.01,70.63,3856
     +5.69,251.03,163.13,96671.11,556.01,0.0/,EA3/0.0,18982.19,41488.29
     +,325.83,188.88,58214.37,82274.7,441.36,96878.53,102392.9,0.0/,EA4
     +/0.0,51925.54,119927.6,22826.76,22032.67,172394.6,82360.9,29161.2
     +1,188013.6,102581.9,0.0/,EA5/0.0,0.0,124037.9,48612.65,47022.6,17
     +2629.6,82477.68,62122.39,0.0,102847.3,0.0/
      DATA EA6/2*0.0,126751.5,106119.9,67853.92,0.0,145329.5,86710.7,0.
     +0,182696.4,0.0/,EA7/2*0.0,134624.4,110474.4,132690.4,0.0,188457.4
     +,172560.5,3*0.0/,EA8/2*0.0,136495.7,124624.6,157117.7,6*0.0/,EA9/
     +2*0.0,137430.9,127501.4,207425.7,6*0.0/,EA10/2*0.0,139345.7,13734
     +9.2,214457.8,6*0.0/,EA11/2*0.0,140700.2,138426.9,7*0.0/,EA12/2*0.
     +0,143374.8,140145.5,7*0.0/
      DATA EA13/2*0.0,149232.3,142554.1,7*0.0/,EA14/2*0.0,149958.1,1433
     +97.,7*0.0/,EA15/2*0.0,150714.4,145489.5,7*0.0/,EA16/3*0.0,146901.
     +,7*0.0/,EA17/3*0.0,147326.,7*0.0/,EA18/3*0.0,147685.7,7*0.0/,EA19
     +/3*0.0,147978.3,7*0.0/,EA20/3*0.0,148040.3,7*0.0/,EA21/3*0.0,1494
     +23.1,7*0.0/
C
C
C     DEFINE USEFUL QUANTITIES
C
      R=0.83169E 08
      RT=R*T
      MGAS=28.9667
      RGAS=R/MGAS
      RGAST=RGAS*T
      ITYPE = 2
      IF (ITYPE.EQ.2) GO TO 2
C     GOTO(1,2),ITYPE
C
C     PERFECT GAS CALCULATION
C
```

```
    1 GAMA=1.4
      E=(1./(GAMA-1.))*RGAST
      ALPHA=0.
      RO=P/RGAST
      H=(E+RGAST)/RGAS
      A=SQRT(GAMA*RGAST)
      ZSR=((GAMA/(GAMA-1.0))*ALOG(T/300.0))-ALOG(P/1.0)
      GAMMAE=GAMA
      RETURN
C
C     REAL GAS CALCULATION
C
C     CALCULATE PARTITION FUNCTIONS FOR EACH SPECIES
C
    2 DO 20 ID=1,11
      IF(ID.GE.3)GOTO 10
      CALL RVPART(TETR,TETV,T,SIGMA,LNQRV)
      GOTO 15
   10 LNQRV(ID)=0.0
   15 CALL TEPART(T,P,LA,GA,EA,MGS,LNQT,LNQE)
      LNQ(ID)=LNQT(ID)+LNQRV(ID)+LNQE(ID)
      LNQP(ID)=LNQ(ID)+ALOG(P)
   20 CONTINUE
C
C     CALCULATE EQUILIBRIUM CONSTANTS FOR EACH REACTION
C
      DO 40 ID=1,8
      IDREAC=ID
      IF(ID.GE.3)GOTO 30
      LNKP(IDREAC)=((-TETE(ID))/T)+(2.*LNQP(ID+2))-LNQP(ID)
      GOTO 40
   30 LNKP(IDREAC)=((-TETE(ID))/T)+LNQP(ID+2)+LNQP(11)-LNQP(ID)
   40 CONTINUE
      DO 50 IDREAC=1,8
      IF(LNKP(IDREAC).LE.(-85.0))GOTO 45
      KP(IDREAC)=EXP(LNKP(IDREAC))
      GOTO 50
   45 KP(IDREAC)=0.0
   50 CONTINUE
      DO 60 I=4,8,2
      IDA=(I-2)/2
   60 KPA(IDA)=(0.2*KP(I)+(0.8*KP(I-1)))
C
C     CALCULATE THE DISSOCIATION AND IONIZATION FACTORS
C
      EPS1=0.0
      EPS2=0.0
      EPS3=0.0
      EPS4=0.0
      EPS5=0.0
      IF(KP(2).LT.1.0E-05)GOTO 61
      XHOLD1=(1.+((4.0*P)/KP(2)))
      EPS1=((-0.8)+SQRT(0.64+(0.8*XHOLD1)))/(2.0*XHOLD1)
```

```
   61 IF(KP(1).LT.1.0E-05)GOTO 62
      XHOLD2=(1.+((4.0*P)/KP(1)))
      EPS2=((-0.4)+SQRT(0.16+(3.84*XHOLD2)))/(2.0*XHOLD2)
   62 IF(KPA(1).LT.1.0E-05)GOTO 63
      EPS3=1./SQRT(1.0+(P/KPA(1)))
   63 IF(KPA(2).LT.1.0E-05)GOTO 64
      ZHOLD=1.0+(P/KPA(2))
      EPS4=((-ZHOLD)+SQRT((ZHOLD*ZHOLD)+(8.0*ZHOLD)))/(2.0*ZHOLD)
   64 IF(KPA(3).LT.1.0E-05)GOTO 65
      AHOLD=2.0+((2.0*P)/KPA(3))
      BHOLD=1.0+(P/KPA(3))
      EPS5=((-AHOLD)+SQRT((AHOLD*AHOLD)+(12.0*BHOLD)))/(2.0*BHOLD)
   65 IF(EPS1.GT.0.2)EPS1=0.2
      IF(EPS2.GT.0.8)EPS2=0.8
      IF(EPS3.GT.1.0)EPS3=1.0
      IF(EPS4.GT.1.0)EPS4=1.0
      IF(EPS5.GT.1.0)EPS5=1.0
      ALPHA=EPS1+EPS2+(2.0*EPS3)+(2.0*EPS4)+(2.0*EPS5)
      Z=1.0+ALPHA
      COMPRES=Z
      RO=P/(Z*RGAST)
      RHO=RO
C
C     CALCULATE THE MOLE FRACTION FOR EACH SPECIES
C
      CALL MOLFRA(Z,EPS1,EPS2,EPS3,EPS4,EPS5,X)
C
C     CALCULATE THE INTERNAL ENERGY, ENTHALPY, AND EQUILIBRIUM RATIO
C     OF SPECIFIC HEATS FOR EACH SPECIES
C
      DO 70 ID=1,11
      CALL ENTHSP(T,LA,GA,EA,TETV,EMEO,HMEO,CV,CP)
   70 CONTINUE
C
C     CALCULATE THE ENTROPY FOR EACH SPECIES
C
      DO 21 LH=1,11
   21 SR(LH)=LNQP(LH)+HMEO(LH)
      XSUM=0.0
      YSUM=0.0
      DO 68 LP=1,11
      YHO=X(LP)*SR(LP)
      YSUM=YSUM+YHO
      IF(X(LP).LE.0.0)GOTO 68
      XHO=X(LP)*ALOG(X(LP))
      XSUM=XSUM+XHO
   68 CONTINUE
      ZSR=Z*(YSUM-XSUM-ALOG(P))
C
C     CALCULATE APPROPRIATE DERIVITIVES FOR THE EQUILIBRIUM RATIO OF
C     SPECIFIC HEATS FOR AIR MIXTURE
C
      DO 80 ID=1,7
```

```
      CALL DERLNK(T,TETE,EMEO,TDRLKC,TDRLKP)
   80 CONTINUE
      CALL DERZ(T,Z,TDRLKC,TDRLKP,EPS1,EPS2,EPS3,EPS4,EPS5,DERZP,DERZRO
     +,DERXP,DERXR)
      ERT=0.0
      DO 90 I=1,11
      SAVE=X(I)*(EMEO(I)+(TETH(I)/T))
      ERT=ERT+SAVE
   90 CONTINUE
      ZHRT=(ERT*Z)+Z
      H=(ZHRT*T)
      ENTH=H*RGAS
      CVR1=0.0
      CVR2=0.0
      CPR1=0.0
      CPR2=0.0
      DO 91 MM=1,11
      TEMP1=X(MM)*CV(MM)
      TEMP2=X(MM)*CP(MM)
      CVR1=CVR1+TEMP1
      CPR1=CPR1+TEMP2
   91 CONTINUE
      DO 94 IZ=1,11
      TEMP3=(EMEO(IZ)+(TETH(IZ)/T))*(DERXR(IZ)*Z)
      TEMP4=(HMEO(IZ)+(TETH(IZ)/T))*(DERXP(IZ)*Z)
      CVR2=CVR2+TEMP3
      CPR2=CPR2+TEMP4
   94 CONTINUE
      ZCVR=(Z*CVR1)+(T*CVR2)
      ZCPR=(Z*CPR1)+(T*CPR2)
      GAMMAE=ZCPR/ZCVR
      A=SQRT((GAMMAE*((1.0+((T/Z)*DERZRO)))/(1.0+((T/Z)*DERZP)))*(P/RO)
     +)
      H=ERT*Z*RGAST
      ENRG=H
      RETURN
      END
C
*****************************************************************************
*
      SUBROUTINE ENTHSP(T,LA,GA,EA,TETV,EMEO,HMEO,CV,CP)
*
*****************************************************************************
C
C
C     THE SUBROUTINE ENTHSP CALCULATES THE INTERNAL ENERGY, ENTHALPY,
C     AND THE SPECIFIC HEATS FOR THE COMPONENTS OF AIR GIVEN THE
C     TEMPERATURE AND THE PARTITION FUNCTION DATA.
C
      COMMON/RGASP/ID
      DIMENSION LA(*),EA(11,*),EMEO(*),HMEO(*),CV(*),CP(*),TETV(*)
      INTEGER GA(11,*)
      SIGO=0.0
```

```
      SIG1=0.0
      SIG2=0.0
      LAN=LA(ID)
      DO 10 IJ=1,LAN
      IF((EA(ID,IJ)/T).GE.85.0)GOTO 10
      SUM1=GA(ID,IJ)*EXP((-EA(ID,IJ))/T)
      SUM2=(EA(ID,IJ)/T)*SUM1
      SUM3=(EA(ID,IJ)/T)*SUM2
      SIG0=SIG0+SUM1
      SIG1=SIG1+SUM2
      SIG2=SIG2+SUM3
   10 CONTINUE
      SIG10=SIG1/SIG0
      SIG20=SIG2/SIG0
      EMEO(ID)=(1.5+(SIG10))
      HMEO(ID)=EMEO(ID)+1.0
      IF(SIG10.LT.1.0E-05)GOTO 15
      CV(ID)=(1.5+SIG20-(SIG10*SIG10))
      GOTO 16
   15 CV(ID)=(1.5+SIG20)
   16 IF(ID.GE.3)GOTO 20
      E=(1.0+(TETV(ID)/T)*(1.0/(EXP(TETV(ID)/T)-1.0)))
      XHOLD=TETV(ID)/(2.0*T)
      C=(1.0+((XHOLD*XHOLD)*(1.0/(SINH(XHOLD)*SINH(XHOLD)))))
      EMEO(ID)=EMEO(ID)+E
      HMEO(ID)=HMEO(ID)+E
      CV(ID)=CV(ID)+C
   20 CP(ID)=CV(ID)+1.0
      RETURN
C
      END
C
*************************************************************************
*
      SUBROUTINE RVPART(TETAR,TETAV,T,SIGMA,LNQRV)
*
*************************************************************************
C
C
C     THE SUBROUTINE RVPART CALCULATES THE ROTATIONAL AND VIBRATIONAL
C     PARTITION FUNCTIONS FOR THE SPECIFIED GAS AT A GIVEN TEMPERATURE.
C     THE SUBROUTINE THEN RETURNS THE SUM OF THE NATURAL LOGARITHMS
C     OF THE ROTATIONAL AND VIBRATIONAL PARTITION FUNCTIONS. THE
C     SUBROUTINE IS ONLY NECESSARY FOR MOLECULES. (DIATOMIC)
C
      COMMON/RGASP/ID
      DIMENSION TETAR(*),TETAV(*)
      REAL LNQRV(*),LNQR,LNQV
      INTEGER SIGMA(*)
      IF(ABS((TETAV(ID)/T)).GT.85.0)GOTO 10
      QV=1./(1.-EXP((-TETAV(ID))/T))
      IF(QV.LE.0.0)GOTO 20
      LNQV=ALOG(QV)
```

```
C
      QR=T/(SIGMA(ID)*TETAR(ID))
      IF(QR.LE.0.0)GOTO 20
      LNQR=ALOG(QR)
C
      LNQRV(ID)=LNQR+LNQV
      RETURN
   10 WRITE(6,100)
      RETURN
   20 WRITE(6,101)
      RETURN
  100 FORMAT(' ***CAUTION, ARGUMENT OF EXP IN RVPART IS TOO LARGE')
  101 FORMAT(' ***CAUTION, ARGUMENT OF ALOG IN RVPART IS NEGATIVE')
      END
C
*****************************************************************************
*
      SUBROUTINE TEPART(T,P,LA,GA,EA,MGSXX,LNQT,LNQE)
*
*****************************************************************************
C
C
C     THE SUBROUTINE TEPART CALCULATES THE TRANSLATIONAL AND
C     ELECTRONIC EXCITATION PARTITION FUNCTIONS FOR THE SPECIFIED GAS
C     AT A GIVEN TEMPERATURE AND PRESSURE. THE SUBROUTINE THEN RETURNS
C     THE NATURAL LOGARITHMS OF THE TRANSLATIONAL AND ELECTRONIC
C     EXCITATION PARTITION FUNCTIONS. THE SUBROUTINE IS ONLY NECESSARY
C     FOR ATOMS. (MONATOMIC)
C
      COMMON/RGASP/ID
      INTEGER GA(11,*)
      REAL MGSXX(*),LNQT(*),LNQE(*)
      DIMENSION LA(*),EA(11,*)
      QE=0.0
      R=8.31696E 07
      IF(T.LE.0.0)GOTO 10
      IF(P.LE.0.0)GOTO 20
      LNQT(ID)=(2.5*ALOG(T))-ALOG(P/1.013E6)+(1.5*ALOG(MGSXX(ID)*4.5530
     +7E-07))+ALOG(R)
      GOTO 25
   10 WRITE(6,100)T
   20 WRITE(6,101)P
   25 LAH=LA(ID)
      DO 40 I=1,LAH
      IF(ABS((EA(ID,I)/T)).GT.85.0)GOTO 40
      QEI=GA(ID,I)*EXP(((-EA(ID,I))/T))
      QE=QE+QEI
   40 CONTINUE
      LNQE(ID)=ALOG(QE)
  100 FORMAT(' ***CAUTION, NEGATIVE TEMPERATURE',E12.5,' BEING EMPLOYED
     +IN TEPART')
  101 FORMAT(' ***CAUTION, NEGATIVE PRESSURE ',E12.5,' BEING EMPLOYED
     +IN TEPART')
```

```
      RETURN
      END
C
*****************************************************************************
*
      SUBROUTINE DERLNK(T,TETE,EMEO,TDRLKC,TDRLKP)
*
*****************************************************************************
C
C
C     THE SUBROUTINE DERLNK CALCULATES THE DERIVITIVE OF THE
C     EQUILIBRIUM CONSTANT FOR EACH REACTION AT CONSTANT PRESSURE
C     AND AT CONSTANT DENSITY GIVEN THE TEMPERATURE, THE CHARACTERISTIC
C     TEMPERATURES OF DISSOCIATION AND IONIZATION AND THE INTERNAL
C     ENERGY CALCULATIONS.
C
      COMMON/RGASP/ID
      DIMENSION TETE(*),EMEO(*),TDRLKC(*),TDRLKP(*)
      IF(ID.GT.2)GOTO 10
      IDE=ID
      TDRLKC(IDE)=-(TETE(IDE)/T)+(2.0*EMEO(IDE+2))-EMEO(IDE)
      GOTO 20
   10 IF((ID.EQ.4).OR.(ID.EQ.6))RETURN
      IDE=(ID+3)/2
      TDRLKC(IDE)=-(((TETE(ID)/T)+(EMEO(11)+EMEO(ID+2))-EMEO(ID))*0.8)+(
     +((TETE(ID+1)/T)+(EMEO(11)+EMEO(ID+3))-EMEO(ID+1))*0.2)
   20 TDRLKP(IDE)=TDRLKC(IDE)+1.0
      RETURN
      END
C
*****************************************************************************
*
      SUBROUTINE DERZ(T,Z,TDRLKC,TDRLKP,EPS1,EPS2,EPS3,EPS4,EPS5,DERZP,
*
*****************************************************************************
C
     +DERZRO,DERXP,DERXR)
C
C     SUBROUTINE DERZ CALCULATES THE DERIVITIVES OF THE DISSOCIATION
C     AND IONIZATION FACTORS GIVEN THE RESULTS OF THE SUBROUTINE
C     DERLNK, THE TEMPERATURE, AND THE COMPRESSIBILITY FACTOR.
C
      DIMENSION TDRLKC(*),TDRLKP(*),DERXP(*),DERXR(*)
      DPEPS1=0.0
      DPEPS2=0.0
      DPEPS3=0.0
      DPEPS4=0.0
      DPEPS5=0.0
      DREPS1=0.0
      DREPS2=0.0
      DREPS3=0.0
      DREPS4=0.0
      DREPS5=0.0
```

```
      IF(((0.2-EPS1).LT.1.0E-05).OR.(EPS1.LT.1.0E-05))GOTO 1
      DPEPS1=(TDRLKP(2)/T)/((2.0/EPS1)-(1.0/(1.0+EPS1))+(1.0/(0.2-EPS1)
     +))
      DREPS1=(TDRLKC(2)/T)/((2.0/EPS1)+(1.0/(0.2-EPS1)))
    1 IF(((0.8-EPS2).LT.1.0E-05).OR.(EPS2.LT.1.0E-05))GOTO 2
      DPEPS2=(TDRLKP(1)/T)/((2.0/EPS2)-(1.0/(1.0+EPS2))+(1.0/(0.8-EPS2)
     +))
      DREPS2=(TDRLKC(1)/T)/((2.0/EPS2)+(1.0/(0.8-EPS2)))
    2 IF(((1.0-EPS3).LT.1.0E-05).OR.(EPS3.LT.1.0E-05))GOTO 3
      DPEPS3=(TDRLKP(3)/T)/((2.0/EPS3)-(1.0/(1.0+EPS3))+(1.0/(1.0-EPS3)
     +))
      DREPS3=(TDRLKC(3)/T)/((2.0/EPS3)+(1.0/(1.0-EPS3)))
    3 IF(((2.0-(2.0*EPS4)).LT.1.0E-05).OR.(EPS4.LT.1.0E-05))GOTO 4
      DPEPS4=(TDRLKP(4)/T)/((2.0/EPS4)-(1.0/(4.0+(2.0*EPS4)))+(1.0/(2.0
     +-(2.0*EPS4))))
      DREPS4=(TDRLKC(4)/T)/((2.0/EPS4)+(1.0/(2.0-(2.0*EPS4))))
    4 IF(((2.0-(2.0*EPS5)).LT.1.0E-05).OR.(EPS5.LT.1.0E-05))GOTO 5
      DPEPS5=(TDRLKP(5)/T)/((2.0/EPS5)-(1.0/(6.0+(2.0*EPS5)))+(1.0/(2.0
     +-(2.0*EPS5))))
      DREPS5=(TDRLKC(5)/T)/((2.0/EPS5)+(1.0/(2.0-(2.0*EPS5))))
    5 DERZP=DPEPS1+DPEPS2+(2.0*DPEPS3)+(2.0*DPEPS4)+(2.0*DPEPS5)
      DERZRO=DREPS1+DREPS2+(2.0*DREPS3)+(2.0*DREPS4)+(2.0*DREPS5)
      DERXP(1)=((-1.0)/Z)*DPEPS2
      DERXP(2)=((-1.0)/Z)*DPEPS1
      DERXP(3)=((2.0/Z)*DPEPS2)+((-1.6/Z)*DPEPS3)
      DERXP(4)=((2.0/Z)*DPEPS1)+((-0.4/Z)*DPEPS3)
      DERXP(5)=(((2.0*DPEPS3)-(2.0*DPEPS4))/Z)*0.8
      DERXP(6)=DERXP(5)/4.0
      DERXP(7)=(((4.0*DPEPS4)-(4.0*DPEPS5))/Z)*0.4
      DERXP(8)=DERXP(7)/4.0
      DERXP(9)=((6.0*DPEPS5)/Z)*(0.8/3.0)
      DERXP(10)=DERXP(9)/4.0
      DERXP(11)=((2.0*DPEPS3)+(2.0*DPEPS4)+(2.0*DPEPS5))/Z
      DERXR(1)=((-1.0)/Z)*DREPS2
      DERXR(2)=((-1.0)/Z)*DREPS1
      DERXR(3)=((2.0/Z)*DREPS2)+((-1.6/Z)*DREPS3)
      DERXR(4)=((2.0/Z)*DREPS1)+((-0.4/Z)*DREPS3)
      DERXR(5)=(((2.0*DREPS3)-(2.0*DREPS4))/Z)*0.8
      DERXR(6)=DERXR(5)/4.0
      DERXR(7)=(((4.0*DREPS4)-(4.0*DREPS5))/Z)*0.4
      DERXR(8)=DERXR(7)/4.0
      DERXR(9)=((6.0*DREPS5)/Z)*(0.8/3.0)
      DERXR(10)=DERXR(9)/4.0
      DERXR(11)=((2.0*DREPS3)+(2.0*DREPS4)+(2.0*DREPS5))/Z
      RETURN
      END
C
*****************************************************************************
*
      SUBROUTINE MOLFRA(Z,EPS1,EPS2,EPS3,EPS4,EPS5,X)
*
*****************************************************************************
C
```

```
C
C     THE SUBROUTINE MOLFRA CALCULATES THE MOLE FRACTIONS OF THE
C     CONSTITUENTS FROM THE COMPRESSIBILITY FACTOR AND THE DISSOCIATION
C     AND IONIZATION FACTORS.
C
      DIMENSION X(*)
      X(1)=(0.8-EPS2)/Z
      X(2)=(0.2-EPS1)/Z
      X(3)=((2.0*EPS2)-(1.6*EPS3))/Z
      X(4)=((2.0*EPS1)-(0.4*EPS3))/Z
      X(5)=(((2.0*EPS3)-(2.0*EPS4))/Z)*0.8
      X(6)=X(5)/4.0
      X(7)=(((4.0*EPS4)-(4.0*EPS5))/Z)*0.4
      X(8)=X(7)/4.0
      X(9)=((6.0*EPS5)/Z)*(0.8/3.0)
      X(10)=X(9)/4.0
      X(11)=((2.0*EPS3)+(2.0*EPS4)+(2.0*EPS5))/Z
      RETURN
C
      END
```

APPENDIX B

PROGRAM LISTING FOR THE ANNULUS PROBLEM

```
*COMDECK COMMON
      LOGICAL RESTART
      REAL MASSIN,MASSOUT
      INTEGER T,T1,TSTEPS,TLAST
      CHARACTER PROBLEM*13
      PARAMETER (NT=120,MT=40,DB=2.,DT=3.532,DS=3.,TSTEPS=20)
      COMMON / HWM /
     +   U(0:NT+1,0:MT+1,0:1),  UR(0:NT+1,0:MT+1),  UT(0:NT+1,0:MT+1),
     +   V(0:NT+1,0:MT+1,0:1),  VR(0:NT+1,0:MT+1),  VT(0:NT+1,0:MT+1),
     +   R(0:NT+1,0:MT+1,0:1),  RR(0:NT+1,0:MT+1),  RT(0:NT+1,0:MT+1),
     +   P(0:NT+1,0:MT+1,0:1),  PR(0:NT+1,0:MT+1),  PT(0:NT+1,0:MT+1),
     +   E(0:NT+1,0:MT+1,0:1),  ER(0:NT+1,0:MT+1),  ET(0:NT+1,0:MT+1),
     +  RL(0:NT+1,0:MT+1,0:1),  WR(0:NT+1,0:MT+1),  WT(0:NT+1,0:MT+1),
     +AREA(0:NT+1,0:MT+1,0:1),
     +
     +W1(0:NT+1,0:MT+1),     SR(0:NT+1,0:MT+1),  DPOSR(0:NT+1,0:MT+1),
     +W3(0:NT+1,0:MT+1),     ST(0:NT+1,0:MT+1),  DNEGR(0:NT+1,0:MT+1),
     +W4(0:NT+1,0:MT+1),    PHI(0:NT+1,0:MT+1),  DPOST(0:NT+1,0:MT+1),
     + Y(0:NT+1,0:MT+1), RADIUS(0:NT+1,0:MT+1),  DNEGT(0:NT+1,0:MT+1),
     + Q(0:NT+1,0:MT+1),  OMEGA(0:NT+1,0:MT+1),
     +
     +UINIT,VINIT,RINIT,PINIT,EINIT,TINIT,GAMMA,TAU,T,T1,TIME,RESTART,
     +PMIN,PCD(0:50),FPCD(0:50),TT(8),THETA(0:NT+1),
     +TEMP(0:NT+1,0:MT+1),SONIC(0:NT+1,0:MT+1),
     +G5(0:NT+1,0:MT+1),G6(0:NT+1,0:MT+1),GMAX,GMIN,ETA
      LEVEL 2,/HWM/
*DECK AXIS
      PROGRAM AXIS
*CALL COMMON
C THIS PROGRAM COMPUTES PROPERTIES IN ANNULAR REGION BETWEEN JET/WALL
C LIST OF VARIABLES
C U,V,R,P,E: AXIAL VELOCITY, RADIAL VEL, DENSITY, PRESSURE, TOT ENERGY
C UINF ,VINF ,RINF ,PINF ,EINF ,TINF : U,V,R,P,E,TEMP OF FREE STREAM
C UINIT,VINIT,RINIT,PINIT,EINIT,TINIT: INITIAL U,V,R,P,E,TEMP IN CELLS
C UR,VR,RR,PR,ER: PROPERTIES (AS ABOVE) ON RADIAL BOUNDARIES (RIEMANN)
C UT,VT,RT,PT,ET: PROPERTIES ON CIRCUMFERENTIAL BOUNDARIES (RIEMANN)
C W,W1,W2,W3,W4: FLUID VEL COMPONENT NORMAL TO THE BOUNDARY
C Y: FLUID VELOCITY COMPONENT PARALLEL TO THE BOUNDARY
C RL: POSITION OF NODES MEASURED FROM SPHERE CENTER ALONG RAYS
C SR,ST: LENGTH OF RADIAL AND CIRCUMFERENTIAL BOUNDARIES
C PHI: ANGLE BETWEEN NEGATIVE X AXIS AND CIRCUMFERENTIAL BOUNDARY
C THETA: ANGLE BETWEEN NEGATIVE X AXIS AND RADIAL BOUNDARY
C DPOSR: ABSOLUTE VEL OF POSITIVE RUNNING WAVE FOR RADIAL BOUNDARIES
C DNEGR: ABSOLUTE VEL OF NEGATIVE RUNNING WAVE FOR RADIAL BOUNDARIES
C DPOST: ABSOLUTE VEL OF POSITIVE RUNNING WAVE FOR CIRCUM BOUNDARIES
C DNEGT: ABSOLUTE VEL OF NEGATIVE RUNNING WAVE FOR CIRCUM BOUNDARIES
C OMEGA: VELOCITY OF NODES ALONG THE RAY
C Q: VELOCITY OF CIRCUMFERENTIAL BOUNDARIES
C AREA, RADIUS: CELL AREA AND DISTANCE OF CENTROID TO X AXIS
C VELGRAD: RATIO OF V/R (RADIAL VEL/RADIUS) AT THE AXIS OF SYMMETRY
C T: TIME STEP INDEX
C TAU: LENGTH OF TIME STEP IN SECONDS
C TIME: ELAPSED TIME IN SECONDS
```

```
C TSTEPS: NUMBER OF TIME STEPS TO BE COMPUTED
C TEMP: AIR TEMPERATURE IN KELVINS
C SONIC: SPEED OF SOUND IN THE AIR
C G5,G6: REAL GAS CONSTANTS, REPLACE GAMMA=1.4, SEE SUBR FLUX FOR DEFT
C GMAX,GMIN: MAXIMUM AND MINIMUM VALUES FOR G5 AND G6
C PMIN: MINIMUM ALLOWABLE PRESSURE IN RIEMANN ITERATIONS
C A,B: MASS VEL OF NEG AND POS RUNNING WAVE IN RIEMANN PROBLEM
C NT,MT: NUMBER OF CELLS IN THE AXIAL AND RADIAL DIRECTIONS
C DB: DIAMETER OF THE BODY (DIMENSIONLESS)
C DT: DIAMETER OF THE TUBE (DIMENSIONLESS)
C DS: DOWNSTREAM LENGTH OF THE GRID IN MULTIPLES OF CHANNEL WIDTH
C
C CONSTANTS
      GAMMA=1.4
      GMAX=1.667
      GMIN=1.000
      PMIN=1.
      ETA=0.1
C
C IF RESTARTING A PREVIOUS RUN, SET RESTART EQUAL TO TRUE.
      RESTART=.TRUE.
C     RESTART=.FALSE.
C INITIAL CONDITIONS
      UINIT=1506.
      VINIT=0.
      RINIT=1.
      PINIT=101300.
      TINIT=273.
C THE AIR IS CONSIDERED TO BE INITIALLY AT STANDARD ATMOSPHERIC
C CONDITIONS, SO IT CAN BE CONSIDERED IDEAL.  THEREFORE, EINIT IS:
      EINIT=(PINIT/((GAMMA-1.)*RINIT))+(UINIT**2.+VINIT**2.)/2.
C
C INPUT/OUTPUT DESCRIPTION
C TAPE5: OUTPUT DATA FROM CONSERVATION EQ'S (U,V,R,P,E,RL,ETC)
C TAPE6: INPUT (BOUNDARY CONDITION) FROM SPHERE PROBLEM
C TAPE7: OUTPUT DATA FROM RIEMANN PROBLEM (UR,VR,RR,PR,ER,UT,...ET,ETC)
C TAPE8: RESTART DATA (N,M,U,V,R,P,E,G5,G6,TEMP FOR EACH CELL)
C
C
C
*****************************************************************************
C
C MAIN COMPUTATION
C
C
*****************************************************************************
C
C
      IF (RESTART) THEN
      READ (8,103) T1,TAU,TIME
      ELSE
      T1=0
      TIME=0.
```

```
      TAU=.000001
      END IF
C
      CALL IC
      CALL GRID
      DO 1 T=1,TSTEPS
      TIME=TIME+TAU
C
      CALL RAY
      CALL ARC
C     CALL BODY
      CALL FLUX
      CALL TIMESTP
      CALL UPDATE
    1 CONTINUE
  103 FORMAT (1X,I6,2E16.9)
      END
C
C
C
*******************************************************************************
C
C
      SUBROUTINE IC
C
C
*******************************************************************************
C
*CALL COMMON
C INITIAL CONDITIONS IN ALL COMPUTATIONAL CELLS:
      DO 31 N=1,NT
      DO 32 M=1,MT
      IF (RESTART) THEN
      READ (8,304) N1,M1,U(N,M,0),V(N,M,0),R(N,M,0),P(N,M,0),E(N,M,0),
     +TEMP(N,M),G5(N,M),G6(N,M)
      ELSE
      U(N,M,0)=UINIT
      V(N,M,0)=VINIT
      R(N,M,0)=RINIT
      P(N,M,0)=PINIT
      E(N,M,0)=EINIT
      TEMP(N,M)=TINIT
      G5(N,M)=1.4
      G6(N,M)=1.4
      END IF
   32 CONTINUE
   31 CONTINUE
C
C UPSTREAM BOUNDARY CONDITIONS (FROM SPHERE SOLUTION):
      READ (6,301,END=302) (U(0,M,0),V(0,M,0),R(0,M,0),P(0,M,0),
     +E(0,M,0),TEMP(0,M),G5(0,M),G6(0,M),M=1,MT)
  302 CONTINUE
  301 FORMAT (1X,4E16.9,E11.5,F6.0,2F6.3)
```

```
  304 FORMAT (1X,2I4,8E15.8)
      RETURN
      END
C
C
C
C*********************************************************************
C
      SUBROUTINE GRID
C
C *********************************************************************
C
*CALL COMMON
C
C DB=BODY DIAMETER
C DT=TUNNEL DIAMETER
C DS=DOWNSTREAM LENGTH OF GRID IN MULTIPLES OF CHANNEL WIDTH
      GRIDY=(DT-DB)/(2.*MT)
      GRIDX=((DT-DB)*DS)/(2.*NT)
C
      DO 11, N=0,NT
      DO 12, M=0,MT
      RL(N,M,0)=DT/2.-M*GRIDY
      IF (M.GT.0) SR(N,M)=GRIDY
      IF (N.GT.0) ST(N,M)=GRIDX
      PHI(N,M)=3.1415926535898
      IF (M.EQ.MT) THETA(N)=3.1415926535898/2.
      IF ((N.GT.0).AND.(M.GT.0)) THEN
      AREA(N,M,0)=GRIDX*GRIDY
      AREA(N,M,1)=AREA(N,M,0)
      RADIUS(N,M)=(RL(N-1,M,0)+RL(N-1,M-1,0))/2.
      END IF
C THE BOUNDARIES WILL NOT BE ALLOWED TO MOVE IN THE PRESENT FORMULATION
      Q(N,M)=0.
      OMEGA(N,M)=0.
   12 CONTINUE
   11 CONTINUE
      RETURN
      END
C
C
C *********************************************************************
C
      SUBROUTINE RAY
C
C *********************************************************************
C
*CALL COMMON
C THIS SUBROUTINE COMPUTES THE RIEMANN PRBLM ON RADIAL (RAY) BOUNDARIES
C
C DOWNSTREAM BOUNDARY CONDITIONS
C
      DO 41 M=1,MT
```

```
      U(NT+1,M,0)=U(NT,M,0)
      V(NT+1,M,0)=V(NT,M,0)
      R(NT+1,M,0)=R(NT,M,0)
      P(NT+1,M,0)=P(NT,M,0)
      E(NT+1,M,0)=E(NT,M,0)
      G5(NT+1,M)=G5(NT,M)
      G6(NT+1,M)=G6(NT,M)
   41 CONTINUE
C
C
      DO 42 N=0,NT
      DO 43 M=1,MT
C VEL COMPONENTS NORMAL (W) AND TANGENTIAL (Y) TO RADIAL BOUNDARY (N,M)
      W1(N,M)=U(N,M,0)*SIN(THETA(N))+V(N,M,0)*COS(THETA(N))
      W1(N+1,M)=U(N+1,M,0)*SIN(THETA(N))+V(N+1,M,0)*COS(THETA(N))
      Y(N,M)=-U(N,M,0)*COS(THETA(N))+V(N,M,0)*SIN(THETA(N))
      Y(N+1,M)=-U(N+1,M,0)*COS(THETA(N))+V(N+1,M,0)*SIN(THETA(N))
C
C DETERMINE IF NON-LINEAR EQUATIONS ARE REQUIRED
C     IF ((ABS(P(N,M,0)-P(N+1,M,0)).GT.(P(N,M,0)/10.)).OR.
C    +(ABS(W1(N,M)-W1(N+1,M)).GT.(ABS(W1(N,M)/10.)))) THEN
      PTEST1=ABS((P(N,M,0)-P(N+1,M,0))/P(N,M,0))
      WTEST1=ABS((W1(N,M)-W1(N+1,M))/W1(N,M))
      IF (((PTEST1.GT.ETA).AND.(P(N,M,0).GT.1.)).OR.
     +((WTEST1.GT.ETA).AND.(ABS(W1(N,M)).GT.1.))) THEN
      CALL NONLRAY (N,M,P0,W0,A,B)
      GO TO 44
      END IF
C
C LINEAR EQUATIONS ARE:
      G6BAR=(G6(N,M)+G6(N+1,M))/2.
      A2=.25*G6BAR*(P(N,M,0)+P(N+1,M,0))*(R(N,M,0)+R(N+1,M,0))
      A=SQRT(A2)
      B=A
      P0=(P(N,M,0)+P(N+1,M,0)+A*(W1(N,M)-W1(N+1,M)))/2.
      W0=(W1(N,M)+W1(N+1,M)+(1./A)*(P(N,M,0)-P(N+1,M,0)))/2.
C
   44 CONTINUE
      DNEGR(N,M)=W1(N,M)-A/R(N,M,0)
      DPOSR(N,M)=W1(N+1,M)+B/R(N+1,M,0)
C
      IF (DNEGR(N,M).GT.0.) THEN
      PR(N,M)=P(N,M,0)
      RR(N,M)=R(N,M,0)
      WR(N,M)=W1(N,M)
      UR(N,M)=U(N,M,0)
      VR(N,M)=V(N,M,0)
      ER(N,M)=E(N,M,0)
      ELSE IF (DPOSR(N,M).LT.0.) THEN
      PR(N,M)=P(N+1,M,0)
      RR(N,M)=R(N+1,M,0)
      WR(N,M)=W1(N+1,M)
      UR(N,M)=U(N+1,M,0)
```

```
      VR(N,M)=V(N+1,M,0)
      ER(N,M)=E(N+1,M,0)
      ELSE IF (W0.GT.0.) THEN
      RNEG=1./((1./R(N,M,0))-((P0-P(N,M,0))/A**2.))
      PR(N,M)=P0
      RR(N,M)=RNEG
      WR(N,M)=W0
      UR(N,M)=W0*SIN(THETA(N))-Y(N,M)*COS(THETA(N))
      VR(N,M)=W0*COS(THETA(N))+Y(N,M)*SIN(THETA(N))
      ER(N,M)=E(N,M,0)+((1./R(N,M,0))-(P0/A**2.))*(P(N,M,0)-P0)
      ELSE IF (W0.LE.0.) THEN
      RPOS=1./((1./R(N+1,M,0))-((P0-P(N+1,M,0))/B**2.))
      PR(N,M)=P0
      RR(N,M)=RPOS
      WR(N,M)=W0
      UR(N,M)=W0*SIN(THETA(N))-Y(N+1,M)*COS(THETA(N))
      VR(N,M)=W0*COS(THETA(N))+Y(N+1,M)*SIN(THETA(N))
      ER(N,M)=E(N+1,M,0)+((1./R(N+1,M,0))-(P0/B**2.))*(P(N+1,M,0)-P0)
      END IF
   43 CONTINUE
   42 CONTINUE
      RETURN
      END
C
C
C ***************************************************************************
C
      SUBROUTINE ARC
C
C ***************************************************************************
C
*CALL COMMON
C THIS SUBROUTINE COMPUTES THE RIEMANN PROBLEM ON TANGENTIAL BOUNDARIES
C
      DO 61 N=1,NT
C REFLECTION BOUNDARY CONDITION ON WALL
C
      U(N,0,0)=U(N,1,0)
      V(N,0,0)=-V(N,1,0)
      R(N,0,0)=R(N,1,0)
      P(N,0,0)=P(N,1,0)
      E(N,0,0)=E(N,1,0)
      G5(N,0)=G5(N,1)
      G6(N,0)=G6(N,1)
C
C REFLECTION BOUNDARY CONDITION ON BODY
C
      U(N,MT+1,0)=U(N,MT,0)
      V(N,MT+1,0)=-V(N,MT,0)
      R(N,MT+1,0)=R(N,MT,0)
      P(N,MT+1,0)=P(N,MT,0)
      E(N,MT+1,0)=E(N,MT,0)
      G5(N,MT+1)=G5(N,MT)
```

```
      G6(N,MT+1)=G6(N,MT)
C
   61 CONTINUE
C
      DO 62 N=1,NT
      DO 63 M=0,MT
C
      W3(N,M)=-U(N,M,0)*SIN(PHI(N-1,M))-V(N,M,0)*COS(PHI(N-1,M))
      W3(N,M+1)=-U(N,M+1,0)*SIN(PHI(N-1,M))-V(N,M+1,0)*COS(PHI(N-1,M))
      Y(N,M)=-U(N,M,0)*COS(PHI(N-1,M))+V(N,M,0)*SIN(PHI(N-1,M))
      Y(N,M+1)=-U(N,M+1,0)*COS(PHI(N-1,M))+V(N,M+1,0)*SIN(PHI(N-1,M))
C
C DETERMINE IF NON-LINEAR EQUATIONS ARE REQUIRED
C     IF ((ABS(P(N,M,0)-P(N,M+1,0)).GT.(P(N,M,0)/10.)).OR.
C    +(ABS(W3(N,M)-W3(N,M+1)).GT.(ABS(W3(N,M)/10.)))) THEN
      PTEST2=ABS((P(N,M,0)-P(N,M+1,0))/P(N,M,0))
      WTEST2=ABS((W3(N,M)-W3(N,M+1))/W3(N,M))
      IF (((PTEST2.GT.ETA).AND.(P(N,M,0).GT.1.)).OR.
     +((WTEST2.GT.ETA).AND.(ABS(W3(N,M)).GT.1.))) THEN
      CALL NONLARC (N,M,P0,W0,A,B)
      GO TO 64
      END IF
C
C LINEAR EQUATIONS ARE:
      G6BAR=(G6(N,M)+G6(N,M+1))/2.
      A2=.25*G6BAR*(P(N,M,0)+P(N,M+1,0))*(R(N,M,0)+R(N,M+1,0))
      A=SQRT(A2)
      B=A
      P0=(P(N,M,0)+P(N,M+1,0)+A*(W3(N,M+1)-W3(N,M)))/2.
      W0=(W3(N,M)+W3(N,M+1)+(1./A)*(P(N,M+1,0)-P(N,M,0)))/2.
C
   64 CONTINUE
      DNEGT(N,M)=W3(N,M+1)-A/R(N,M+1,0)
      DPOST(N,M)=W3(N,M)+B/R(N,M,0)
C
      IF (DNEGT(N,M).GT.0.) THEN
      PT(N,M)=P(N,M+1,0)
      RT(N,M)=R(N,M+1,0)
      WT(N,M)=W3(N,M+1)
      UT(N,M)=U(N,M+1,0)
      VT(N,M)=V(N,M+1,0)
      ET(N,M)=E(N,M+1,0)
      ELSE IF (DPOST(N,M).LT.0.) THEN
      PT(N,M)=P(N,M,0)
      RT(N,M)=R(N,M,0)
      WT(N,M)=W3(N,M)
      UT(N,M)=U(N,M,0)
      VT(N,M)=V(N,M,0)
      ET(N,M)=E(N,M,0)
      ELSE IF (W0.GT.0.) THEN
      RNEG=1./((1./R(N,M+1,0))-((P0-P(N,M+1,0))/A**2.))
      PT(N,M)=P0
      RT(N,M)=RNEG
```

```
      WT(N,M)=W0
      UT(N,M)=-W0*SIN(PHI(N-1,M))-Y(N,M+1)*COS(PHI(N-1,M))
      VT(N,M)=-W0*COS(PHI(N-1,M))+Y(N,M+1)*SIN(PHI(N-1,M))
      ET(N,M)=E(N,M+1,0)+((1./R(N,M+1,0))-(P0/A**2.))*(P(N,M+1,0)-P0)
      ELSE IF (W0.LE.0.) THEN
      RPOS=1./((1./R(N,M,0))-((P0-P(N,M,0))/B**2.))
      PT(N,M)=P0
      RT(N,M)=RPOS
      WT(N,M)=W0
      UT(N,M)=-W0*SIN(PHI(N-1,M))-Y(N,M)*COS(PHI(N-1,M))
      VT(N,M)=-W0*COS(PHI(N-1,M))+Y(N,M)*SIN(PHI(N-1,M))
      ET(N,M)=E(N,M,0)+((1./R(N,M,0))-(P0/B**2.))*(P(N,M,0)-P0)
      END IF
C
   63 CONTINUE
   62 CONTINUE
      RETURN
      END
C
C
C ***********************************************************************
C
      SUBROUTINE NONLRAY (N,M,P0,W0,A,B)
C
C ***********************************************************************
C
*CALL COMMON
      LEVEL 0,N,M,P0,W0,A,B
C THIS SUBROUTINE COMPUTES THE RIEMANN PROBLEM ON RADIAL BOUNDARIES
C BY ITERATION OF THE NON-LINEAR EQUATIONS
C
      G5BAR=(G5(N,M)+G5(N+1,M))/2.
      G6BAR=(G6(N,M)+G6(N+1,M))/2.
      PCD(0)=(P(N,M,0)+P(N+1,M,0))/2.
      J=0
   58 IF (J.GT.50) THEN
      P0=PCD(J)
      GO TO 59
      END IF
C COMPUTATION OF MASS VELOCITIES
C COMPUTATION FOR NEGATIVE-MOST CELL
C       IF (PCD(J).EQ.P(N,M,0)) THEN
        PTEST3=ABS((PCD(J)-P(N,M,0))/P(N,M,0))
        IF (PTEST3.LT.ETA) THEN
        A=SQRT(G5(N,M)*P(N,M,0)*R(N,M,0))
        GO TO 56
        END IF
      GHATNEG=G5(N,M)+(1.-(G5BAR/G6BAR))*(G5BAR-1.)*
     +        ((PCD(J)-P(N,M,0))/(0.5*(PCD(J)+P(N,M,0))))
      GNEG=MAX(GMIN,MIN(GHATNEG,GMAX))
      A11=(PCD(J)-P(N,M,0))*(PCD(J)+0.5*(GNEG-1.)*(PCD(J)+P(N,M,0)))
      A12=(PCD(J)/R(N,M,0))-((GNEG-1.)*P(N,M,0)/((G5(N,M)-1.)*R(N,M,0))
     +)
```

```
      A=SQRT(ABS(A11/A12))
C
C COMPUTATION FOR POSITIVE-MOST CELL
   56   PTEST4=ABS((PCD(J)-P(N+1,M,0))/P(N+1,M,0))
        IF (PTEST4.LT.ETA) THEN
        B=SQRT(G5(N+1,M)*P(N+1,M,0)*R(N+1,M,0))
        GO TO 57
        END IF
      GHATPOS=G5(N+1,M)+(1.-(G5BAR/G6BAR))*(G5BAR-1.)*
     +        ((PCD(J)-P(N+1,M,0))/(0.5*(PCD(J)+P(N+1,M,0))))
      GPOS=MAX(GMIN,MIN(GHATPOS,GMAX))
      B11=(PCD(J)-P(N+1,M,0))*(PCD(J)+0.5*(GPOS-1.)*(PCD(J)+P(N+1,M,0))
     +)
      B12=(PCD(J)/R(N+1,M,0))-((GPOS-1.)*P(N+1,M,0)/((G5(N+1,M)-1.)*R(
     +N+1,M,0)))
      B=SQRT(ABS(B11/B12))
C
   57 F=(B*P(N,M,0)+A*P(N+1,M,0)+A*B*(W1(N,M)-W1(N+1,M)))/(A+B)
      FPCD(J)=MAX(PMIN,F)
      IF (J.EQ.0) THEN
      PCD(J+1)=FPCD(J)
      J=J+1
      GO TO 58
      END IF
      IF ((FPCD(J-1).EQ.PMIN).AND.(FPCD(J).EQ.PMIN)) THEN
      P0=PMIN
      GO TO 59
      END IF
      DPCD=PCD(J)-PCD(J-1)
      DFPCD=FPCD(J)-FPCD(J-1)
      IF (ABS(DPCD).LT.ABS(PCD(J)/10000.)) THEN
      P0=PCD(J)
      ELSE
      PCD(J+1)=(FPCD(J)*DPCD-PCD(J)*DFPCD)/(DPCD-DFPCD)
      J=J+1
      GO TO 58
      END IF
   59 CONTINUE
      W0=(A*W1(N,M)+B*W1(N+1,M)+P(N,M,0)-P(N+1,M,0))/(A+B)
C
      RETURN
      END
C
C
C ***************************************************************************
C
      SUBROUTINE NONLARC (N,M,P0,W0,A,B)
C
C ***************************************************************************
C
      COMMON A11,A12,B11,B12
*CALL COMMON
      LEVEL 0,N,M,P0,W0,A,B
```

```
C THIS SUBROUTINE COMPUTES THE RIEMANN PROBLEM
C BY ITERATION OF THE NON-LINEAR EQUATIONS
C
      G5BAR=(G5(N,M)+G5(N,M+1))/2.
      G6BAR=(G6(N,M)+G6(N,M+1))/2.
      PCD(0)=(P(N,M+1,0)+P(N,M,0))/2.
      J=0
   58 IF (J.GT.50) THEN
      P0=PCD(J)
      GO TO 59
      END IF
C
C COMPUTATION OF MASS VELOCITIES
C
C COMPUTATION FOR NEGATIVE-MOST CELL
        PTEST5=ABS((PCD(J)-P(N,M+1,0))/P(N,M+1,0))
        IF (PTEST5.LT.ETA) THEN
        A=SQRT(G5(N,M+1)*P(N,M+1,0)*R(N,M+1,0))
        GO TO 56
        END IF
      GHATNEG=G5(N,M+1)+(1.-(G5BAR/G6BAR))*(G5BAR-1.)*
     +        ((PCD(J)-P(N,M+1,0))/(0.5*(PCD(J)+P(N,M+1,0))))
      GNEG=MAX(GMIN,MIN(GHATNEG,GMAX))
      A11=(PCD(J)-P(N,M+1,0))*(PCD(J)+0.5*(GNEG-1.)*(PCD(J)+P(N,M+1,0))
     +)
      A12=(PCD(J)/R(N,M+1,0))-((GNEG-1.)*P(N,M+1,0)/((G5(N,M+1)-1.)*R(
     +N,M+1,0)))
      A=SQRT(ABS(A11/A12))
C COMPUTATION FOR POSITIVE-MOST CELL
   56   PTEST6=ABS((PCD(J)-P(N,M,0))/P(N,M,0))
        IF (PTEST6.LT.ETA) THEN
        B=SQRT(G5(N,M)*P(N,M,0)*R(N,M,0))
        GO TO 57
        END IF
      GHATPOS=G5(N,M)+(1.-(G5BAR/G6BAR))*(G5BAR-1.)*
     +        ((PCD(J)-P(N,M,0))/(0.5*(PCD(J)+P(N,M,0))))
      GPOS=MAX(GMIN,MIN(GHATPOS,GMAX))
      B11=(PCD(J)-P(N,M,0))*(PCD(J)+0.5*(GPOS-1.)*(PCD(J)+P(N,M,0)))
      B12=(PCD(J)/R(N,M,0))-((GPOS-1.)*P(N,M,0)/((G5(N,M)-1.)*R(N,M,0))
     +)
      B=SQRT(ABS(B11/B12))
C
   57 F=(B*P(N,M+1,0)+A*P(N,M,0)+A*B*(W3(N,M+1)-W3(N,M)))/(A+B)
      FPCD(J)=MAX(PMIN,F)
      IF (J.EQ.0) THEN
      PCD(J+1)=FPCD(J)
      J=J+1
      GO TO 58
      END IF
      IF ((FPCD(J-1).EQ.PMIN).AND.(FPCD(J).EQ.PMIN)) THEN
      P0=PMIN
      GO TO 59
      END IF
```

```
      DPCD=PCD(J)-PCD(J-1)
      DFPCD=FPCD(J)-FPCD(J-1)
      IF (ABS(DPCD).LT.ABS(PCD(J)/10000.)) THEN
      P0=PCD(J)
      ELSE
      PCD(J+1)=(FPCD(J)*DPCD-PCD(J)*DFPCD)/(DPCD-DFPCD)
      J=J+1
      GO TO 58
      END IF
   59 CONTINUE
      W0=(A*W3(N,M+1)+B*W3(N,M)+P(N,M+1,0)-P(N,M,0))/(A+B)
C
      RETURN
      END
C
C
C ***************************************************************************
C
      SUBROUTINE BODY
C
C ***************************************************************************
C
*CALL COMMON
C THIS SUBROUTINE COMPUTES THE PROJECTILE BOUNDARY CONDITION.
C COMPUTE REFLECTED PRESSURE BY ITERATION OF NON-LINEAR EQUATIONS.
C THE BOUNDARY ON THE BODY IS A ONE-D REFLECTION PROBLEM, WHERE
C W = VEL OF INCIDENT FLUID, WT = VEL BEHIND REFLECTED SHOCK = 0.
      P1=0.
      PMIN=1.0
C
      DO 72 N=1,NT
      WT(N,MT)=0.
C VALUES FOR UT,VT,RT AND ET ON THE BODY SURFACE BOUNDARY ARE NOT
C REQUIRED, SINCE AT THIS BOUNDARY WT = Q = 0 , SO THESE TERMS DROP OUT
C OF THE CONSERVATION EQUATIONS.  HOWEVER, FOR THE SAKE OF PROGRAMMING
C COMPLETENESS, THEY WILL BE SET TO ZERO.
      UT(N,MT)=0.
      VT(N,MT)=0.
      RT(N,MT)=0.
      ET(N,MT)=0.
      W4(N,MT)=-U(N,MT,0)*SIN(PHI(N-1,MT))-V(N,MT,0)*COS(PHI(N-1,MT))
      L=0
      G5BAR=G5(N,MT)
      G6BAR=G6(N,MT)
      PCD(L)=P(N,MT,0)
   73 IF (L.GE.50) THEN
      PT(N,MT)=PCD(L)
      DPOST(N,MT)=W4(N,MT)+B/R(N,MT,0)
      GO TO 77
      END IF
C COMPUTE MASS VELOCITY OF THE RIEMANN WAVE
C       IF (PCD(L).EQ.P(N,MT,0)) THEN
        PTEST7=ABS((PCD(L)-P(N,MT,0))/P(N,MT,0))
```

```
          IF (PTEST7.LT.ETA) THEN
          B=SQRT(G5(N,MT)*P(N,MT,0)*R(N,MT,0))
          GO TO 71
          END IF
        GHATPOS=G5(N,MT)+(1.-(G5BAR/G6BAR))*(G5BAR-1.)*
       +        ((PCD(L)-P(N,MT,0))/(0.5*(PCD(L)+P(N,MT,0))))
        GPOS=MAX(GMIN,MIN(GHATPOS,GMAX))
        B11=(PCD(L)-P(N,MT,0))*(PCD(L)+0.5*(GPOS-1.)*(PCD(L)+P(N,MT,0)))
        B12=(PCD(L)/R(N,MT,0))-((GPOS-1.)*P(N,MT,0)/((G5(N,MT)-1.)*R(N,MT
       +,0)))
        B=SQRT(ABS(B11/B12))
C COMPUTE PRESSURE BEHIND THE RIEMANN WAVE
   71 F=P(N,MT,0)-W4(N,MT)*B
        FPCD(L)=MAX(PMIN,F)
        IF (L.EQ.0) THEN
        PCD(L+1)=FPCD(L)
        L=L+1
        GO TO 73
        END IF
        IF ((FPCD(L-1).EQ.PMIN).AND.(FPCD(L).EQ.PMIN)) THEN
        PT(N,MT)=PMIN
        DPOST(N,MT)=W4(N,MT)+B/R(N,MT,0)
        GO TO 77
        END IF
        DPCD=PCD(L)-PCD(L-1)
        DFPCD=FPCD(L)-FPCD(L-1)
        IF (ABS(DPCD).LT.ABS(PCD(L)/10000.)) THEN
        PT(N,MT)=PCD(L)
        DPOST(N,MT)=W4(N,MT)+B/R(N,MT,0)
        ELSE
        PCD(L+1)=(FPCD(L)*DPCD-PCD(L)*DFPCD)/(DPCD-DFPCD)
          IF (PCD(L+1).LE.0.) THEN
          LZ=L+1
          PCD(0)=PCD(L)
          L=0
          GO TO 73
          END IF
        L=L+1
        GO TO 73
        END IF
   77 CONTINUE
   72 CONTINUE
        END
C
C
C ***************************************************************************
C
      SUBROUTINE FLUX
C
C ***************************************************************************
C
*CALL COMMON
C
```

```
      DO 81 N=1,NT
      DO 82 M=1,MT
C
C CONSERVATION OF MASS
      C1=RR(N,M)*WR(N,M)*SR(N,M)
      C2=RT(N,M-1)*(WT(N,M-1)-Q(N,M-1))*ST(N,M-1)
      C3=RR(N-1,M)*(-WR(N-1,M))*SR(N-1,M)
      C4=RT(N,M)*(Q(N,M)-WT(N,M))*ST(N,M)
       C5=R(N,M,0)*V(N,M,0)*AREA(N,M,0)/RADIUS(N,M)
      C6=R(N,M,0)*AREA(N,M,0)
      R(N,M,1)=(C6-TAU*(C1+C2+C3+C4+C5))/AREA(N,M,1)
C
C CONSERVATION OF AXIAL MOMENTUM
      AM1=SR(N,M)*(RR(N,M)*UR(N,M)*WR(N,M)+PR(N,M)*SIN(THETA(N)
     +))
      AM2=ST(N,M-1)*(RT(N,M-1)*UT(N,M-1)*(WT(N,M-1)-Q(N,M-1))-
     +PT(N,M-1)*SIN(PHI(N-1,M-1)))
      AM3=SR(N-1,M)*(RR(N-1,M)*UR(N-1,M)*(-WR(N-1,M))-PR(N-1,M)*
     +SIN(THETA(N-1)))
      AM4=ST(N,M)*(RT(N,M)*UT(N,M)*(Q(N,M)-WT(N,M))+
     +PT(N,M)*SIN(PHI(N-1,M)))
       AM5=R(N,M,0)*U(N,M,0)*V(N,M,0)*AREA(N,M,0)/RADIUS(N,M)
      AM6=R(N,M,0)*U(N,M,0)*AREA(N,M,0)
      U(N,M,1)=(AM6-TAU*(AM1+AM2+AM3+AM4+AM5))/(R(N,M,1)*AREA(N,M,1))
C
C CONSERVATION OF RADIAL MOMENTUM
      RM1=SR(N,M)*(RR(N,M)*VR(N,M)*WR(N,M)+PR(N,M)*COS(THETA(N)
     +))
      RM2=ST(N,M-1)*(RT(N,M-1)*VT(N,M-1)*(WT(N,M-1)-Q(N,M-1))-
     +PT(N,M-1)*COS(PHI(N-1,M-1)))
      RM3=SR(N-1,M)*(RR(N-1,M)*VR(N-1,M)*(-WR(N-1,M))-PR(N-1,M)*
     +COS(THETA(N-1)))
      RM4=ST(N,M)*(RT(N,M)*VT(N,M)*(Q(N,M)-WT(N,M))+PT(N,M)*
     +COS(PHI(N-1,M)))
       RM5=R(N,M,0)*V(N,M,0)*V(N,M,0)*AREA(N,M,0)/RADIUS(N,M)
      RM6=R(N,M,0)*V(N,M,0)*AREA(N,M,0)
      V(N,M,1)=(RM6-TAU*(RM1+RM2+RM3+RM4+RM5))/(R(N,M,1)*AREA(N,M,1))
C
C CONSERVATION OF ENERGY
      E1=(PR(N,M)+RR(N,M)*ER(N,M))*WR(N,M)*SR(N,M)
      E2=(PT(N,M-1)*WT(N,M-1)+RT(N,M-1)*ET(N,M-1)*(WT(N,M-1)-
     +Q(N,M-1)))*ST(N,M-1)
      E3=(PR(N-1,M)+RR(N-1,M)*ER(N-1,M))*(-WR(N-1,M))*SR(N-1,M)
      E4=(PT(N,M)*(-WT(N,M))+RT(N,M)*ET(N,M)*(Q(N,M)-WT(N,M)
     +))*ST(N,M)
       E5=(P(N,M,0)+R(N,M,0)*E(N,M,0))*V(N,M,0)*AREA(N,M,0)/
     +RADIUS(N,M)
      E6=R(N,M,0)*E(N,M,0)*AREA(N,M,0)
      E(N,M,1)=(E6-TAU*(E1+E2+E3+E4+E5))/(R(N,M,1)*AREA(N,M,1))
C
      PROBLEM='R AND E GIVEN'
      DENSITY=R(N,M,1)
      ENERGY=E(N,M,1)-(U(N,M,1)**2.+V(N,M,1)**2.)/2.
```

```
      ESAVE=ENERGY
      OLDP=P(N,M,0)
      OLDT=TEMP(N,M)
      CALL REALGAS (DENSITY,ENERGY,SOUND,PRESSUR,TEMPERA,PROBLEM,
     +OLDP,OLDT)
      P(N,M,1)=PRESSUR
      TEMP(N,M)=TEMPERA
      SONIC(N,M)=SOUND
      G5(N,M)=1.+P(N,M,1)/(R(N,M,1)*ESAVE)
      G6(N,M)=(SONIC(N,M)**2.)*R(N,M,1)/P(N,M,1)
      IF (P(N,M,1).LT.0) P(N,M,1)=PMIN
   82 CONTINUE
   81 CONTINUE
C
C     IF (T.EQ.TSTEPS) THEN
      TLAST=T1+T
      REWIND 8
      WRITE (8,803) TLAST,TAU,TIME
      WRITE (8,804) ((N,M,U(N,M,1),V(N,M,1),R(N,M,1),P(N,M,1),E(N,M,1),
     +TEMP(N,M),G5(N,M),G6(N,M),M=1,MT),N=1,NT)
      IF (N.LE.NT) GO TO 89
      WRITE (5,808) TLAST,TIME
      WRITE (5,811)
      WRITE (7,808) TLAST,TIME
      WRITE (7,812)
      DO 83 N=0,NT,10
      DO 84 M=0,MT
      IF ((N.EQ.0).OR.(M.EQ.0)) THEN
      WRITE (5,810) N,M,RL(N,M,0),SR(N,M),ST(N,M),RADIUS(N,M),
     +AREA(N,M,0),PHI(N,M),Q(N,M),U(N,M,0),V(N,M,0),R(N,M,0),P(N,M,0),
     +E(N,M,0)
      ELSE
      WRITE (5,810) N,M,RL(N,M,0),SR(N,M),ST(N,M),RADIUS(N,M),
     +AREA(N,M,0),PHI(N,M),Q(N,M),U(N,M,1),V(N,M,1),R(N,M,1),P(N,M,1),
     +E(N,M,1)
      END IF
      WRITE (7,802) N,M,UR(N,M),VR(N,M),WR(N,M),RR(N,M),PR(N,M),
     +ER(N,M),UT(N,M),VT(N,M),WT(N,M),RT(N,M),PT(N,M),ET(N,M)
   84 CONTINUE
   83 CONTINUE
   89 CONTINUE
      MASSIN=0.
      MASSOUT=0.
      DO 85 M=1,MT
      MASSIN=MASSIN+(6.283185*R(1,M,1)*U(1,M,0)*RADIUS(1,M)*SR(0,M))
      MASSOUT=MASSOUT+6.283185*R(NT,M,1)*U(NT,M,0)*RADIUS(NT,M)*SR(NT,M
     +)
   85 CONTINUE
      PRINT*, TLAST,TIME,MASSIN,MASSOUT
      END IF
C
C
  800 FORMAT (1X,E14.7)
```

```
  801 FORMAT (1X,I5,2F10.4,10X,2F10.4)
  802 FORMAT (1X,2I3,3F10.3,F7.4,2E12.5,3F10.3,F7.4,2E12.5)
  803 FORMAT (1X,I6,2E16.9)
  804 FORMAT (1X,2I4,8E15.8)
  808 FORMAT (///1H1,1X,'TIME(',I4,')=',E14.7/)
  810 FORMAT (1X,2I3,6F10.7,F12.5,2F11.5,F7.4,2E12.5)
  811 FORMAT (3X,'N',2X,'M',5X,'RL',8X,'SR',8X,'ST',6X,'RADIUS',5X,
     +'AREA',6X,'PHI',9X,'Q',10X,'U',10X,'V',8X,'R',9X,'P',11X,'E'/)
  812 FORMAT (//3X,'N',2X,'M',5X,'UR',8X,'VR',8X,'WR',6X,'RR',8X,
     +'PR',10X,'ER',8X,'UT',8X,'VT',8X,'WT',7X,'RT',8X,'PT',10X,
     +'ET'/)
  824 FORMAT (1X,I5,F14.7)
  825 FORMAT (1X,I5,9E14.7)
      RETURN
      END
C
C
C ***************************************************************************
C
      SUBROUTINE UPDATE
C
C ***************************************************************************
C
*CALL COMMON
C
      DO 93 N=1,NT
      DO 94 M=1,MT
      U(N,M,0)=U(N,M,1)
      V(N,M,0)=V(N,M,1)
      R(N,M,0)=R(N,M,1)
      P(N,M,0)=P(N,M,1)
      E(N,M,0)=E(N,M,1)
   94 CONTINUE
   93 CONTINUE
C
  900 FORMAT (1X,2I5,6E19.12)
  901 FORMAT (1X,I10,E20.13)
      RETURN
      END
C
C
C ***************************************************************************
C
      SUBROUTINE TIMESTP
C
C ***************************************************************************
C
*CALL COMMON
      SF=0.9
      DO 101 N=1,NT
      DO 102 M=1,MT
C
      TT(1)=ST(N,M)*SIN(PHI(N-1,M)-THETA(N-1))/DPOSR(N-1,M)
```

```
      TT(2)=ST(N,M-1)*SIN(PHI(N-1,M-1)-THETA(N-1))/DPOSR(N-1,M)
C
      TT(3)=ST(N,M)*SIN(PHI(N-1,M)-THETA(N))/(-DNEGR(N,M))
      TT(4)=ST(N,M-1)*SIN(PHI(N-1,M-1)-THETA(N))/(-DNEGR(N,M))
C
      TT(5)=(RL(N,M-1,0)-RL(N,M,0))/
     +((DPOST(N,M)/SIN(PHI(N-1,M)-THETA(N)))-OMEGA(N,M-1))
      TT(6)=(RL(N-1,M-1,0)-RL(N-1,M,0))/
     +((DPOST(N,M)/SIN(PHI(N-1,M)-THETA(N-1)))-OMEGA(N-1,M-1))
C
      TT(7)=(RL(N,M-1,0)-RL(N,M,0))/
     +(OMEGA(N,M)-(DNEGT(N,M-1)/SIN(PHI(N-1,M-1)-THETA(N))))
      TT(8)=(RL(N-1,M-1,0)-RL(N-1,M,0))/
     +(OMEGA(N-1,M)-(DNEGT(N,M-1)/SIN(PHI(N-1,M-1)-THETA(N-1))))
C
      TAUT=1.E100
      TAUR=1.E100
      DO 1006 J=1,8
      IF (J.LE.4) THEN
      IF ((TT(J).GT.0.).AND.(TT(J).LT.TAUT)) TAUT=TT(J)
      ELSE
      IF ((TT(J).GT.0.).AND.(TT(J).LT.TAUR)) TAUR=TT(J)
      END IF
 1006 CONTINUE
      TAU9=TAUT*TAUR/(TAUT+TAUR)
      IF ((N.EQ.1).AND.(M.EQ.1)) THEN
      TAUBAR=TAU9
      ELSE
      TAUBAR=MIN(TAUBAR,TAU9)
      END IF
  102 CONTINUE
  101 CONTINUE
      TAU=SF*TAUBAR
C
      RETURN
      END
C
C
C*********************************************************************
C ////////////////////////////////////////////////////////////////////
C*********************************************************************
C
C
C*********************************************************************
C
      SUBROUTINE REALGAS(DENSITY,ENERGY,SOUND,PRESSUR,TEMPERA,PROBLEM,
     +OLDP,OLDT)
C
C*********************************************************************
C
C THIS SUBROUTINE WILL RETURN THE THERMODYNAMIC PROPERTIES OF REAL AIR,
C GIVEN THE DENSITY AND INTERNAL ENERGY OF THE AIR (PROBLEM='R AND E
C GIVEN'), OR GIVEN THE PRESSURE AND TEMPERATURE OF THE AIR (PROBLEM=
```

```
C 'P AND T GIVEN').
      CHARACTER PROBLEM*13
      COMMON/XYZ/GAMMAE
      COMMON/ENTRO/ZSR
      COMMON/BERT/ENRG,ENTH,RHO,COMPRES
      LEVEL 0,DENSITY,ENERGY,SOUND,PRESSUR,TEMPERA,PROBLEM,OLDP,OLDT
C
C VARIABLES AND UNITS ARE:
C    ROGIVE:     GIVEN DENSITY, KG/M**3
C    EGIVE:      GIVEN ENERGY, J/KG
C    P:          PRESSURE, N/M**2
C    T:          KELVIN
C    GAMMA:      RATIO OF SPECIFIC HEATS, DIMENSIONLESS
C    Z:          COMPRESSIBILITY, DIMENSIONLESS
C    ALPHA:      DEGREE OF DISOCCIATION, DIMENSIONLESS
C    A:          SONIC VELOCITY, M/S
C    ZSR:        DIMENSIONLESS ENTROPY, -S/R, S-ENTROPY, R-GAS CONSTANT
C
C CONVERT SI UNITS (USED IN MAIN PROGRAM) TO CGS (USED IN SUBROUTINE)
      DENSITY=DENSITY*(1.E-3)
      ENERGY=ENERGY*(1.E4)
C     PRESSUR=PRESSUR*(1.E1)
C     TEMPERA=TEMPERA
C     SOUND=SOUND*(1.E2)
C
C COMPUTE PROPERTIES OF THE REAL GAS
      IF (PROBLEM.EQ.'R AND E GIVEN') THEN
        CALL USERGP (DENSITY,ENERGY,SOUND,PRESSUR,TEMPERA,OLDP,OLDT)
      ELSE IF (PROBLEM.EQ.'P AND T GIVEN') THEN
        CALL RGP (PRESSUR,TEMPERA,ALPHA,DENSITY,ENERGY,SOUND)
      ELSE
        PRINT*, 'TROUBLE IN SUBROUTINE REALGAS'
      END IF
C
C CONVERT CGS UNITS TO SI
      DENSITY=DENSITY*(1.E3)
      ENERGY=ENERGY*(1.E-4)
      PRESSUR=PRESSUR*(1.E-1)
      TEMPERA=TEMPERA
      SOUND=SOUND*(1.E-2)
C
      RETURN
      END
C
*****************************************************************************
*
      SUBROUTINE USERGP(ROGIVE,EGIVE,A,P,T,OLDP,OLDT)
*
*****************************************************************************
C
      COMMON /RGPCOM/ GAMA,GAMAE,IRGPOPT,PLEFT,TLEFT,GAMLFT,ROLEFT
      LEVEL 0,ROGIVE,EGIVE,A,P,T,OLDP,OLDT
```

```
      DIMENSION AJAC(2,2),F(2),DELTA(2)

      DATA GAMA,GAMAE/1.4,1.4/
      DATA EMAX/1.E+13/
      EGIVE=AMIN1(EGIVE,EMAX)
C SUBROUTINE GUESS IS NOT USED HERE - STARTING POINT FOR ITERATION IS
C TAKEN AS THE T AND P IN THE CELL FROM THE PREVIOUS TIME STEP
C     CALL GUESS(P,T,ROGIVE,EGIVE)
      P=OLDP
      T=OLDT
      DEL=.01
      TOLER = 2.0E-5
      IRGPOPT = 1
C        NEWTON ITERATION TO FIND P,T WITH GIVEN RO,E
      DO 500 ITER=1,10
        ITNUM=ITER
      CALL RGP(P,T,ALPHA,RONEW,ENEW,ANEW)
      DELP=DEL*P
       P1=P+DELP
      CALL RGP(P1,T,ALPHA,RO1,E1,A)
      DELT=DEL*T
       T2=T+DELT
      CALL RGP(P,T2,ALPHA,RO2,E2,A)
      AJAC(1,1)=(RO1-RONEW)/DELP
      DRODP=AJAC(1,1)
        AJAC(2,1)=(E1-ENEW)/DELP
      DEDP=AJAC(2,1)
        AJAC(1,2)=(RO2-RONEW)/DELT
      DRODT=AJAC(1,2)
        AJAC(2,2)=(E2-ENEW)/DELT
      DEDT=AJAC(2,2)
        F(1)=-RONEW+ROGIVE
      F(2)=-ENEW+EGIVE
      CALL SOL2BY2(AJAC,DELTA,F)
      IF(ABS(DELTA(1)) .GT. TOLER*P)GO TO 300
      IF(ABS(DELTA(2)) .GT. TOLER*T)GO TO 300
      GO TO 600
  300 CONTINUE
      P=P+DELTA(1)
      T=T+DELTA(2)
  500 CONTINUE
C        NO CONVERGENCE
C     WRITE(6,1234)
 1234 FORMAT(' NO CONVERGENCE IN USERGP ITERATION')
  600 CONTINUE
      PBACK=P
      GBACK = PBACK/(ROGIVE*EGIVE) + 1.
      GCBACK = ANEW*ANEW*ROGIVE/PBACK
        PLEFT=P
        TLEFT=T
        ROLEFT=ROGIVE
      RETURN
       END
```

```
C
*******************************************************************************
*
      SUBROUTINE SOL2BY2(A,X,B)
*
*******************************************************************************
C

      LEVEL 0,A,X,B
      REAL A(2,2),X(2),B(2)

      DET = A(1,1) * A(2,2)  -  A(1,2) * A(2,1)
      X(1) = (A(2,2) * B(1)  -  A(1,2) * B(2)) / DET
      X(2) = (-A(2,1) * B(1)  +  A(1,1) * B(2)) / DET

      RETURN
C
      END
C
*******************************************************************************
*
      SUBROUTINE GUESS(P,T,RO,E)
*
*******************************************************************************
C
      LEVEL 0,P,T,RO,E
      DATA R,GM1 /2.9677E6,.4/
      P=GM1*RO*E
      T=GM1*E/R
      RETURN
C
       END
C
*******************************************************************************
*
      SUBROUTINE RGP(P,T,ALPHA,RO,H,A)
*
*******************************************************************************
C
C     ****************************************
C     *                                      *
C     *   AN EQUATION OF STATE FOR REAL AIR  *
C     *                                      *
C     *   UNIVERSITY OF TORONTO              *
C     *   INSTITUTE FOR AEROSPACE STUDIES    *
C     *                                      *
C     *   WRITTEN BY ROBERT DESCHAMBAULT     *
C     *   VERSION 1.2  JUNE, 1980            *
C     *                                      *
C     ****************************************
C
C     THE SUBROUTINE RGP IS AN ENGINEERING APPROXIMATION OF THE
C     EOS (EQUATION OF STATE) FOR PERFECT AND REAL AIR.
```

```
C     RGP CALCULATES VARIOUS THERMODYNAMIC QUANTITIES GIVEN THE EQUILIB
C     PRESSURE AND TEMPERATURE.  IT IS ADAPTED FROM THE NASA TECHNICAL
C     REPORT TR R-50 BY DR. C. F. HANSEN(1959).  EXTENSIONS HAVE BEEN
C     MADE TO THE ORIGINAL WORK TO INCLUDE TWO MORE LEVELS OF
C     IONIZATION.  HENCE, THE CALCULATION IS RELIABLE TO 50000 DEGREES
C     KELVIN IF DENSITIES ARE KEPT UNDER 100 TIMES STANDARD ATMOSPHERIC
C     CONDITIONS.
C     THE MODEL ASSUMES A MIXTURE OF 20 PERCENT OXYGEN AND 80 PERCENT
C     NITROGEN AT STP CONDITIONS.  AS THE TEMPERATURE IS INCREASED,
C     FOR A GIVEN INITIAL PRESSURE, A TOTAL OF 11 DIFFERENT SPECIES
C     INVOLVED IN 8 REACTIONS MAY BE PRODUCED.
C
C     VARIABLE LIST
C
C     P - PRESSURE (ATMOSPHERE)
C     T - TEMPERATURE (DEGREE KELVIN)
C     ITYPE - TYPE OF EOS USED, 1 = PERFECT GAS, 2 = REAL GAS
C     ALPHA - DEGREE OF DISSOCIATION AND IONIZATION
C     RO - EQUILIBRIUM DENSITY (GRAMS PER CUBIC CENTIMETER)
C     H - EQUILIBRIUM ENTHALPY (ERGS)
C     A - EQUILIBRIUM SPEED OF SOUND (CENTIMETER PER SECOND)
C     GAMMAE - EQUILIBRIUM RATIO OF SPECIFIC HEATS
C     R - UNIVERSAL GAS CONSTANT (ERG PER GRAMMOLE PER DEGREE KELVIN)
C     ZSR - NONDIMENSIONAL ENTROPY
C
C     REQUIRED SUBROUTINES FOR RGP (SIX ROUTINES)
C     ENTHSP
C     RVPART
C     TEPART
C     DERLNK
C     DERZ
C     MOLFRA
C
      COMMON/ABC/ITYPE
      COMMON/RGASP/ID
      COMMON/XYZ/GAMMAE
      COMMON/ENTRO/ZSR
      COMMON/BERT/ENRG,ENTH,RHO,COMPRES
      LEVEL 0,P,T,ALPHA,RO,H,A
      DIMENSION LA(11),EA(11,21),TETE(11),TETV(2),TETR(2),X(11),TDRLKC(
     +5),TDRLKP(5),DERXR(11),DERXP(11),HMEO(11),EMEO(11),CP(11),CV(11),
     +TETH(11),SR(11)
      DIMENSION EA1(11),EA2(11),EA3(11),EA4(11),EA5(11),EA6(11),EA7(11)
     +,EA8(11),EA9(11),EA10(11),EA11(11),EA12(11),EA13(11),EA14(11),EA
     +15(11),EA16(11),EA17(11),EA18(11),EA19(11),EA20(11),EA21(11)
      REAL MGAS,MGS(11),LNQ(11),LNQP(11),LNQT(11),LNQRV(11),LNQE(11),LN
     +KP(8),KP(8),KPA(3)
      INTEGER GA(11,21),SIGMA(2)
      INTEGER GA1(11),GA2(11),GA3(11),GA4(11),GA5(11),GA6(11),GA7(11),
     +GA8(11),GA9(11),GA10(11),GA11(11),GA12(11),GA13(11),GA14(11),GA15
     +(11),GA16(11),GA17(11),GA18(11),GA19(11),GA20(11),GA21(11)
      EQUIVALENCE (GA(1,1),GA1(1)),(GA(1,2),GA2(1)),(GA(1,3),GA3(1)),(G
     +A(1,4),GA4(1)),(GA(1,5),GA5(1)),(GA(1,6),GA6(1)),(GA(1,7),GA7(1))
```

```
     +,(GA(1,8),GA8(1)),(GA(1,9),GA9(1)),(GA(1,10),GA10(1)),(GA(1,11),G
     +A11(1)),(GA(1,12),GA12(1)),(GA(1,13),GA13(1)),(GA(1,14),GA14(1)),
     +(GA(1,15),GA15(1)),(GA(1,16),GA16(1)),(GA(1,17),GA17(1)),(GA(1,18
     +),GA18(1)),(GA(1,19),GA19(1)),(GA(1,20),GA20(1)),(GA(1,21),GA21(1
     +))
      EQUIVALENCE (EA(1,1),EA1(1)),(EA(1,2),EA2(1)),(EA(1,3),EA3(1)),(E
     +A(1,4),EA4(1)),(EA(1,5),EA5(1)),(EA(1,6),EA6(1)),(EA(1,7),EA7(1))
     +,(EA(1,8),EA8(1)),(EA(1,9),EA9(1)),(EA(1,10),EA10(1)),(EA(1,11),E
     +A11(1)),(EA(1,12),EA12(1)),(EA(1,13),EA13(1)),(EA(1,14),EA14(1)),
     +(EA(1,15),EA15(1)),(EA(1,16),EA16(1)),(EA(1,17),EA17(1)),(EA(1,18
     +),EA18(1)),(EA(1,19),EA19(1)),(EA(1,20),EA20(1)),(EA(1,21),EA21(1
     +))
C
C      INITIALIZE CONSTANTS REQUIRED FOR PARTITION FUNCTION CALCULATIONS
C
      DATA TETH/0.0,0.0,56608.,29669.5,225469.,187726.,569172.,595759.,
     +1119774.,1233519.,0.0/
      DATA MGS/28.0134,31.9988,14.0067,15.9994,14.00615,15.99885,14.005
     +6,15.9983,14.00505,15.99775,0.54905E-03/
      DATA LA/2,14,15,21,10,5,7,7,4,6,1/
      DATA TETE/113216.,59339.8,168861.,158056.,343703.,408033.6,550602
     +.4,637760.5,898381.8,896989.,0.0/
      DATA TETV/3371.0,2256.0/
      DATA TETR/2.88,2.069/
      DATA SIGMA/2,2/
      DATA GA1/1,3,4,5,1,4,2,1,1,2,2/,GA2/3,2,10,3,3,10,4,3,4,4,2/,GA3/
     +0,1,6,1,5,6,2,5,5,2,0/,GA4/0,3,12,5,5,6,4,5,3,4,0/,GA5/0,0,6,1,1,
     +6,6,1,0,6,0/,GA6/2*0,12,5,5,0,10,5,0,10,0/,GA7/2*0,2,3,15,0,2,15,
     +3*0/,GA8/2*0,20,15,9,6*0/,GA9/2*0,12,9,5,6*0/,GA10/2*0,14,5,12,6*
     +0/,GA11/2*0,6,3,7*0/,GA12/2*0,10,45,7*0/,GA13/2*0,12,15,7*0/,GA14
     +/2*0,6,9,7*0/,GA15/2*0,34,15,7*0/,GA16/3*0,5,7*0/,GA17/3*0,3,7*0/
     +,GA18/3*0,5,7*0/,GA19/3*0,25,7*0/,GA20/3*0,15,7*0/,GA21/3*0,9,7*0
     +/
      DATA EA1/11*0.0/,EA2/72224.73,11390.85,27653.59,228.01,70.63,3856
     +5.69,251.03,163.13,96671.11,556.01,0.0/,EA3/0.0,18982.19,41488.29
     +,325.83,188.88,58214.37,82274.7,441.36,96878.53,102392.9,0.0/,EA4
     +/0.0,51925.54,119927.6,22826.76,22032.67,172394.6,82360.9,29161.2
     +1,188013.6,102581.9,0.0/,EA5/0.0,0.0,124037.9,48612.65,47022.6,17
     +2629.6,82477.68,62122.39,0.0,102847.3,0.0/
      DATA EA6/2*0.0,126751.5,106119.9,67853.92,0.0,145329.5,86710.7,0.
     +0,182696.4,0.0/,EA7/2*0.0,134624.4,110474.4,132690.4,0.0,188457.4
     +,172560.5,3*0.0/,EA8/2*0.0,136495.7,124624.6,157117.7,6*0.0/,EA9/
     +2*0.0,137430.9,127501.4,207425.7,6*0.0/,EA10/2*0.0,139345.7,13734
     +9.2,214457.8,6*0.0/,EA11/2*0.0,140700.2,138426.9,7*0.0/,EA12/2*0.
     +0,143374.8,140145.5,7*0.0/
      DATA EA13/2*0.0,149232.3,142554.1,7*0.0/,EA14/2*0.0,149958.1,1433
     +97.,7*0.0/,EA15/2*0.0,150714.4,145489.5,7*0.0/,EA16/3*0.0,146901.
     +,7*0.0/,EA17/3*0.0,147326.,7*0.0/,EA18/3*0.0,147685.7,7*0.0/,EA19
     +/3*0.0,147978.3,7*0.0/,EA20/3*0.0,148040.3,7*0.0/,EA21/3*0.0,1494
     +23.1,7*0.0/
C
C      DEFINE USEFUL QUANTITIES
C
```

```
      R=0.83169E 08
      RT=R*T
      MGAS=28.9667
      RGAS=R/MGAS
      RGAST=RGAS*T
      ITYPE = 2
      IF (ITYPE.EQ.2) GO TO 2
C     GOTO(1,2),ITYPE
C
C     PERFECT GAS CALCULATION
C
    1 GAMA=1.4
      E=(1./(GAMA-1.))*RGAST
      ALPHA=0.
      RO=P/RGAST
      H=(E+RGAST)/RGAS
      A=SQRT(GAMA*RGAST)
      ZSR=((GAMA/(GAMA-1.0))*ALOG(T/300.0))-ALOG(P/1.0)
      GAMMAE=GAMA
      RETURN
C
C     REAL GAS CALCULATION
C
C     CALCULATE PARTITION FUNCTIONS FOR EACH SPECIES
C
    2 DO 20 ID=1,11
      IF(ID.GE.3)GOTO 10
      CALL RVPART(TETR,TETV,T,SIGMA,LNQRV)
      GOTO 15
   10 LNQRV(ID)=0.0
   15 CALL TEPART(T,P,LA,GA,EA,MGS,LNQT,LNQE)
      LNQ(ID)=LNQT(ID)+LNQRV(ID)+LNQE(ID)
      LNQP(ID)=LNQ(ID)+ALOG(P)
   20 CONTINUE
C
C     CALCULATE EQUILIBRIUM CONSTANTS FOR EACH REACTION
C
      DO 40 ID=1,8
      IDREAC=ID
      IF(ID.GE.3)GOTO 30
      LNKP(IDREAC)=((-TETE(ID))/T)+(2.*LNQP(ID+2))-LNQP(ID)
      GOTO 40
   30 LNKP(IDREAC)=((-TETE(ID))/T)+LNQP(ID+2)+LNQP(11)-LNQP(ID)
   40 CONTINUE
      DO 50 IDREAC=1,8
      IF(LNKP(IDREAC).LE.(-85.0))GOTO 45
      KP(IDREAC)=EXP(LNKP(IDREAC))
      GOTO 50
   45 KP(IDREAC)=0.0
   50 CONTINUE
      DO 60 I=4,8,2
      IDA=(I-2)/2
   60 KPA(IDA)=(0.2*KP(I)+(0.8*KP(I-1)))
```

```
C
C     CALCULATE THE DISSOCIATION AND IONIZATION FACTORS
C
      EPS1=0.0
      EPS2=0.0
      EPS3=0.0
      EPS4=0.0
      EPS5=0.0
      IF(KP(2).LT.1.0E-05)GOTO 61
      XHOLD1=(1.+((4.0*P)/KP(2)))
      EPS1=((-0.8)+SQRT(0.64+(0.8*XHOLD1)))/(2.0*XHOLD1)
   61 IF(KP(1).LT.1.0E-05)GOTO 62
      XHOLD2=(1.+((4.0*P)/KP(1)))
      EPS2=((-0.4)+SQRT(0.16+(3.84*XHOLD2)))/(2.0*XHOLD2)
   62 IF(KPA(1).LT.1.0E-05)GOTO 63
      EPS3=1./SQRT(1.0+(P/KPA(1)))
   63 IF(KPA(2).LT.1.0E-05)GOTO 64
      ZHOLD=1.0+(P/KPA(2))
      EPS4=((-ZHOLD)+SQRT((ZHOLD*ZHOLD)+(8.0*ZHOLD)))/(2.0*ZHOLD)
   64 IF(KPA(3).LT.1.0E-05)GOTO 65
      AHOLD=2.0+((2.0*P)/KPA(3))
      BHOLD=1.0+(P/KPA(3))
      EPS5=((-AHOLD)+SQRT((AHOLD*AHOLD)+(12.0*BHOLD)))/(2.0*BHOLD)
   65 IF(EPS1.GT.0.2)EPS1=0.2
      IF(EPS2.GT.0.8)EPS2=0.8
      IF(EPS3.GT.1.0)EPS3=1.0
      IF(EPS4.GT.1.0)EPS4=1.0
      IF(EPS5.GT.1.0)EPS5=1.0
      ALPHA=EPS1+EPS2+(2.0*EPS3)+(2.0*EPS4)+(2.0*EPS5)
      Z=1.0+ALPHA
      COMPRES=Z
      RO=P/(Z*RGAST)
      RHO=RO
C
C     CALCULATE THE MOLE FRACTION FOR EACH SPECIES
C
      CALL MOLFRA(Z,EPS1,EPS2,EPS3,EPS4,EPS5,X)
C
C     CALCULATE THE INTERNAL ENERGY, ENTHALPY, AND EQUILIBRIUM RATIO
C     OF SPECIFIC HEATS FOR EACH SPECIES
C
      DO 70 ID=1,11
      CALL ENTHSP(T,LA,GA,EA,TETV,EMEO,HMEO,CV,CP)
   70 CONTINUE
C
C     CALCULATE THE ENTROPY FOR EACH SPECIES
C
      DO 21 LH=1,11
   21 SR(LH)=LNQP(LH)+HMEO(LH)
      XSUM=0.0
      YSUM=0.0
      DO 68 LP=1,11
      YHO=X(LP)*SR(LP)
```

```
      YSUM=YSUM+YHO
      IF(X(LP).LE.0.0)GOTO 68
      XHO=X(LP)*ALOG(X(LP))
      XSUM=XSUM+XHO
   68 CONTINUE
      ZSR=Z*(YSUM-XSUM-ALOG(P))
C
C     CALCULATE APPROPRIATE DERIVITIVES FOR THE EQUILIBRIUM RATIO OF
C     SPECIFIC HEATS FOR AIR MIXTURE
C
      DO 80 ID=1,7
      CALL DERLNK(T,TETE,EMEO,TDRLKC,TDRLKP)
   80 CONTINUE
      CALL DERZ(T,Z,TDRLKC,TDRLKP,EPS1,EPS2,EPS3,EPS4,EPS5,DERZP,DERZRO
     +,DERXP,DERXR)
      ERT=0.0
      DO 90 I=1,11
      SAVE=X(I)*(EMEO(I)+(TETH(I)/T))
      ERT=ERT+SAVE
   90 CONTINUE
      ZHRT=(ERT*Z)+Z
      H=(ZHRT*T)
      ENTH=H*RGAS
      CVR1=0.0
      CVR2=0.0
      CPR1=0.0
      CPR2=0.0
      DO 91 MM=1,11
      TEMP1=X(MM)*CV(MM)
      TEMP2=X(MM)*CP(MM)
      CVR1=CVR1+TEMP1
      CPR1=CPR1+TEMP2
   91 CONTINUE
      DO 94 IZ=1,11
      TEMP3=(EMEO(IZ)+(TETH(IZ)/T))*(DERXR(IZ)*Z)
      TEMP4=(HMEO(IZ)+(TETH(IZ)/T))*(DERXP(IZ)*Z)
      CVR2=CVR2+TEMP3
      CPR2=CPR2+TEMP4
   94 CONTINUE
      ZCVR=(Z*CVR1)+(T*CVR2)
      ZCPR=(Z*CPR1)+(T*CPR2)
      GAMMAE=ZCPR/ZCVR
      A=SQRT((GAMMAE*((1.0+((T/Z)*DERZRO)))/(1.0+((T/Z)*DERZP)))*(P/RO)
     +)
      H=ERT*Z*RGAST
      ENRG=H
      RETURN
      END
C
*******************************************************************************
*
      SUBROUTINE ENTHSP(T,LA,GA,EA,TETV,EMEO,HMEO,CV,CP)
*
```

```
*************************************************************************
C
C
C     THE SUBROUTINE ENTHSP CALCULATES THE INTERNAL ENERGY, ENTHALPY,
C     AND THE SPECIFIC HEATS FOR THE COMPONENTS OF AIR GIVEN THE
C     TEMPERATURE AND THE PARTITION FUNCTION DATA.
C
      COMMON/RGASP/ID
      LEVEL 0,T,LA,GA,EA,TETV,EMEO,HMEO,CV,CP
      DIMENSION LA(*),EA(11,*),EMEO(*),HMEO(*),CV(*),CP(*),TETV(*)
      INTEGER GA(11,*)
      SIG0=0.0
      SIG1=0.0
      SIG2=0.0
      LAN=LA(ID)
      DO 10 IJ=1,LAN
      IF((EA(ID,IJ)/T).GE.85.0)GOTO 10
      SUM1=GA(ID,IJ)*EXP((-EA(ID,IJ))/T)
      SUM2=(EA(ID,IJ)/T)*SUM1
      SUM3=(EA(ID,IJ)/T)*SUM2
      SIG0=SIG0+SUM1
      SIG1=SIG1+SUM2
      SIG2=SIG2+SUM3
   10 CONTINUE
      SIG10=SIG1/SIG0
      SIG20=SIG2/SIG0
      EMEO(ID)=(1.5+(SIG10))
      HMEO(ID)=EMEO(ID)+1.0
      IF(SIG10.LT.1.0E-05)GOTO 15
      CV(ID)=(1.5+SIG20-(SIG10*SIG10))
      GOTO 16
   15 CV(ID)=(1.5+SIG20)
   16 IF(ID.GE.3)GOTO 20
      E=(1.0+(TETV(ID)/T)*(1.0/(EXP(TETV(ID)/T)-1.0)))
      XHOLD=TETV(ID)/(2.0*T)
      C=(1.0+((XHOLD*XHOLD)*(1.0/(SINH(XHOLD)*SINH(XHOLD)))))
      EMEO(ID)=EMEO(ID)+E
      HMEO(ID)=HMEO(ID)+E
      CV(ID)=CV(ID)+C
   20 CP(ID)=CV(ID)+1.0
      RETURN
      END
C
*************************************************************************
*
      SUBROUTINE RVPART(TETAR,TETAV,T,SIGMA,LNQRV)
*
*************************************************************************
C
C
C     THE SUBROUTINE RVPART CALCULATES THE ROTATIONAL AND VIBRATIONAL
C     PARTITION FUNCTIONS FOR THE SPECIFIED GAS AT A GIVEN TEMPERATURE.
C     THE SUBROUTINE THEN RETURNS THE SUM OF THE NATURAL LOGARITHMS
```

```
C     OF THE ROTATIONAL AND VIBRATIONAL PARTITION FUNCTIONS. THE
C     SUBROUTINE IS ONLY NECESSARY FOR MOLECULES. (DIATOMIC)
C
      COMMON/RGASP/ID
      LEVEL 0,TETAR,TETAV,T,SIGMA,LNQRV
      DIMENSION TETAR(*),TETAV(*)
      REAL LNQRV(*),LNQR,LNQV
      INTEGER SIGMA(*)
      IF(ABS((TETAV(ID)/T)).GT.85.0)GOTO 10
      QV=1./(1.-EXP((-TETAV(ID))/T))
      IF(QV.LE.0.0)GOTO 20
      LNQV=ALOG(QV)
C
      QR=T/(SIGMA(ID)*TETAR(ID))
      IF(QR.LE.0.0)GOTO 20
      LNQR=ALOG(QR)
C
      LNQRV(ID)=LNQR+LNQV
      RETURN
   10 WRITE(6,100)
      RETURN
   20 WRITE(6,101)
      RETURN
  100 FORMAT(' ***CAUTION, ARGUMENT OF EXP IN RVPART IS TOO LARGE')
  101 FORMAT(' ***CAUTION, ARGUMENT OF ALOG IN RVPART IS NEGATIVE')
      END
C
**********************************************************************
*
      SUBROUTINE TEPART(T,P,LA,GA,EA,MGSXX,LNQT,LNQE)
*
**********************************************************************
C
C
C     THE SUBROUTINE TEPART CALCULATES THE TRANSLATIONAL AND
C     ELECTRONIC EXCITATION PARTITION FUNCTIONS FOR THE SPECIFIED GAS
C     AT A GIVEN TEMPERATURE AND PRESSURE. THE SUBROUTINE THEN RETURNS
C     THE NATURAL LOGARITHMS OF THE TRANSLATIONAL AND ELECTRONIC
C     EXCITATION PARTITION FUNCTIONS. THE SUBROUTINE IS ONLY NECESSARY
C     FOR ATOMS. (MONATOMIC)
C
      COMMON/RGASP/ID
      LEVEL 0,T,P,LA,GA,EA,MGSXX,LNQT,LNQE
      INTEGER GA(11,*)
      REAL MGSXX(*),LNQT(*),LNQE(*)
      DIMENSION LA(*),EA(11,*)
      QE=0.0
      R=8.31696E 07
      IF(T.LE.0.0)GOTO 10
      IF(P.LE.0.0)GOTO 20
      LNQT(ID)=(2.5*ALOG(T))-ALOG(P/1.013E6)+(1.5*ALOG(MGSXX(ID)*4.5530
     +7E-07))+ALOG(R)
      GOTO 25
```

```
   10 WRITE(6,100)T
   20 WRITE(6,101)P
   25 LAH=LA(ID)
      DO 40 I=1,LAH
      IF(ABS((EA(ID,I)/T)).GT.85.0)GOTO 40
      QEI=GA(ID,I)*EXP(((-EA(ID,I))/T))
      QE=QE+QEI
   40 CONTINUE
      LNQE(ID)=ALOG(QE)
  100 FORMAT(' ***CAUTION, NEGATIVE TEMPERATURE',E12.5,' BEING EMPLOYED
     +IN TEPART')
  101 FORMAT(' ***CAUTION, NEGATIVE PRESSURE ',E12.5,' BEING EMPLOYED
     +IN TEPART')
      RETURN
      END
C
*******************************************************************************
*
      SUBROUTINE DERLNK(T,TETE,EMEO,TDRLKC,TDRLKP)
*
*******************************************************************************
C
C
C     THE SUBROUTINE DERLNK CALCULATES THE DERIVITIVE OF THE
C     EQUILIBRIUM CONSTANT FOR EACH REACTION AT CONSTANT PRESSURE
C     AND AT CONSTANT DENSITY GIVEN THE TEMPERATURE, THE CHARACTERISTIC
C     TEMPERATURES OF DISSOCIATION AND IONIZATION AND THE INTERNAL
C     ENERGY CALCULATIONS.
C
      COMMON/RGASP/ID
      LEVEL 0,T,TETE,EMEO,TDRLKC,TDRLKP
      DIMENSION TETE(*),EMEO(*),TDRLKC(*),TDRLKP(*)
      IF(ID.GT.2)GOTO 10
      IDE=ID
      TDRLKC(IDE)=(TETE(IDE)/T)+(2.0*EMEO(IDE+2))-EMEO(IDE)
      GOTO 20
   10 IF((ID.EQ.4).OR.(ID.EQ.6))RETURN
      IDE=(ID+3)/2
      TDRLKC(IDE)=(((TETE(ID)/T)+(EMEO(11)+EMEO(ID+2))-EMEO(ID))*0.8)+(
     +((TETE(ID+1)/T)+(EMEO(11)+EMEO(ID+3))-EMEO(ID+1))*0.2)
   20 TDRLKP(IDE)=TDRLKC(IDE)+1.0
      RETURN
      END
C
*******************************************************************************
*
      SUBROUTINE DERZ(T,Z,TDRLKC,TDRLKP,EPS1,EPS2,EPS3,EPS4,EPS5,DERZP,
*
*******************************************************************************
C
     +DERZRO,DERXP,DERXR)
C
C     SUBROUTINE DERZ CALCULATES THE DERIVITIVES OF THE DISSOCIATION
```

```
C     AND IONIZATION FACTORS GIVEN THE RESULTS OF THE SUBROUTINE
C     DERLNK, THE TEMPERATURE, AND THE COMPRESSIBILITY FACTOR.
C
      LEVEL 0,T,Z,TDRLKC,TDRLKP,EPS1,EPS2,EPS3,EPS4,EPS5,DERZP,
     +DERZRO,DERXP,DERXR
      DIMENSION TDRLKC(*),TDRLKP(*),DERXP(*),DERXR(*)
      DPEPS1=0.0
      DPEPS2=0.0
      DPEPS3=0.0
      DPEPS4=0.0
      DPEPS5=0.0
      DREPS1=0.0
      DREPS2=0.0
      DREPS3=0.0
      DREPS4=0.0
      DREPS5=0.0
      IF(((0.2-EPS1).LT.1.0E-05).OR.(EPS1.LT.1.0E-05))GOTO 1
      DPEPS1=(TDRLKP(2)/T)/((2.0/EPS1)-(1.0/(1.0+EPS1))+(1.0/(0.2-EPS1)
     +))
      DREPS1=(TDRLKC(2)/T)/((2.0/EPS1)+(1.0/(0.2-EPS1)))
    1 IF(((0.8-EPS2).LT.1.0E-05).OR.(EPS2.LT.1.0E-05))GOTO 2
      DPEPS2=(TDRLKP(1)/T)/((2.0/EPS2)-(1.0/(1.0+EPS2))+(1.0/(0.8-EPS2)
     +))
      DREPS2=(TDRLKC(1)/T)/((2.0/EPS2)+(1.0/(0.8-EPS2)))
    2 IF(((1.0-EPS3).LT.1.0E-05).OR.(EPS3.LT.1.0E-05))GOTO 3
      DPEPS3=(TDRLKP(3)/T)/((2.0/EPS3)-(1.0/(1.0+EPS3))+(1.0/(1.0-EPS3)
     +))
      DREPS3=(TDRLKC(3)/T)/((2.0/EPS3)+(1.0/(1.0-EPS3)))
    3 IF(((2.0-(2.0*EPS4)).LT.1.0E-05).OR.(EPS4.LT.1.0E-05))GOTO 4
      DPEPS4=(TDRLKP(4)/T)/((2.0/EPS4)-(1.0/(4.0+(2.0*EPS4)))+(1.0/(2.0
     +-(2.0*EPS4))))
      DREPS4=(TDRLKC(4)/T)/((2.0/EPS4)+(1.0/(2.0-(2.0*EPS4))))
    4 IF(((2.0-(2.0*EPS5)).LT.1.0E-05).OR.(EPS5.LT.1.0E-05))GOTO 5
      DPEPS5=(TDRLKP(5)/T)/((2.0/EPS5)-(1.0/(6.0+(2.0*EPS5)))+(1.0/(2.0
     +-(2.0*EPS5))))
      DREPS5=(TDRLKC(5)/T)/((2.0/EPS5)+(1.0/(2.0-(2.0*EPS5))))
    5 DERZP=DPEPS1+DPEPS2+(2.0*DPEPS3)+(2.0*DPEPS4)+(2.0*DPEPS5)
      DERZRO=DREPS1+DREPS2+(2.0*DREPS3)+(2.0*DREPS4)+(2.0*DREPS5)
      DERXP(1)=((-1.0)/Z)*DPEPS2
      DERXP(2)=((-1.0)/Z)*DPEPS1
      DERXP(3)=((2.0/Z)*DPEPS2)+((-1.6/Z)*DPEPS3)
      DERXP(4)=((2.0/Z)*DPEPS1)+((-0.4/Z)*DPEPS3)
      DERXP(5)=(((2.0*DPEPS3)-(2.0*DPEPS4))/Z)*0.8
      DERXP(6)=DERXP(5)/4.0
      DERXP(7)=(((4.0*DPEPS4)-(4.0*DPEPS5))/Z)*0.4
      DERXP(8)=DERXP(7)/4.0
      DERXP(9)=((6.0*DPEPS5)/Z)*(0.8/3.0)
      DERXP(10)=DERXP(9)/4.0
      DERXP(11)=((2.0*DPEPS3)+(2.0*DPEPS4)+(2.0*DPEPS5))/Z
      DERXR(1)=((-1.0)/Z)*DREPS2
      DERXR(2)=((-1.0)/Z)*DREPS1
      DERXR(3)=((2.0/Z)*DREPS2)+((-1.6/Z)*DREPS3)
      DERXR(4)=((2.0/Z)*DREPS1)+((-0.4/Z)*DREPS3)
```

```
      DERXR(5)=(((2.0*DREPS3)-(2.0*DREPS4))/Z)*0.8
      DERXR(6)=DERXR(5)/4.0
      DERXR(7)=(((4.0*DREPS4)-(4.0*DREPS5))/Z)*0.4
      DERXR(8)=DERXR(7)/4.0
      DERXR(9)=((6.0*DREPS5)/Z)*(0.8/3.0)
      DERXR(10)=DERXR(9)/4.0
      DERXR(11)=((2.0*DREPS3)+(2.0*DREPS4)+(2.0*DREPS5))/Z
      RETURN
      END
C
*******************************************************************************
*
      SUBROUTINE MOLFRA(Z,EPS1,EPS2,EPS3,EPS4,EPS5,X)
*
*******************************************************************************
C
C
C     THE SUBROUTINE MOLFRA CALCULATES THE MOLE FRACTIONS OF THE
C     CONSTITUENTS FROM THE COMPRESSIBILITY FACTOR AND THE DISSOCIATION
C     AND IONIZATION FACTORS.
C
      LEVEL 0,Z,EPS1,EPS2,EPS3,EPS4,EPS5,X
      DIMENSION X(*)
      X(1)=(0.8-EPS2)/Z
      X(2)=(0.2-EPS1)/Z
      X(3)=((2.0*EPS2)-(1.6*EPS3))/Z
      X(4)=((2.0*EPS1)-(0.4*EPS3))/Z
      X(5)=(((2.0*EPS3)-(2.0*EPS4))/Z)*0.8
      X(6)=X(5)/4.0
      X(7)=(((4.0*EPS4)-(4.0*EPS5))/Z)*0.4
      X(8)=X(7)/4.0
      X(9)=((6.0*EPS5)/Z)*(0.8/3.0)
      X(10)=X(9)/4.0
      X(11)=((2.0*EPS3)+(2.0*EPS4)+(2.0*EPS5))/Z
      RETURN
C
      END
```

DISTRIBUTION LIST

12 Administrator
Defense Technical Info Center
ATTN: DTIC-DDA
Cameron Station
Alexandria, VA 22304-6145

1 HQDA (DAMA-ART-M)
Washington, DC 20310

1 Commander
US Army Materiel Command
ATTN: AMCDRA-ST
5001 Eisenhower Avenue
Alexandria, VA 22333-0001

1 Commander
Armament R&D Center
US Army AMCCOM
ATTN: SMCAR-TSS
Dover, NJ 07801

1 Commander
Armament R&D Center
US Army AMCCOM
ATTN: SMCAR-TDC
Dover, NJ 07801

1 Director
Benet Weapons Laboratory
Armament R&D Center
US Army AMCCOM
ATTN: SMCAR-LCB-TL
Watervliet, NY 12189

1 Commander
US Army Armament, Munitions
and Chemical Command
ATTN: SMCAR-ESP-L
Rock Island, IL 61299

1 Director
US Army Air Mobility Research
and Development Laboratory
Ames Research Center
Moffett Field, CA 94035

1 Commander
US Army Communications-
Electronics Command
ATTN: AMSEL-ED
Fort Monmouth, NJ 07703

1 Commander
ERADCOM Technical Library
ATTN: DELSD-L (Reports
Section)
Fort Monmouth, NJ 07703-5301

1 Commander
US Army Missile Command
Research, Development and
Engineering Center
ATTN: AMSMI-RD
Redstone Arsenal, AL 35898

1 Director
US Army Missile & Space
Intelligence Center
ATTN: AIAMS-YDL
Redstone Arsenal
AL 35898-5500

1 Commander
US Army Tank-Automotive Cmd
ATTN: AMSTA-TSL
Warren, MI 48397-5000

1 Director
US Army TRADOC Systems
Analysis Activity
ATTN: ATAA-SL
White Sands Missile Range,
NM 88002

1 Commander
US Army Aviation Research
and Development Command
ATTN: AMSAV-E
4300 Goodfellow Blvd
St. Louis, MO 63120

1 Commandant
US Army Infantry School
ATTN: ATSH-CD-CSO-OR
Fort Benning, GA 31905

1 Commander
US Army Development and
Employment Agency
ATTN: MODE-TED-SAB
Fort Lewis, WA 98433

1 AFWL/SUL
Kirtland AFB, NM 87117

1 AFATL/DLODL
Eglin AFB, FL 32542-5000

10 Central Intelligence Agency
Office of Central Reference
Dissemination Branch
Room GE-47 HQS
Washington, DC 20502

2 Dir, USAMSAA
ATTN: AMXSY-D
AMXSY-MP (H. Cohen)

1 Cdr, USATECOM
ATTN: AMSTE-TO-F

3 Cdr, CRDC, AMCCOM
ATTN: SMCCR-RSP-A
SMCCR-MU
SMCCR-SPS-IL

USER EVALUATION SHEET/CHANGE OF ADDRESS

This Laboratory undertakes a continuing effort to improve the quality of the reports it publishes. Your comments/answers to the items/questions below will aid us in our efforts.

1. BRL Report Number_____ Date of Report_____

2. Date Report Received_____

3. Does this report satisfy a need? (Comment on purpose, related project, or other area of interest for which the report will be used.)_____

4. How specifically, is the report being used? (Information source, design data, procedure, source of ideas, etc.)_____

5. Has the information in this report led to any quantitative savings as far as man-hours or dollars saved, operating costs avoided or efficiencies achieved, etc? If so, please elaborate._____

6. General Comments. What do you think should be changed to improve future reports? (Indicate changes to organization, technical content, format, etc.)

CURRENT ADDRESS

Name

Organization

Address

City, State, Zip

7. If indicating a Change of Address or Address Correction, please provide the New or Correct Address in Block 6 above and the Old or Incorrect address below.

OLD ADDRESS

Name

Organization

Address

City, State, Zip

(Remove this sheet, fold as indicated, staple or tape closed, and mail.)

FOLD HERE

Director
US Army Ballistic Research Laboratory
ATTN: DRXBR-OD-ST
Aberdeen Proving Ground, MD 21005-5066

NO POSTAGE
NECESSARY
IF MAILED
IN THE
UNITED STATES

OFFICIAL BUSINESS
PENALTY FOR PRIVATE USE, $300

BUSINESS REPLY MAIL
FIRST CLASS PERMIT NO 12062 WASHINGTON, DC
POSTAGE WILL BE PAID BY DEPARTMENT OF THE ARMY

Director
US Army Ballistic Research Laboratory
ATTN: DRXBR-OD-ST
Aberdeen Proving Ground, MD 21005-9989

FOLD HERE

END